A COMPUTER BASED TREND SURFACE STUDY OF STRUCTURAL ANALYSIS: TEST CASE FROM LIPSON COVE, SOUTH AUSTRALIA

Vol. II

by

Peter Haddon Cohen, B.Sc (Hons)

Department of Geology and Mineralogy

University of Adelaide

November, 1983

A Thesis submitted for the

Degree of Doctor of Philosophy

AWARDED 17th JUNE 1986

TABLE OF CONTENTS

VOLUME II

LIST OF FIGURES

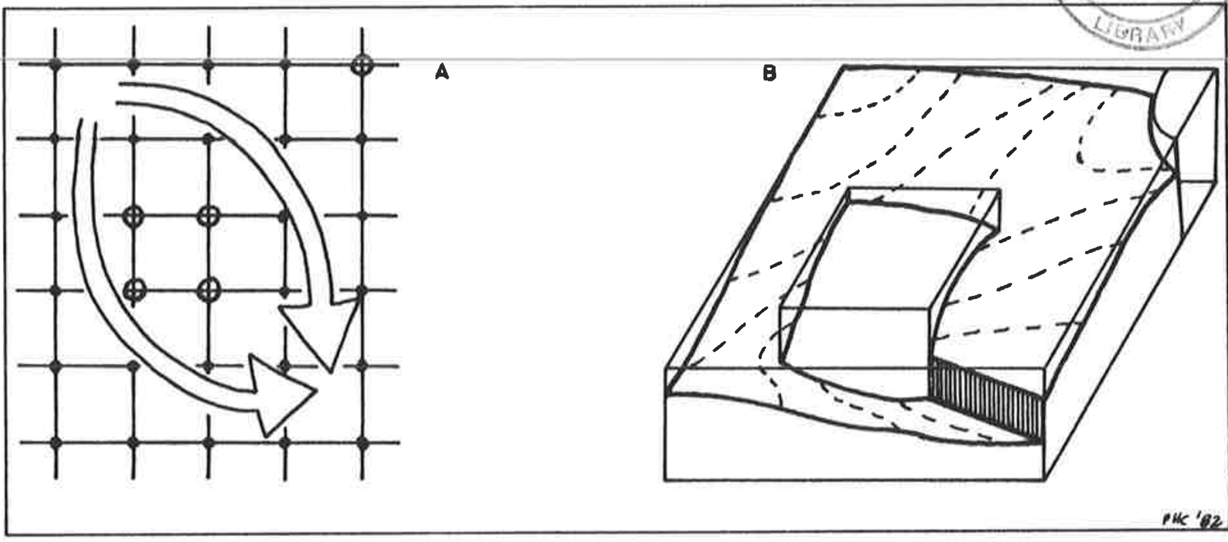

Fig. 1.1 Fitting a surface to a regular grid of gradient data, ".", by taking independent paths (a) around missing data, "o", can give rise to discontinuities (b).

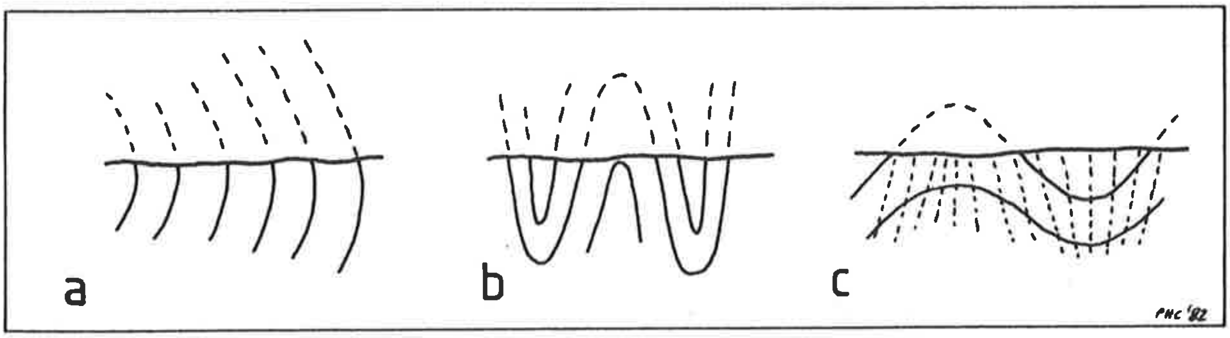

Fig. 1.2 Some situations not suitable for Type I trend surface analysis.
a) Hinge regions of reclined folds.
b) Very tight upright folds.
c) Subvertical foliations.

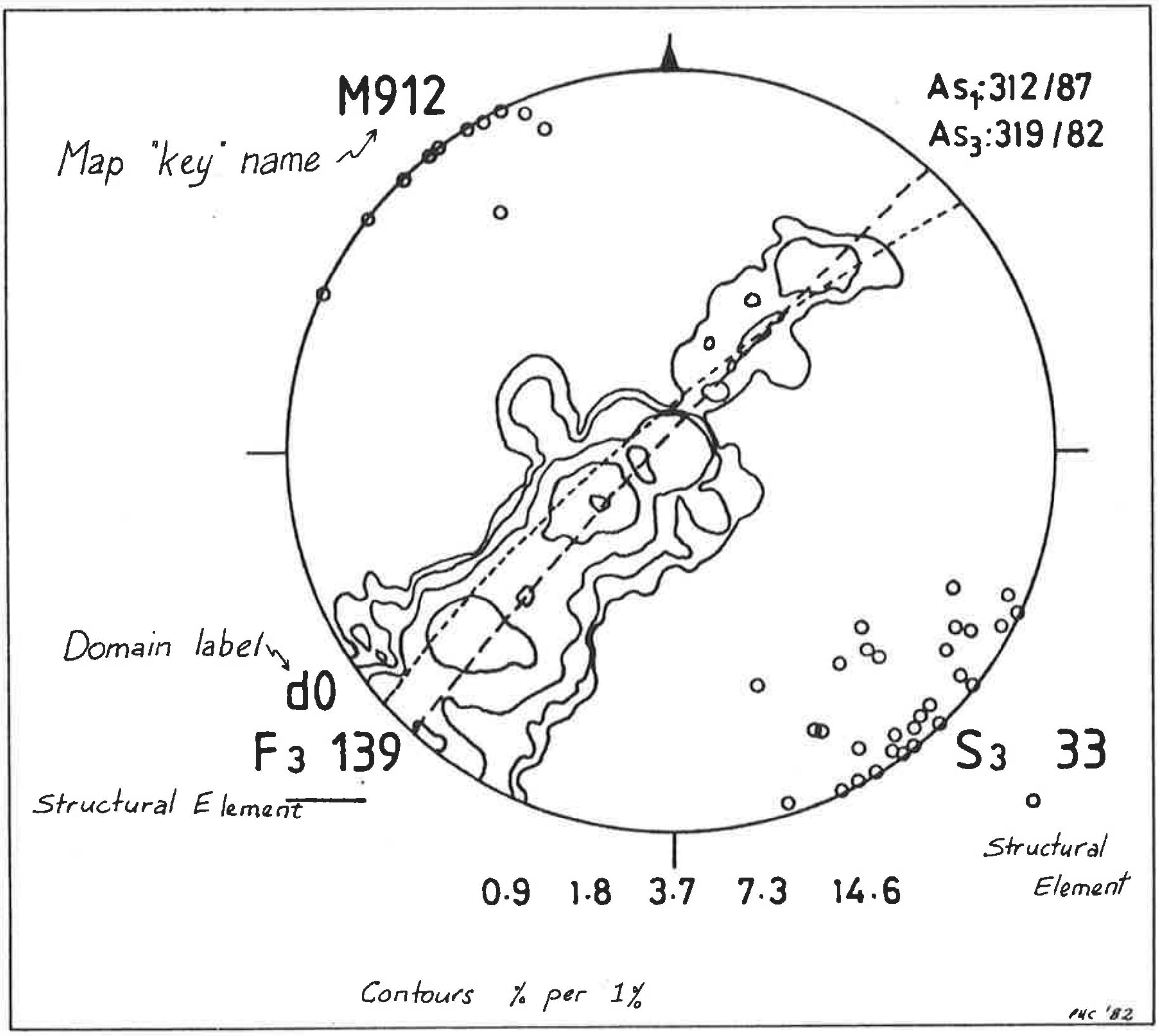

Fig. 1.3 Design of stereonet, stereoplot, and pi figures used in this thesis (except colour plates). All figures are equal-area lower hemisphere plots unless otherwise stated.

M: = mean (subscripted refers to the appropriate domain).

A: = axial plane.

C: = centre of conical distribution.

P: = pole to great circle distribution.

π: = as above, but for pi figure.

π_c: = as above, using a conical distribution.

π_f: = fitted π when distribution is poorly weighted.

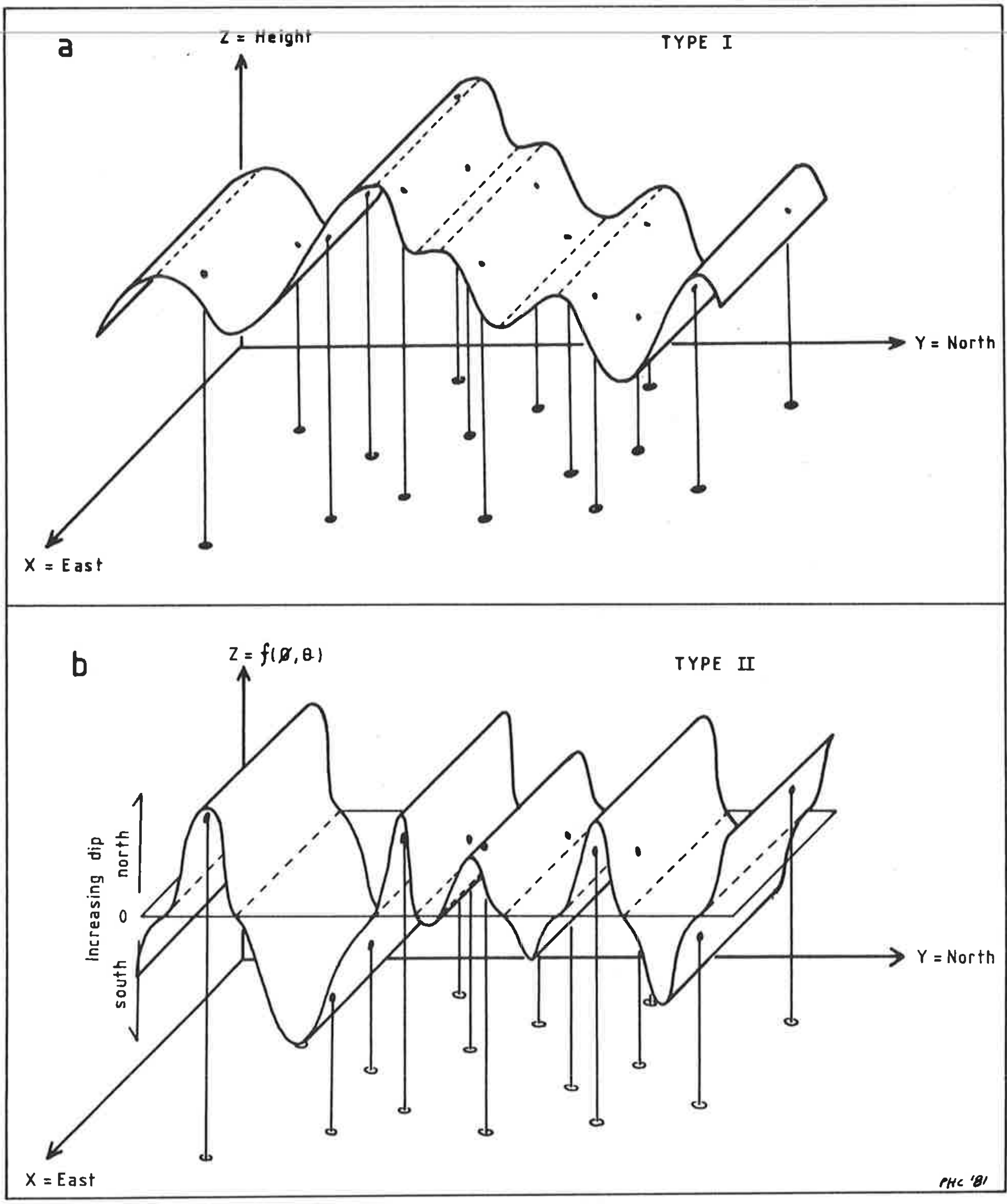

Fig. 2.1 Two types of trend surfaces applicable to structural geology.
a) Type I: trend surfaces are identical to structure surfaces.
b) Type II: trend surfaces of properties of structural data.

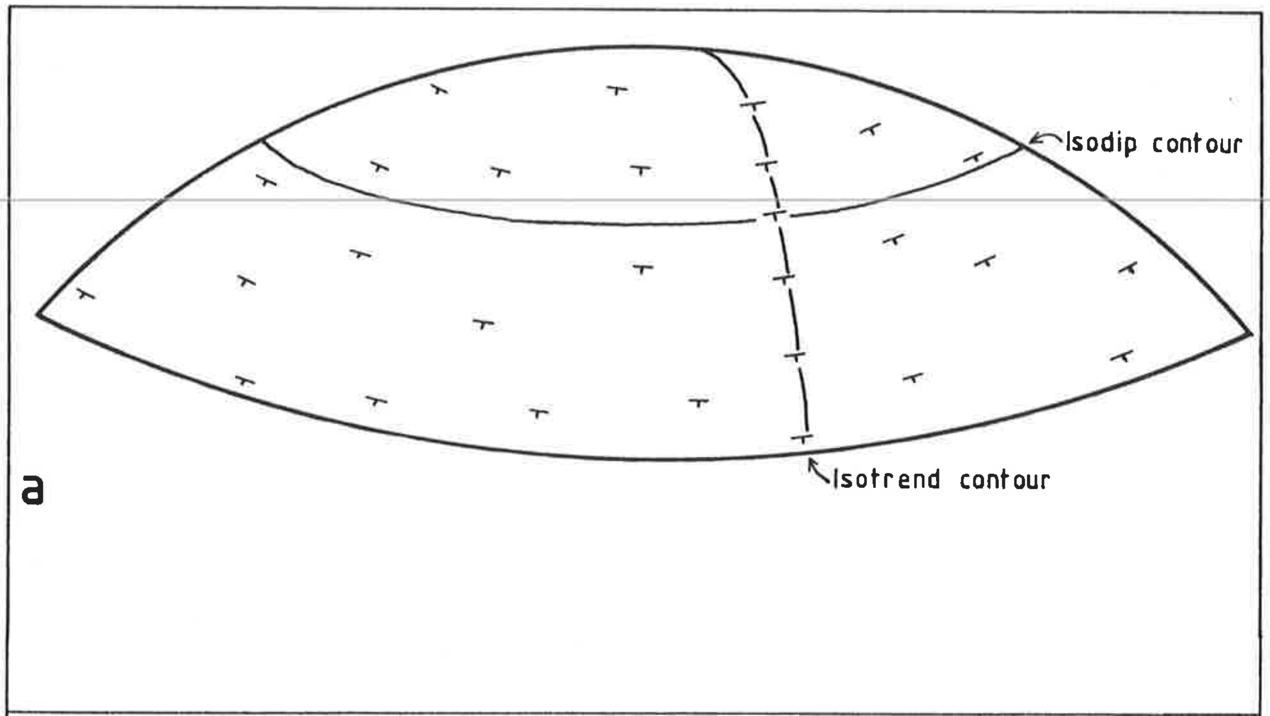

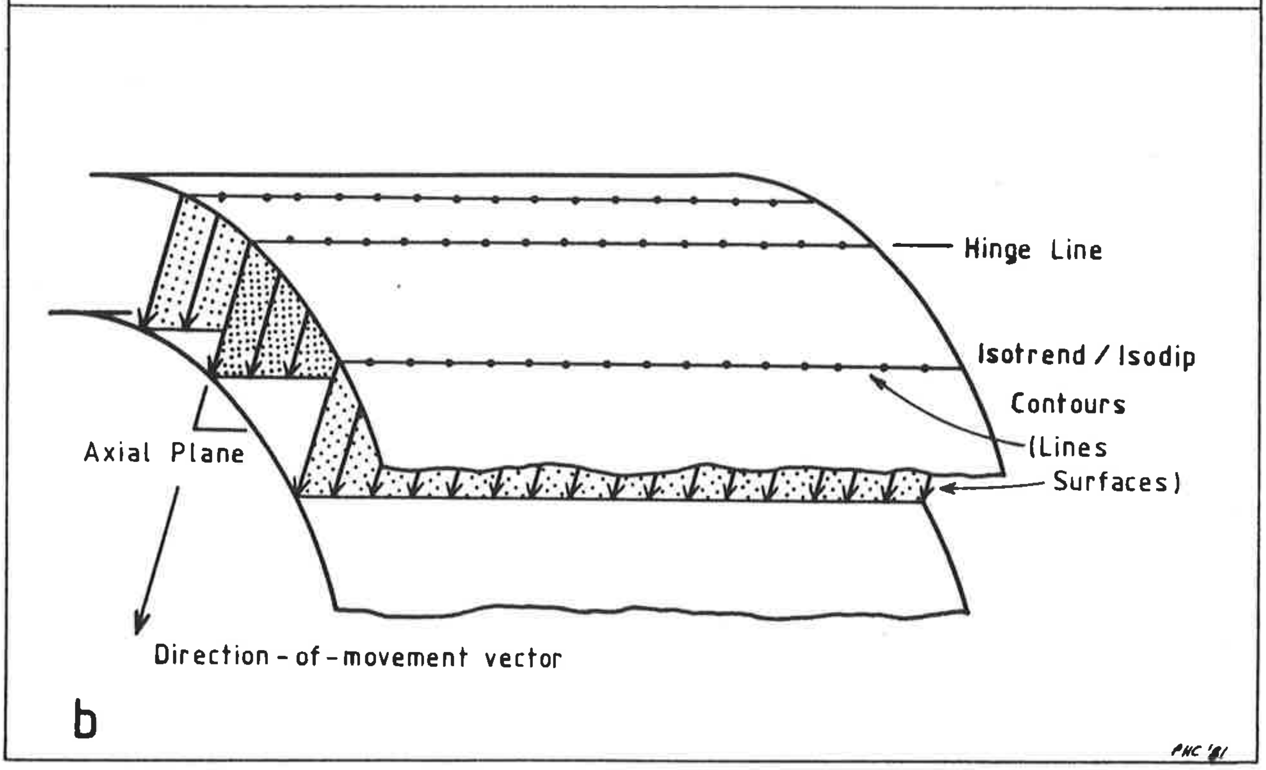

Fig. 2.2

a) Definition of isotrend contour lines and isodip contour lines on a structural surface. Isotrends join points of equal trend, and isodips join points of equal dip.

b) General definition of isotrend/isodip contour lines and surfaces (see text). The figure does not need to distinguish isotrends from isodips.

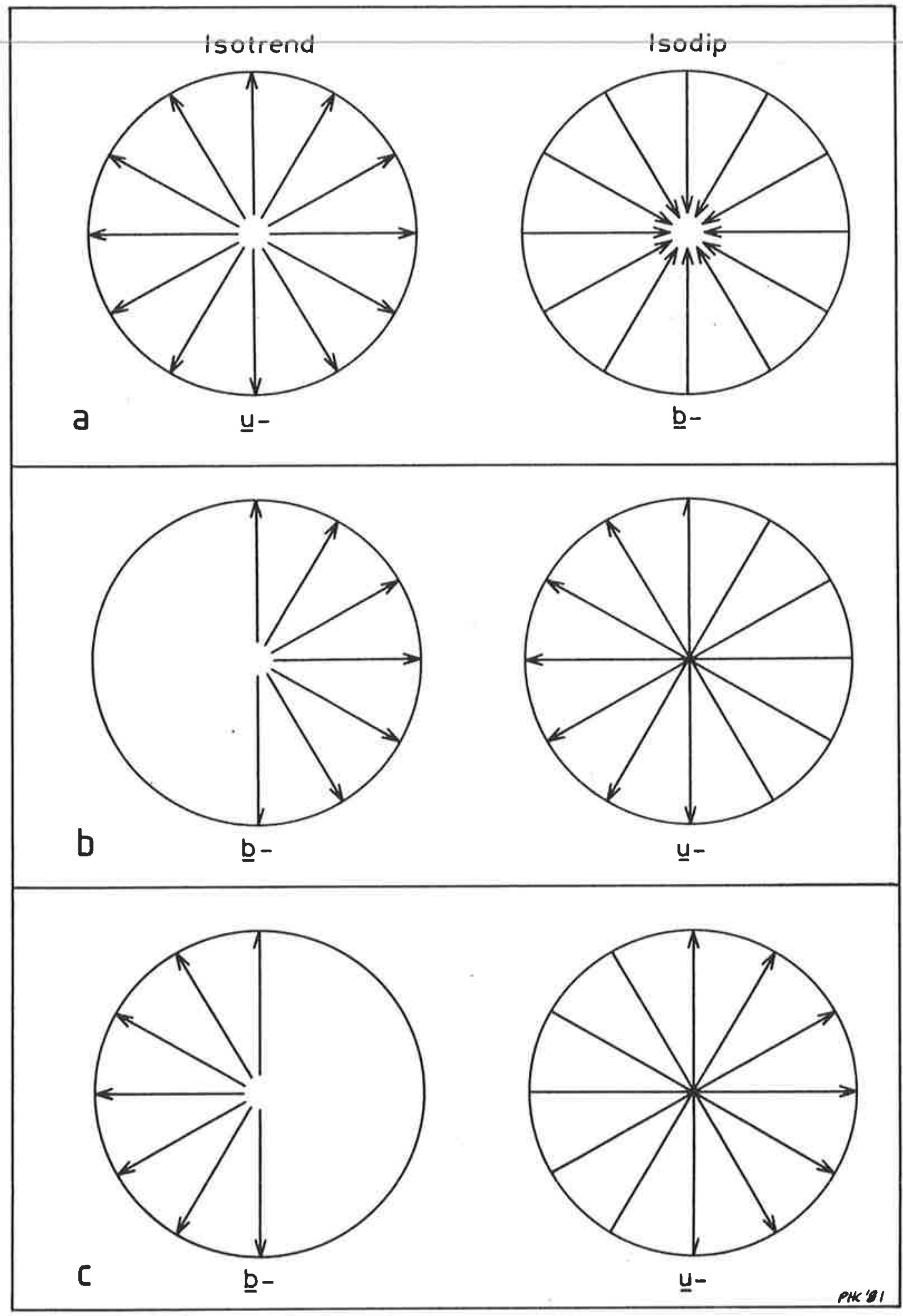

Fig. 2.3 Stereoplot pairs of ranges of values for isotrends and isodip contours to uniquely define every non-directed orientation, except vertical (see text). u- represents uni-directional data, b- represents bi-directional data. A full arrowhead at the end of a range of values indicates that the corresponding azimuthal range is closed, and a half arrowhead indicates that it is open.

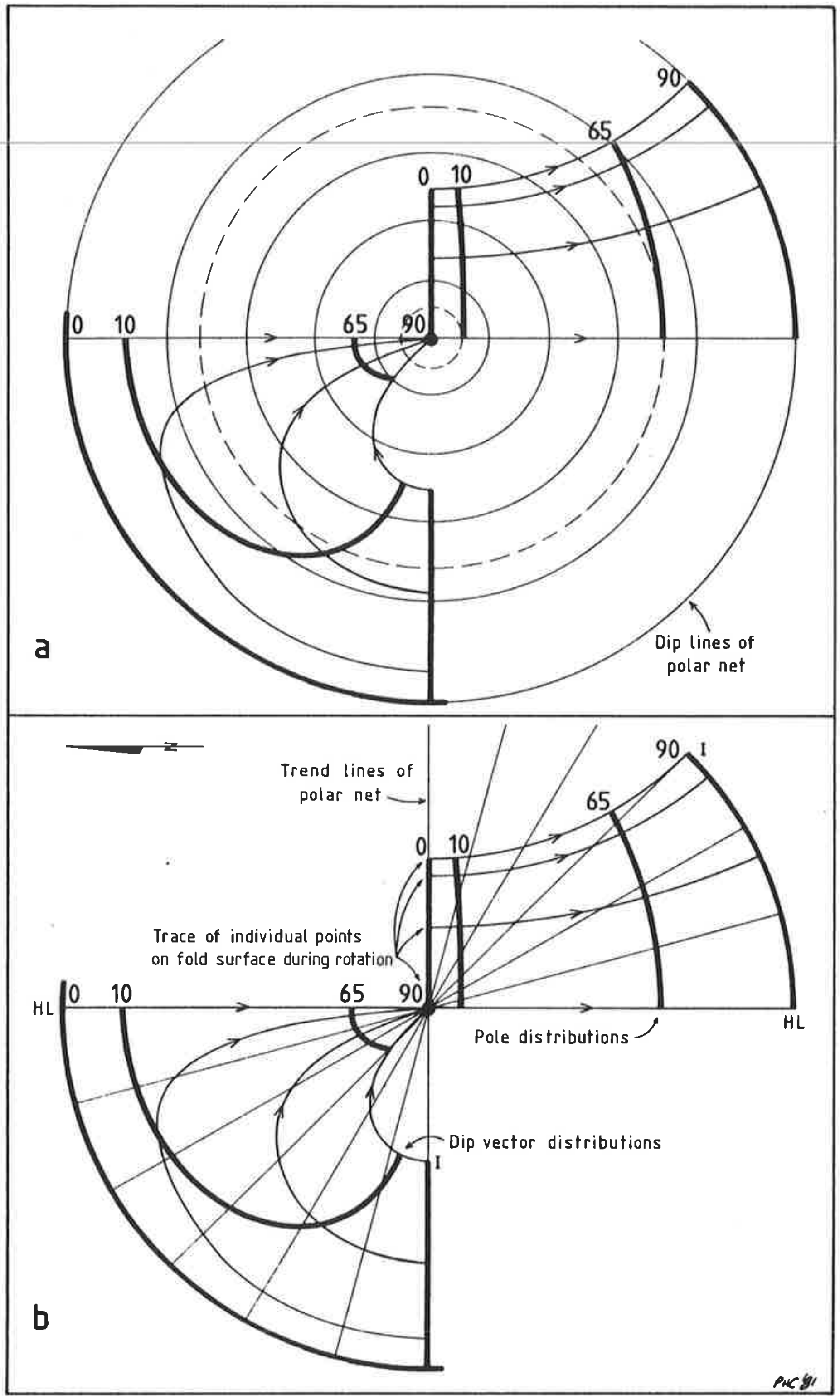

Fig. 2.4 Behaviour of the dip vector distribution of the western limb of an upright, north-south cylindrical fold during rotation (see §4.2.3). The corresponding pole figures are included. The fold is rotated anticlockwise about the axial plane normal (090°/00°) by: 0°, 10°, 65°, and 90°. Four points (hinge line, HL; limb extremity or inflection point, I; and two intermediate points) are traced (arrowed lines) during rotation.

a) Superimposed isodip contours of a polar net for every 18° of dip (as used by the standard colour chart, Fig. CP.1d, Appendix X).
b) Superimposed isotrend contours of a polar net at every 15° (double the resolution of the standard colour chart).

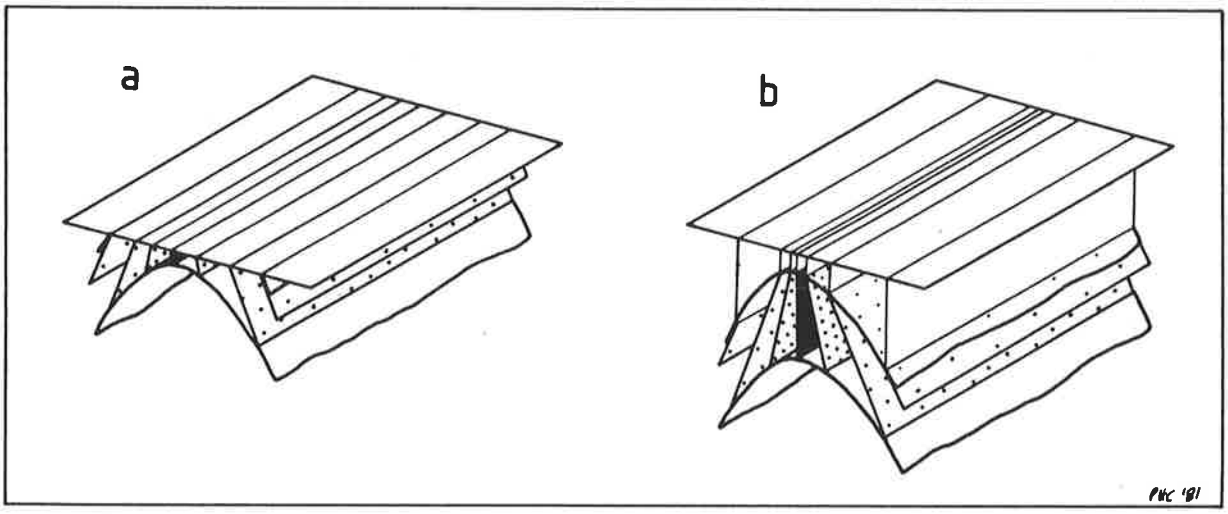

Fig. 2.5 Two sources of data.
a) Transection of structures (e.g. ground surface).
b) orthographic projection of bounding surfaces.

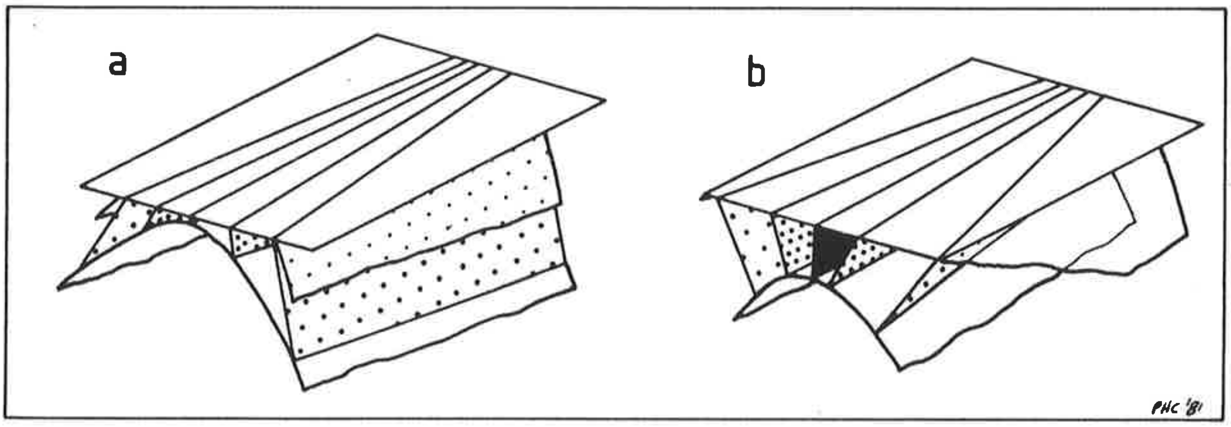

Fig. 2.6 Transected folds have contour patterns that combine cylindricity and profile shape information, i.e. ρ_p and ρ_r respectively.
a) A pattern for plunging cylindrical folds can appear identical to (b) a pattern for horizontal conical folds.

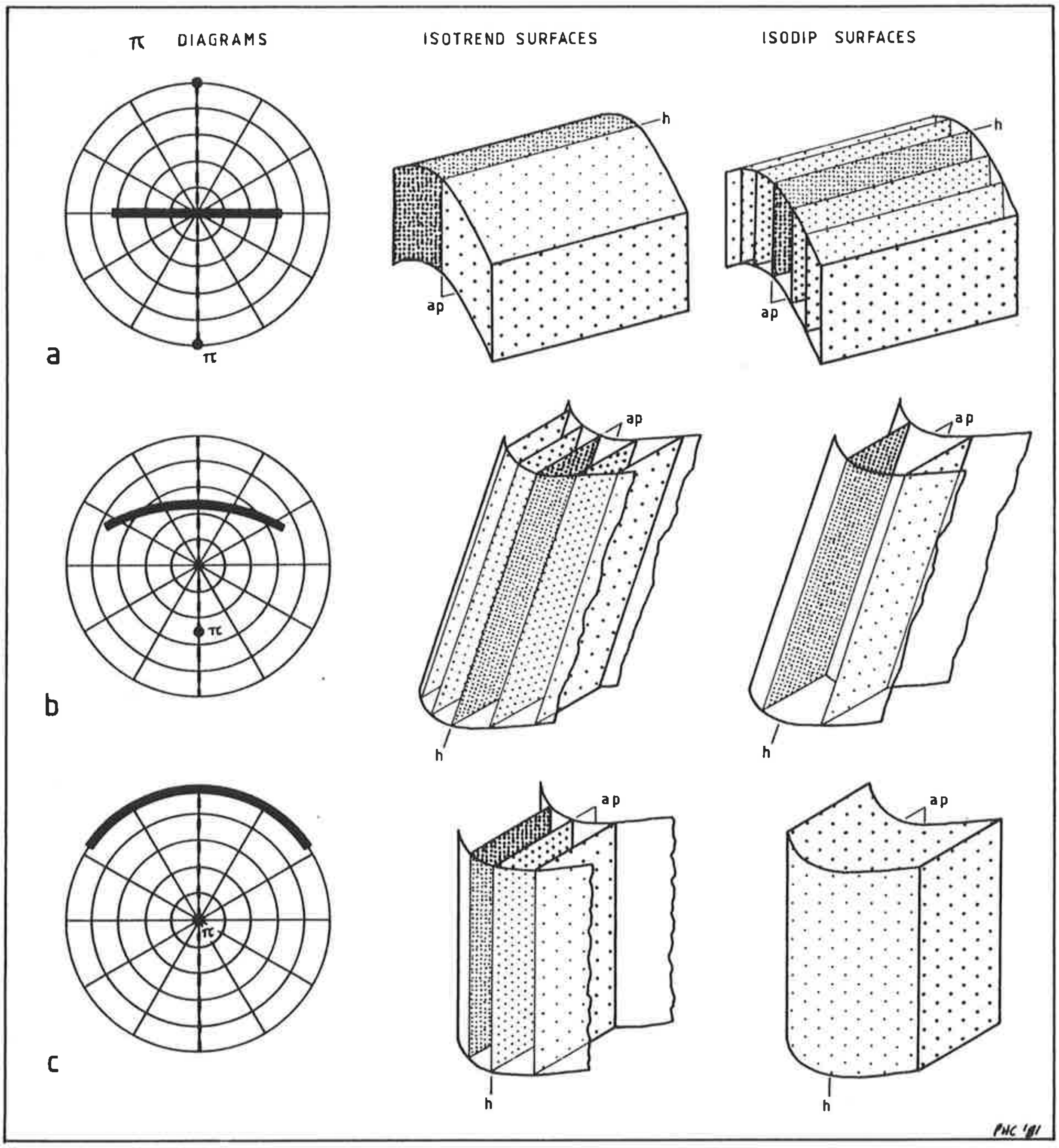

Fig. 2.7 Behaviour of isotrend and isodip contours during rotation of an upright cylindrical fold. (h - hinge line, ap - axial plane.) Isodip contours are intervals of 18° and isotrends in intervals of 30° (equivalent to standard colour chart, Fig. CP.1d) (Note that the block diagrams of (b) are upright, see pole figure.)

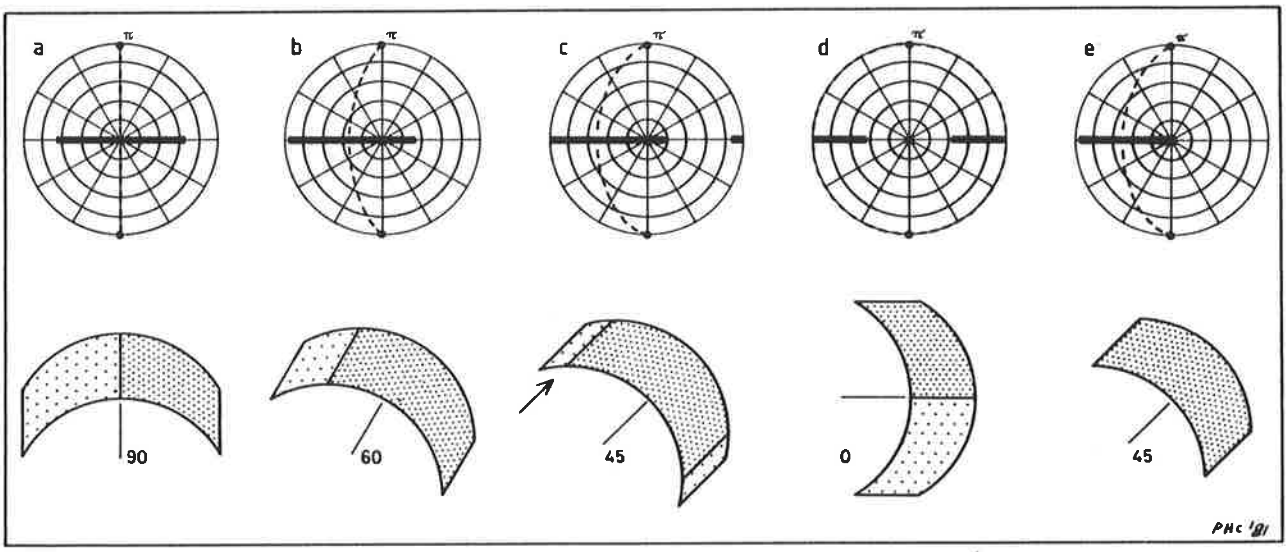

Fig. 2.8 Behaviour of isotrend volumes during the reclining of a horizontal fold profile. Boundary between volumes have infinite density (ρ_p) at horizontal dips (e.g. arrowed), and zero density at vertical dips (see text).
a) to d) Interlimb angle less than 90°.
e) Interlimb angle greater than 90°.

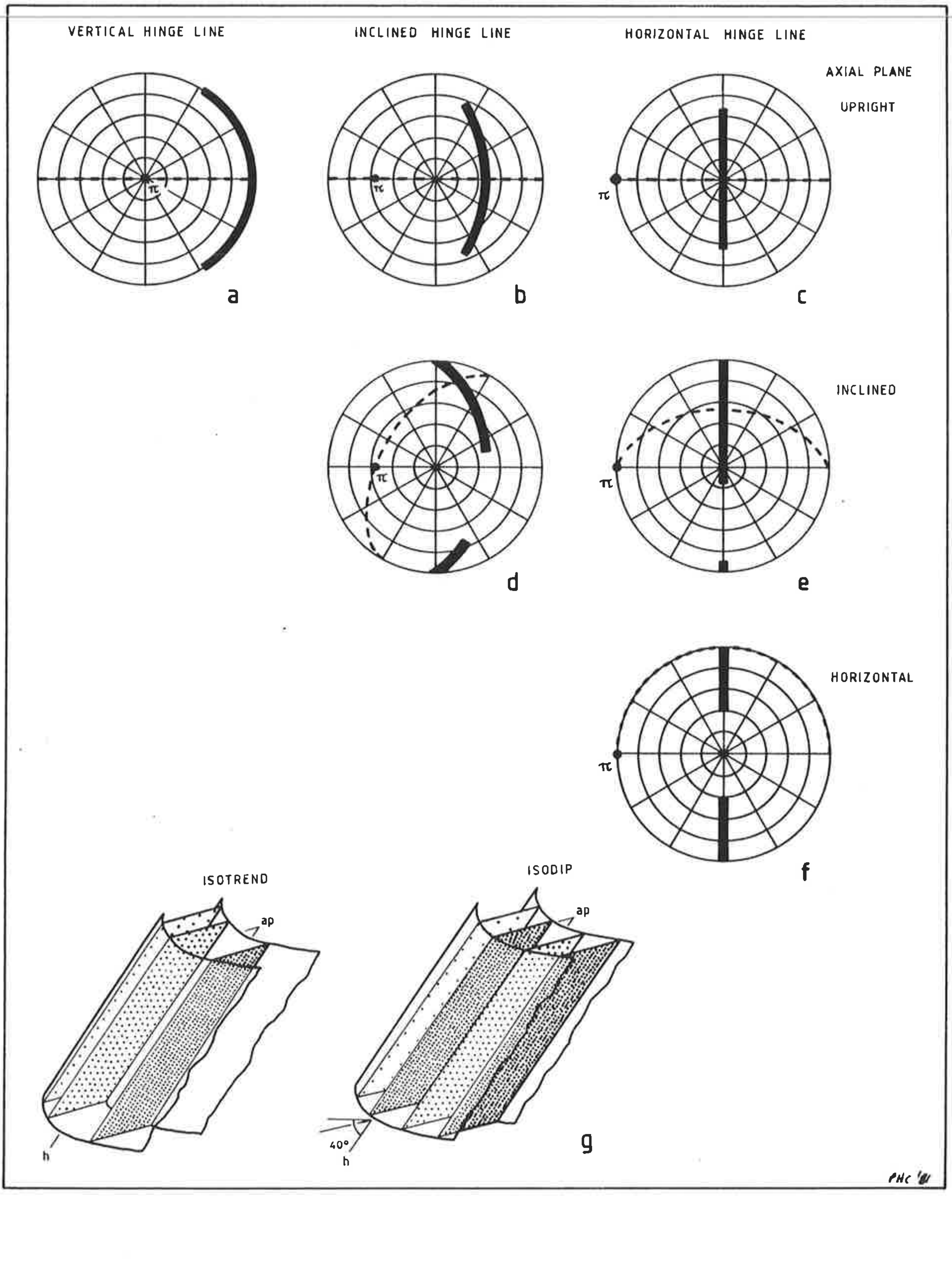

Fig. 2.9 (a-f) Pole figures of various cylindrical fold orientations (see text). Dashed line is axial plane.
(g) Block diagrams corresponding to (d). Number and values of isotrend/isodip contours are found from the pole figure.

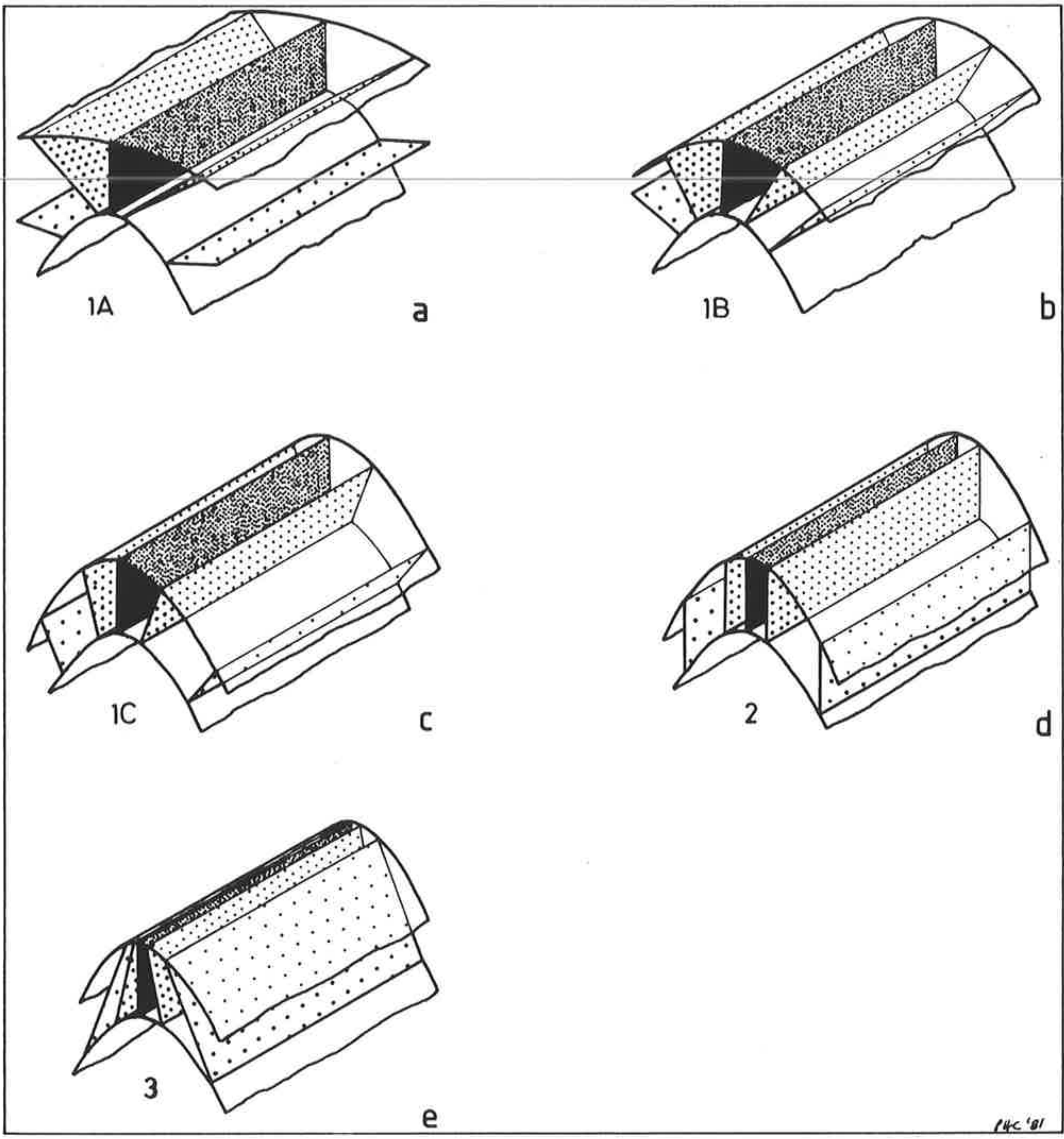

Fig. 2.10 Isodip/isotrend contours for the five Ramsay (1967, Fig. 7.24) fold classes for cylindrical folds in a general orientation.

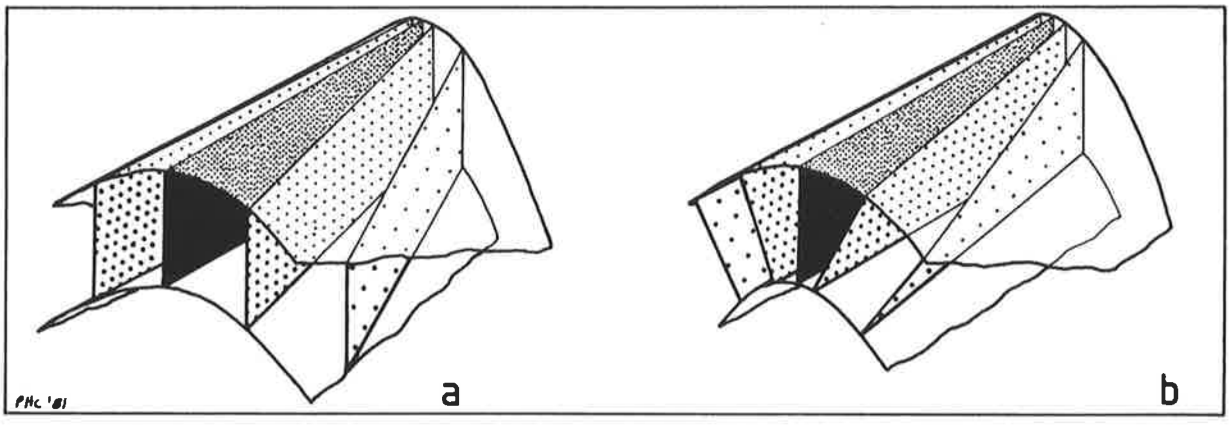

Fig. 2.11 Examples of isodip/isotrend contours for conical folds in a general orientation.
a) Class 2/2 ("similar" at both ends).
b) Class 1C/2 ("1C" at one end, "2" at the other end).

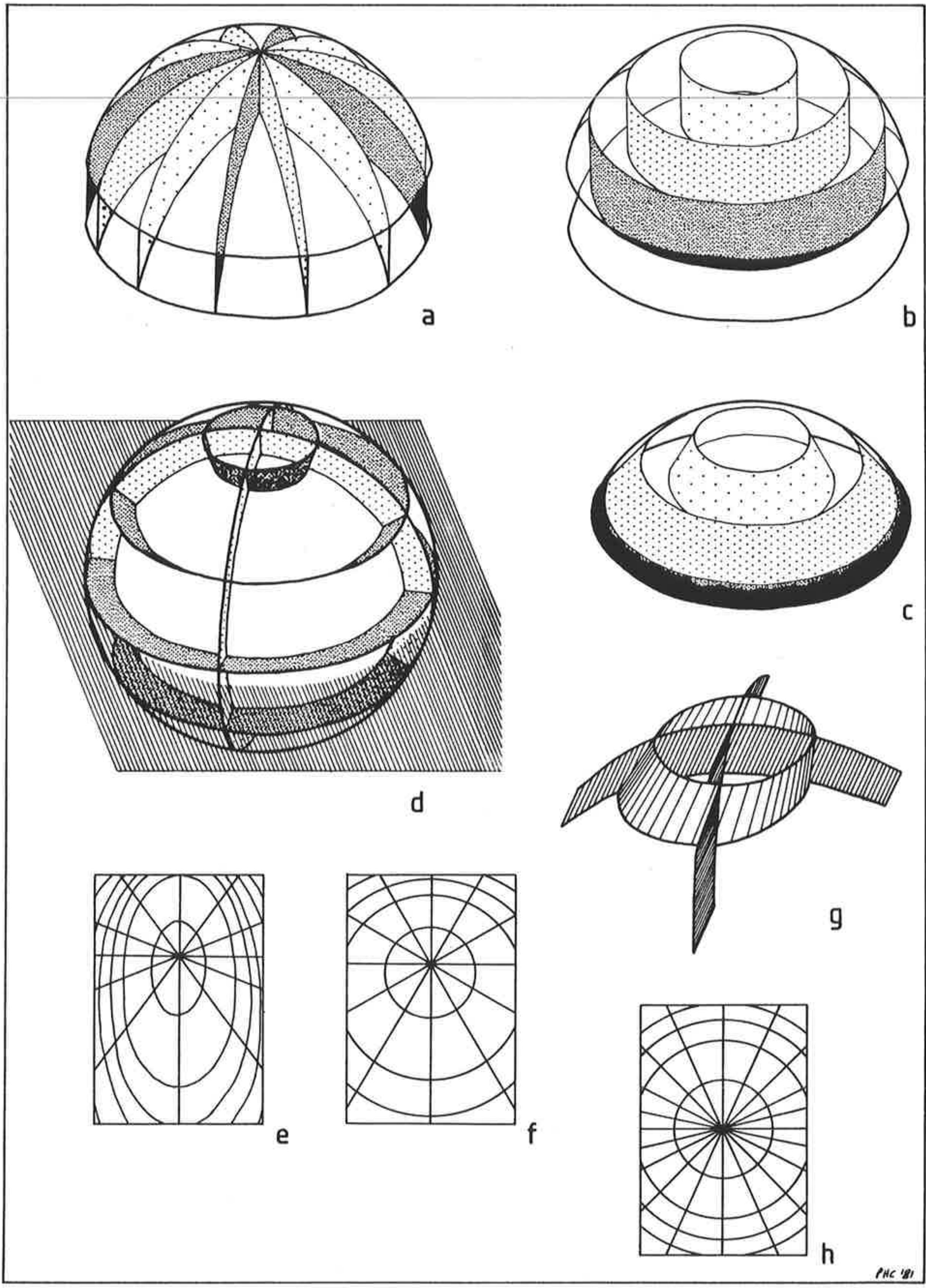

Fig. 2.12 Contours for spherical domes.
(a) Isotrends of a symmetrical dome of any class. (b) Isodips of "similar" style dome. (c) Isodips of class 3 dome. (d) Contours for "parallel" style dome. When transected by an oblique plane, it gives contour patterns of (e), which on projection to a plan map produces (f). (g) Contours of an asymmetric dome produce contour maps such as (h) i.e. varying ρ_r for isotrend contours.

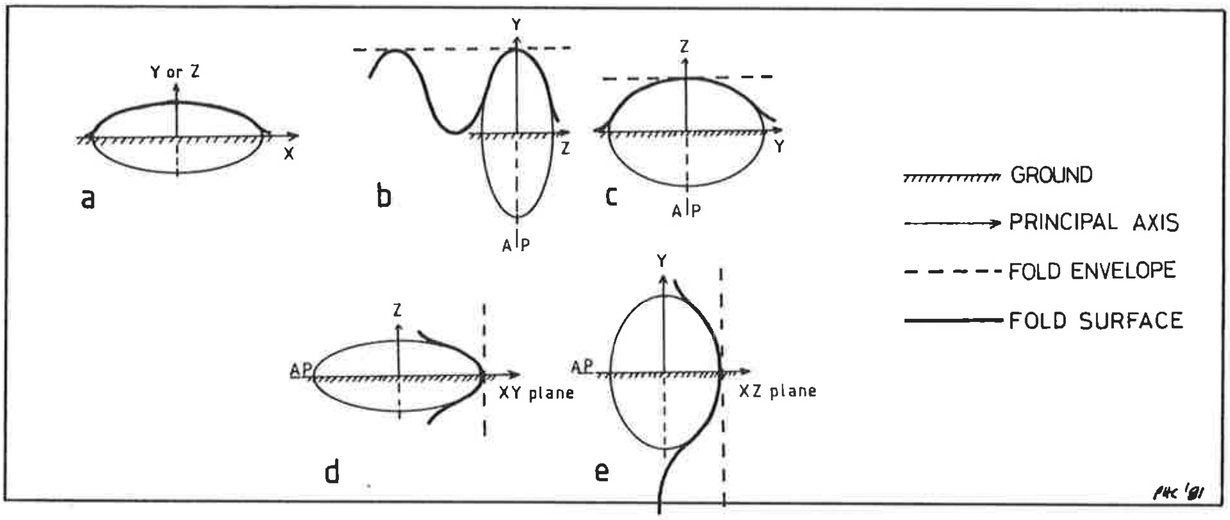

Fig. 2.13 Various geometries of ellipsoidal domes.
a,b,c) Profiles.
d,e) Axial plane sections.
The axial plane is the principal plane, containing x, that best suits the geometry for any given situation. For symmetrical folds axial planes are the planes perpendicular to the fold envelope. For highly asymmetric folds, the axial planes may be ambiguous. Elliptical folds may have axial planes that do not pass through the point of maximum curvature (a,c,e). Geologically, such folds approximate box folds which often have two axial planes passing through the two points of maximum curvature. For mathematical simplicity, the former geometry is adhered to, which does not detract from the understanding of real folds. The fold hinge is the trace of the axial plane on the dome surface.

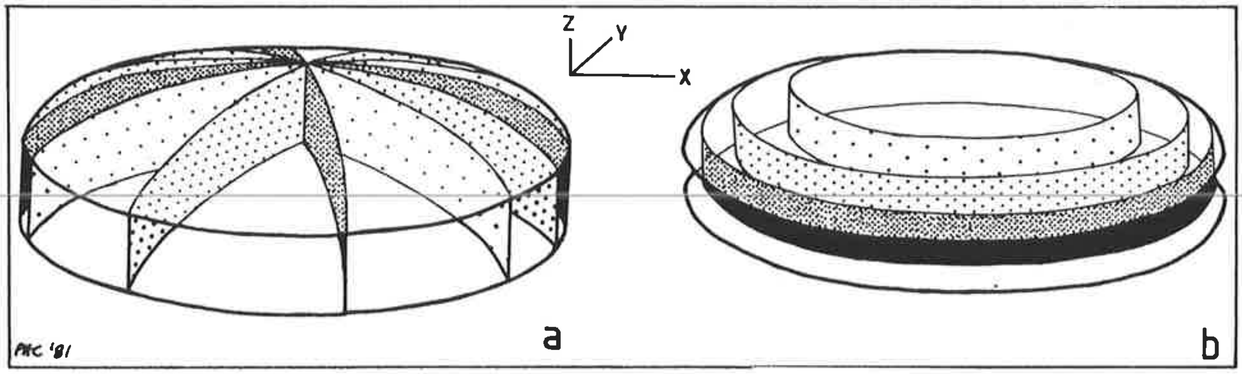

Fig. 2.14 Contours for ellipsoidal domes.
a) Isotrends. b) Isodips.

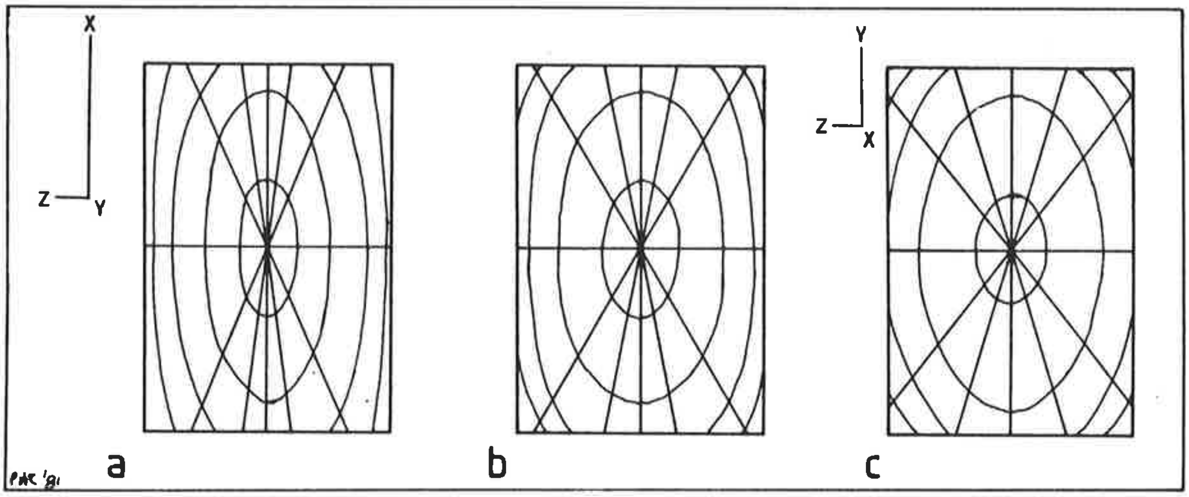

Fig. 2.15 Change in contours of ellipsoidal dome under rotation. Contours are schematic, as for Fig. 2.17e. Precise values and positions can be computed from Appendix E. (a) Model of Fig. 2.13b; (b) Rotation of (a) around the z axis to (c) the vertical.

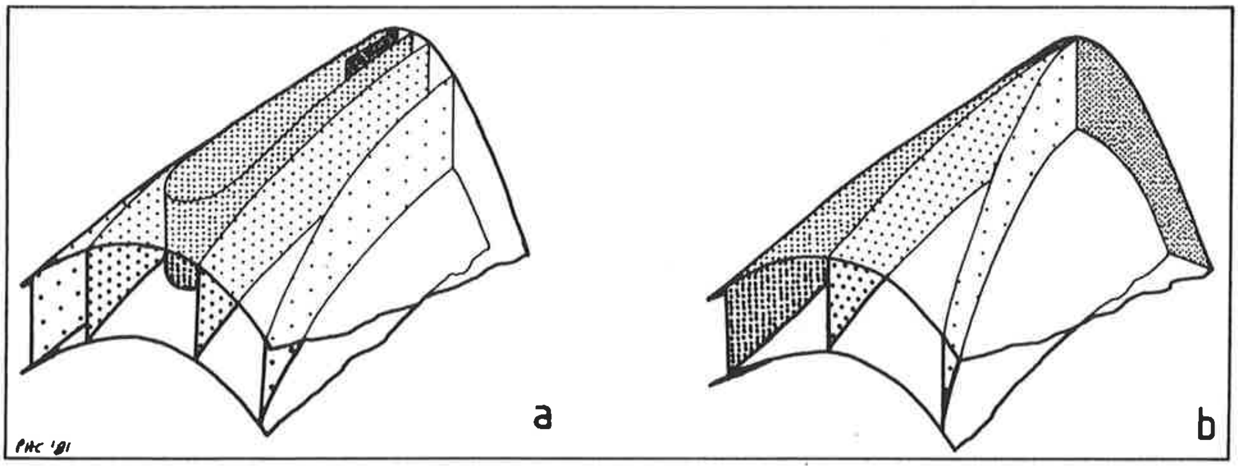

Fig. 2.16 Contours of a fold, in any orientation, consisting of combined conical fold and ellipsoidal dome. (a) Isodips. (b) Isotrends.

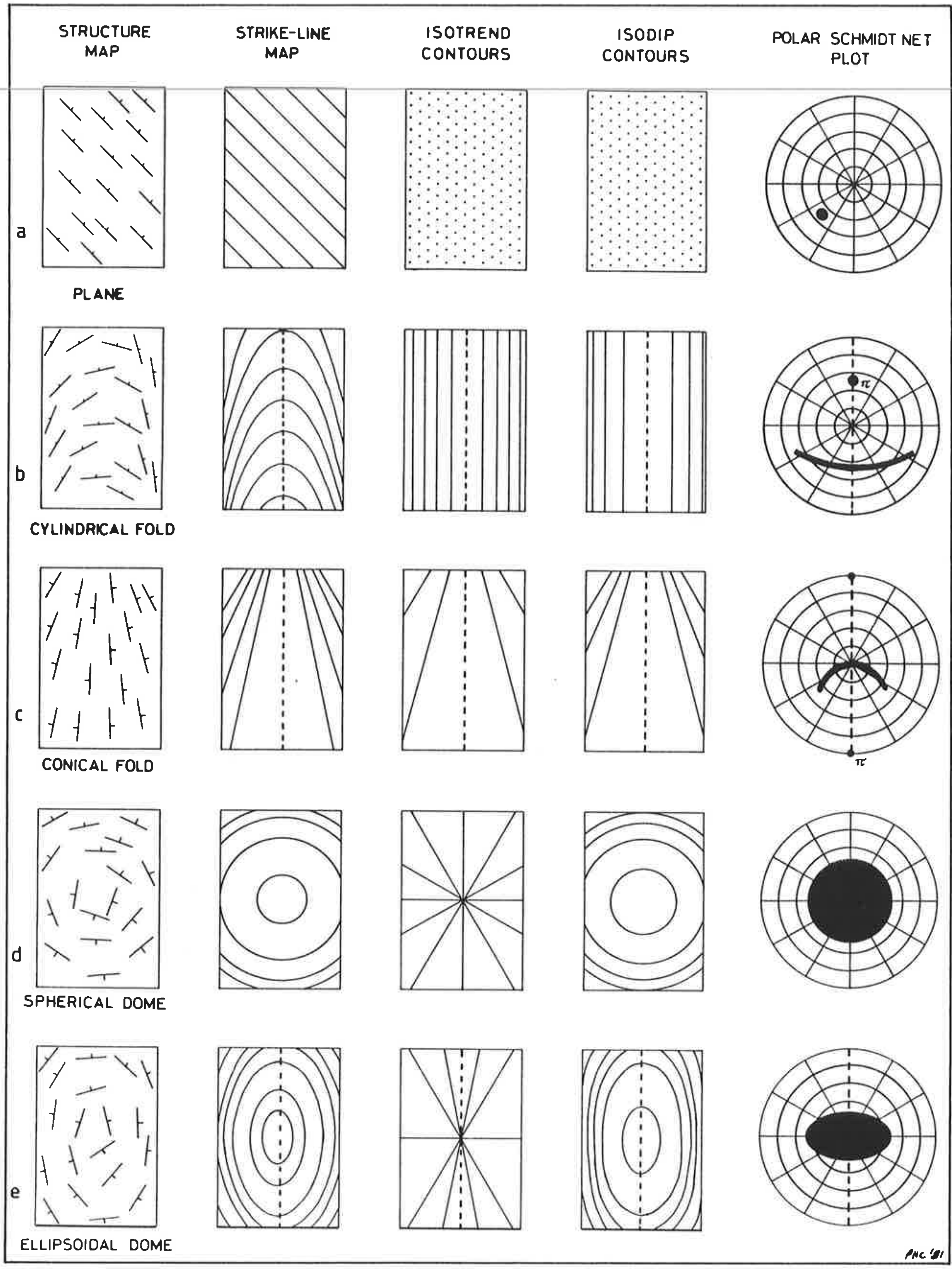

Fig. 2.17 Summary table of sketch maps and pole figures for the five basic structures on which S.O.D.A. analyses are made. Contours are representative only, values would be derived from the pole figures (see text). (Stippled areas represent contour surfaces. Dashed lines represent axial plane traces. Symbols in structure maps are dip and strike of layering.)

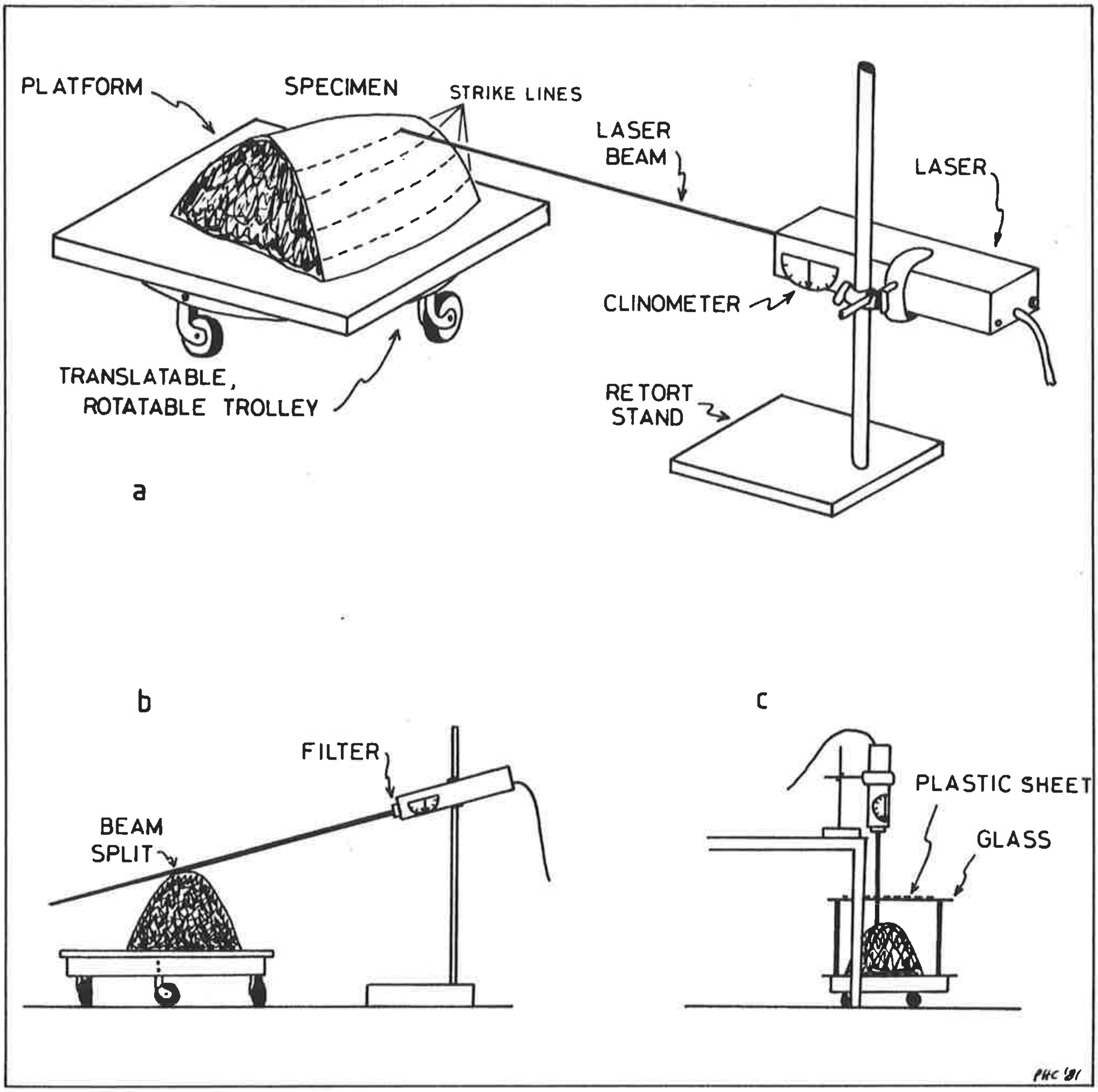

Fig. 2.18 Method of deriving contours from a specimen with a convex surface.
a) Construction of strike-lines (from which isotrends are derived).
b) Construction of isodips.
c) Construction of orthographic map of strike-lines and isodips.

Fig. 2.19 a) Fold of mica schist from Kanmantoo metasediments for §2.7.3 . N and S are fold profiles labelled in Fig. 2.21. Fold hinge is 77cm long.

b) Strike-lines (solid) and isodip contourss (dashed) for (a).

Fig. 2.20 Fold of garnetiferous granitic gneiss for §2.7.4 . Dashed line is fold hinge, which is 27cm long. Note sharp change in fold surface curvature left of the hinge corresponding to that delineated in Fig. 2.22.

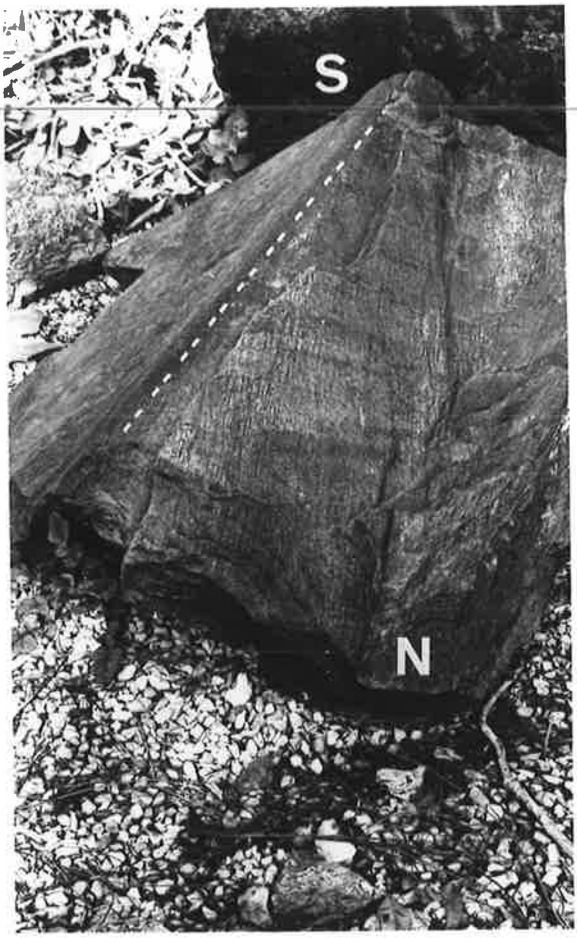
S
N

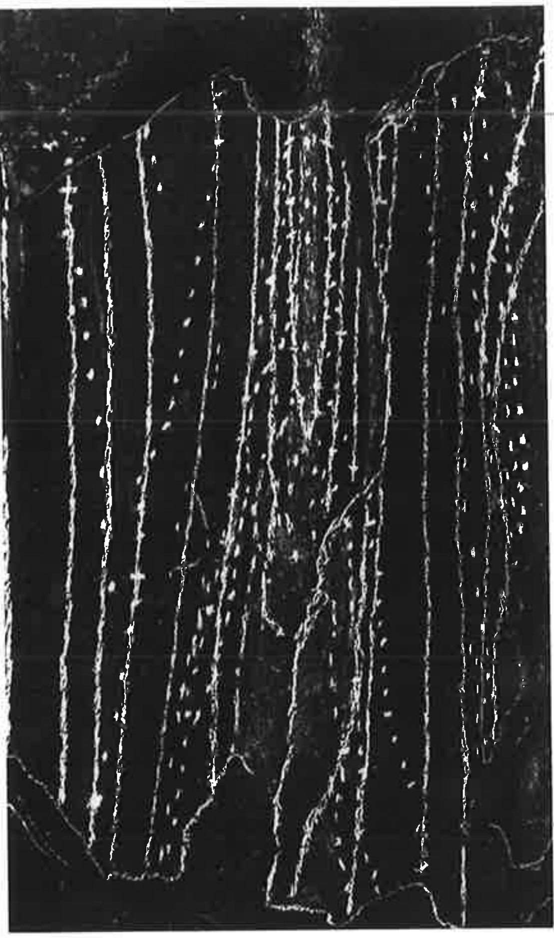

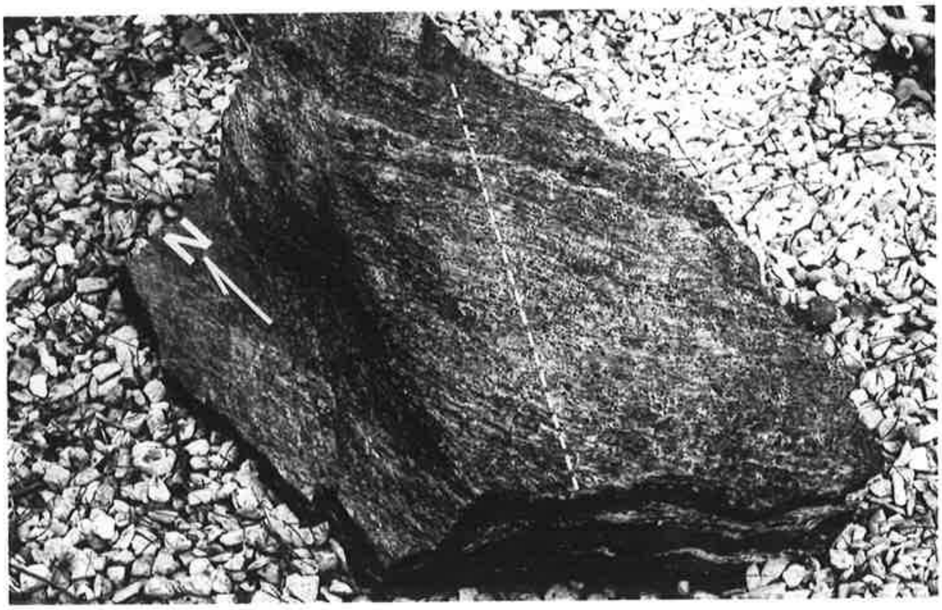
N

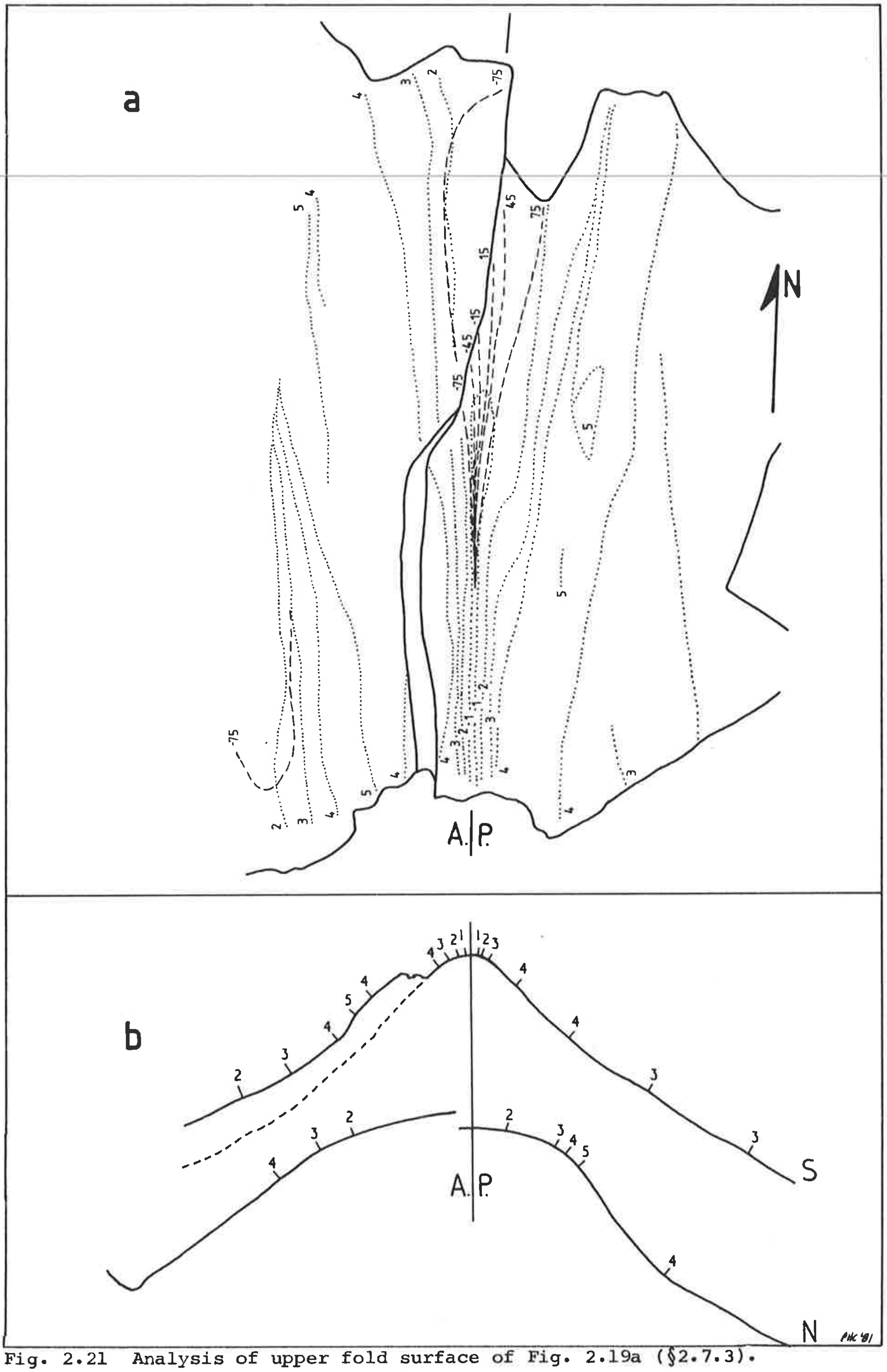

Fig. 2.21 Analysis of upper fold surface of Fig. 2.19a (§2.7.3).

a) Map of isodips (dotted) and isotrends (dashed), producing conical patterns.

b) Profiles of upper surface, northern (N) and southern (S) ends of the fold. Numbers are isodip contour values x10°.

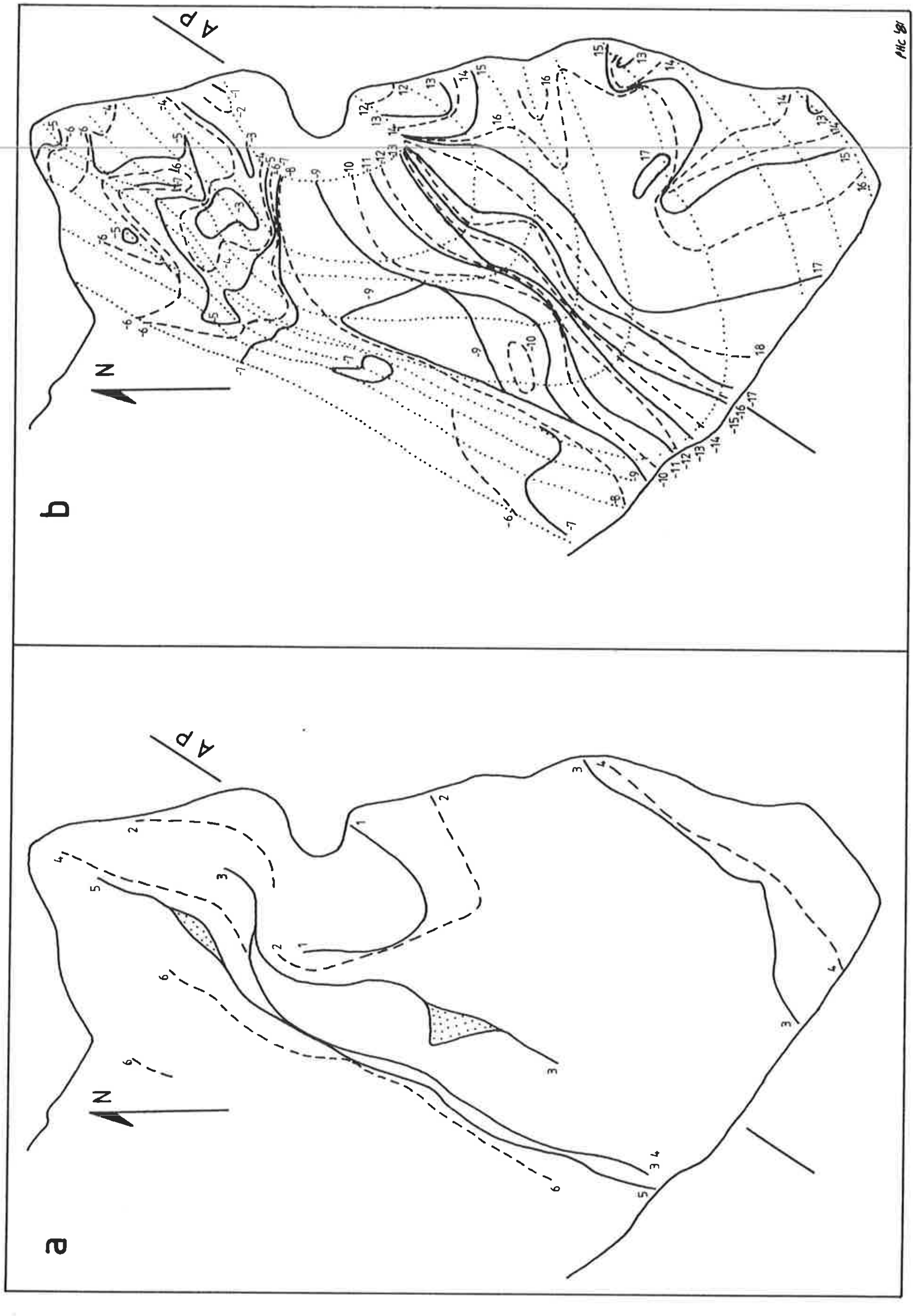

Fig. 2.22 Analysis of upper fold surface of Fig. 2.20 (§2.7.4).
a) Map of isodip contours (solid and dashed lines). Stippled areas are contour surfaces. Numbers are contours values x10°.
b) Map of isotrend contours(solid and dashed) and strike-lines (dotted). Numbers are contour values x10° (positive are clockwise, negative are anticlockwise).

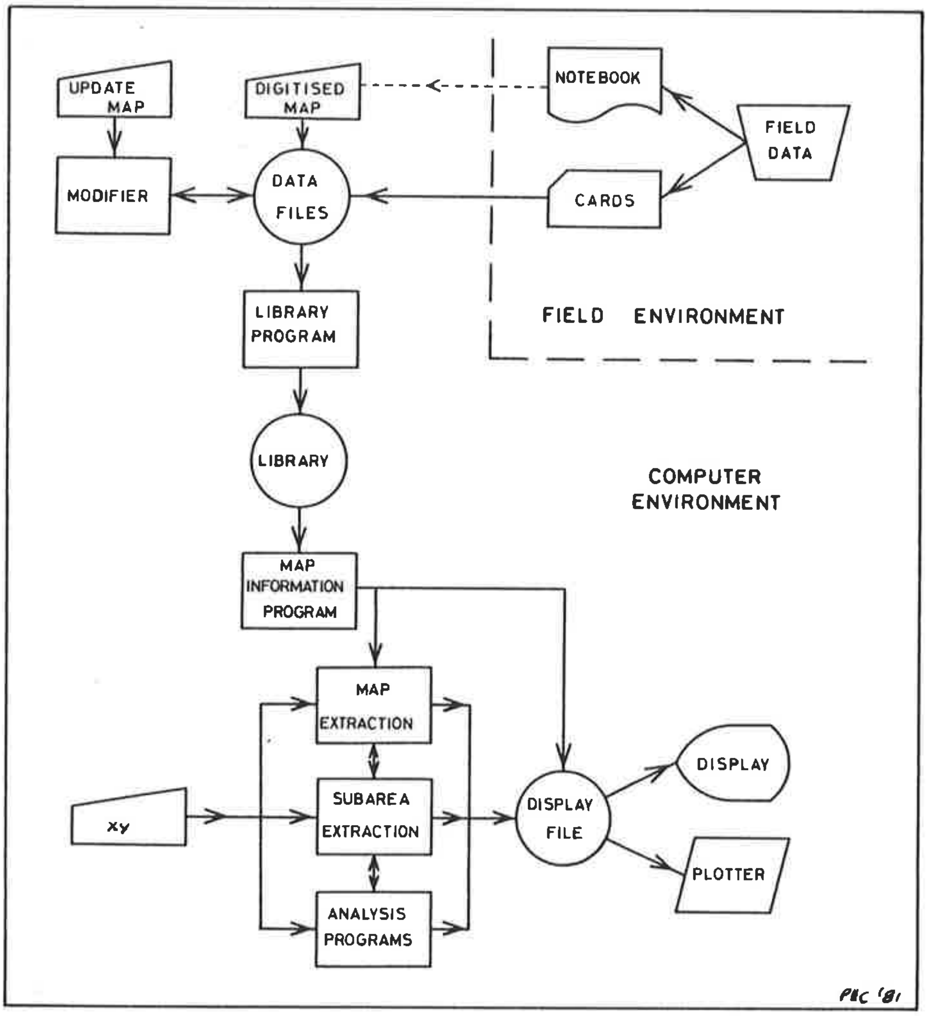

Fig. 3.1 A flow chart for computer analysis of structure data.

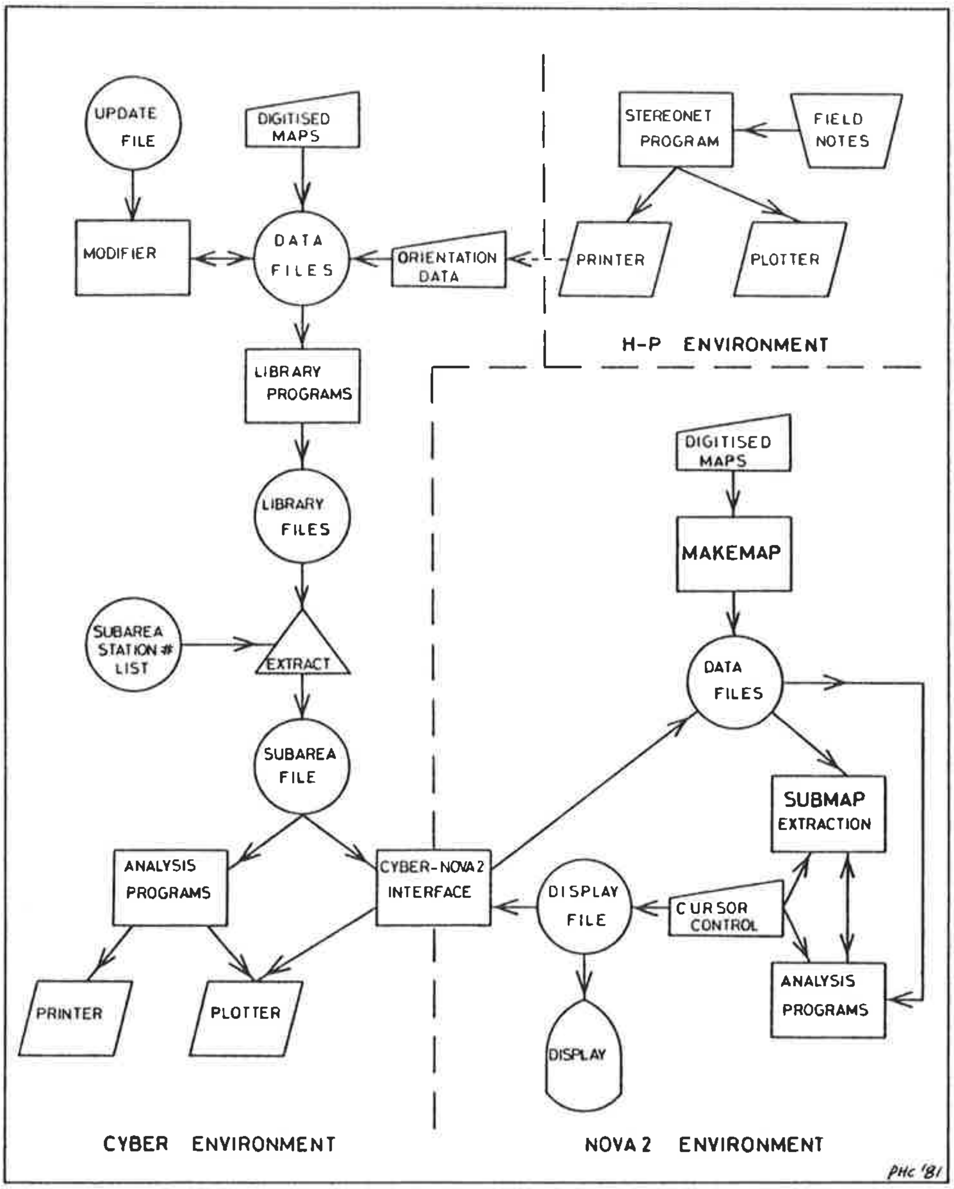

Fig. 3.2 Flow chart of structural data analysis developed for this thesis.

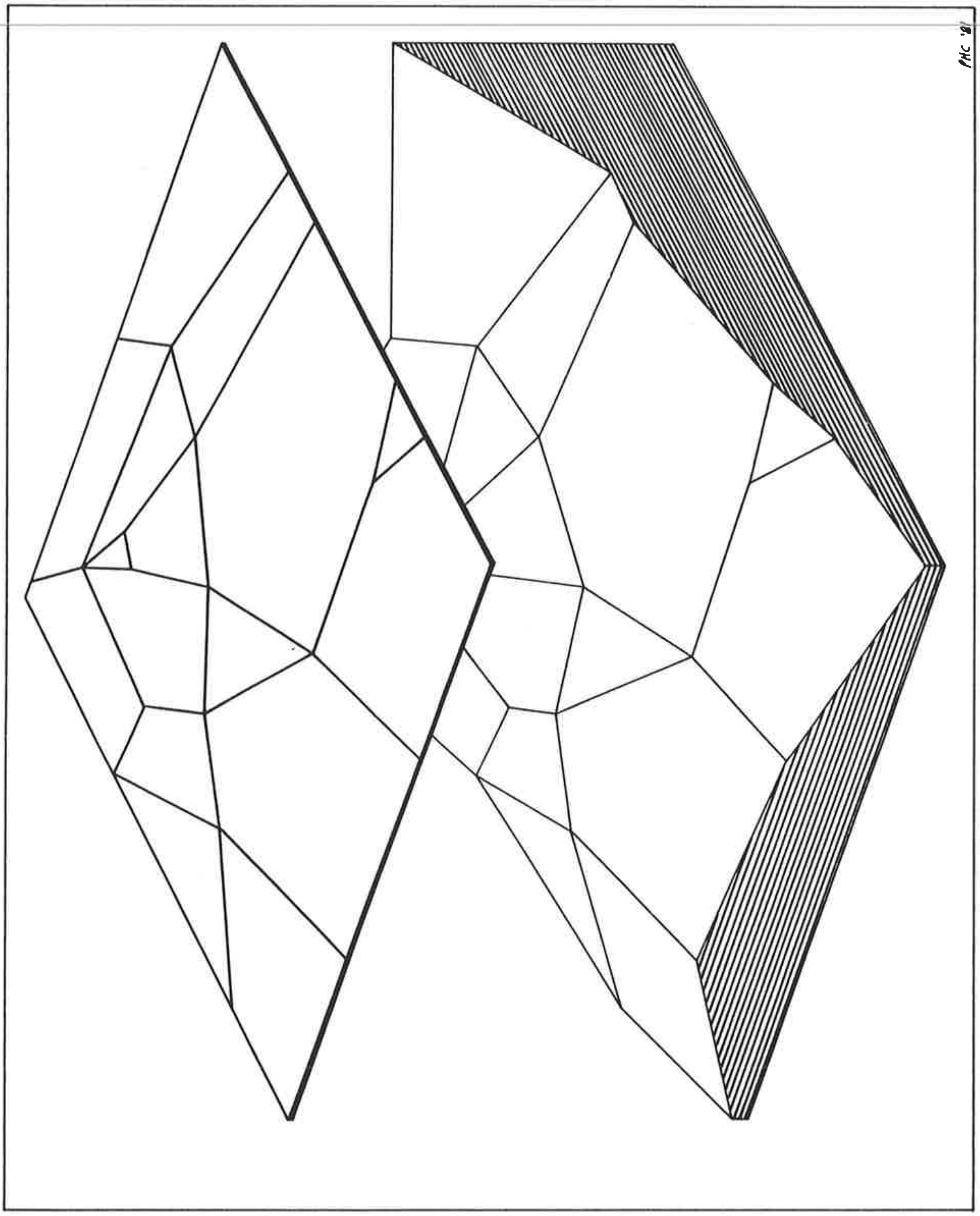

Fig. 3.3 A tessellated map representing a surface approximated by polygons.

Fig. 3.4 The Nova computing facilities.

a) Hardware.

b) Logistics.

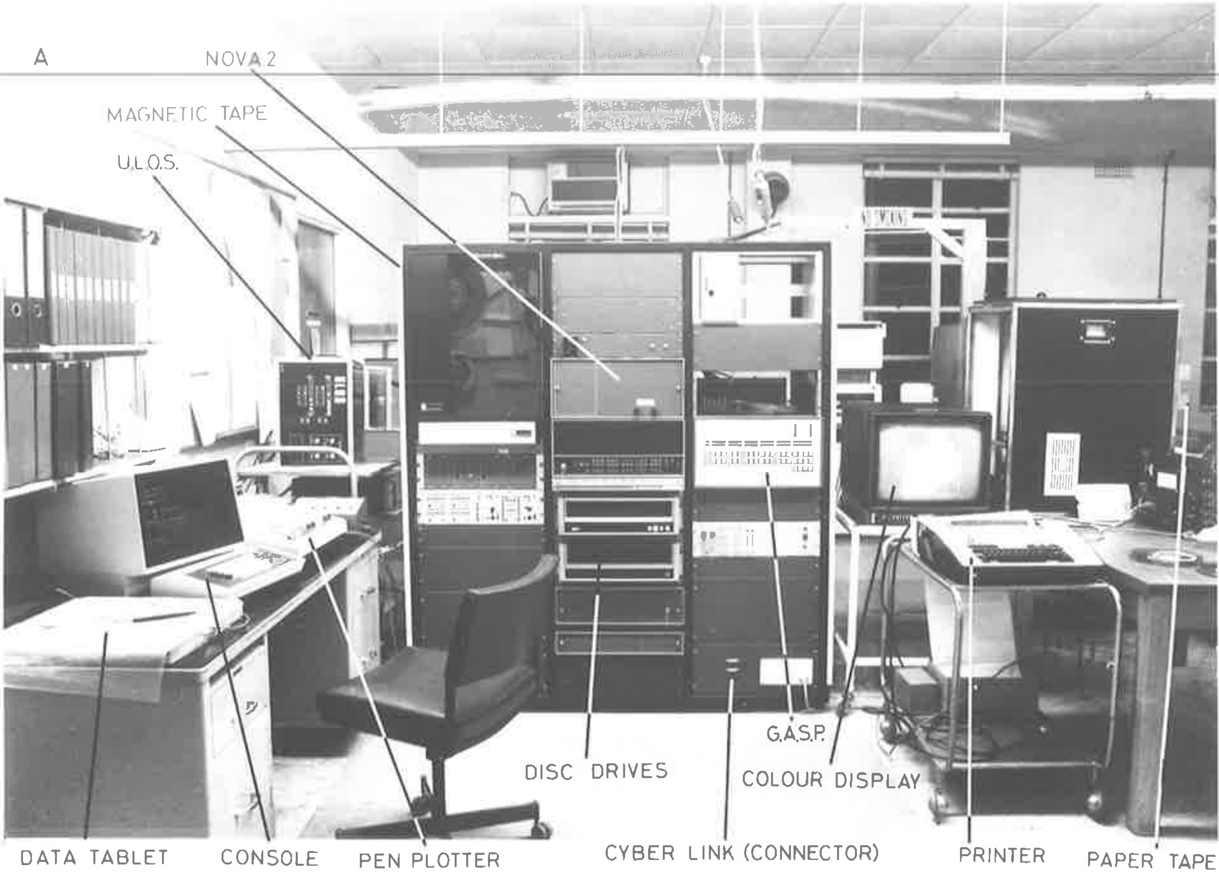
A
NOVA 2
MAGNETIC TAPE
U.L.O.S.
G.A.S.P.
DISC DRIVES
COLOUR DISPLAY
DATA TABLET
CONSOLE
PEN PLOTTER
CYBER LINK (CONNECTOR)
PRINTER
PAPER TAPE

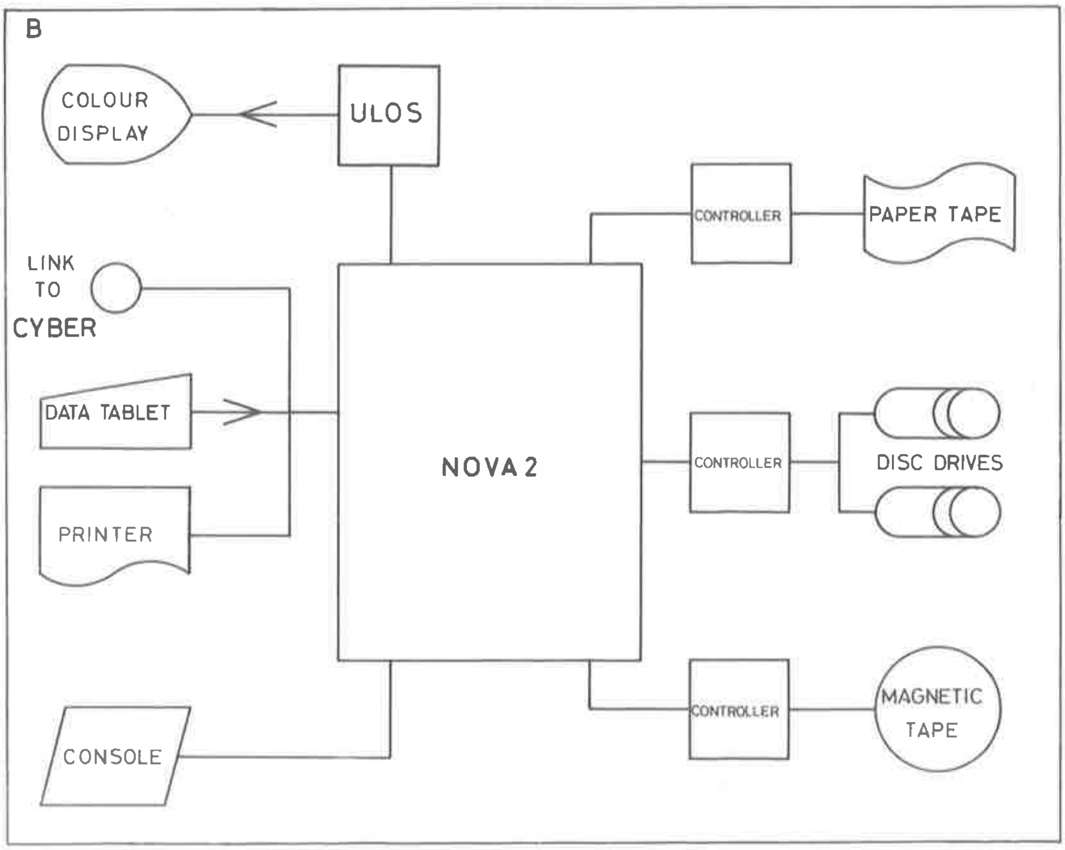
B
COLOUR DISPLAY
ULOS
CONTROLLER
PAPER TAPE
LINK TO CYBER
DATA TABLET
NOVA 2
CONTROLLER
DISC DRIVES
PRINTER
CONSOLE
CONTROLLER
MAGNETIC TAPE

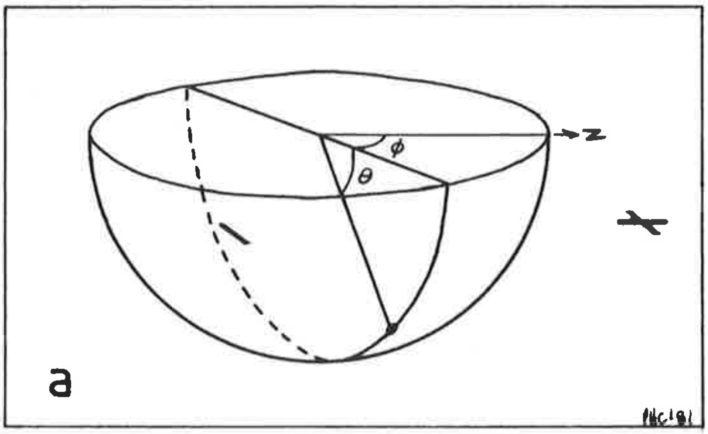

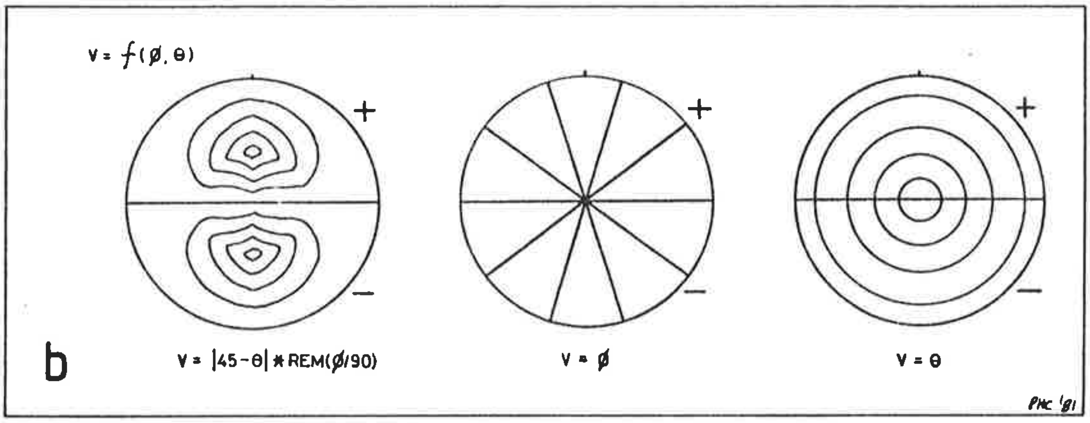

Fig. 3.5 An application of the S.O.D.A. technique on the Cyber.

a) Definition of ø and θ for trend and plunge respectively.

b) Various functions to divide orientations into regions for contouring.

Fig. 4.1 Models of cylindrical "similar" type folds. Fold profiles after Hudleston (1973a, figure 12).
Results of (a),(b),(c) processed by S.O.D.A. are displayed in colour plate, Fig. CP.3.
Results of (d),(e),(f),(g) are displayed in colour plates, Figs. CP.4 and CP.5.

a) Upright horizontal rounded fold, using profile "3B".

b) " " fold, using profile "3D".

c) " " angular (chevron) fold, using profile "3F".

d) " " fold, using profile "1D".

e) Model (d) rotated 10° around the normal to the axial plane.

f) " (d) " 65° " " " " " " " .

g) " (d) " 90° (vertical).

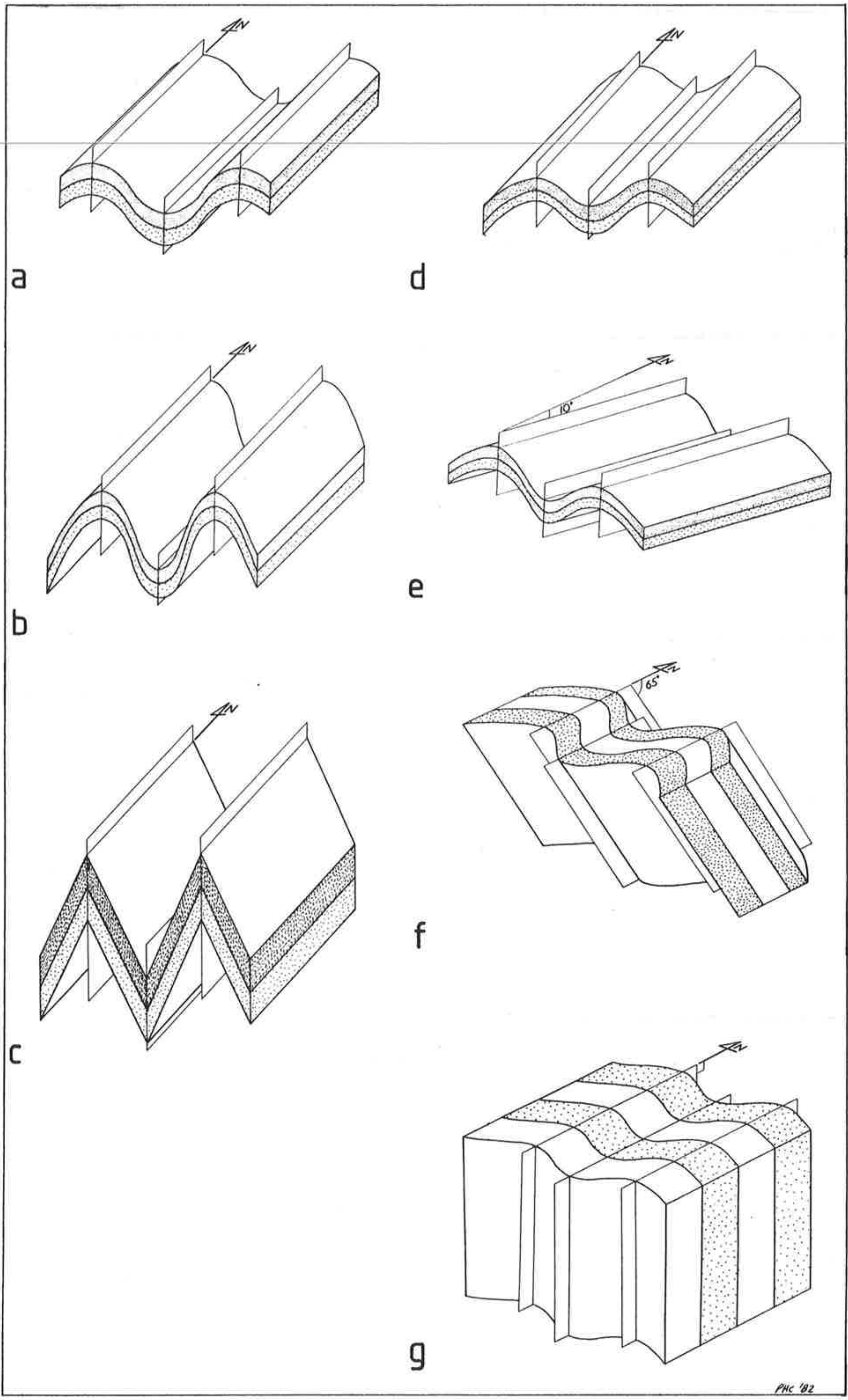
N
a
b
c
d
10°
e
65°
f
g
PHC '82

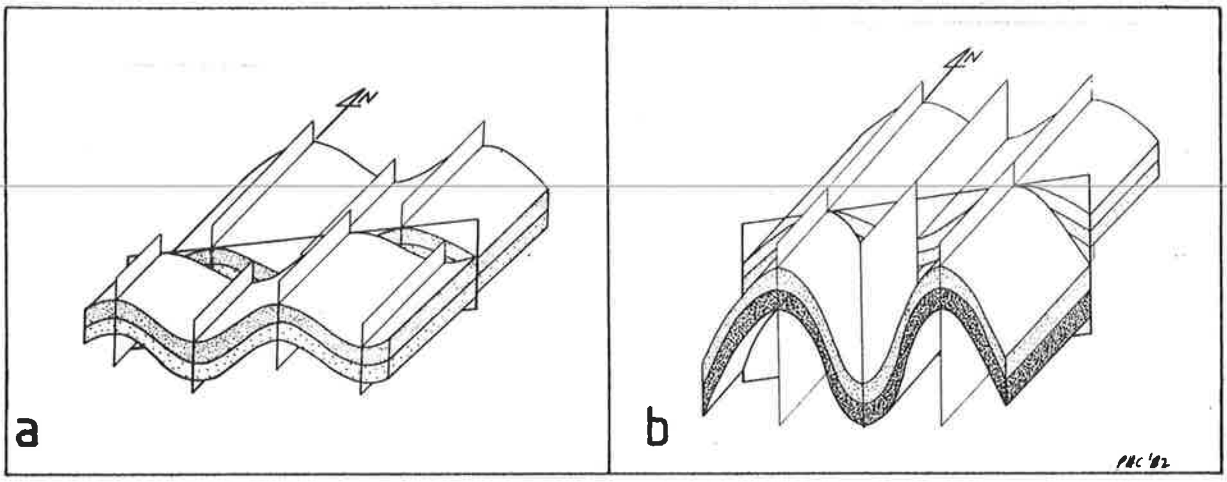

Fig. 4.2 Models of faults.
a) A dextral strike-slip fault, of a quarter wavelength, induced in a previous model (Fig. 4.1d).
b) A vertical fault juxtaposing two different fold models; such that the fold hinge lines appear to pass through the fault unaffected. (Northern portion after Fig. 4.1d, southern portion after Fig. 4.1b).

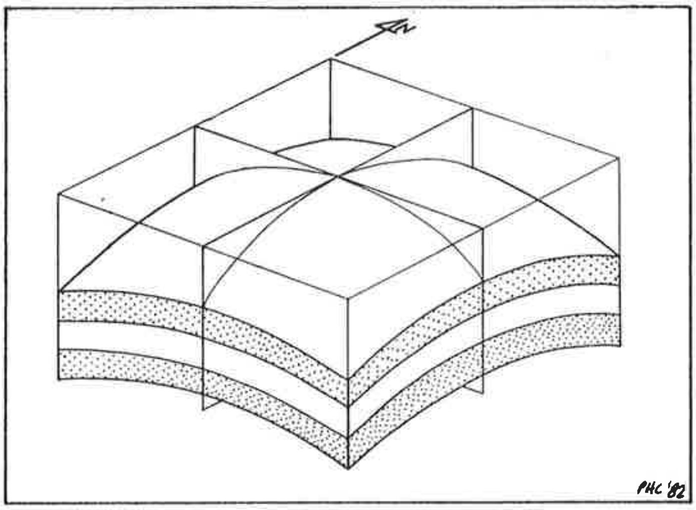

Fig. 4.3 Model of a shallow dome of "similar" style.

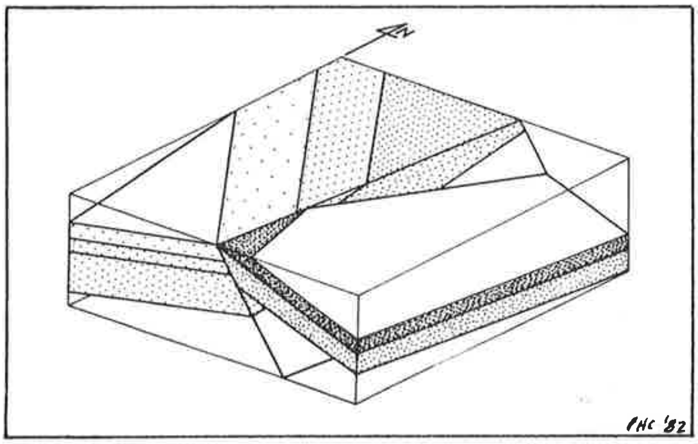

Fig. 4.4 Model of a scissor fault, or alternatively, an angular unconformity. Although shown with perfectly planar strata, the surfaces are undulatory for the purposes of this model.

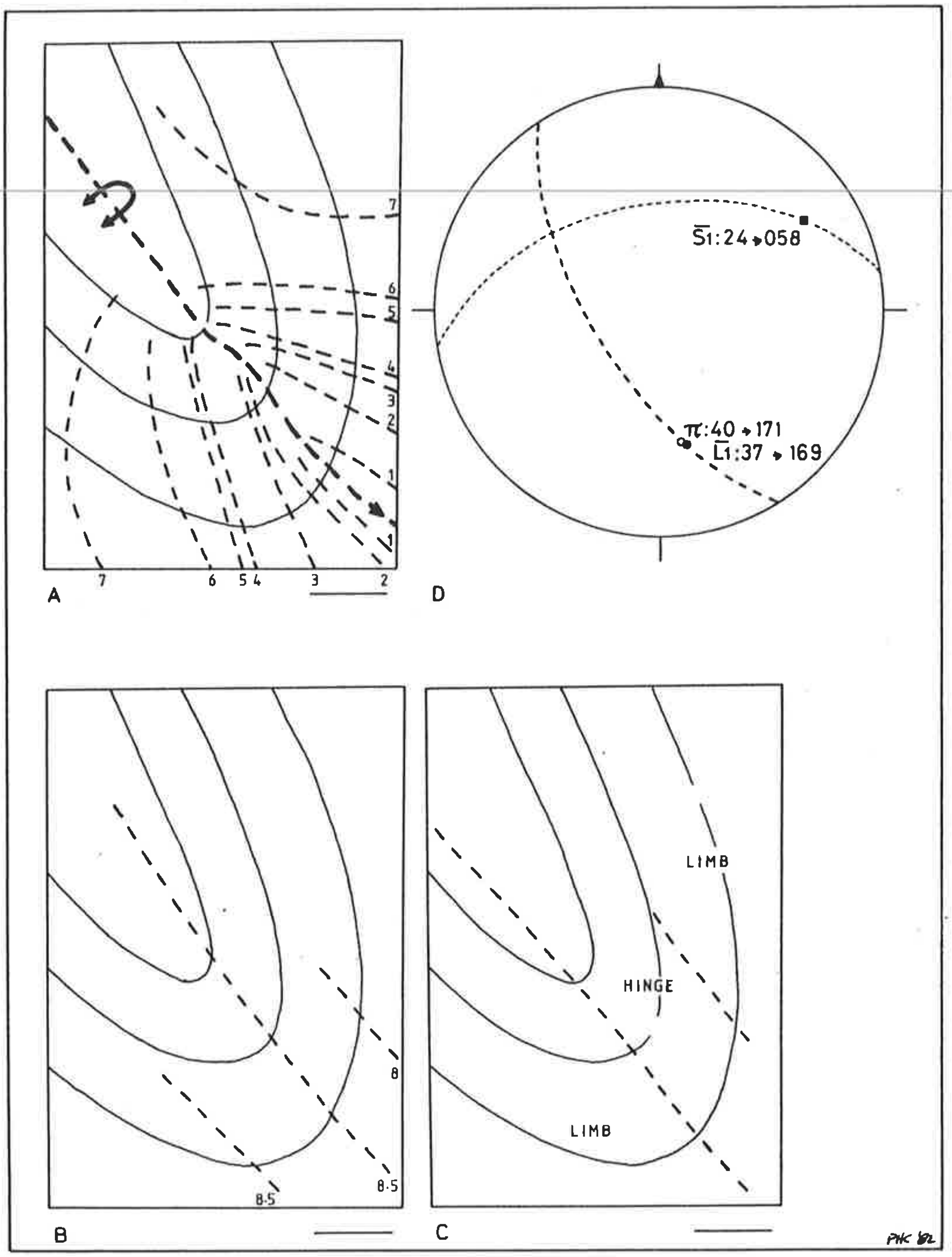

Fig. 5.1 Analysis of Llangedwyn-Dyffryn-Clwyd S.O.D.A. plots (Fig. CP.9). For (a,b,c) dashed lines are contours from the S.O.D.A. plots, and solid lines are lithologic boundaries. Scale bar is 1 km. Contour values are x10°.

a) Light contours are isodips of S_0, from Fig. CP.9a (reference plane is the axial plane, 238°/66°), and heavy contour is isotrend of S_0, from Fig. CP.9c (reference plane is plane R in Fig. 5.2e).

b) Isodip contours of L_1, from Fig. CP.9g.

c) Isotrend contours of S_1, from Fig. CP.9e.

d) Synoptic stereoplot of data, from Fig. CP.9i.

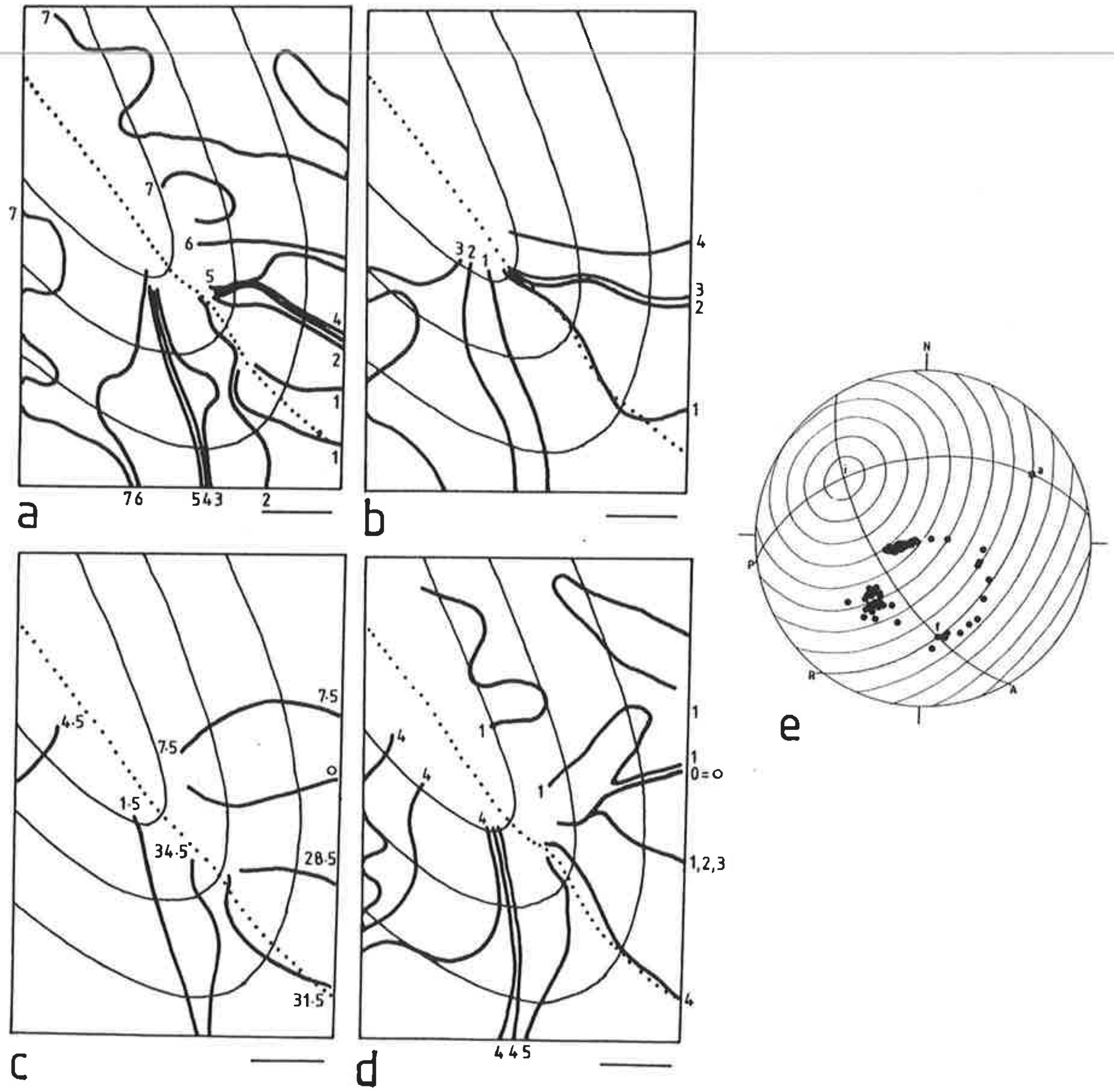

Fig. 5.2

a) S.O.D.A. plot of bedding poles on isodip chart (e).

b) S.O.D.A. plot of bedding dip vectors on isodip chart (e).

c) S.O.D.A. plot of bedding poles on isotrend chart (Fig. CP.2d).

d) S.O.D.A. plot of bedding poles on isodip chart similar to Fig. CP.2f, but with RES=10°.

e) Dip-vector figure of bedding data and superimposed Colour chart: 4 10 ; 035 -50 90 0. A: average axial plane foliation, P: profile plane, R: reference plane 125°/50°, a: pole to A, f: fold axis = pole to profile plane, i: intersection of axial plane foliation in profile plane.

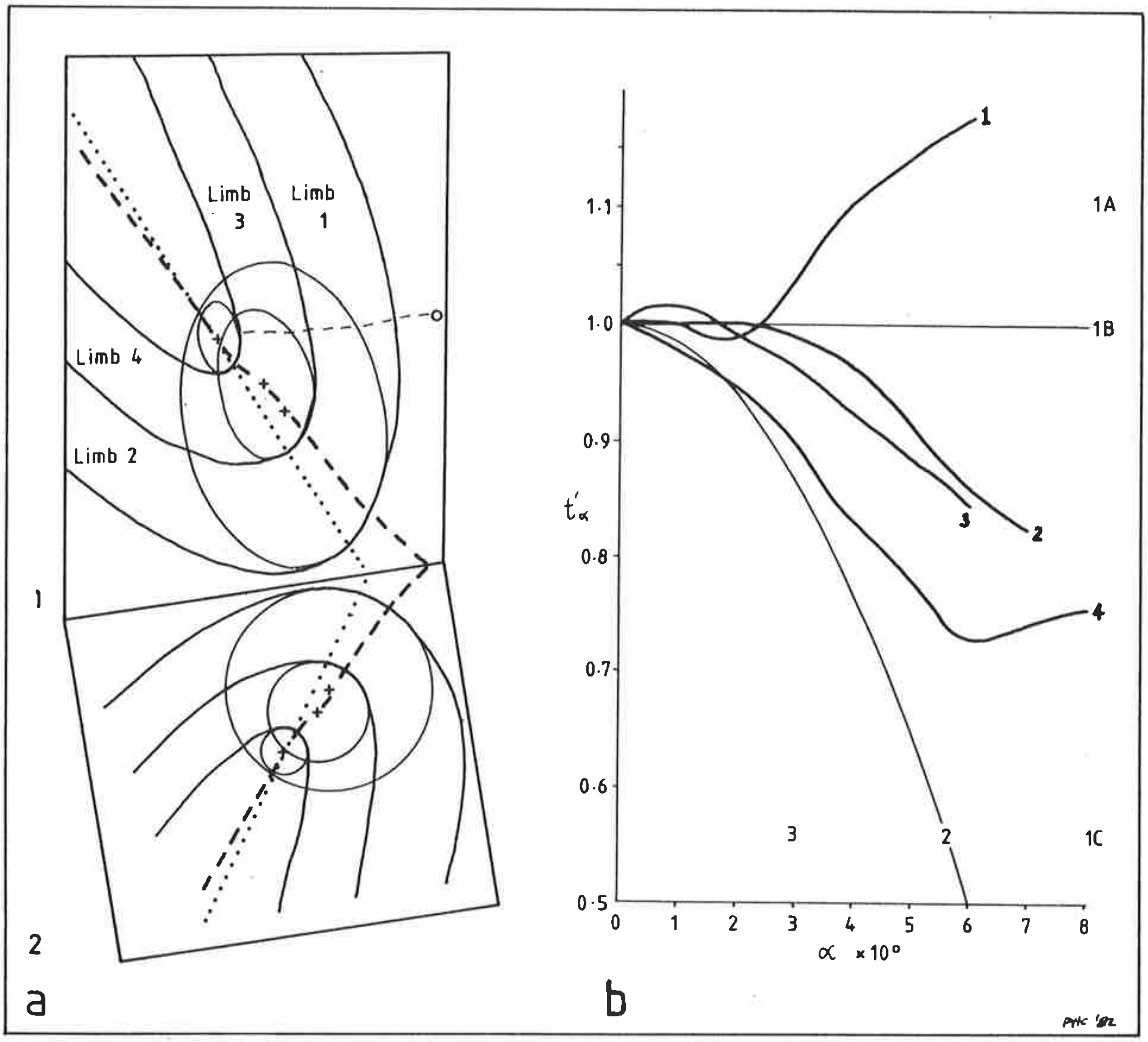

Fig. 5.3

a) Profile plane (2) of outcrop pattern (1) (see Stockwell, 1950, for example of method). Determination of axial plane surface trace by the elliptical-arc method (Stauffer, 1973). Heavy dashed line is axial plane surface determined from S.O.D.A. plot Fig. 5.1a, crosses are centre of ellipses, dotted line is axial plane foliation trace, light dashed line (labeled with "o") is the trace where bedding overturns.

b) t'_α vs α plot of dip isogons for the four limbs (Limbs 1 to 4) in (a).

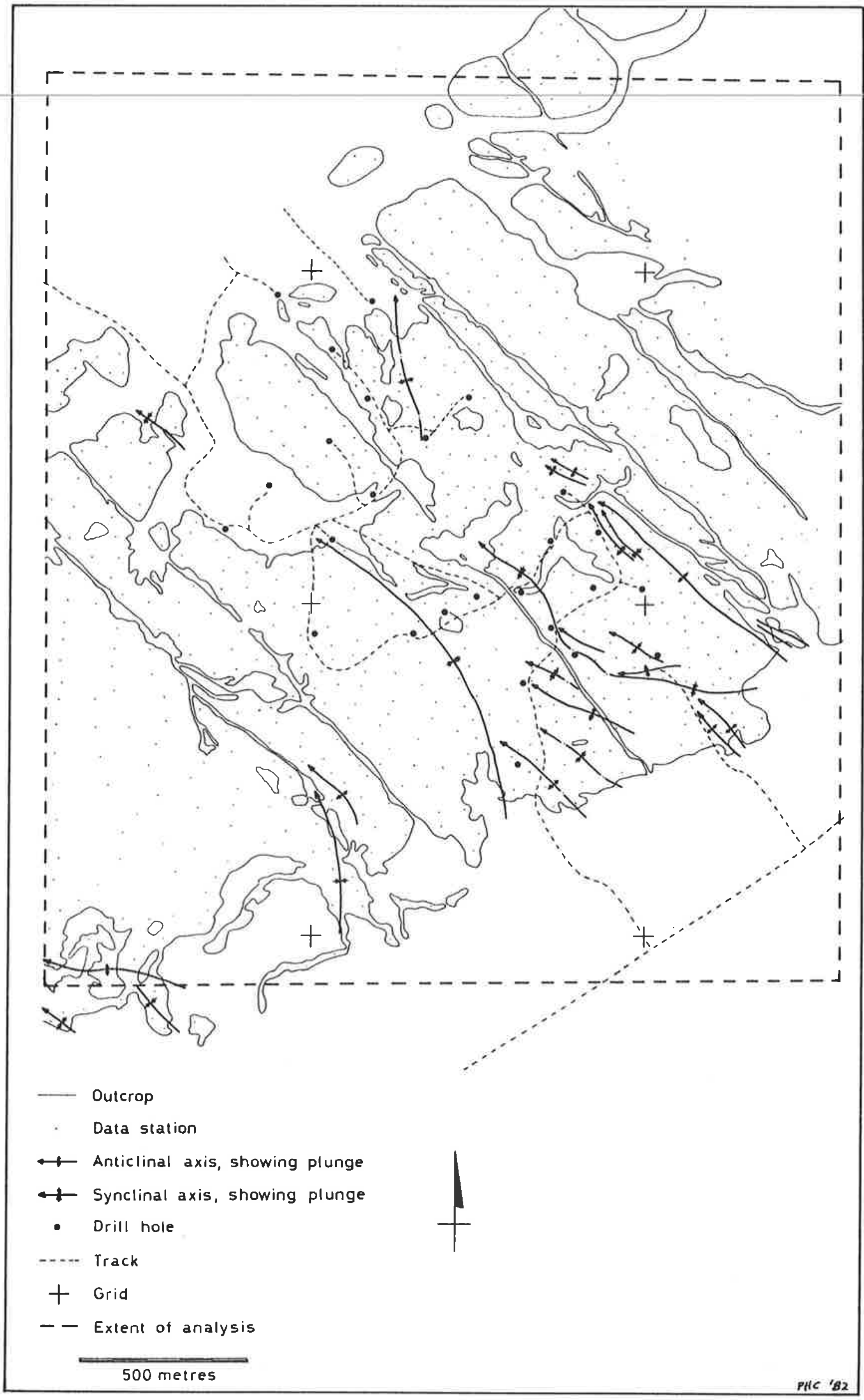

Fig. 5.4 Basic structural map of an area in Brockman Three. (After a geological map by Hamersley Ex. Pty. Ltd.)

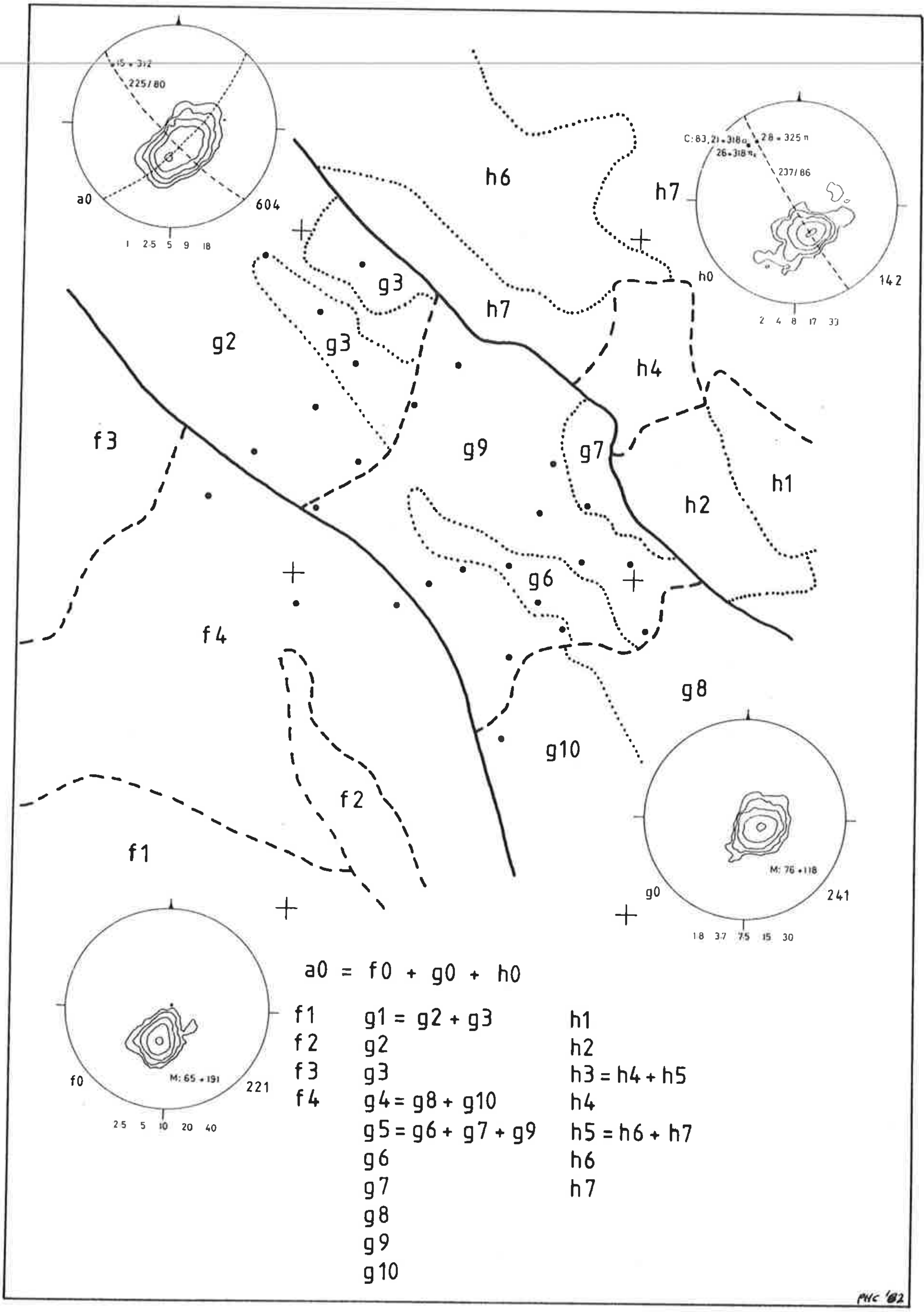

Fig. 5.5 Domain map of Fig. 5.4, derived from the application of the S.O.D.A. technique.

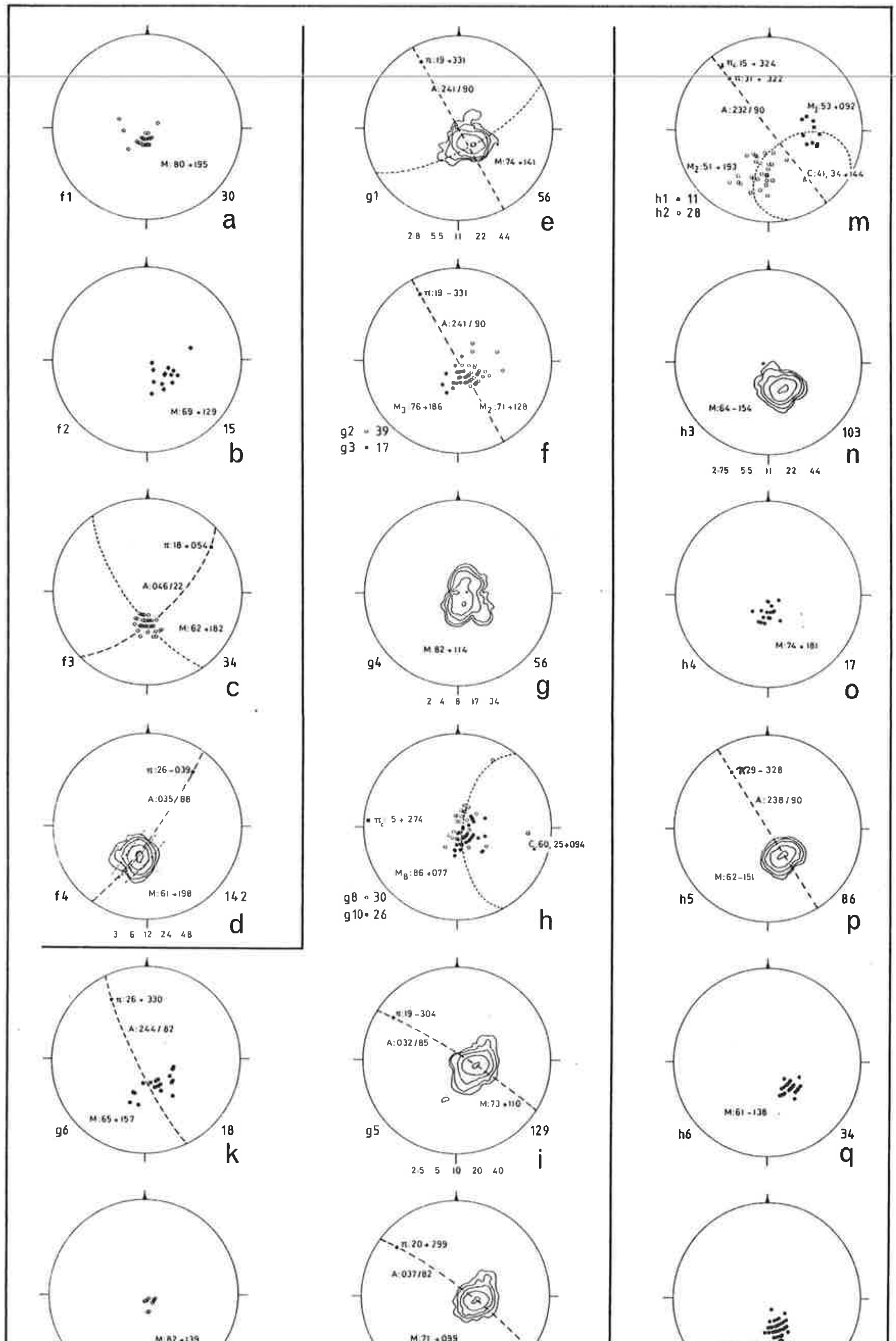

Fig. 5.6 Data stereoplots of domains in Fig. 5.5.

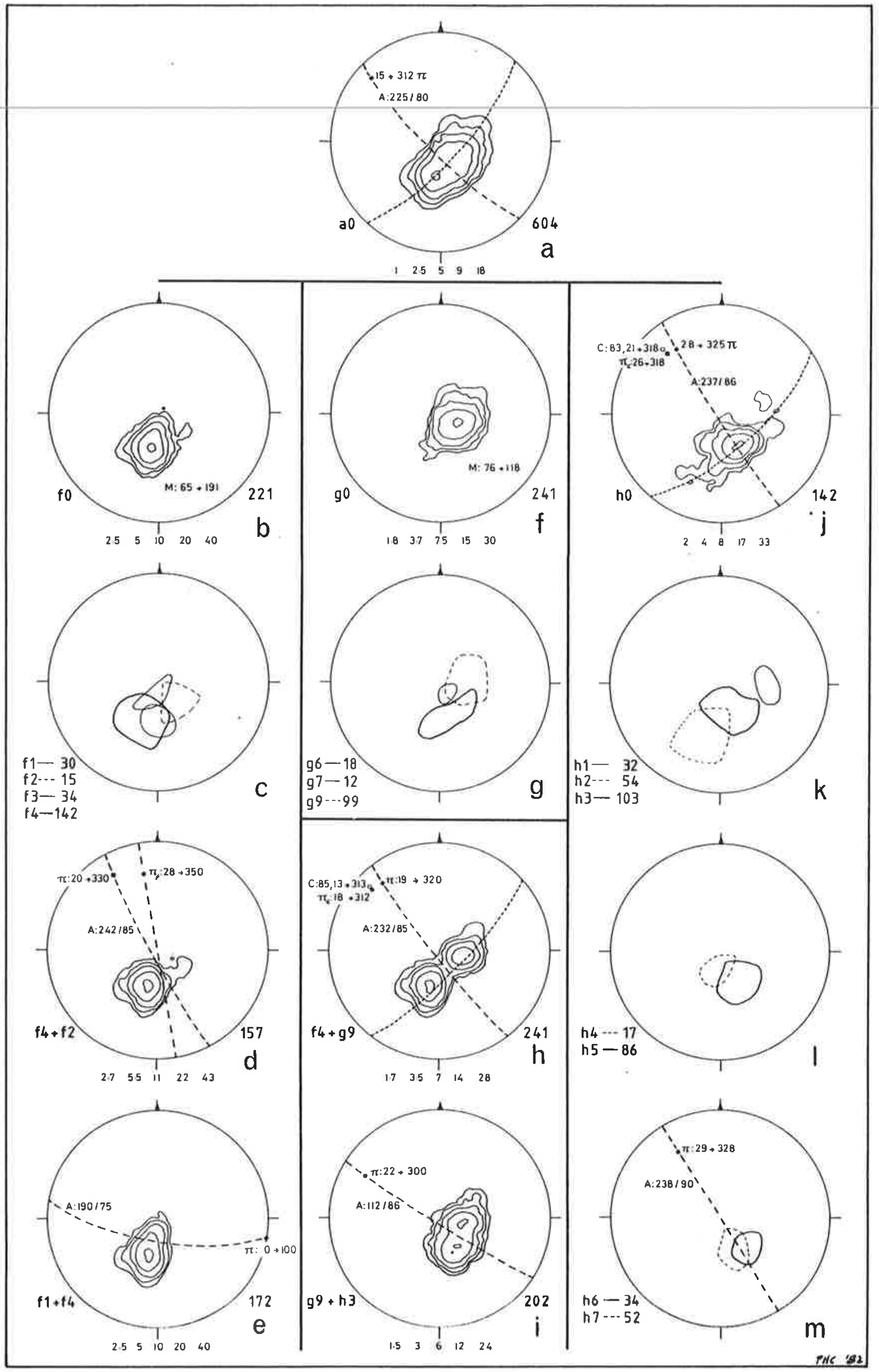

Fig. 5.7 Synoptic stereoplots of domains in Fig. 5.5.

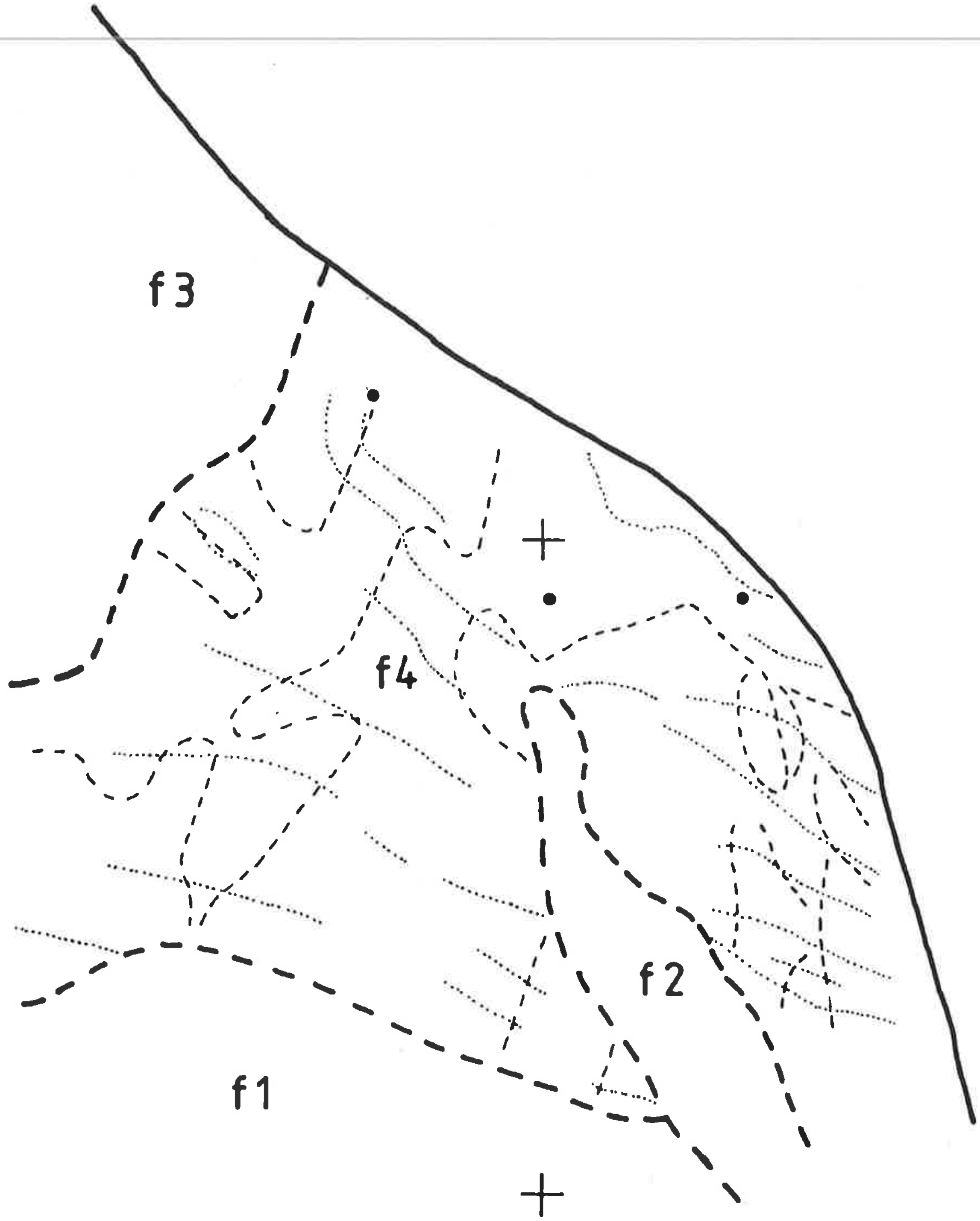

Fig. 5.8 Isotrend contours delineating minor NE-SW and E-W trends (see Fig. 5.6d) for domain f4.

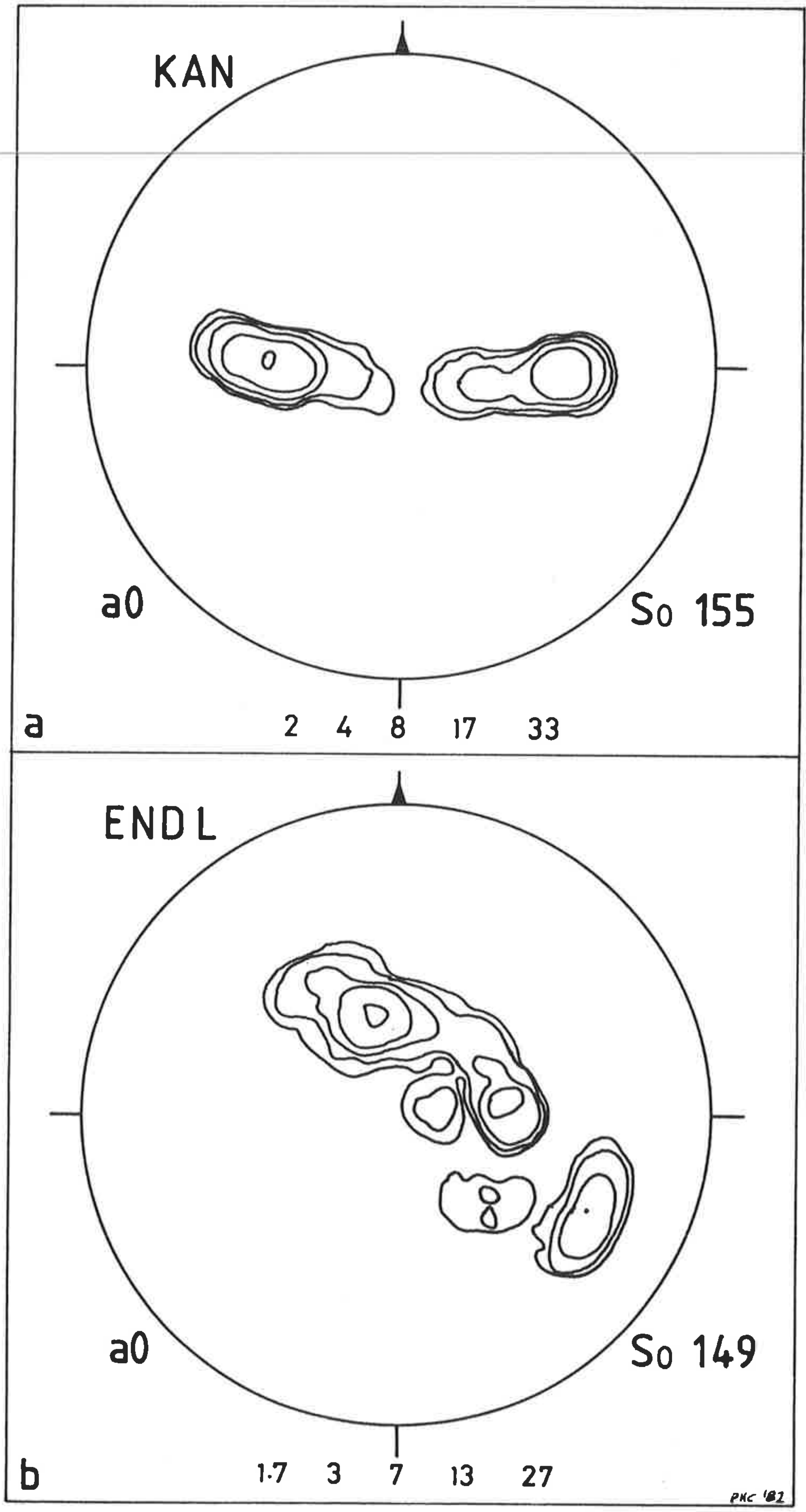

Fig. 5.9 Pi figures of mesoscale examples of (a) §2.7.3 and (b) §2.7.4.

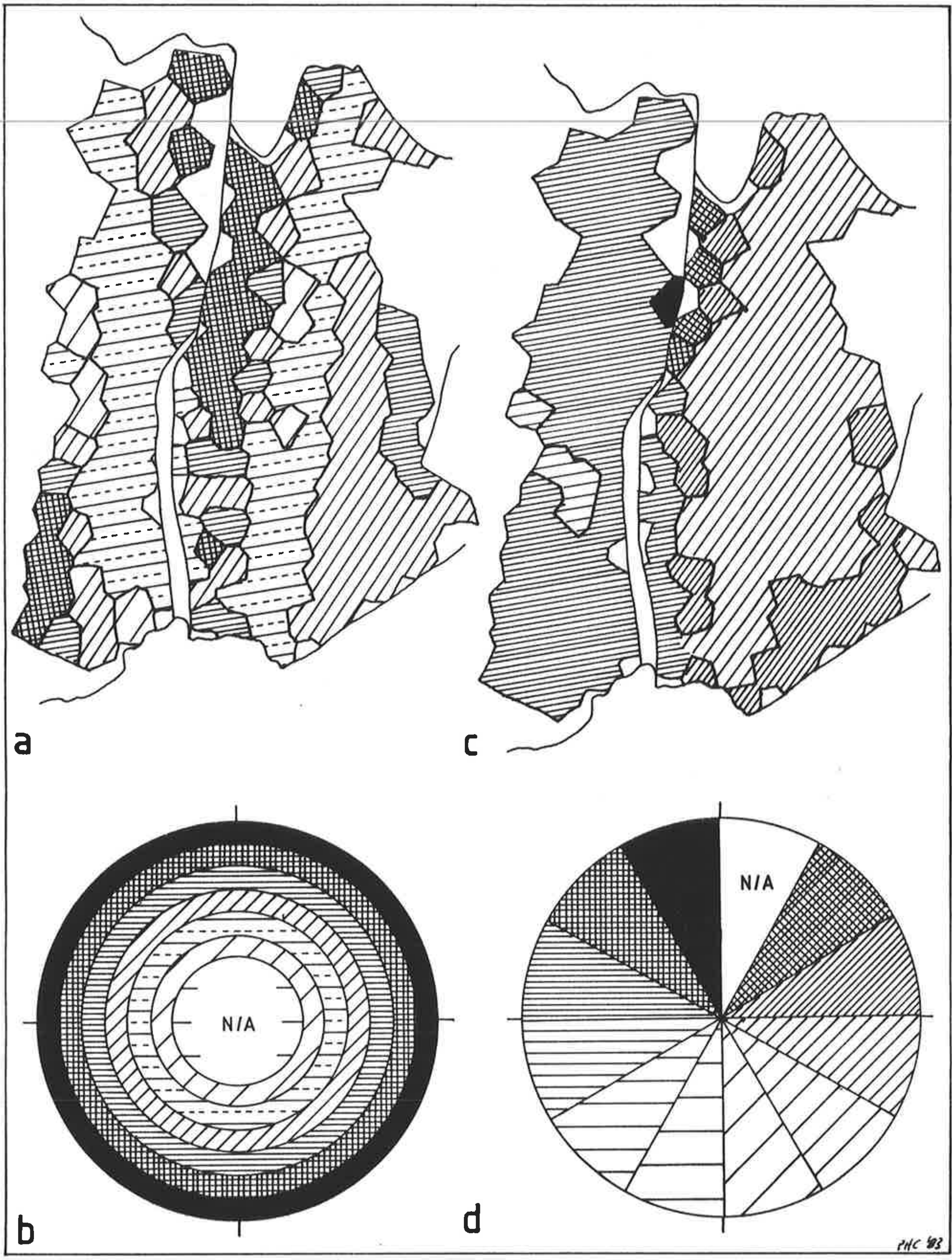

Fig. 5.10 S.O.D.A. plots of mesoscale specimen from §2.7.3 ("KAN"). (a) Isodip S.O.D.A. plot using isodip chart (b) 4 10 ; 0 90 0 00 7 (only dips less than 70° are used and presented, i.e. N/A = not applicable). (c) Isotrend S.O.D.A. plot using isotrend chart (d) 2 30 (15) ; 0 90 0 00 7.

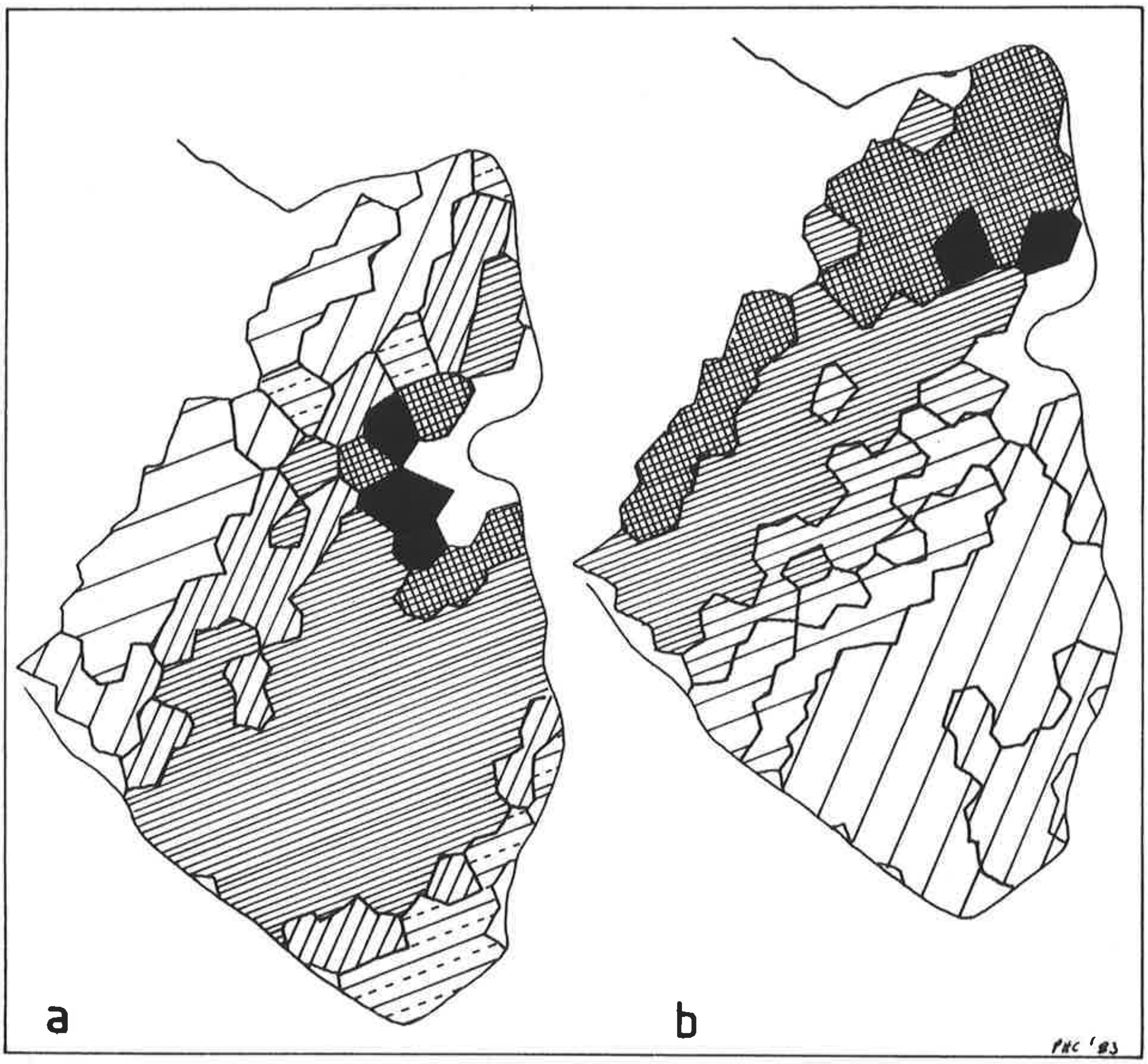

Fig. 5.11 S.O.D.A. plots of mesoscale specimen from §2.7.4 ("ENDL"). (a) Isodip S.O.D.A. plot using isodip chart of Fig. 5.10b. (b) Isotrend S.O.D.A. plot using isotrend chart of Fig. 5.10d.

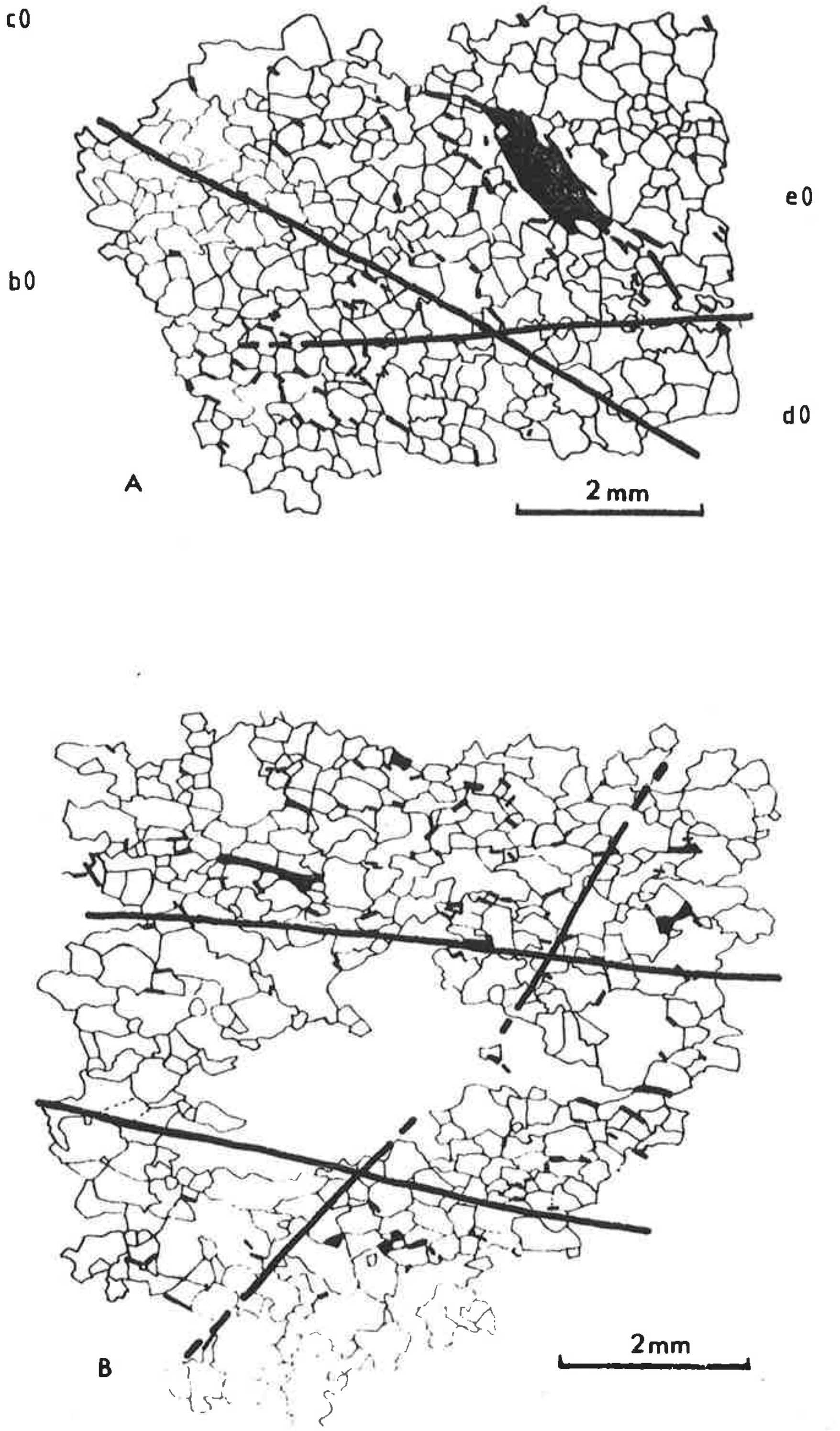

Fig. 5.12 Visible boundaries within S.O.D.A. plots. (a) and (b) correspond to colour plates, Figs. CP.12a,c.

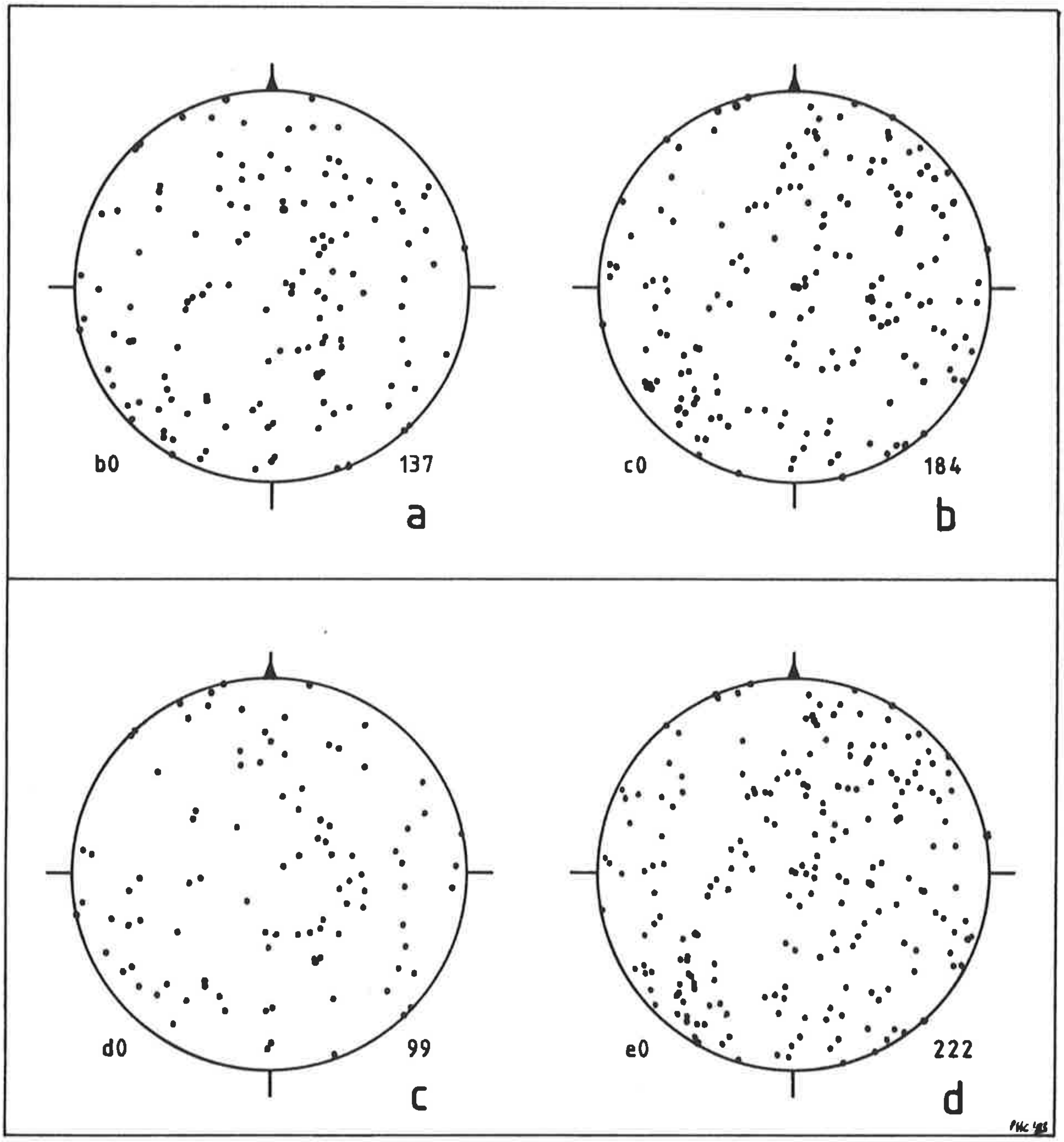

Fig. 5.13 Stereoplot of quartz axes for domains determined in Fig. 5.12a.

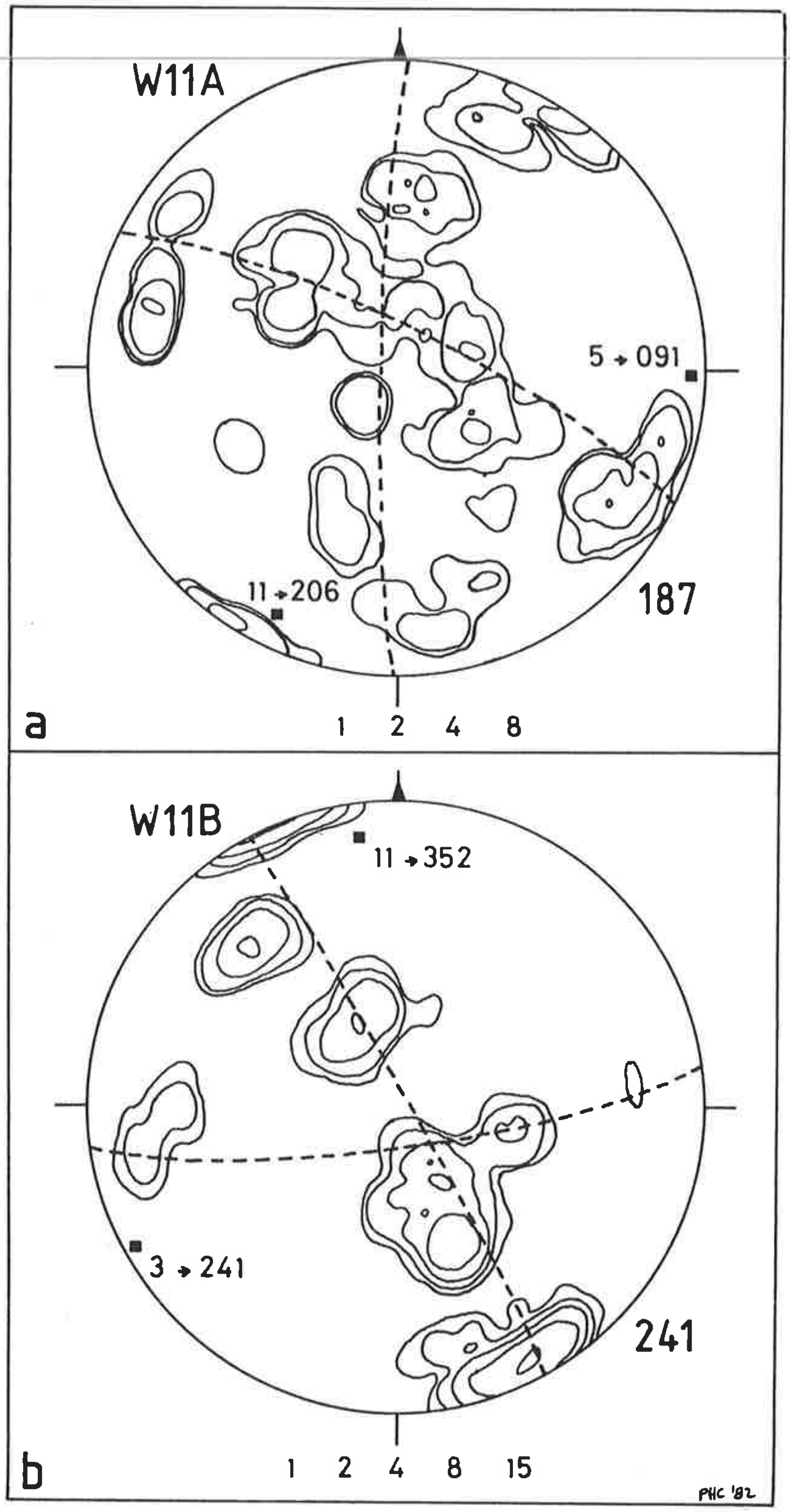

Fig. 5.14 Stereoplots of non-random quartz fabrics. (a,b) after Wilson (1973) figures 11A,B, respectively. W11A and W11B are key names (see Appendix R).

Fig. 5.15 Sketch of thin section slide HB1, showing domains. (Specimen located at Fig. 7.24b.)

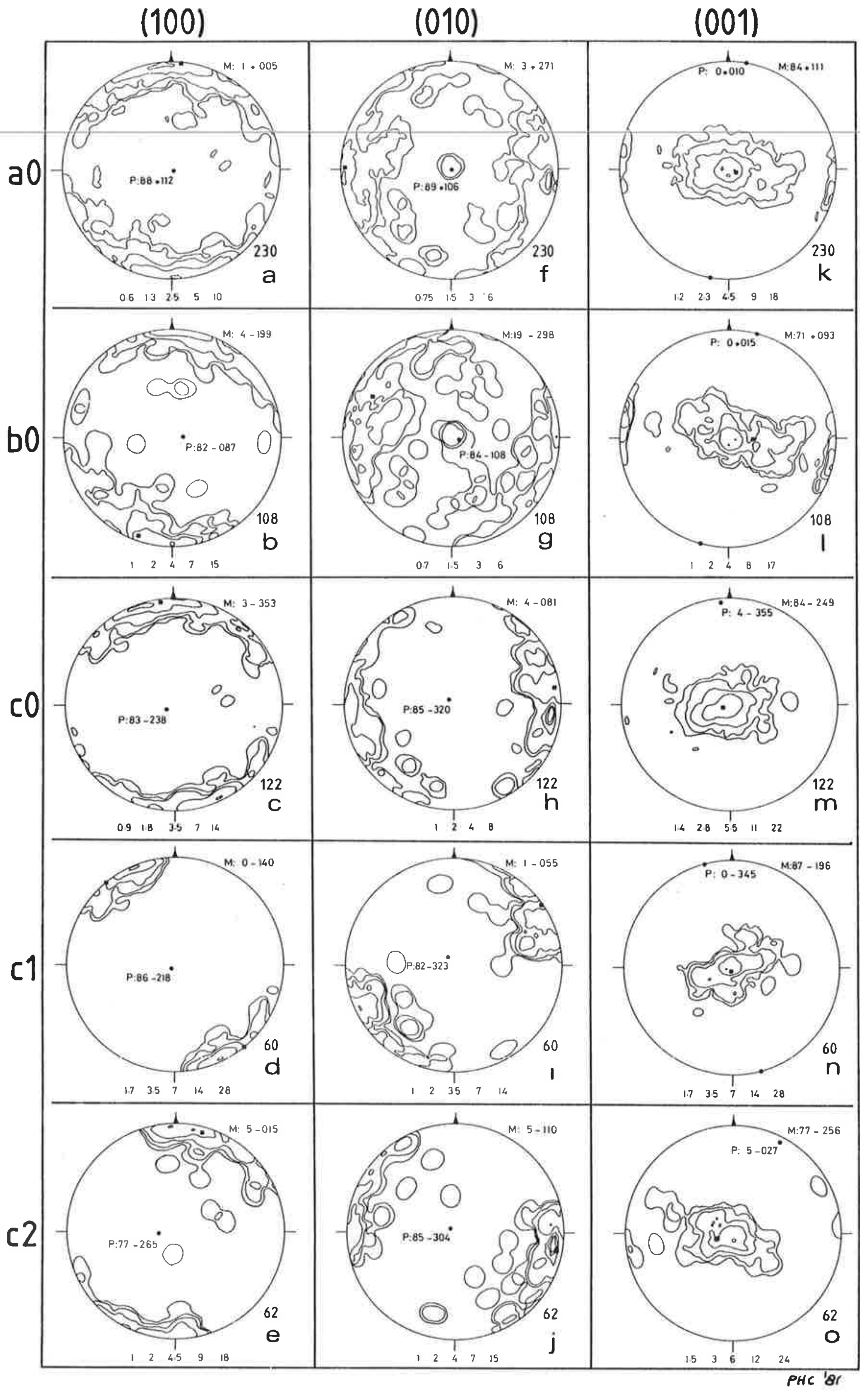

Fig. 5.16 Stereoplots of domains for thin section HB1, using hornblende crystallographic axes (section not orientated) (see Fig. CP.14).

Fig. 5.17 Sketch of thin section slide HB2, with stereoplots of the hornblende crystallographic axes (section not orientated) (see Fig. CP.15). (Specimen located at Fig. 7.24b.)

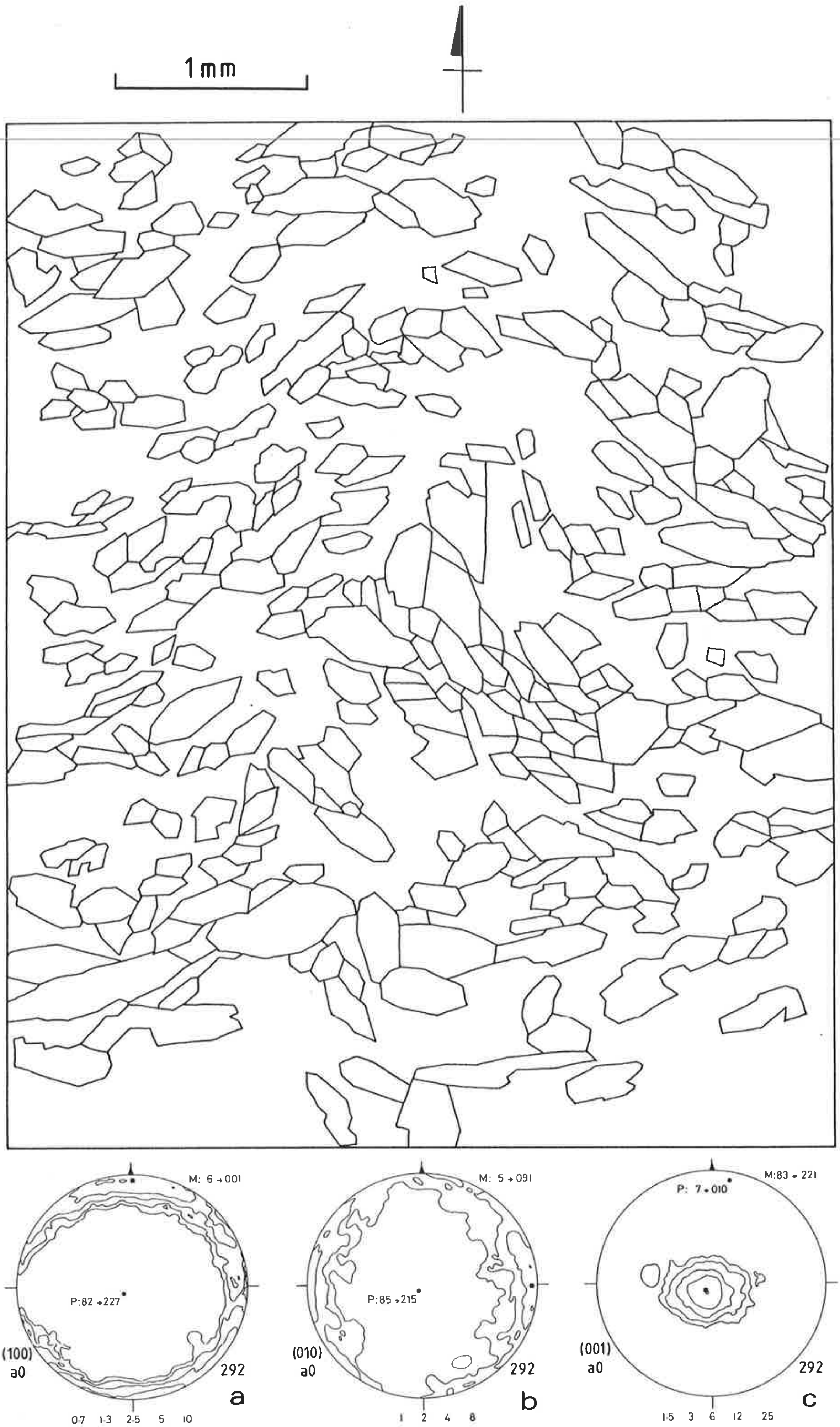

1mm
M: 6 → 001
P:82 → 227
(100)
a0
292
a
0·7 1·3 2·5 5 10
M: 5 → 091
P:85 → 215
(010)
a0
292
b
1 2 4 8
M:83 → 221
P: 7 → 010
(001)
a0
292
c
1·5 3 6 12 25

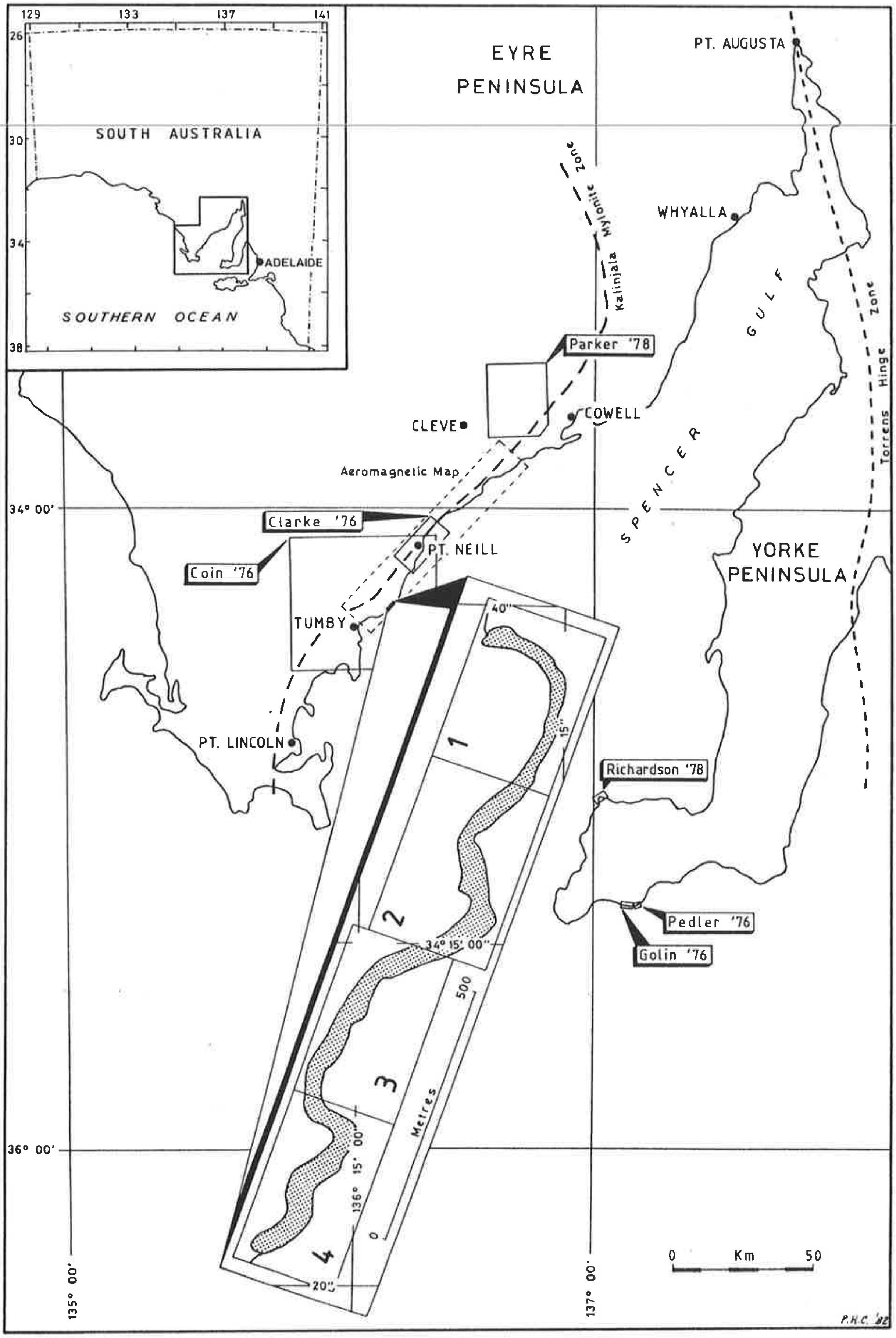

Fig. 6.1 Locality map of detailed thesis area (Lipson Cove North), and other relevant theses areas.

Fig. 6.2 Geology map of Lipson Cove North (in back pocket).

Fig. 6.3 Migmatite and quartz veins in amphibolite.

a) Migmatite veins showing effects of all deformation episodes. (Lens cap is 55mm in diameter.) (Location: 1095,1488)

b) Quartz vein in amphibolite. Scale bar is 30mm. (Location: 1382,1070)

Thin-sections of an amphibolite showing feldspathic veins containing F_2 folds, which fold S_1, and refolded by F_3. (Location 1366,2233). Scale bar is 5mm.

c) (Left) Plane-polarised light. Matrix of hornblende and feldspar, with localised occurrences of biotite.

d) (Right) Plane-polarised light. Same amphibolite as (c).

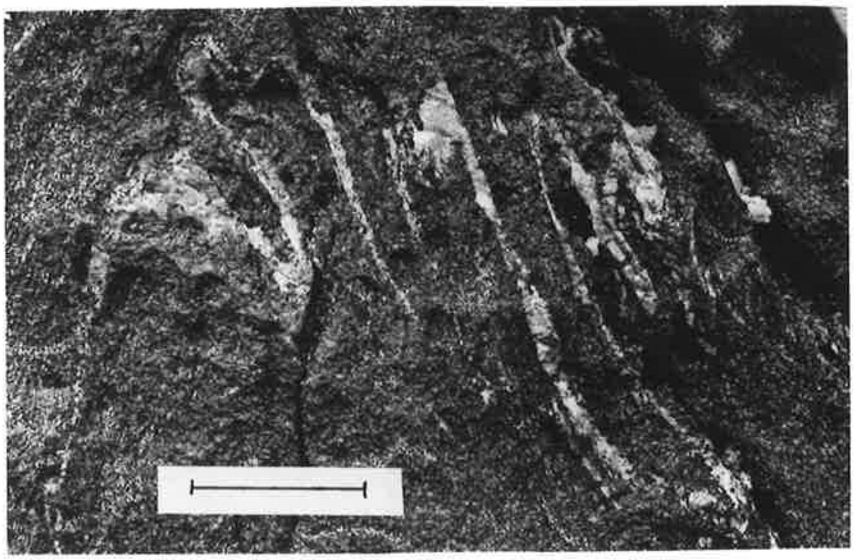

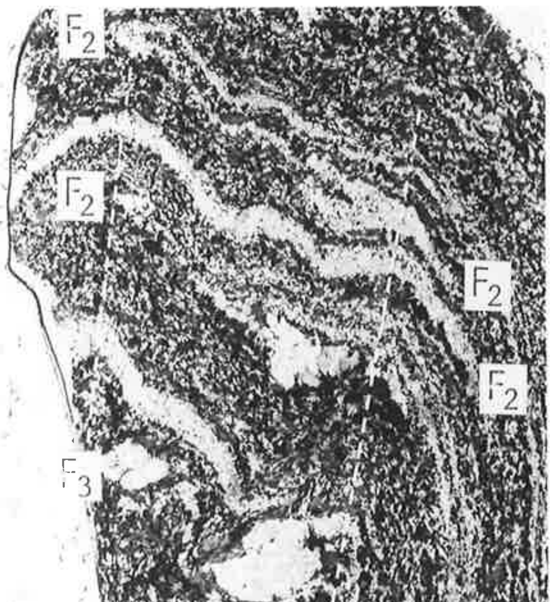
F_2
F_2
F_2
F_2
F_3
F_3

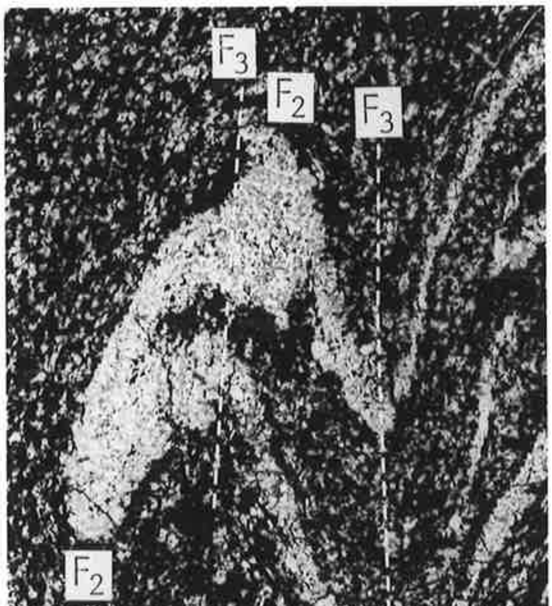
F_3
F_2
F_3
F_2

Fig. 6.4 Pre- to syn-D_3 granitic vein (V) intrusions.

a) View looking southwest showing a granitic vein in parts parallel or subparallel to layering, except to the left of the photograph (labelled 'C'). Scale bar is 30cm. Location (1920,1302).

b) Thin section of a specimen from a granitic vein (concordant with the S_1 foliation in a granitic augen gneiss) in which an S_3 foliation was produced. Scale bar is 2cm. (Location 1407,2081.5).

c) Thin section of a late stage granitic vein showing a possible foliation and much magnetite. Light grey grains are biotites. The vein from which the specimen was derived showed no controlled emplacement by the layering as was seen for the previous two specimens above. The possible foliation was not evident in the outcrop observations. Scale bar is 2cm.


V
C


S_1
S_1
S_3

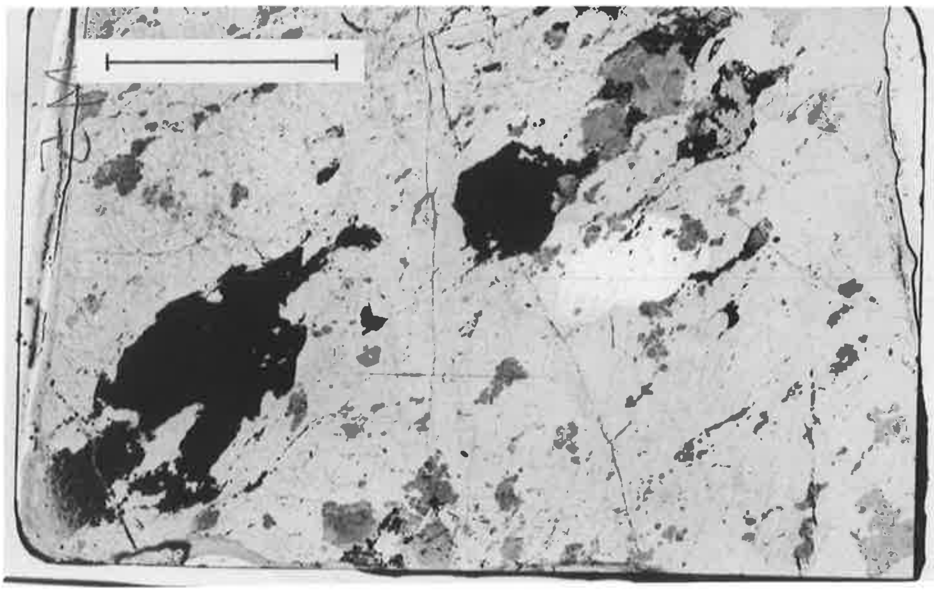

Fig. 6.5 Remnants of a pre- or syn-D_2 granitic vein carrying a high magnetite content portrayed by feldspar augen containing cores of magnetite.

a) Sketch from a photograph portraying two bands of magnetite-centred quartz/feldspar augen which were observed to cross-cut the layering (S_{0-1}) at a low angle to the left. The sketch is of one limb of an F_3 fold where the two bands and the layering are parallel. The folding and cross-cutting relationship of one band is exposed (b) but the second does not outcrop. Granitic veins are shown in black and S_3 is marked by axial plane jointing (see Fig. 7.4a).

b) One of two bands of augen occurring in an amphibolite in submap M13. On the sinistral limb of the F_3 fold (axial plane parallel to pen, looking southwest) the augen are flatter (compared to those in the hinge region where they are more elongate and parallel to L_3), defining a foliation (S_2) at a distinct angle to S_{0-1}, but become subparallel (S_{1-2}) on the dextral limb.
(Location 1382,2219, looking southeast).

c) Similar augen to (a) occurring in granitic and leuco-amphibolite gneisses in submap M45. Squares outline some of the magnetite grains.
(Location 1275,1880).

d) Thin section in plane light of magnetite grain surrounded by quartz and feldspar enclosed in amphibolite. (Such occurrences are possibly remnants of thin pegmatite veins that occurred early in the tectonic history.) Apart from the large magnetite grain, the small dark minerals are primarily hornblende with accessary biotite and magnetite. The light mineral is feldspar. Scale bar is 3mm.
(Location: 1382,2219)

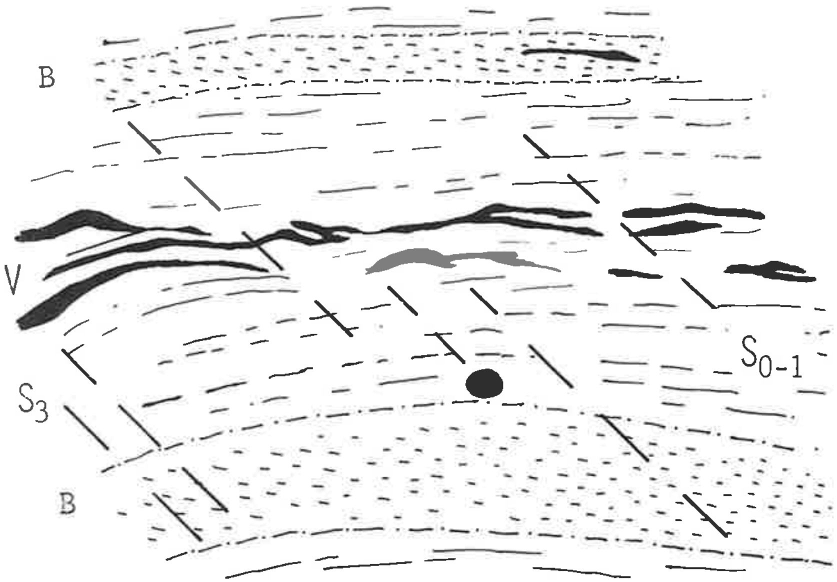

B
V
S0-1
S3
B

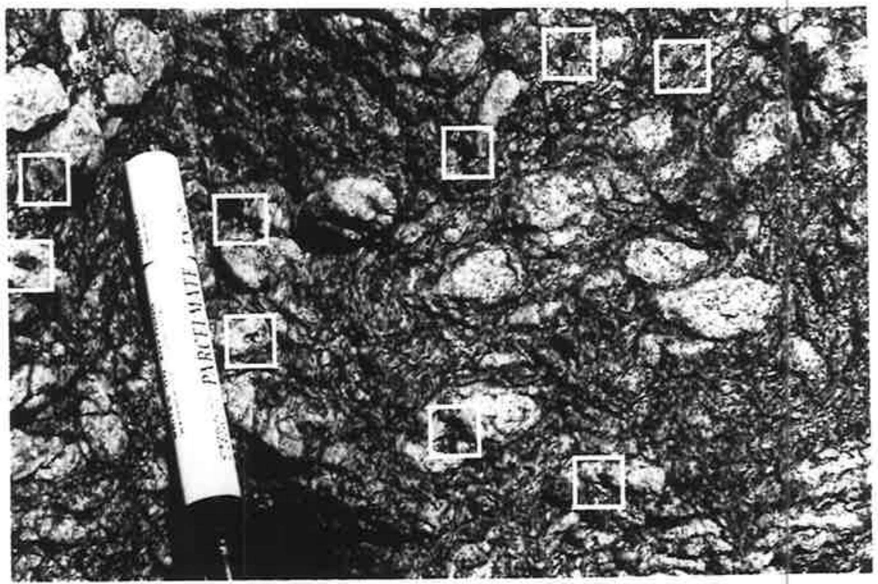

PAPERMATE

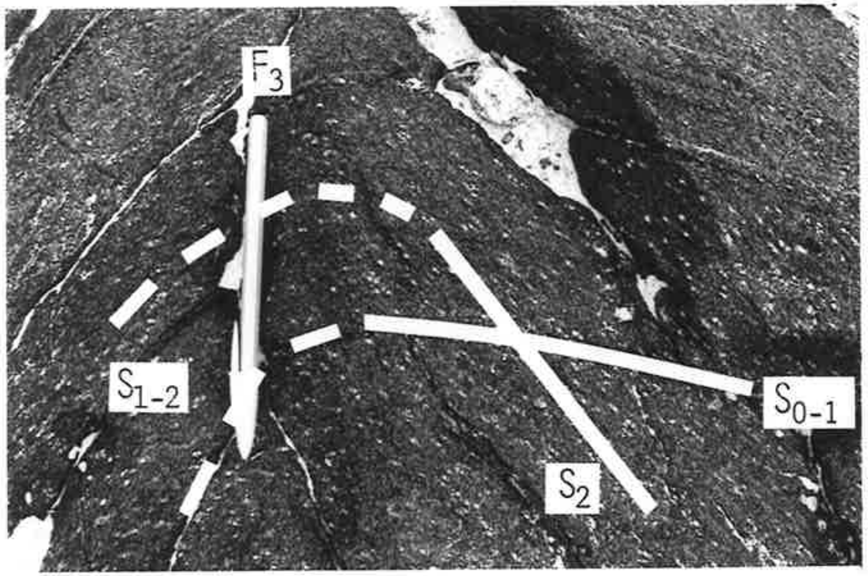

F3
S1-2
S0-1
S2

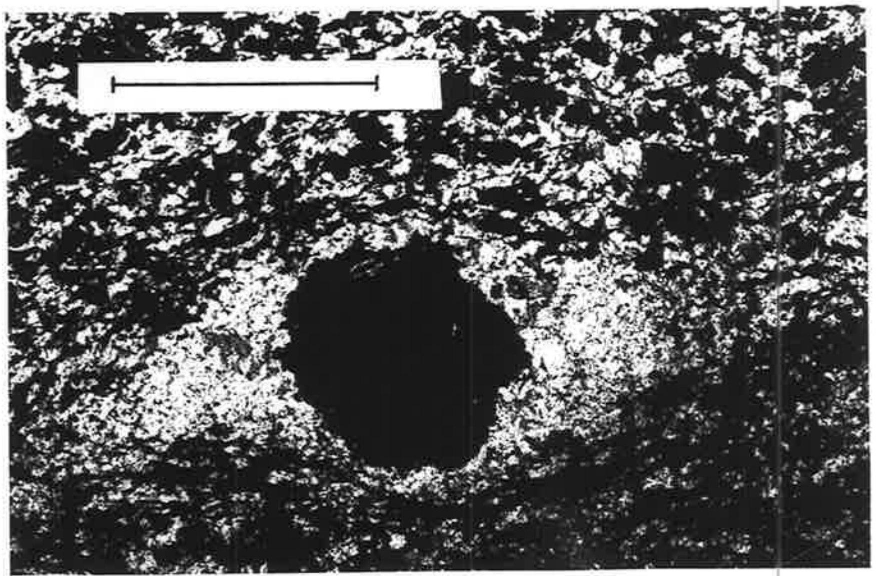

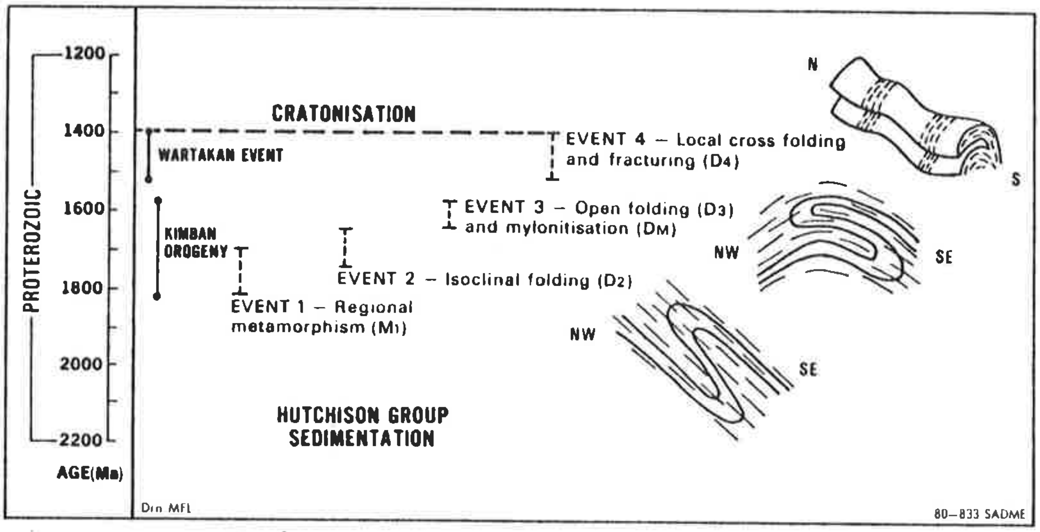

Fig. 6.6 Summary of regional tectonic events (after Parker and Lemon, 1982). The figure does not include the intrusion of the Lincoln Complex rock suite which began between sedimentation and Event 1, and continued into Event 2.

Fig. 6.7 Four appearances of the dominant foliation (S_1) in the mapped area.

a) A layer-parallel foliation, S_{0-1} is openly folded by D_3, producing small wavelength folds with a weak axial plane cleavage S_3 (defined by realignment of biotite, not shown). The rock is a layered amphibolite with the layers defined by varying ratios of feldspar to hornblende. Scale bar is 40cm.
(Location 1290,1917).

b) A weakly layered augen gneiss showing oblate augen in an F_2 fold profile. F_3 folding is not visible but trends from behind-right to front-left. Lens cap is 55mm in diameter.
(Location 1063,1377, looking south).

c) (Left) Similar rock type to (a) a few decimetres to the south. Oblate augen are crenulated by D_3, if not also by D_2.
(Location 1051,1340).

d) (Right) S_1 in an amphibolite gneiss, defined by separated feldspar and hornblende plus minor biotite bands. In this case, D_2 folds S_1, producing subhorizontal, steeply inclined F_2 folds with a weak axial plane cleavage, S_2 (defined by biotite and some hornblende, not shown). D_3 has openly folded F_2, producing an F_3 fold (not shown but parallel to the pen) nearly orthogonal to F_2. Scale bar is 7cm.
(Location 1080,1152.5).

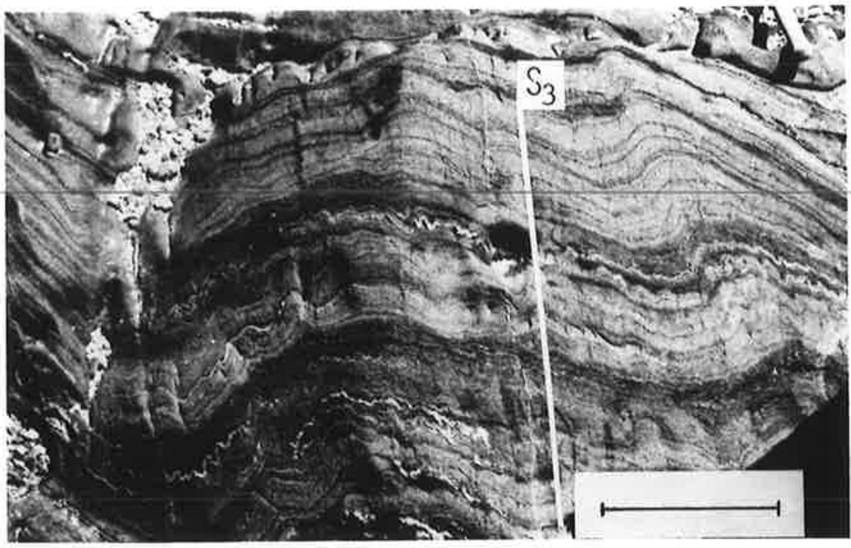
S3


0 1 2 3 4 5
cm

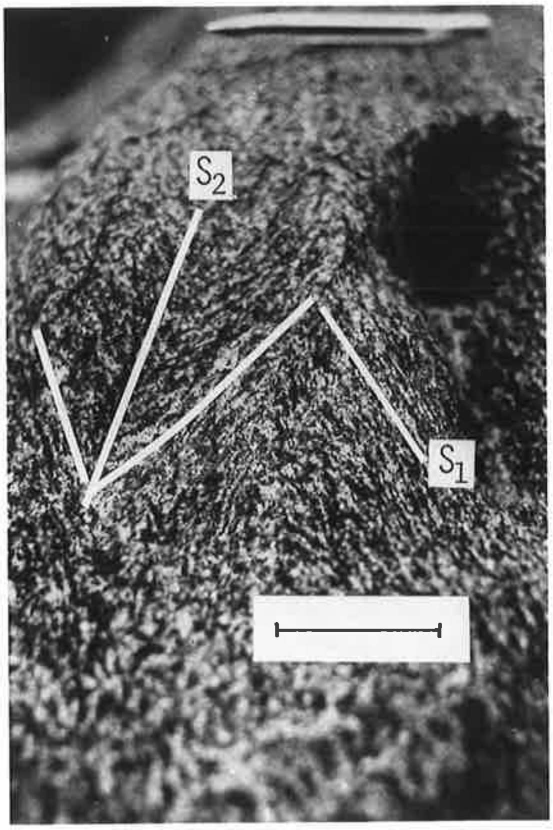
S2
S1

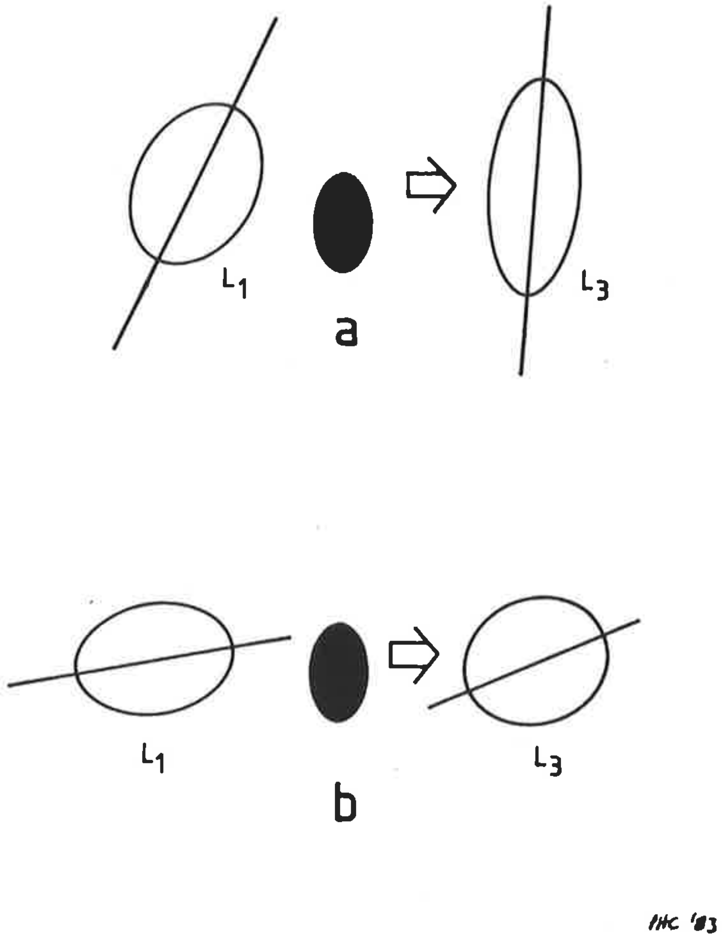

Fig. 6.8 Model demonstrating modification of L_1 to L_3. In (a) D_3 strains (black ellipse) rotates and intensifies L_1 to produce L_3, and (b) the D_3 strain virtually destroys the lineation.

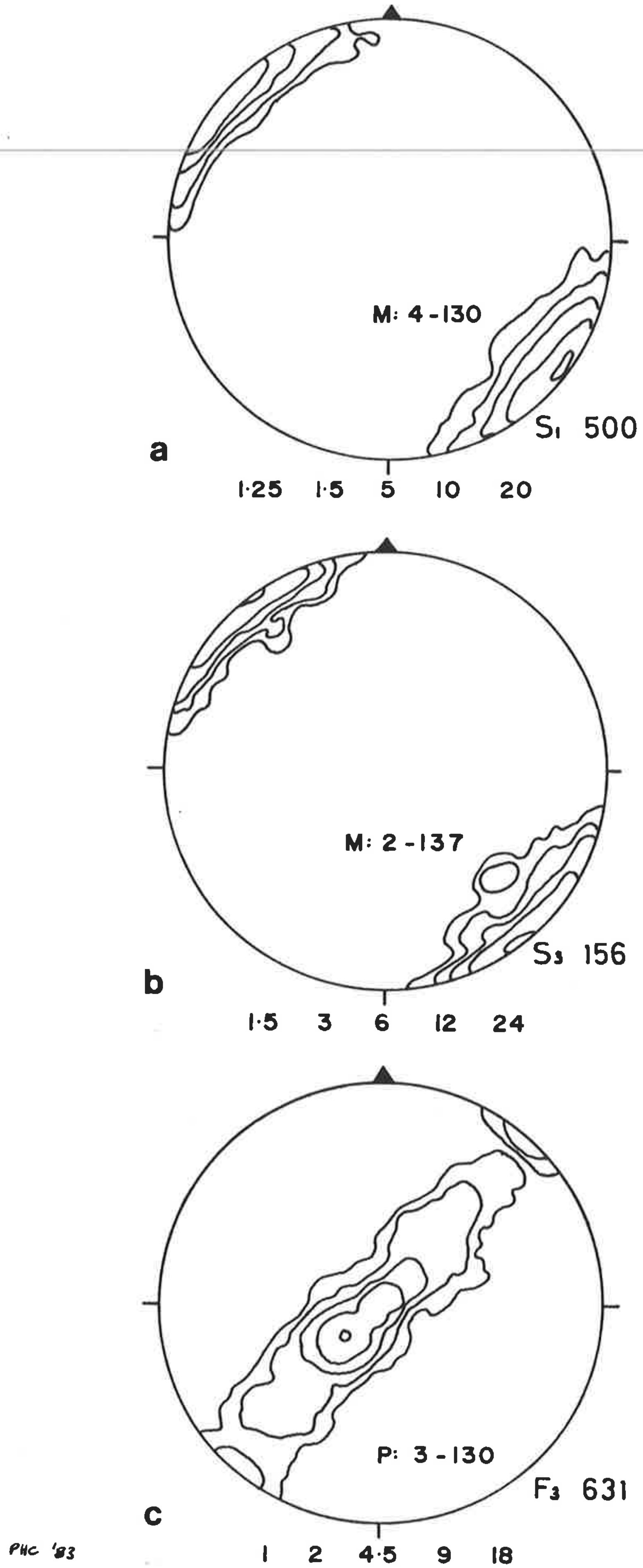

Fig. 7.1 Stereonet plots of each of the structural elements used in the analysis of Lipson Cove, for the whole of the mapped area.

Fig. 7.2 Structural data maps for Geology Sheet 1.

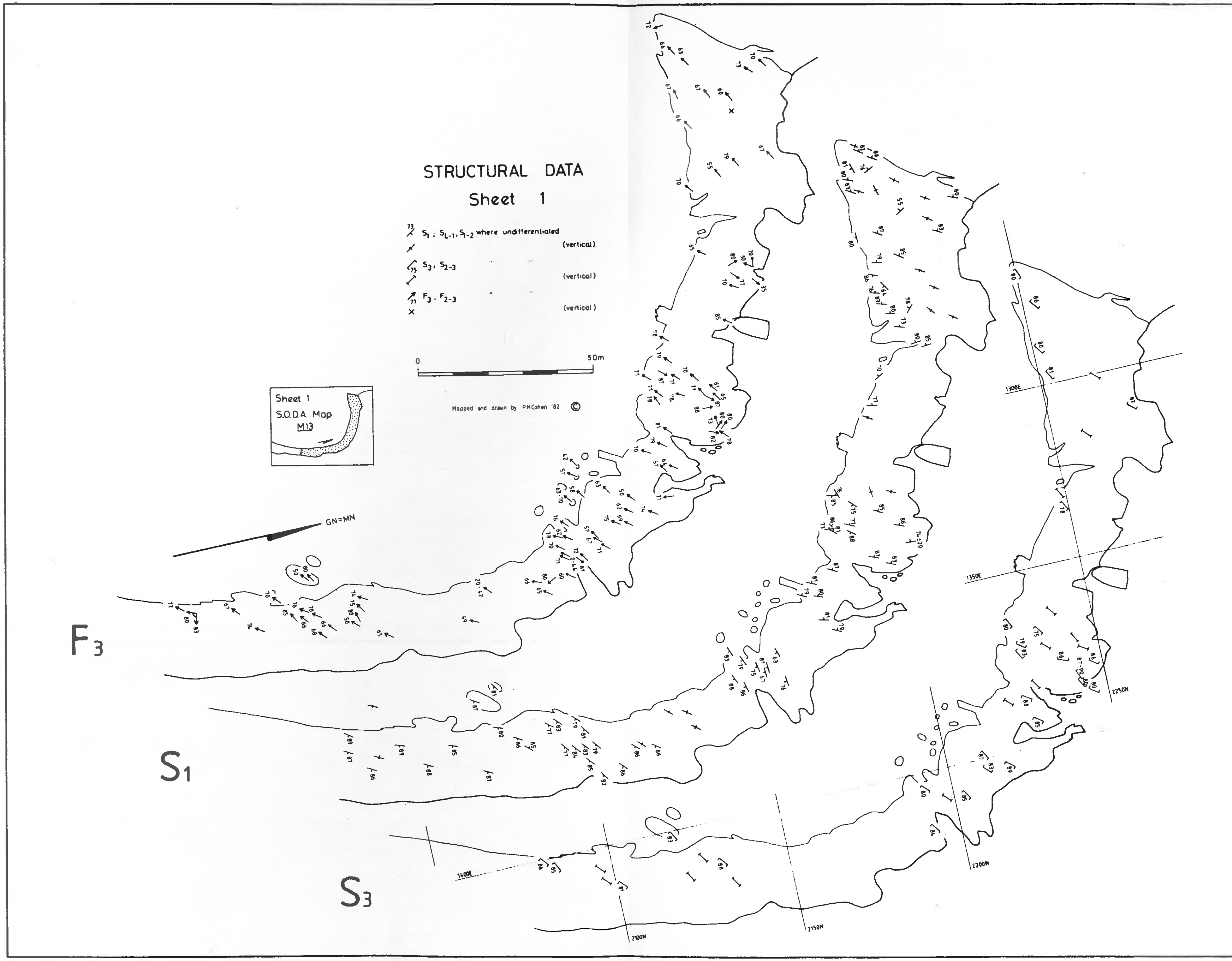

STRUCTURAL DATA
Sheet 1
73 S1 ; SL-1, S1-2 where undifferentiated
(vertical)
75 S3 ; S2-3 " "
(vertical)
77 F3 , F2-3 " "
(vertical)
0
50m
Mapped and drawn by P.H.Cohen '82 ©
Sheet 1
S.O.D.A. Map
M13
GN=MN
F3
S1
S3
1300E
1350E
1400E
2100N
2150N
2200N
2250N

Fig. 7.3 Examples of types of lineations (except the third generation crenulation lineation (see Fig. 7.15a)).

a) Elongation lineation (L_3) produced by D_3 lying in the S_1 gneissosity. Pen for scale is in direction of F_3 axial plane.
(Location 1078,1122 - Sheet 4).

b) Subhorizontal F_2 fold in granitic gneiss, surrounded by amphibolite, folds a D_1 elongation lineation, and is in turned folded by an F_3 fold. Marker pen for scale.
(Location 1340,2264 - Sheet 1).

c) (Left) Steeply plunging F_3 fold hinge (parallel to pen) in fine-grained granitic gneiss showing an intersection lineation (L_i, see text) between S_0 and S_1, caused by a small angular difference in their orientations. Scale bar is 6cm.
(Location 1372,2245 - Sheet 1).

d) (Right) Intersection lineation L_i (between S_0 and S_1) and mineral lineation produced by D_3, in the limb of an F_3 fold in a medium-grained leucogranitic gneiss. Scale bar is 4cm.
(Location 1102,1490 - Sheet 3).

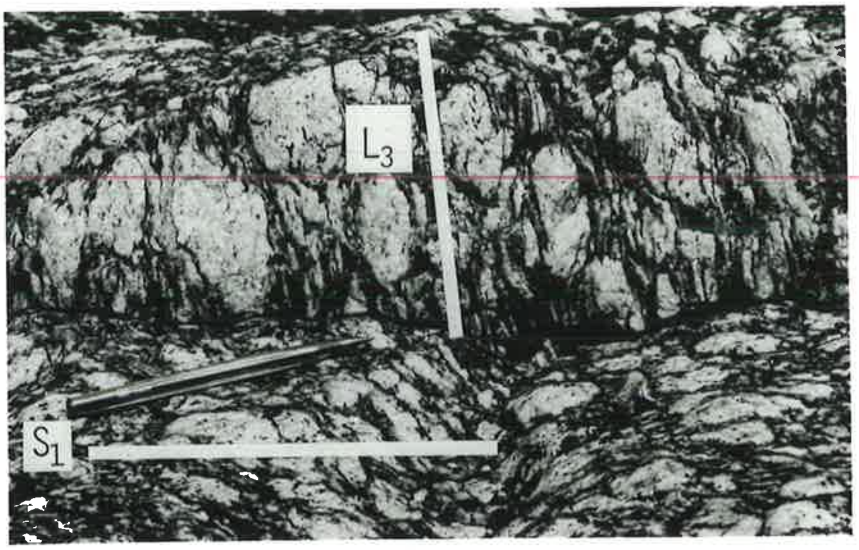
L3
S1

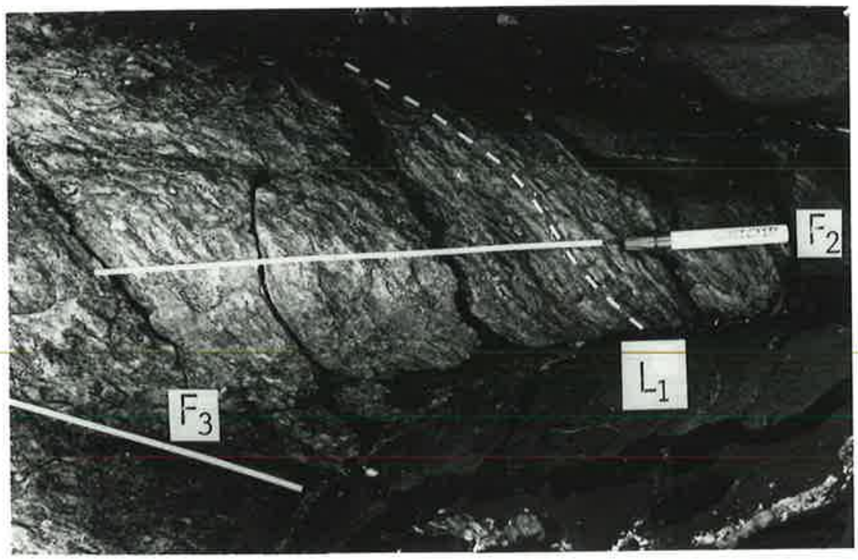
F2
L1
F3

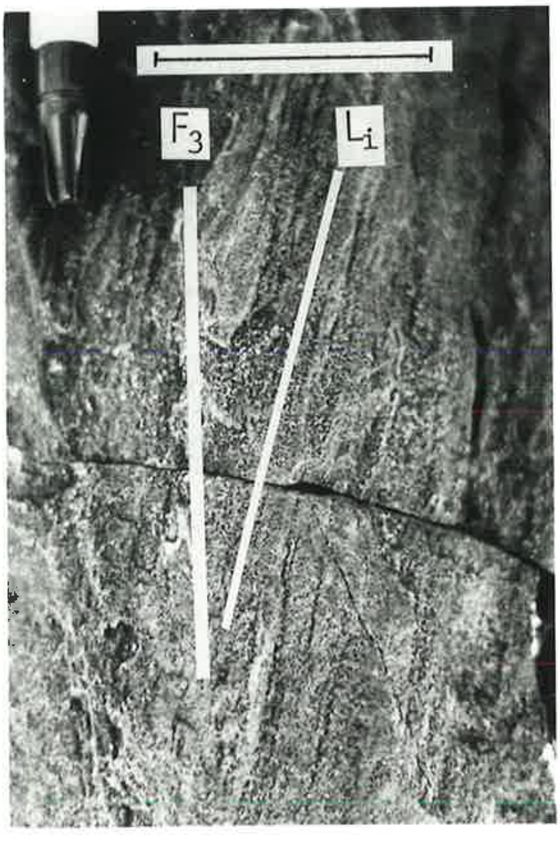
F3
Li

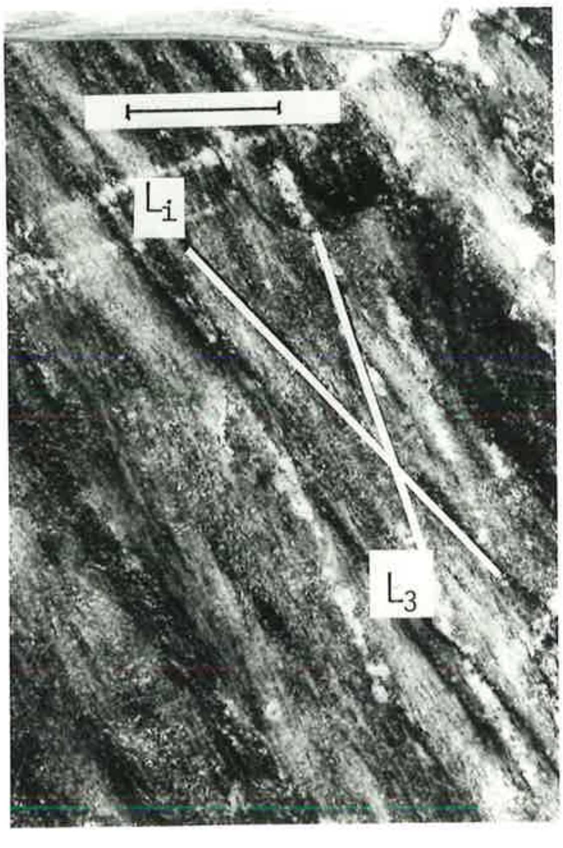
Li
L3

Fig. 7.4 a) Hinge of an F_3 fold in layered granitic gneiss, looking southwest. An 'S_3' jointing parallel to the F_3 axial plane has developed. The scale bar is (25 cm long). (Location 1410,2127 - Sheet 1).

b) An F_3 fold in an augen gneiss. An S_{1-2} foliation (the label on the photograph refers to the S_{1-2} envelope) is strongly crenulated by D_3. (Location 1413,2153 - Sheet 1).

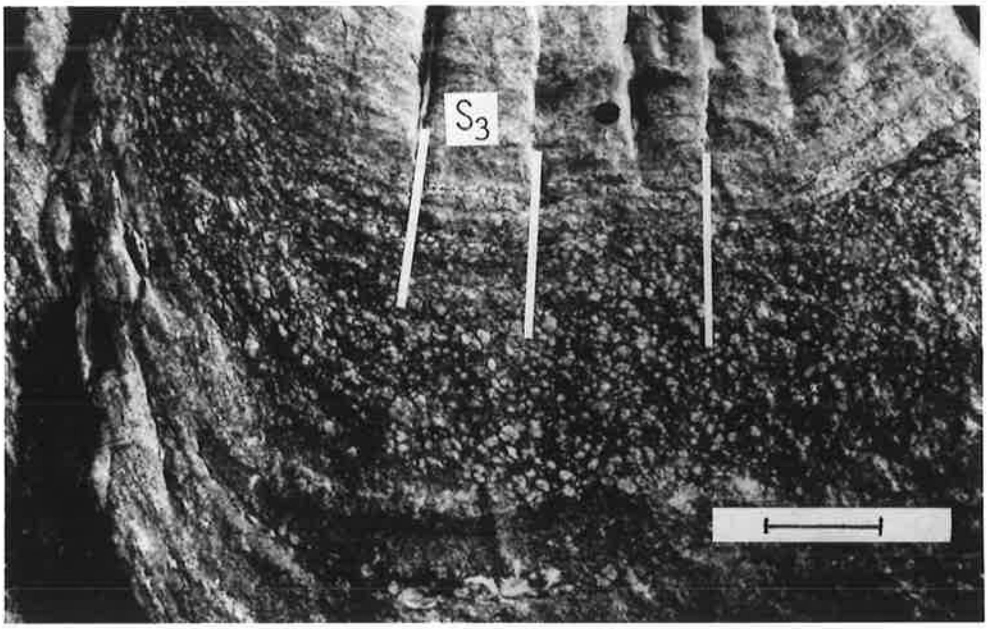
S3


F3
S1-2

Fig. 7.5 Examples of refolded folds in submap M13. In all cases, a layer-parallel foliation, S_{0-1} is folded by F_2 and refolded by F_3.

a) Oblique view (looking southeast) of part of the hinge and sinistral limb of an upright steeply plunging F_3 fold folding an amphibolite layer containing many micro-granitic and quartzo-feldspathic veins. Folds in the veins show evidence of an earlier folding event (D_2). The isoclinal F_2 folds give rise to an S_{1-2} schistosity. (Note pair of S and Z vergence folds.) Marker pen for scale.
(Localation 1356,2230 - Sheet 1).

b) Oblique view (looking northeast) of an upright steeply plunging F_3 fold folding an amphibolite layer containing quartzofeldspathic veins. A Z vergence fold in a vein (arrowed) on the sinistral limg of the F_3 fold indicates an earlier fold forming event (D_2). Arrow is 5cm long. Inset is of a quartzo-feldspathic vein enlarged in (c). The pointer refers to the same fold near the 'F_2' label in (c).
(Location 1359,2227 - Sheet 1)

c) (Left) Enlargement of the inset in (b), but looking southwest. The vein shows a subhorizontal, but variably plunging, F_2 fold refolded by F_3.

d) (Right) Interference minor fold of type S on Z (cf. to a mirror image of Ramsay, 1967, figure 10.19) in a granitic layer
(Location 1345,2240 - Sheet 1)

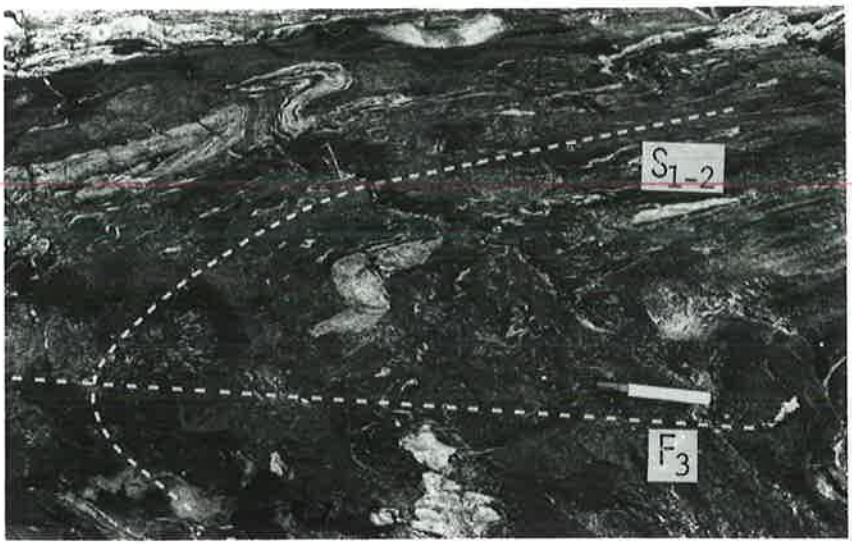
S1-2
F3

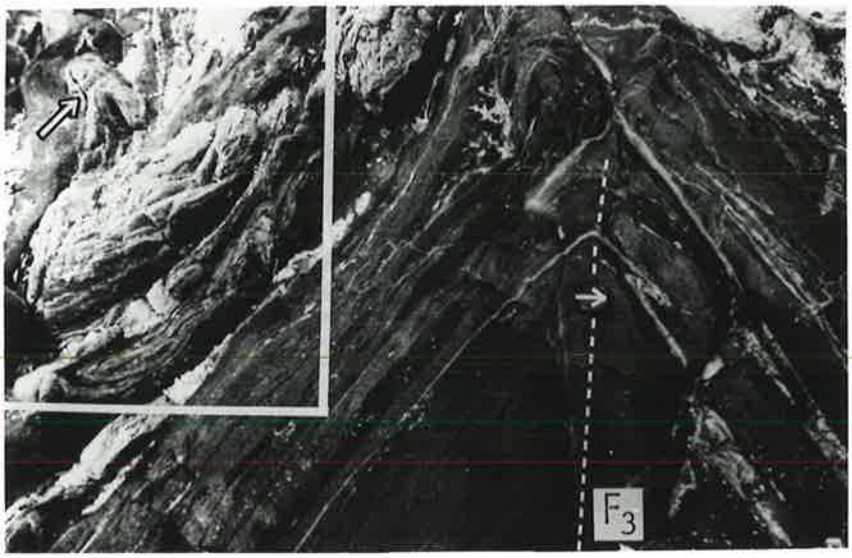
F3

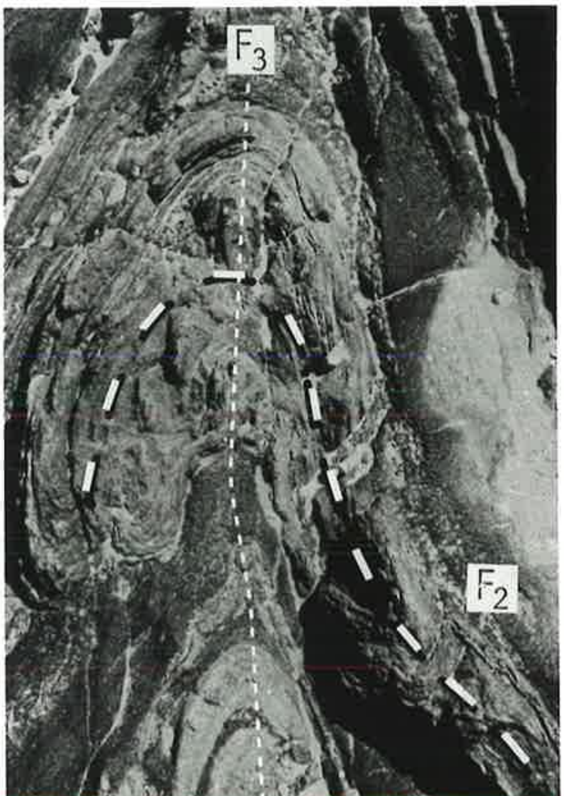
F3
F2

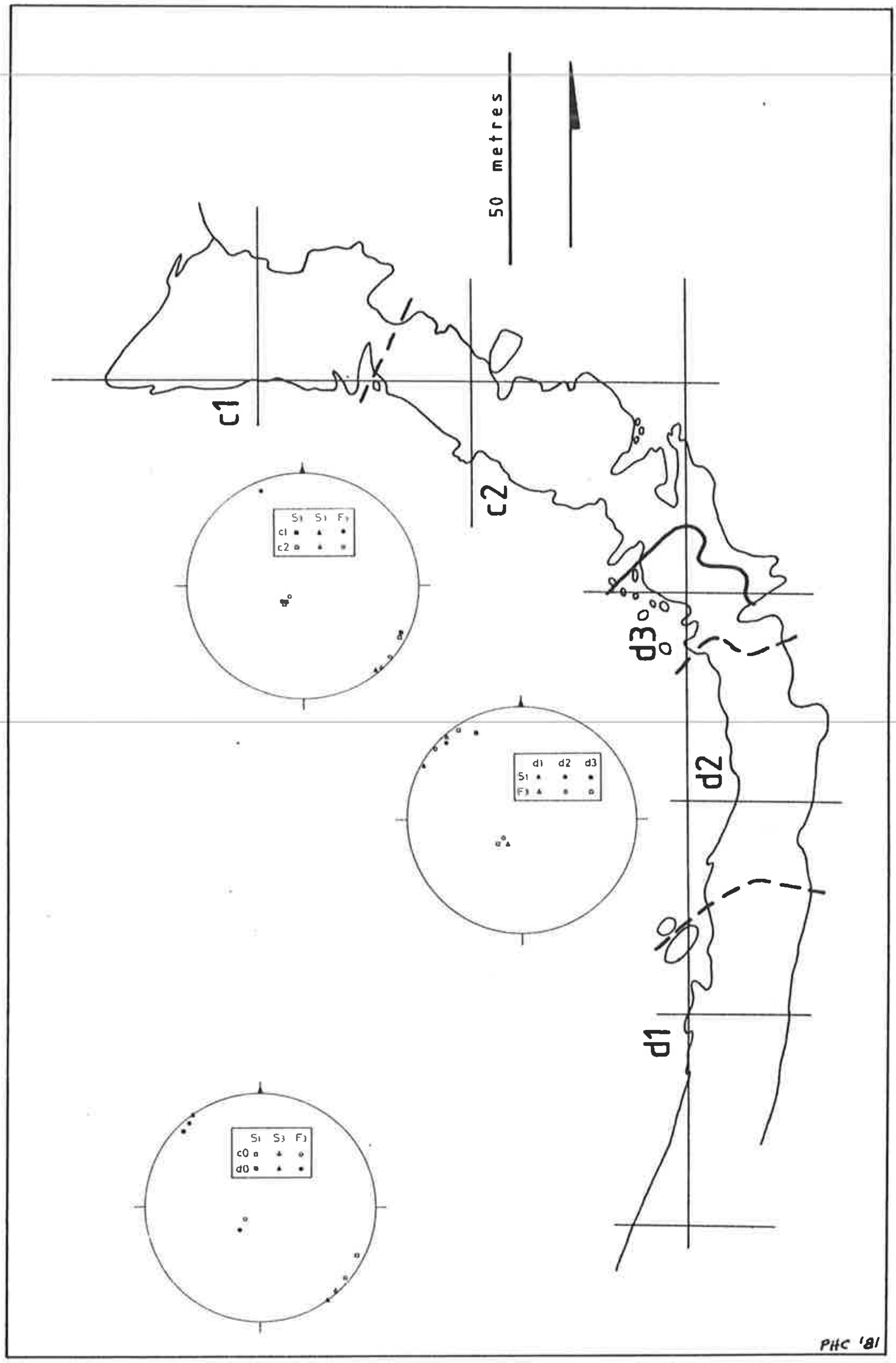

Fig. 7.6 Structural domains of Geology Sheet 1 (Submap M13).
a0 = c0 + d0 , c0 = c1 + c2, d0 = d1 + d2 + d3
The synoptic stereoplots summarise the domain data of Fig. 7.7.

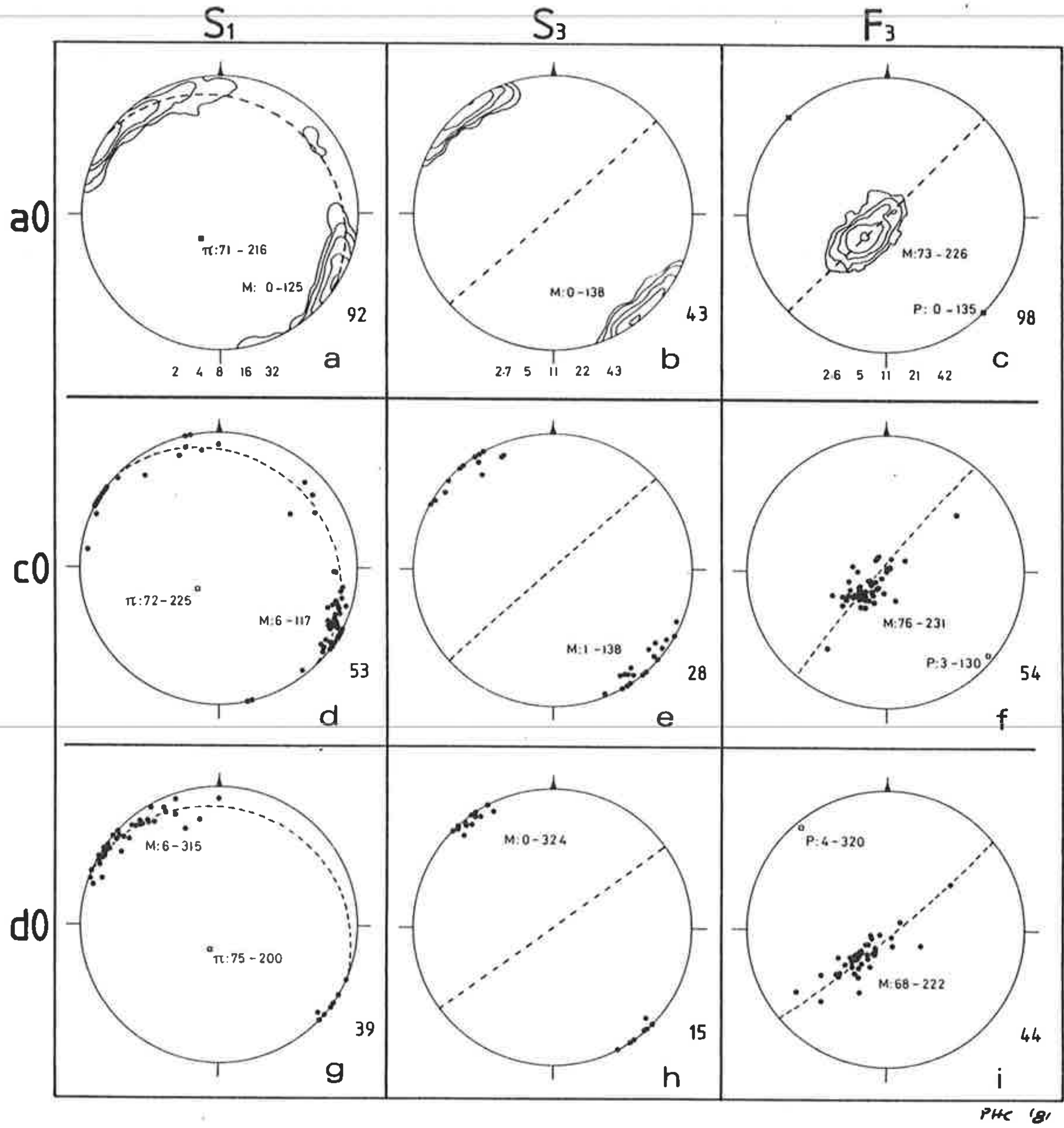

A

Fig. 7.7 Stereoplots of structural domains for Geology Sheet 1. (A) Primary domains; (B) Secondary domains (overleaf).

(Continued)

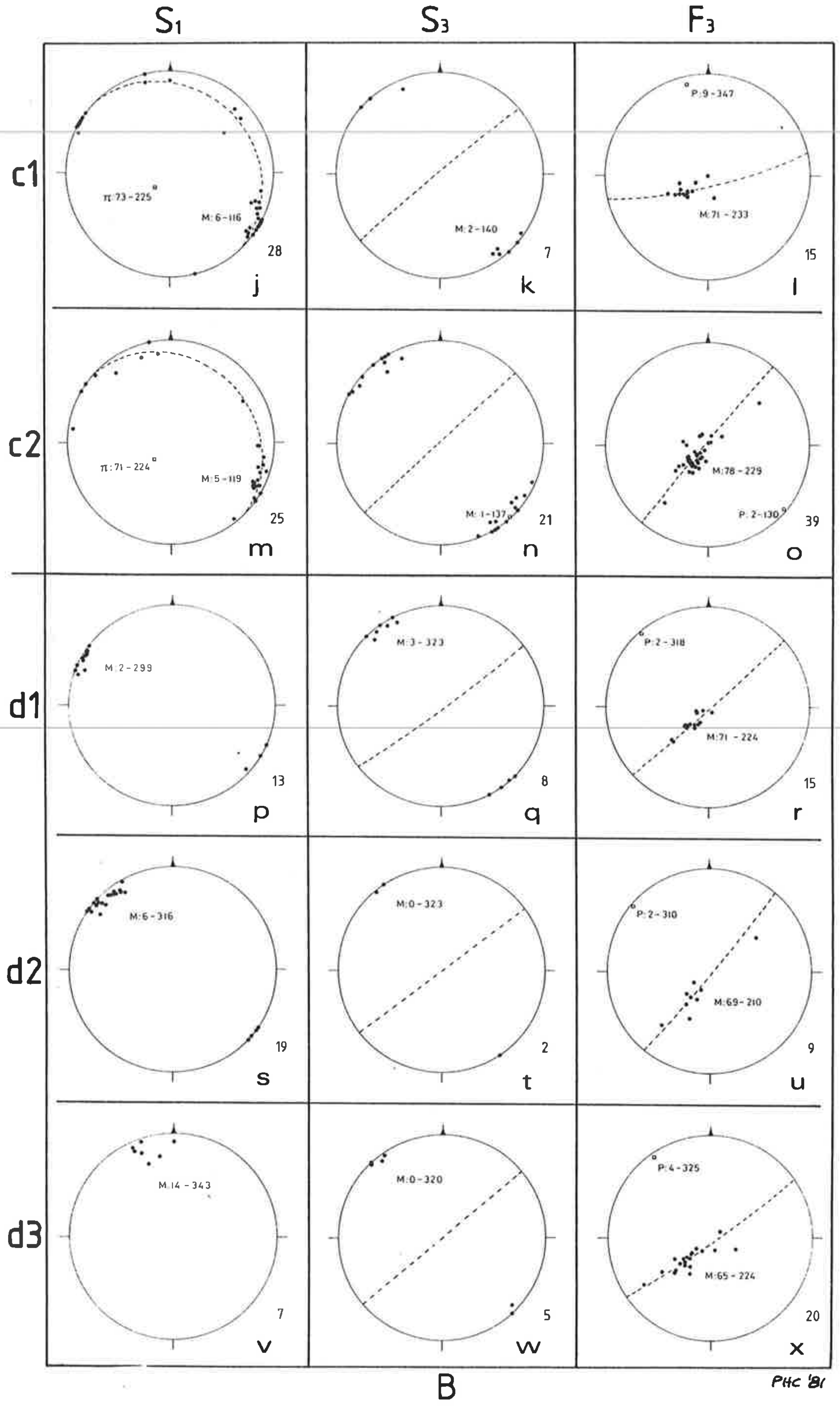
S1
S3
F3
c1
π:73-225
M:6-116
28
j
M:2-140
7
k
P:9-347
M:71-233
15
l
c2
π:71-224
M:5-119
25
m
M:1-137
21
n
M:78-229
P:2-130
39
o
d1
M:2-299
13
p
M:3-323
8
q
P:2-318
M:71-224
15
r
d2
M:6-316
19
s
M:0-323
2
t
P:2-310
M:69-210
9
u
d3
M:14-343
7
v
M:0-320
5
w
P:4-325
M:65-224
20
x
B
PHC '81

Fig. 7.7 (Cont.)

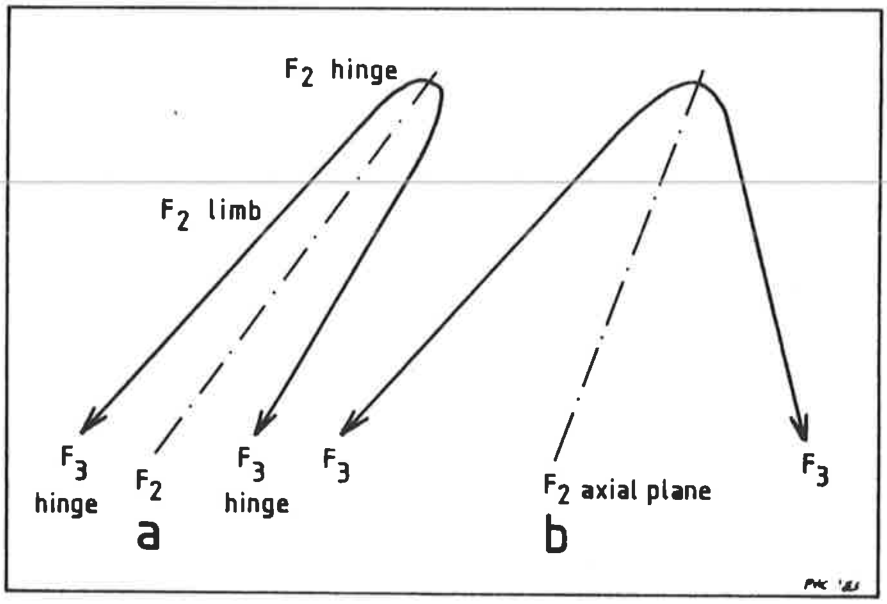

Fig. 7.8 Profiles of steeply inclined F_2 folds demonstrating the orientations of F_3 fold hinges which would arise when the F_2 folds are overprinted by D_3.

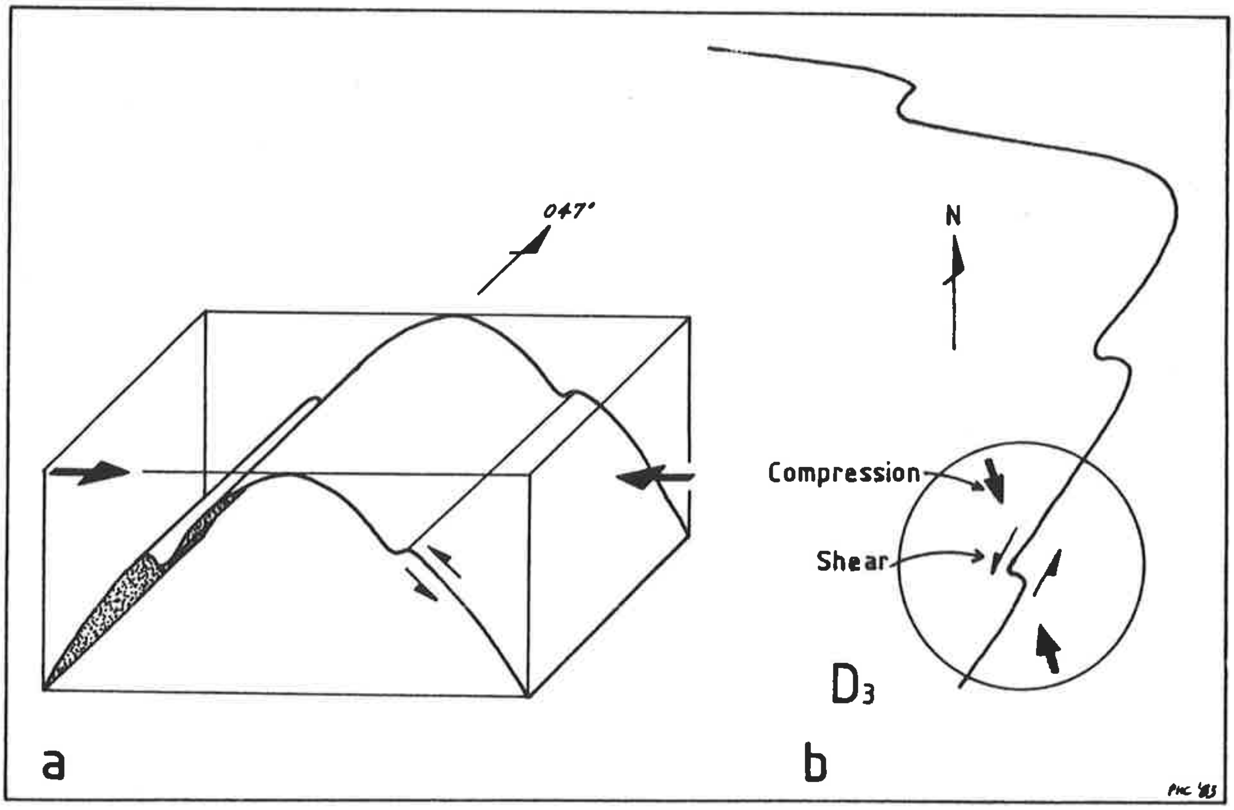

Fig. 7.9 Compression and shear stresses on the limb of D_3 folds. (a) An upright open horizontal F_3 fold (as interpreted by Parker and Lemon (1982) for the Cowell/Cleve area. (b) The effect of (a) if F_3 was plunging NE or (a) overprints a previous steeply inclined D_2 structure.

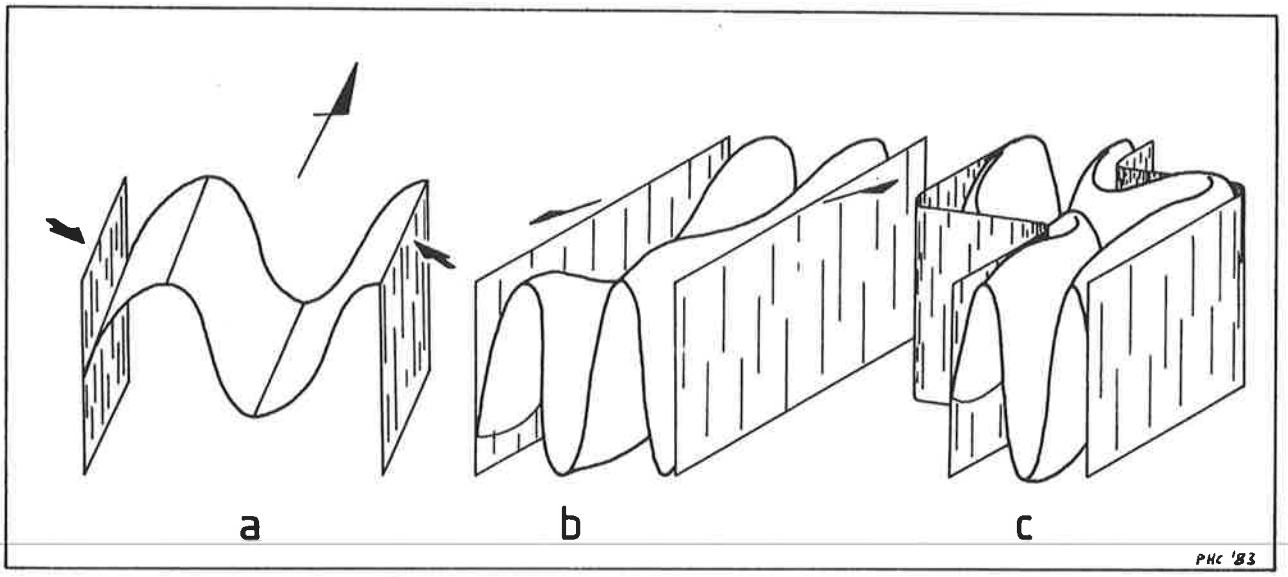

Fig. 7.10 Model demonstrating how (a) N-S subvertical, subhorizontal F_2 folds are modified by D_3 to produce refolded folds as interpreted in Fig. 7.13a. The compressional component of D_3 flattens the folds and may reorientate them (b). The shearing component will refold the modified F_2 folds to produce sinistral folds overprinting the earlier D_2 folds (c). Both (b) and (c) would be operating simultaneously, although significant effects of one may be precede the other.

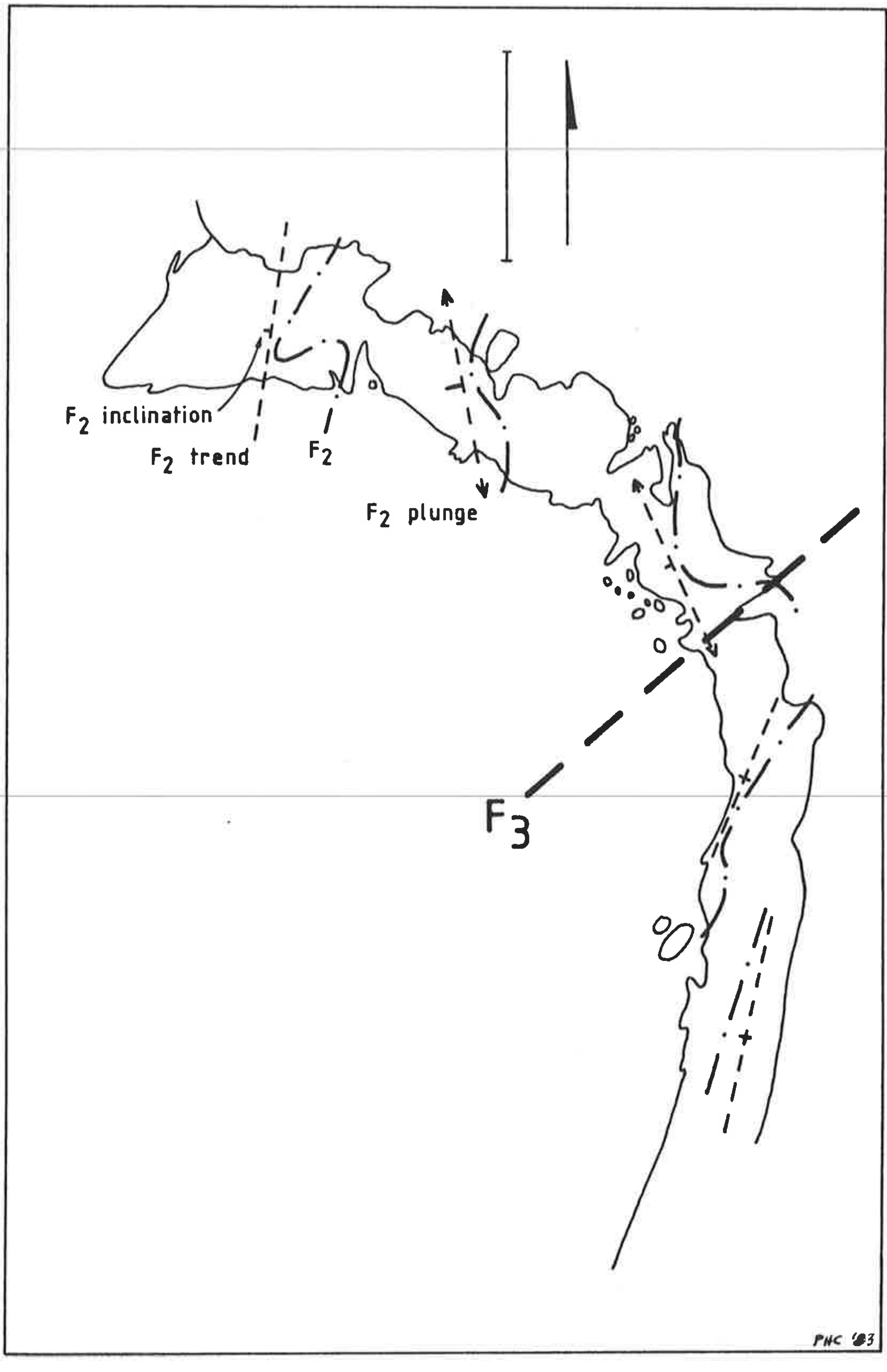

Fig. 7.11 Schematic interpretation of the D_2 structures in submap M13. The dot-dash line is the trace of F_2 hinges (now buckled by D_3) interpreted from the geology sheet 1 (Fig. 6.2). The trend of F_3 fold envelopes for each of the traces is given by the dashed lines. Size of the inclination bar qualitatively represents the degree and direction of inclination (the shorter the bar, the steeper the axial plane). Arrowed trend lines indicate noticable F_2 fold hinge plunges, although overall plunge is subhorizontal. Heavy dashed line is the interpreted trace of the submap-sized F_3 fold axial plane. Scale bar, parallel to the north-arrow, is 50 metres.

Fig. 7.12 Structural data maps for Geology Sheet 2.

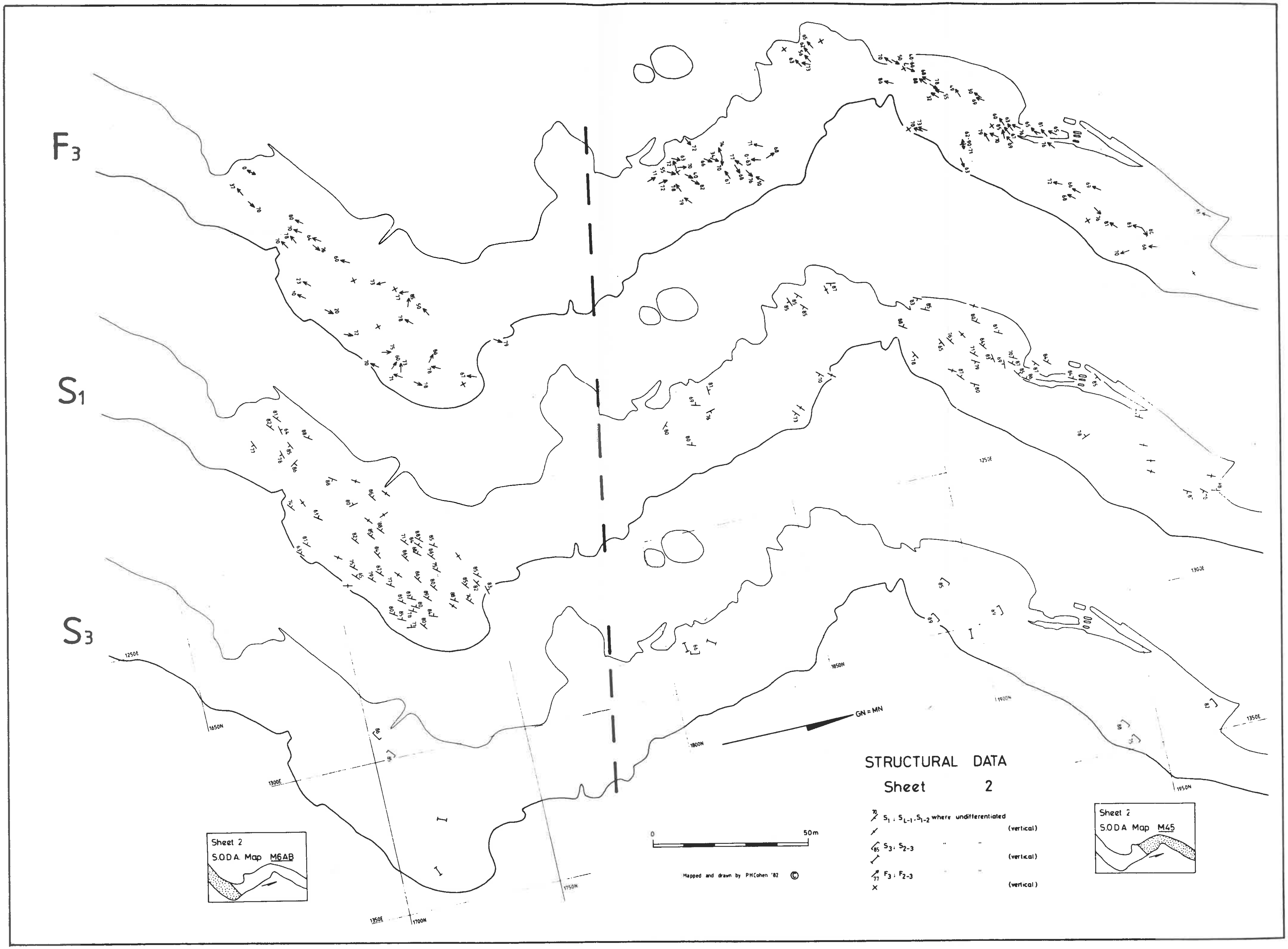
F3
S1
S3
1250E
1300E
1350E
1650N
1700N
1750N
1800N
1850N
1900N
1950N
GN = MN
STRUCTURAL DATA
Sheet 2
S1 ; SL-1 , S1-2 where undifferentiated
(vertical)
S3 ; S2-3
(vertical)
F3 ; F2-3
(vertical)
0
50m
Mapped and drawn by P.H.Cohen '82 ©
Sheet 2
S.O.D.A. Map M6AB
Sheet 2
S.O.D.A Map M45

Fig. 7.13 a) Diagrammatic sketch, looking northwest, of a common type of mesoscopic structure in submap M45 and domain c2 of submap M13. A subhorizontal layer-parallel foliation, S_{0-1}, is folded and transposed by D_2 to produce subhorizontal F_2 folds (stippled axial plane) steeply inclined to the west. This is overprinted by D_3 producing upright sinistral F_3 folds (heavy dashed line) refolding F_2, which causes F_2 hinges to vary in plunge.

b) Looking northwest. This fold shows a remarkable similarity to the style portrayed in (a). Note that topography and the oblique viewpoint has an effect on the fold traces shown.
(Location 1280,1892 - Sheet 2).

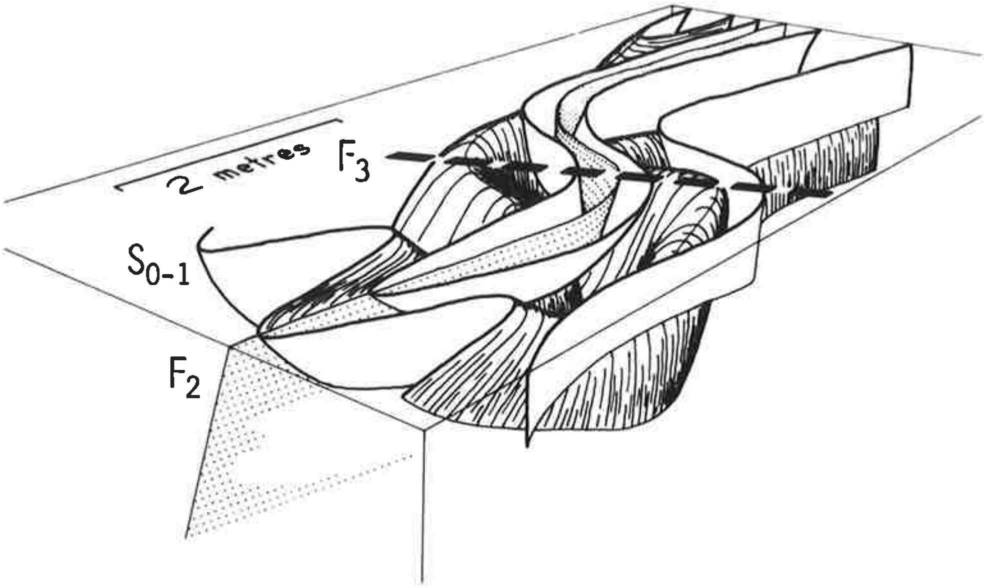
2 metres
F3
S0-1
F2

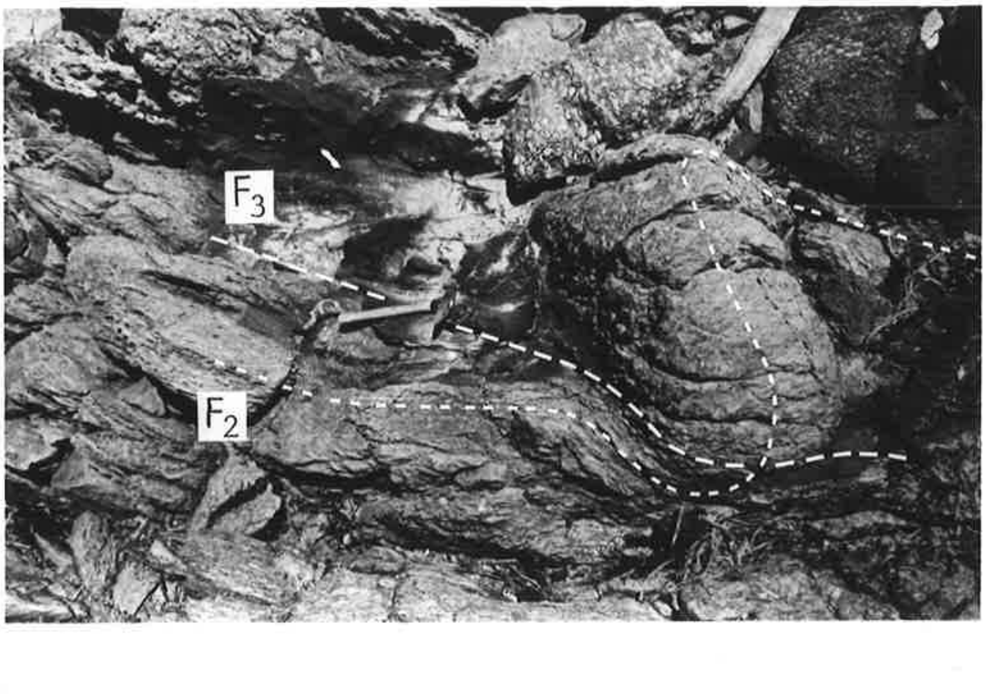
F3
F2

Fig. 7.14 Examples of interference folds in the northern portion of submap M45. In all cases, F_2 folds are folding interlayered granitic and amphibolite gneisses, and are in turn overprinted by F_3 folds.
(Location in the vicinity of 1892,1280 - Sheet 2)

a) Looking down-plunge (south) of F_2 folds refolded by D_3. Rock type is mainly amphibolite with interlayered augen gneiss layers. Scale is provided by pen (parallel to F_3 trace).

b) Looking northeast. Scale bar is 50cm.

c) Refolded F_2 folds folding a hornblende rich layer (outlined) in a more feldspar-rich amphibolite.


F2

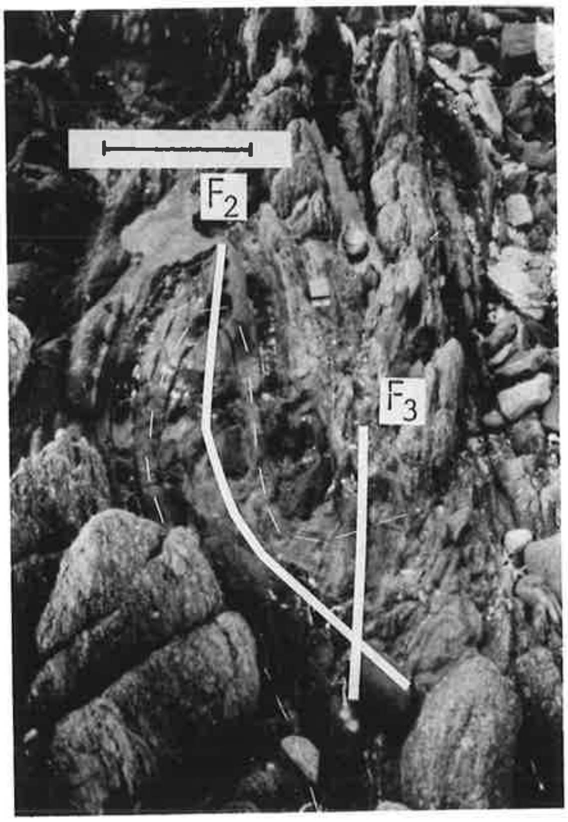
F2
F3

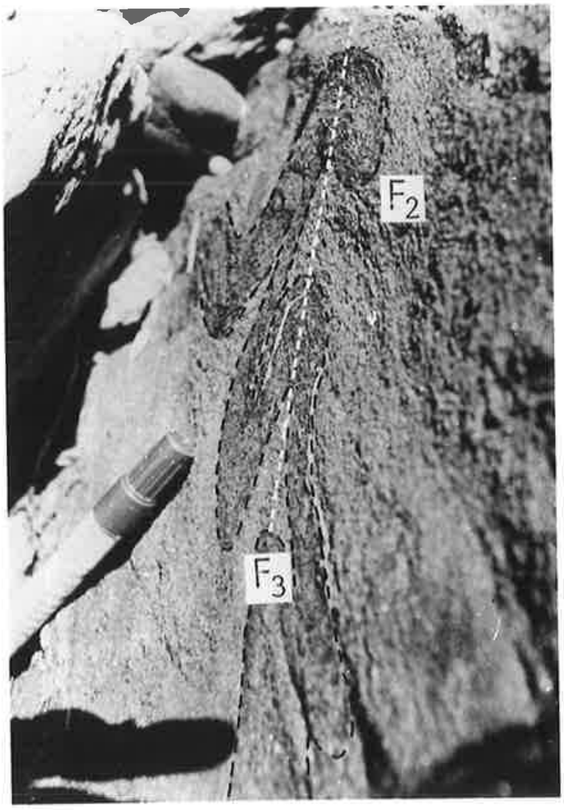
F2
F3

Fig. 7.15 a) An F_2 fold in a granitic layer overprinted by a D_3 crenulation lineation, L_3.
(Location 1287,1815.5 - Sheet 2).

b) An oblique view, looking north, of an F_3 fold which refolds F_2 folds. Field of view is 2m.
(Location 1282,1808 - Sheet 2).

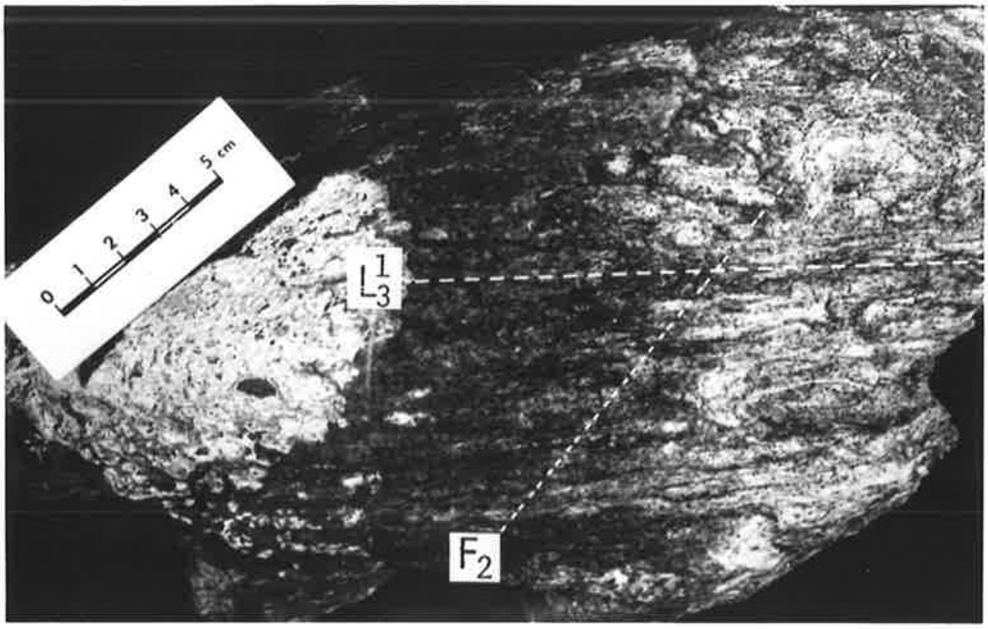
0 1 2 3 4 5 cm
L_3^1
F_2

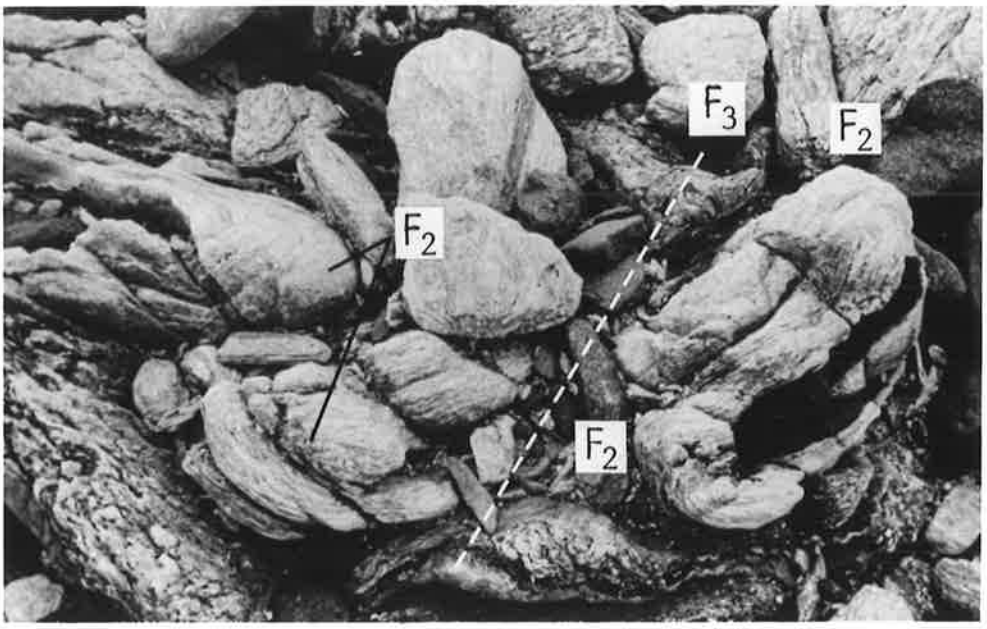
F_3
F_2
F_2
F_2

Fig. 7.16 Possible occurences of F_1 folds in amphibolites.

a) Subvertical section through subhorizontal S_{0-1} folded by F_{2-3}, with a weak subvertical S_{2-3} axial plane. Closures in S_0 suggest possible F_1. (Location 1378,2010 - Sheet 2).

b Sketch of (a). Scale bar is 3cm.

c) Similar situation to (a) although possible F_1 fold closure not seen. (Location in the vicinity of 1280,1892 - Sheet 2).

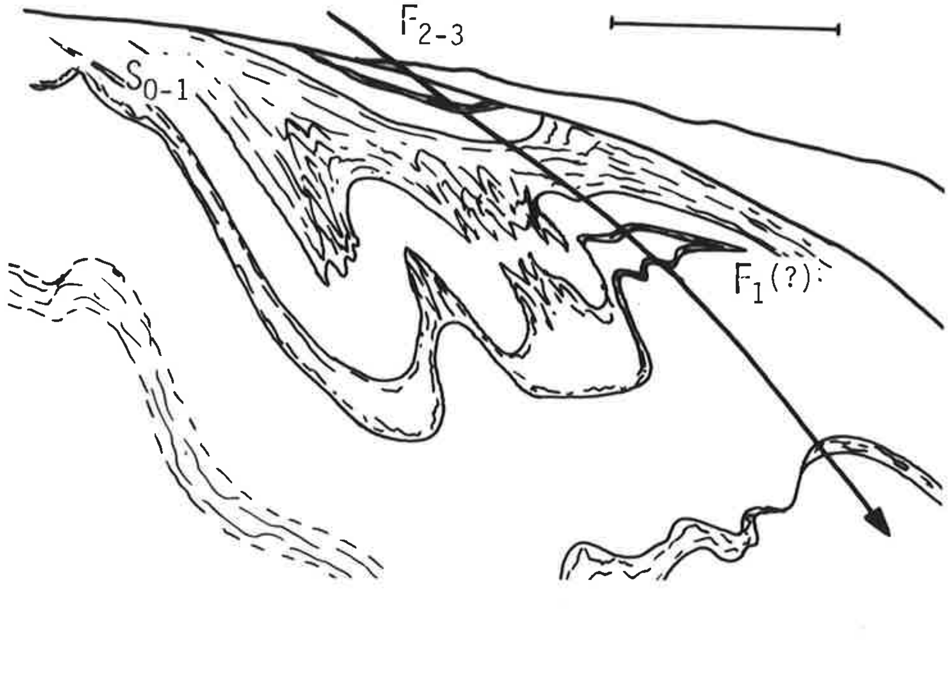

F_{2-3}
S_{0-1}
F_1(?)

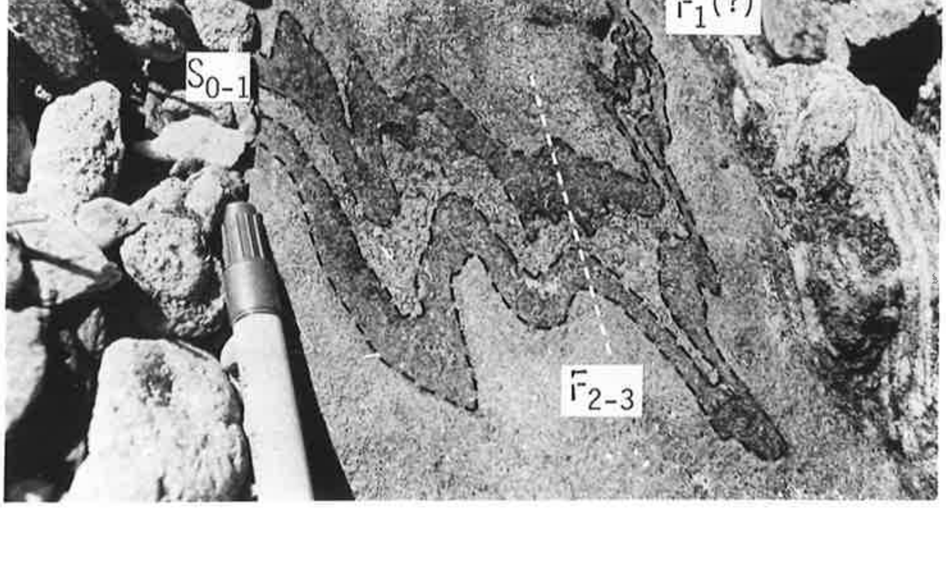

F_1(?)
S_{0-1}
F_{2-3}

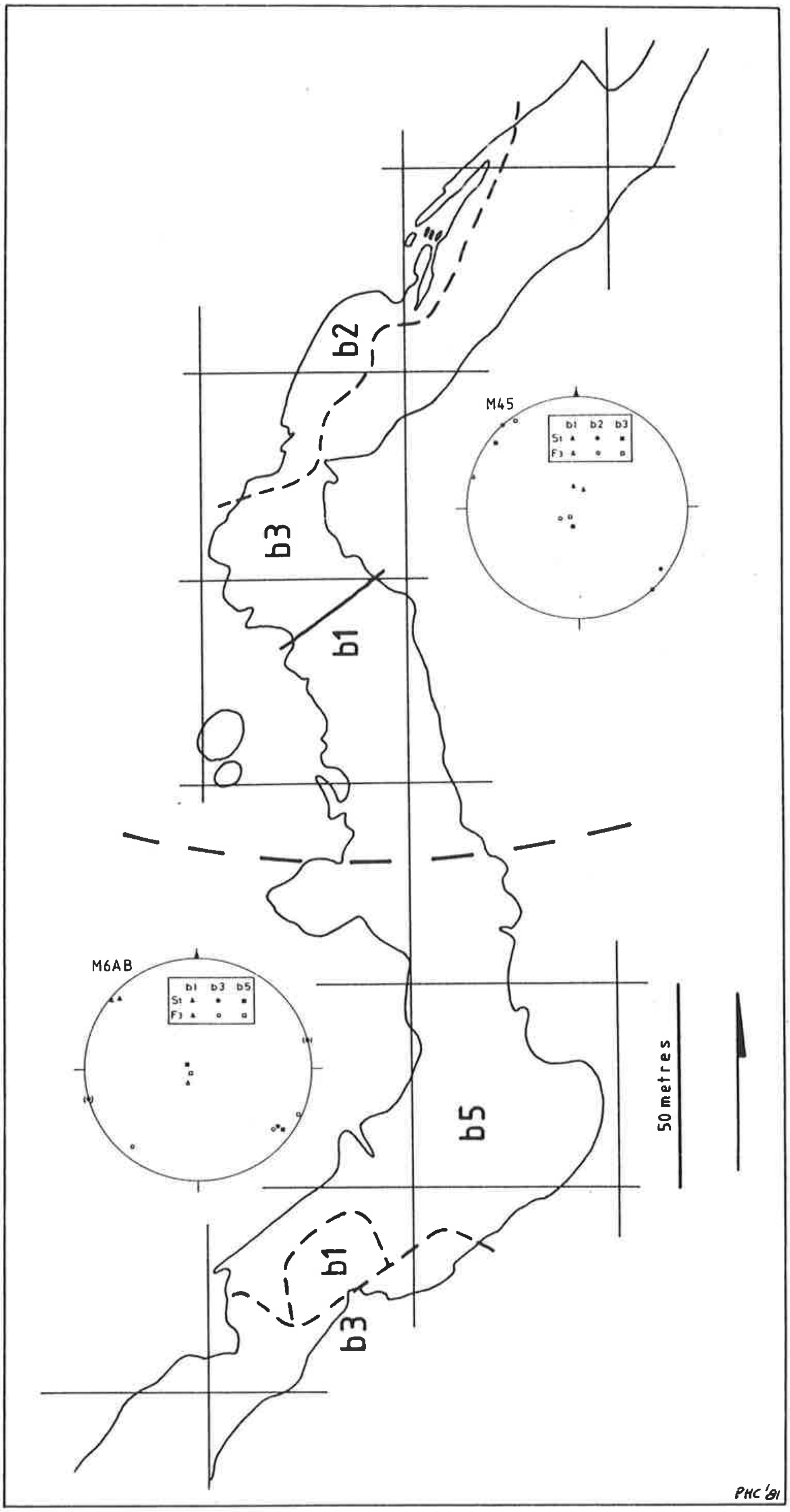

Fig. 7.17 Structural domains of Geology Sheet 2 (Submaps M45 and M6AB).
M6AB: a0 = b1 + b3 + b5 M45: a0 = b1 + b2 + b3
Synoptic stereonets from Figs. 7.18 (M45) and 7.21 (M6AB).

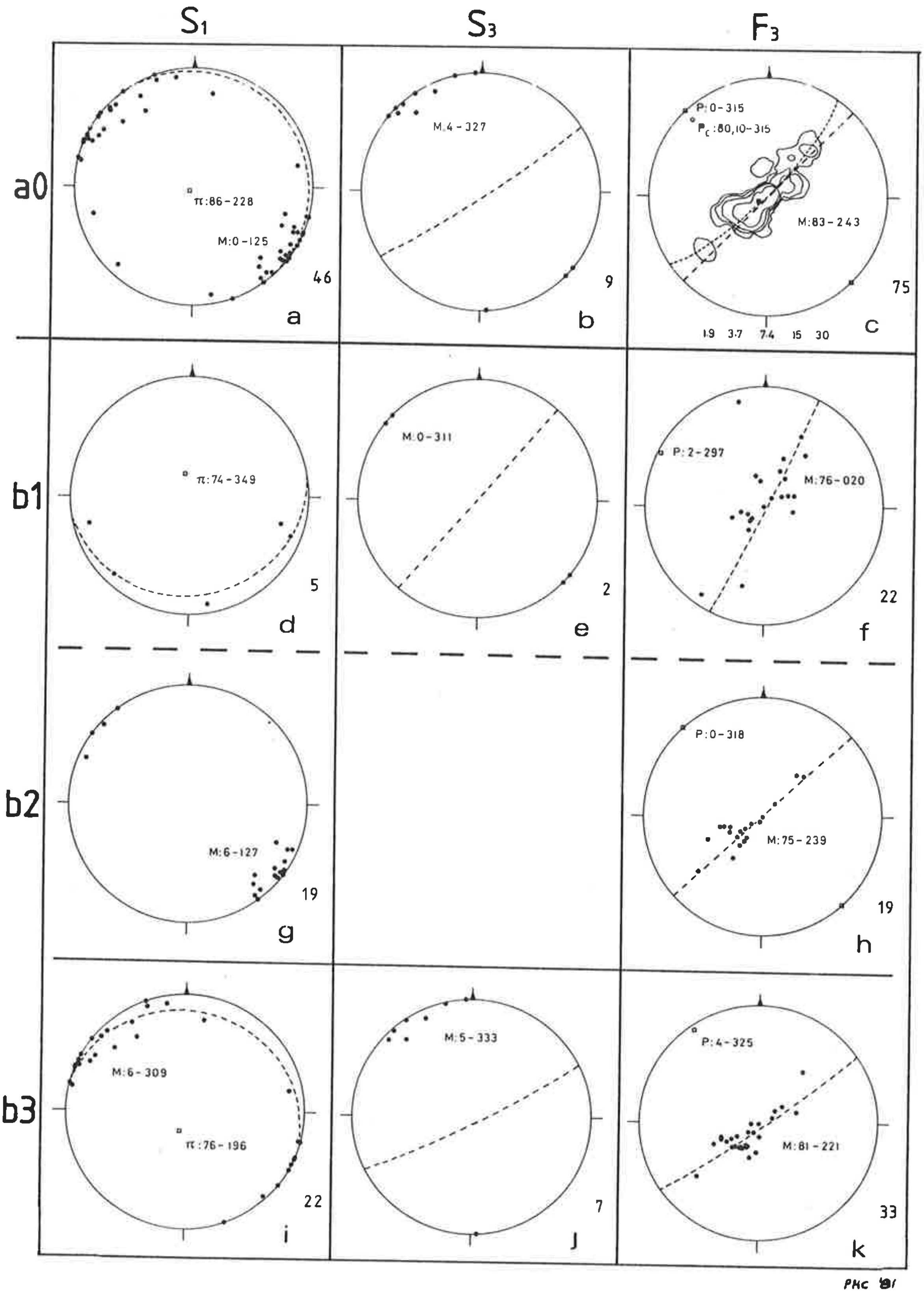

Fig. 7.18 Stereoplots of structural domains for Submap M45 in Geology Sheet 2.

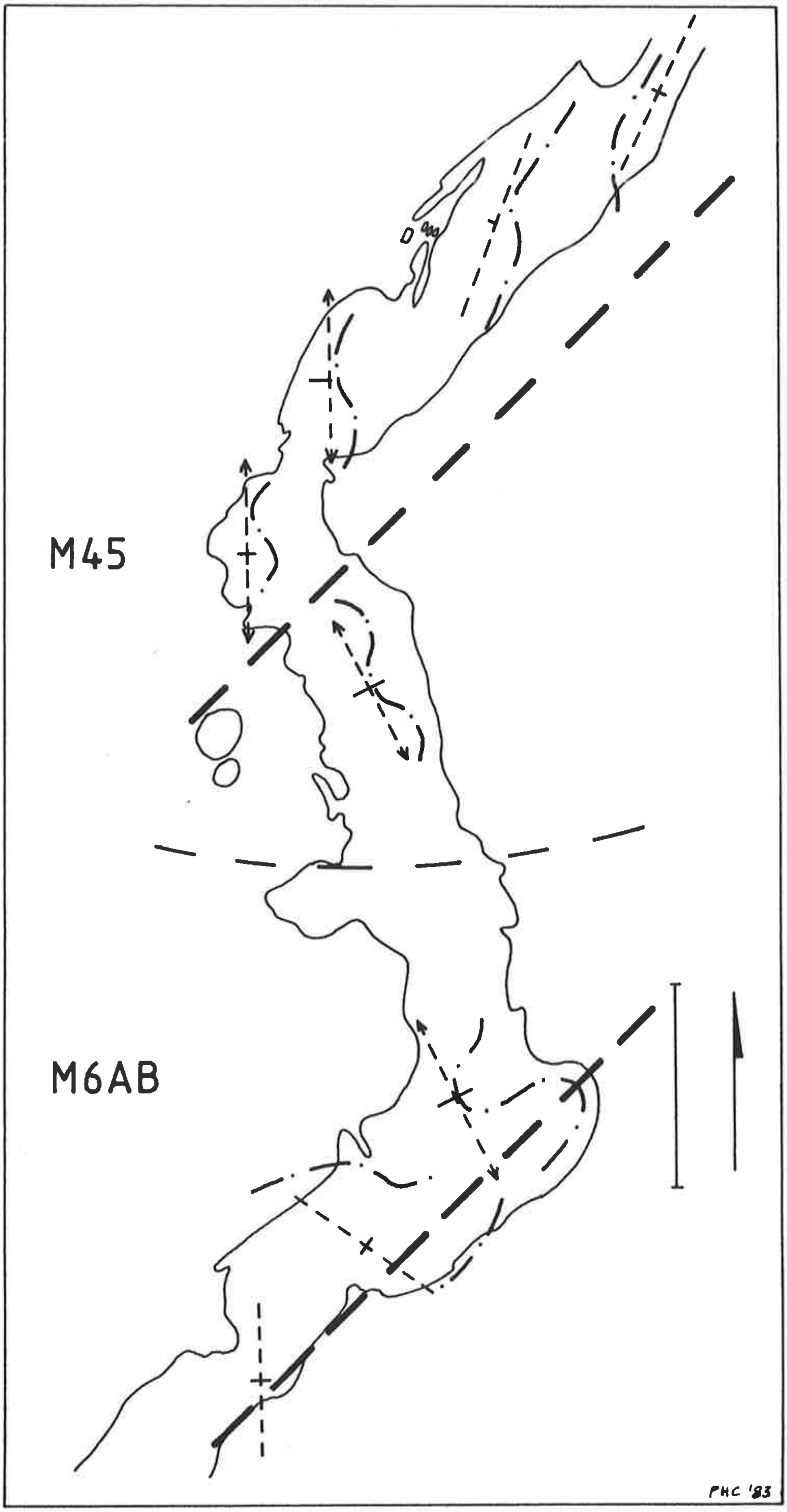

Fig. 7.19 Schematic interpretation of the D_2 structures in submaps M45 and M6AB. Refer to Fig. 7.11 for the meaning of symbols.

Fig. 7.20 Views of the massive granitic augen gneisses in the southern portion of submap M6AB.

a) View looking southwest showing F_3 folds and their fold envelope. Inset is enlarged in (b). Nearest headland above inset is the north shore of submap M912 and the next visible headland is the south end of the beach at Lipson Cove. Scale bar is approximately 3m.
(Location 1291,1680 - Sheet 2)

b) Enlargement of inset in (a), showing layering (layers 'A' to 'D') and strain variation in the gneisses. (Layers 'A' to 'C' show a stronger fabric, S_1, portrayed by flattened augen, than does 'D'.) Scale bar is 40cm.

c) View looking northwest showing complex structures in the augen gneisses highlighted by small biotite gneiss layers. Complexity is caused by small angles (less than 45°) between F_2 and F_3 axial traces (see text). A D_3 crenulation cleavage, S_3, occurs in the biotite layers. Scale bar is 1m. (Location 1265,1662 - Sheet 2).

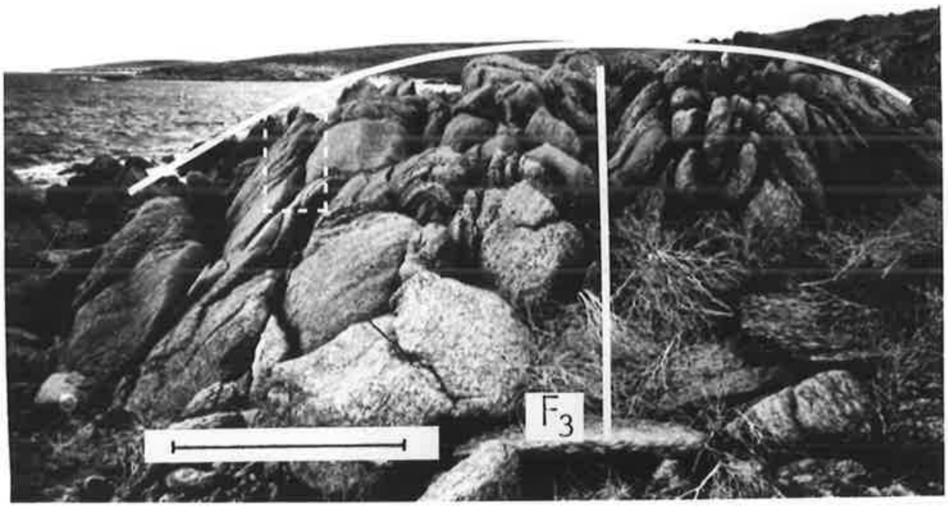
F3

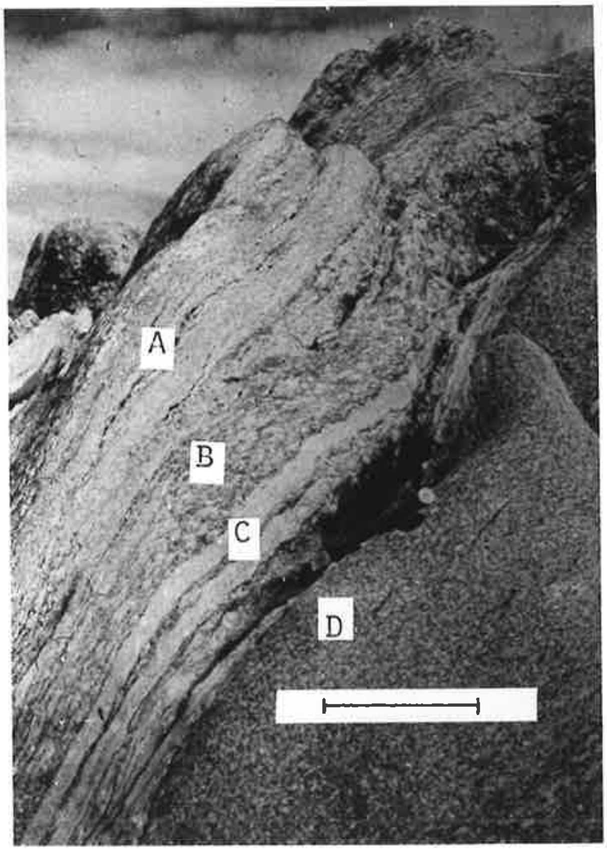
A
B
C
D

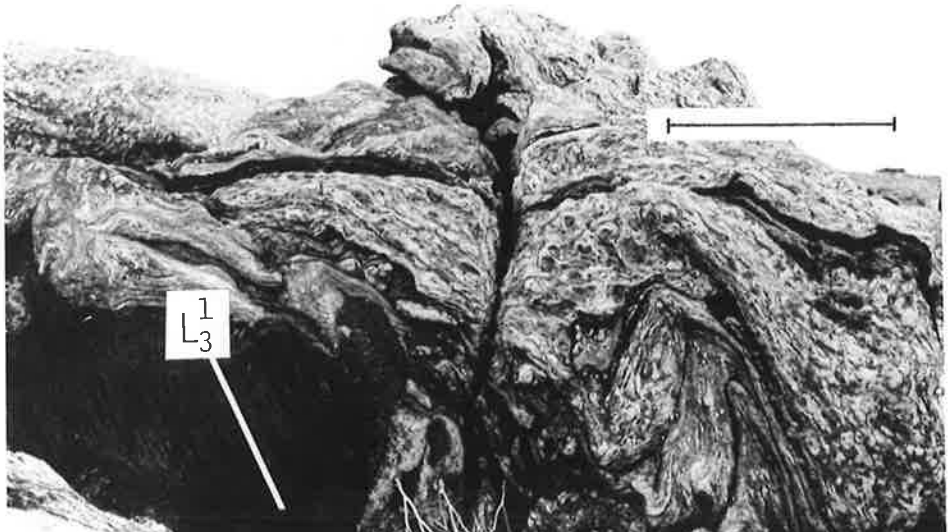
L_3^1

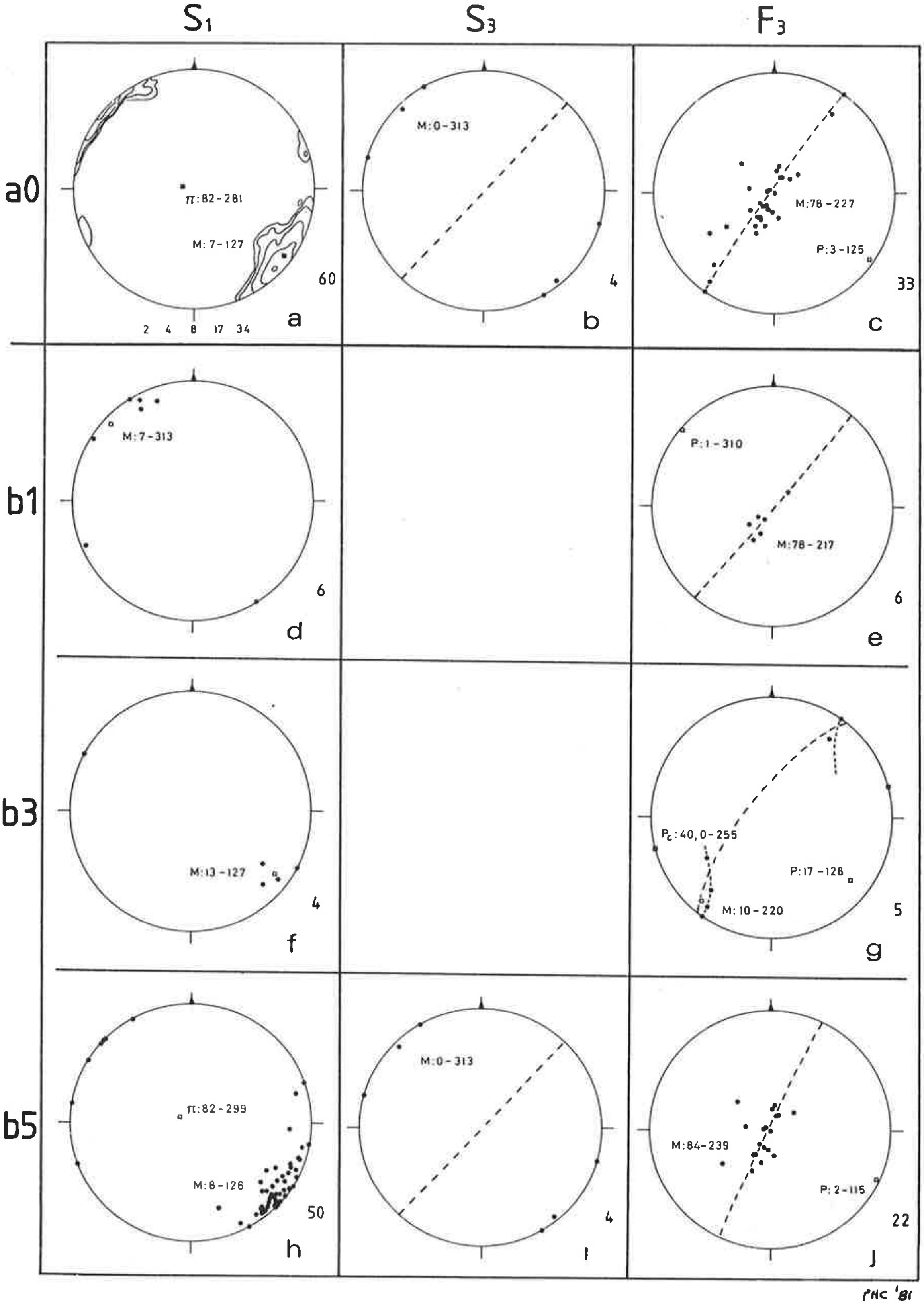

Fig. 7.21 Stereoplots of structural domains for Submap M6AB in Geology Sheet 2.

Fig. 7.22 Structural data maps for Geology Sheet 3.

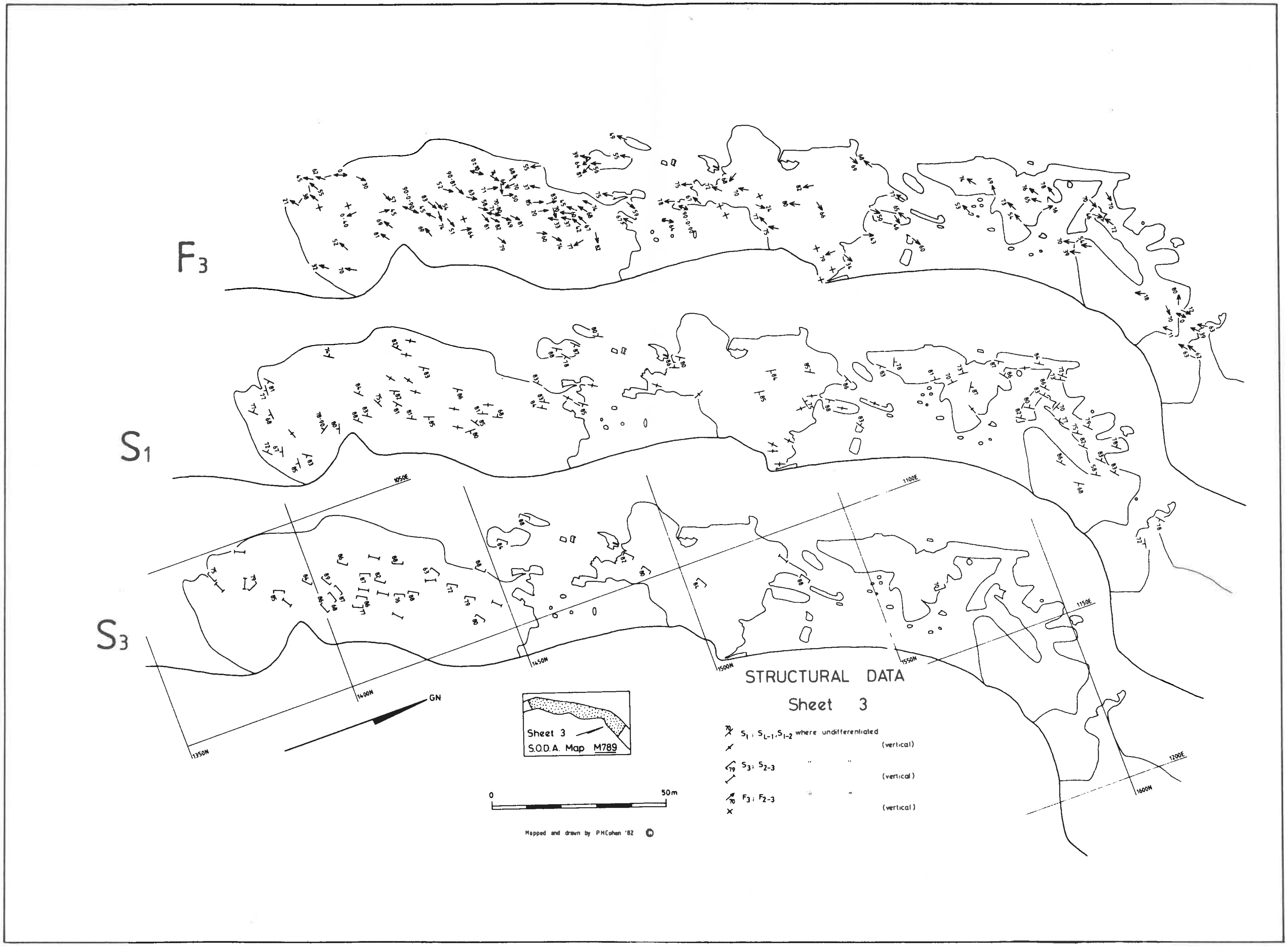
F3
S1
S3
STRUCTURAL DATA
Sheet 3
Sheet 3
S.O.D.A. Map M789
GN
1050E
1100E
1150E
1200E
1350N
1400N
1450N
1500N
1550N
1600N
S1 ; SL-1, S1-2 where undifferentiated
(vertical)
S3 ; S2-3
(vertical)
F3 ; F2-3
(vertical)
0
50m
Mapped and drawn by P.H.Cohen '82 ©

Fig. 7.23 View of F_3 fold (looking southwest) showing variation in granitic gneisses. Scale bar is 1m. (Foreground location 1215,1575 - Sheet 3).

Fig 7.24 a) (Left) View (looking south) of F_2 folds in an amphibolite layer overprinted by D_3. (Location 1058,1373.5 - Sheet 3).

b) (Right) Closeup of (a) near the hammer. S_1 is defined by differentiated layers of hornblende and feldspar and alignment of hornblende and biotite grains (see Fig. V.1, which is a thin-section in plane light from this rock). Small F_2 fold hinges can be seen by the feldspar bands.

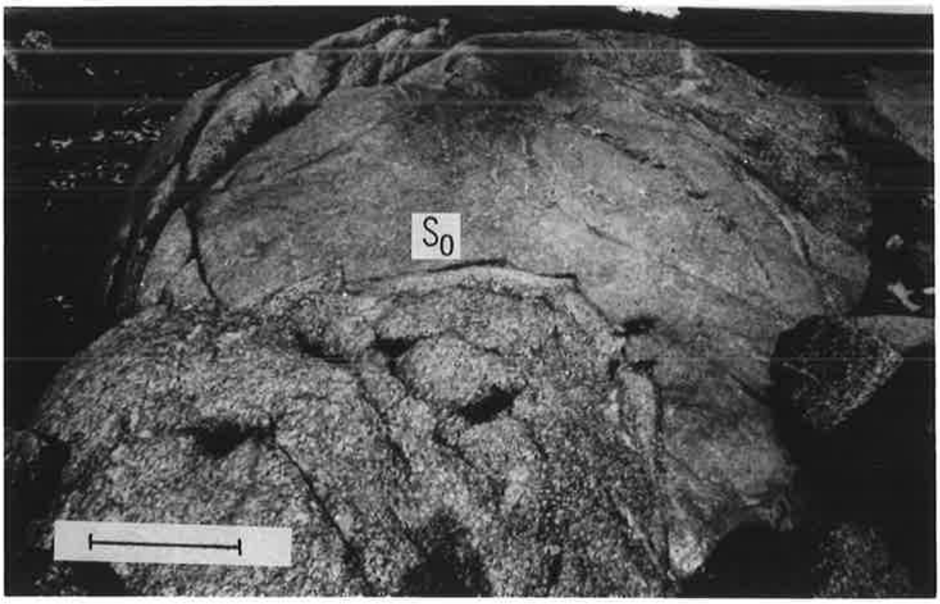
S_0


F_2
F_3
F_2

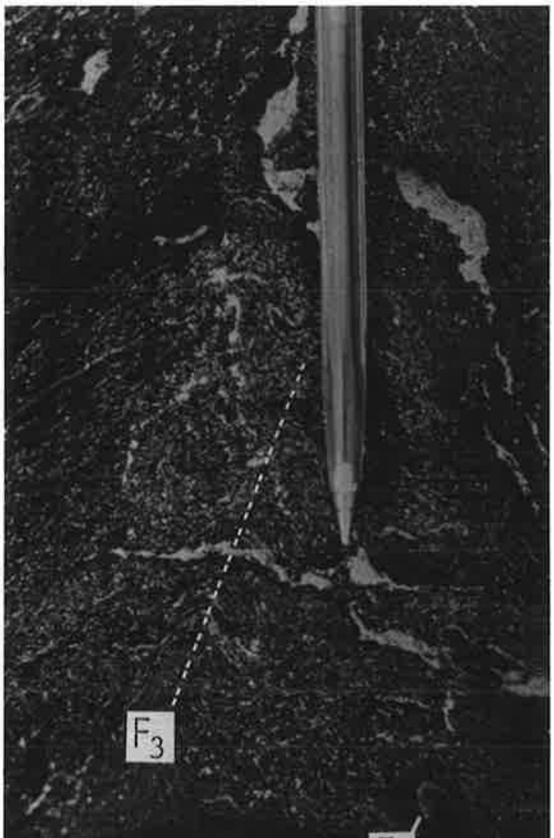
F_3
F_2

Fig. 7.25 Some mesoscopic folds found in submap M789 that are not readily discernable.

a) Isoclinal subhorizontal F_2 fold folding S_{0-1}. Scale bar is 45cm. (Location 1103,1440 - Sheet 3).

b) F_2 fold in amphibolite refolded by F_3. The F_2 fold folds the layer-parallel foliation, S_{0-1}. (Location 1108,1490 - Sheet 3).

c) Complexly folded leuco-granitic gneiss surrounded by amphibolite. This gneiss is related to that shown in Fig. 7.3d. Lens cap is 55mm in diameter. (Location 1095,1471.5 - Sheet 3).

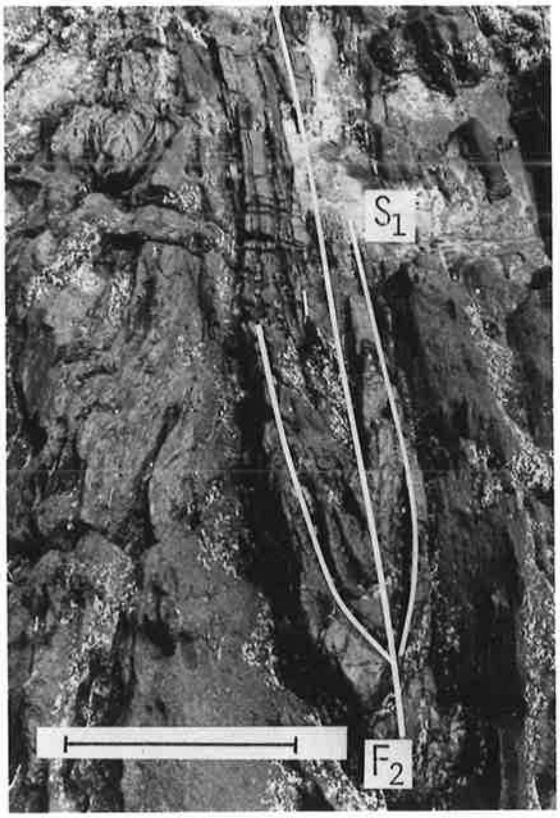
S1
F2

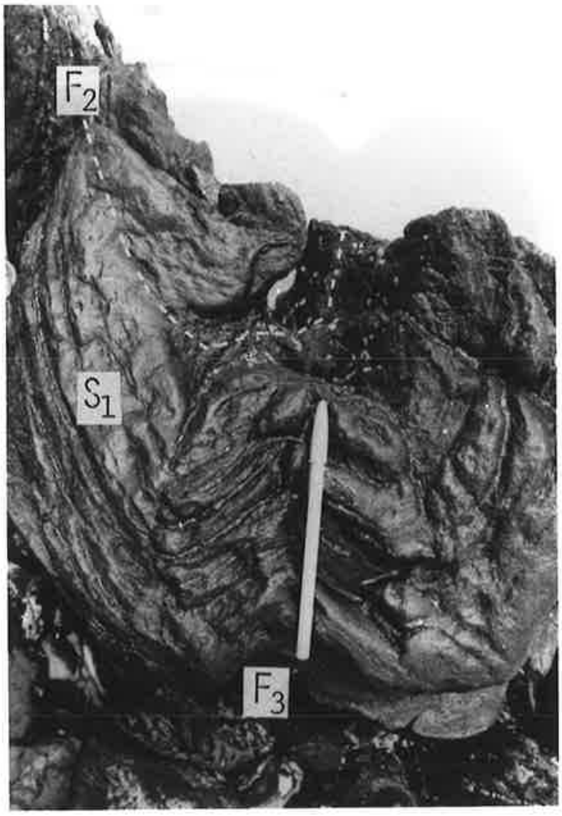
F2
S1
F3

Fig. 7.26 a) Internal very complex folding in a medium-grained granitic gneiss layer (see Fig. 7.Ad) that defines an overall layer concordant with the surrounding amphibolites (see Geology Sheet 3). (Location 1095,1503, looking west - Sheet 3).

b) Detail of in the contact between the layer in (a) and the adjacent massive amphibolite. Scale bar is 10cm.

c) A similar type of vein material to (a) and (b), in the massive amphibolite layer, which was both folded and produced a small axial plane (S_3) vein.
(Location 1103,1505 - Sheet 3).

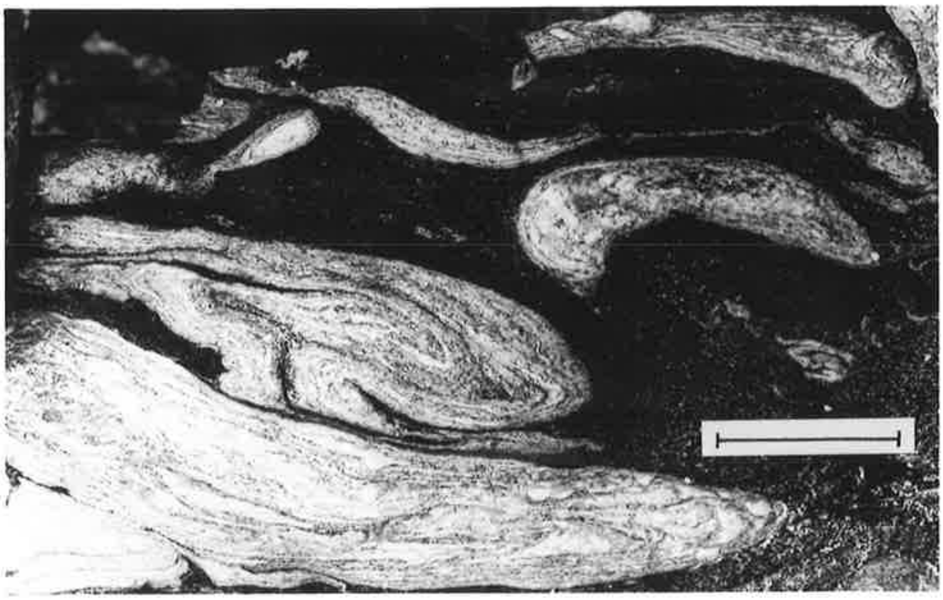

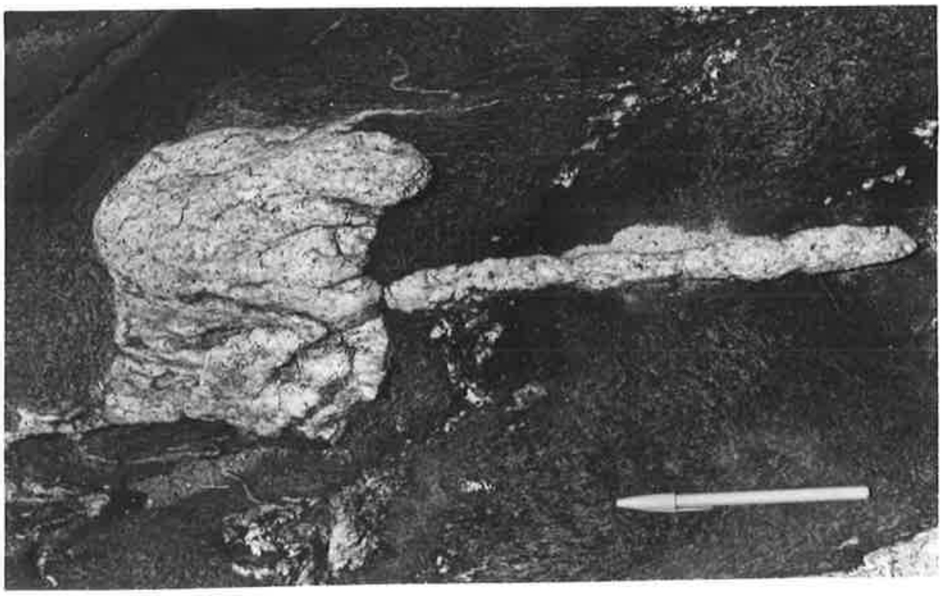

Fig. 7.27 a) A granitic vein containing a layer-parallel foliation is folded by F_2, which is refolded by F_3 (dashed trace is parallel to S_3 defined by the biotite flakes in the surrounding biotite gneiss.
(Location 1066,1392 - sheet 3).

b) Right-hand side view of (a) showing mineral lineation defined by the long axis of biotite flakes in the S_3 schistosity, and the F_2 folds refolded by F_3.

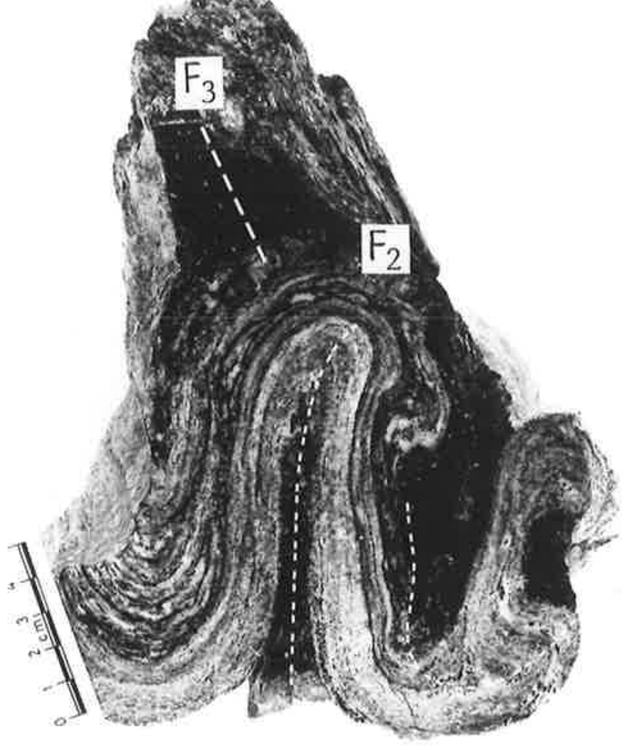
F_3
F_2
cm

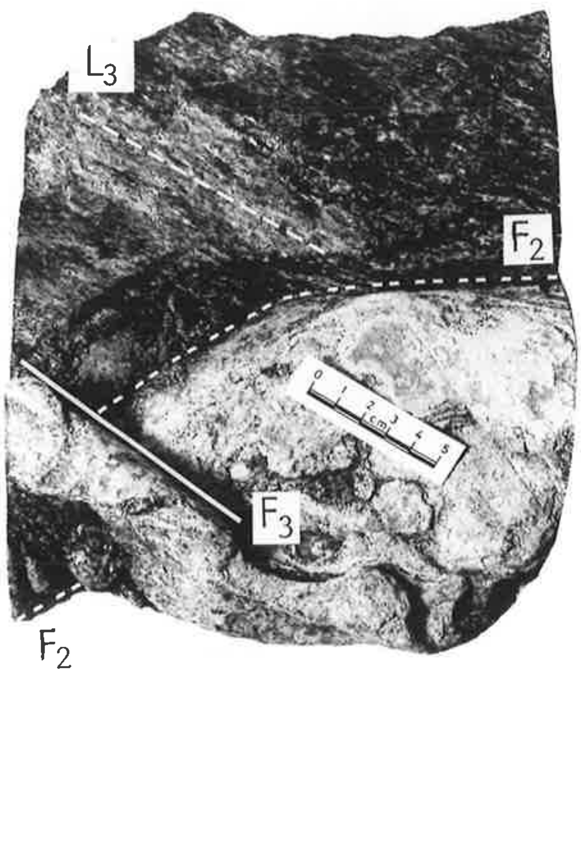
L_3
F_2
cm
F_3
F_2

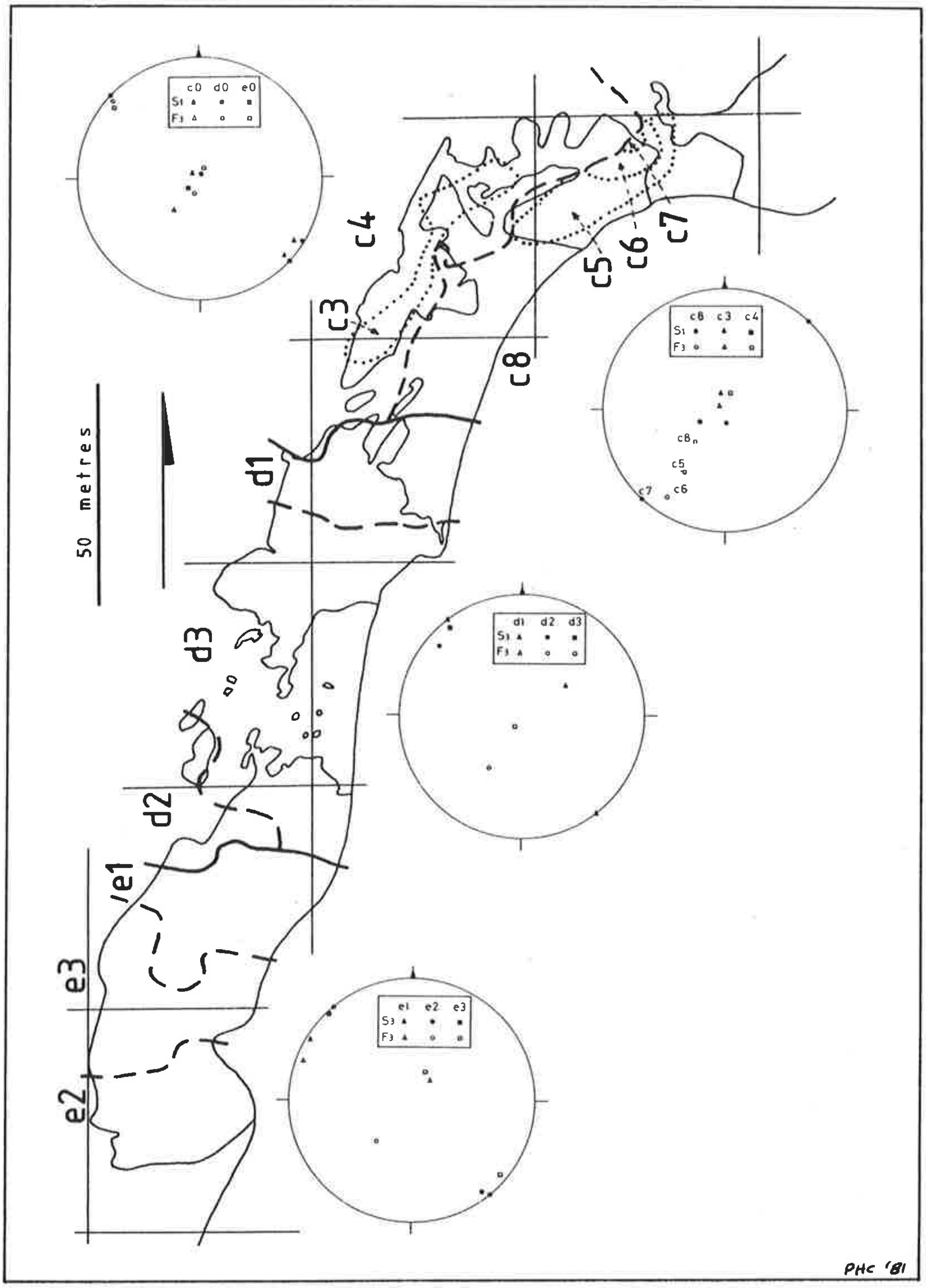

Fig. 7.28 Structural domains of Geology Sheet 3 (Submap M789).
a0 = c0 + d0 + e0, c0 = c1 + c2 (c1 = c5 + c6 + c7 + c8; c2 = c3 + c4), d0 = d1 + d2 + d3, e0 = e1 + e2 + e3
Synoptic stereonets from Fig. 7.29.

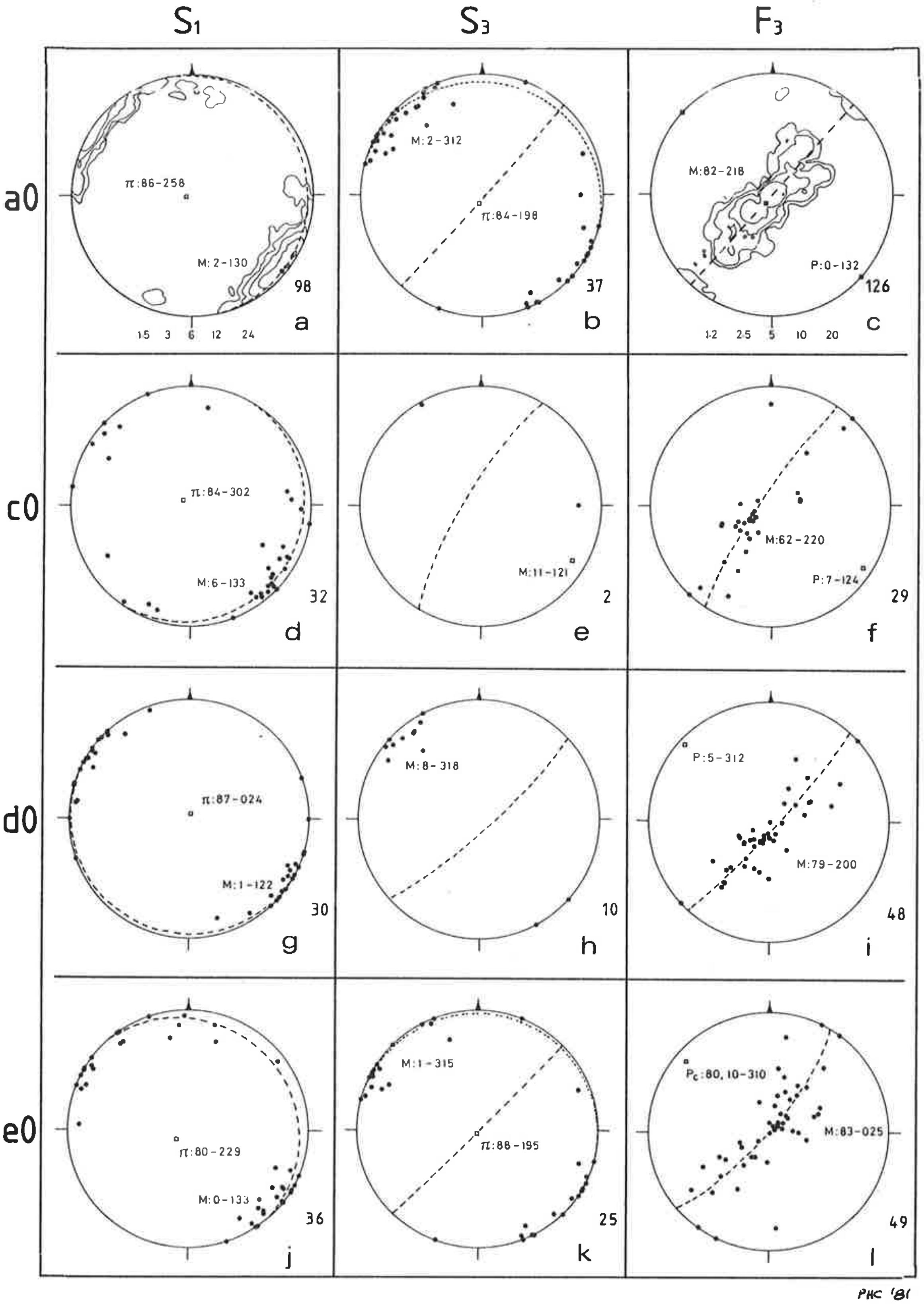

A

Fig. 7.29 Stereoplots of structural domains for Geology Sheet 3. (A) Primary domains; (B) Secondary and tertiary domains of c0 (overleaf); (C) Secondary domains of d0 and e0 (overleaf from (B)).

(Continued)

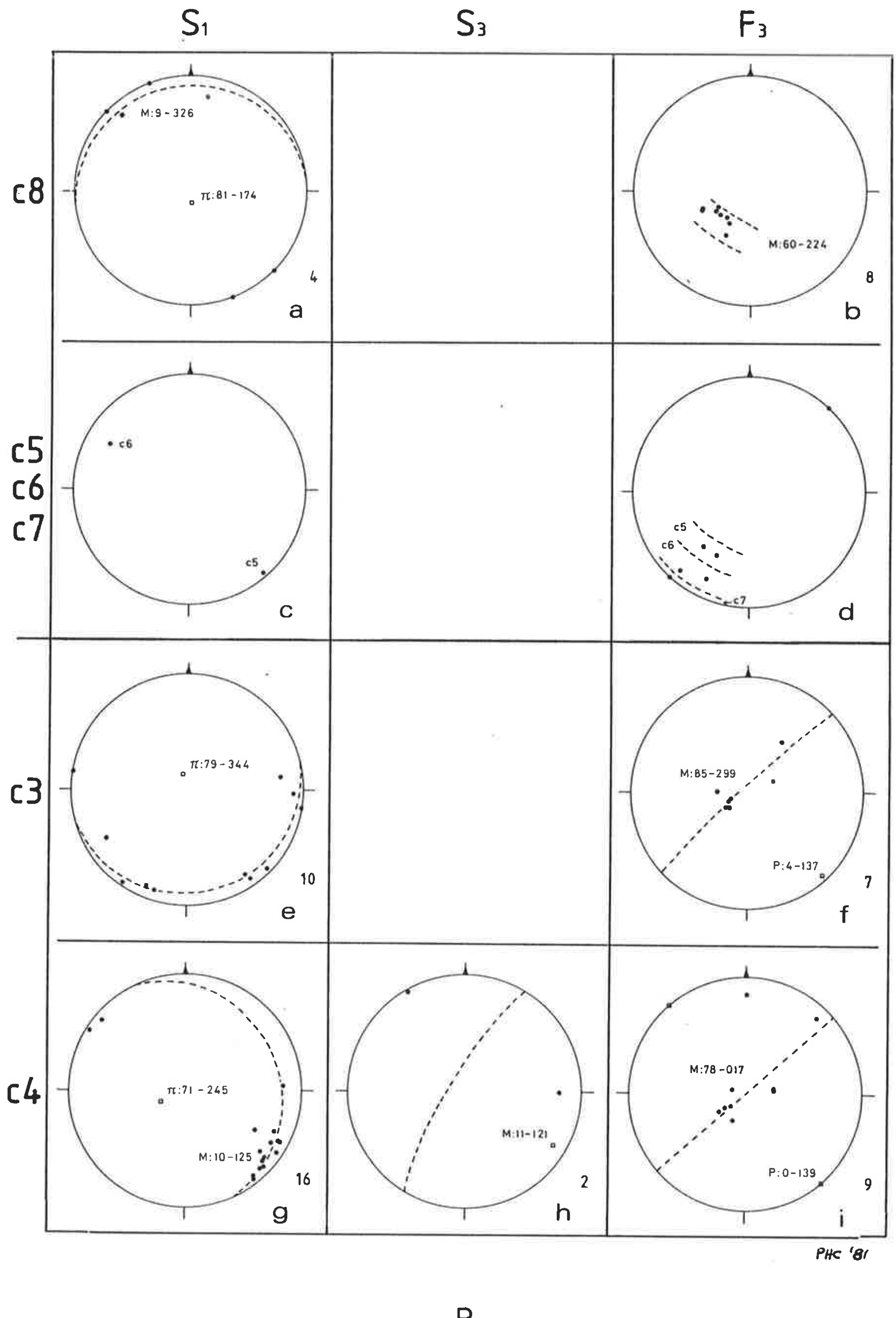
S1
S3
F3
c8
M:9-326
π:81-174
4
a
M:60-224
8
b
c5
c6
c7
c6
c5
c
c5
c6
c7
d
c3
π:79-344
10
e
M:85-299
P:4-137
7
f
c4
π:71-245
M:10-125
16
g
M:11-121
2
h
M:78-017
P:0-139
9
i
PHC '81
B

Fig. 7.29 (Cont.)

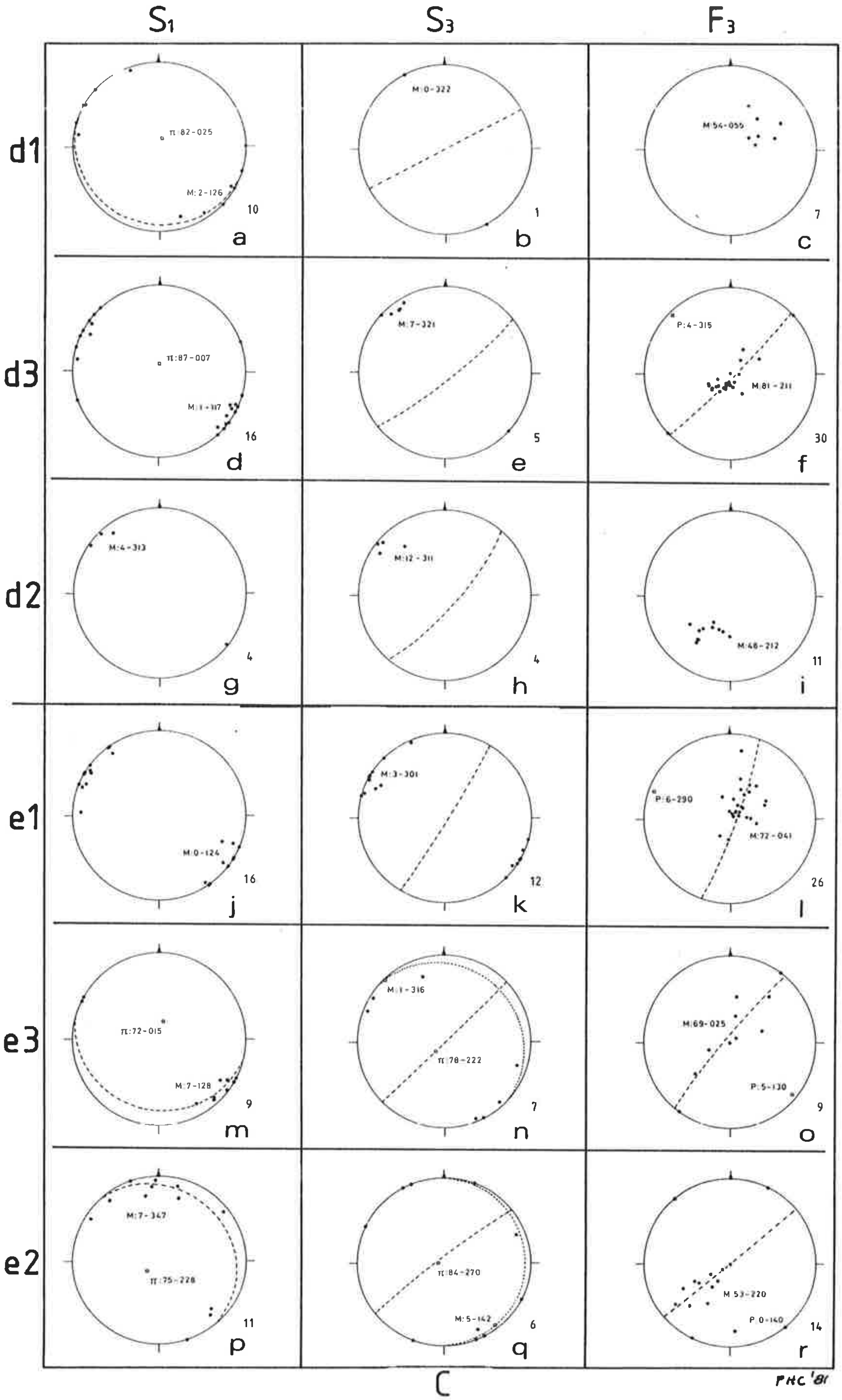
S1
S3
F3
d1
d3
d2
e1
e3
e2
π:82-025
M:2-126
10
a
M:0-322
1
b
M:54-055
7
c
π:87-007
M:1-317
16
d
M:7-321
5
e
P:4-315
M:81-211
30
f
M:4-313
4
g
M:12-311
4
h
M:48-212
11
i
M:0-124
16
j
M:3-301
12
k
P:6-290
M:72-041
26
l
π:72-015
M:7-128
9
m
M:1-316
π:78-222
7
n
M:69-025
P:5-130
9
o
M:7-347
π:75-228
11
p
π:84-270
M:5-142
6
q
M:53-220
P:0-140
14
r
C
PHC '81

Fig. 7.29 (Cont.)

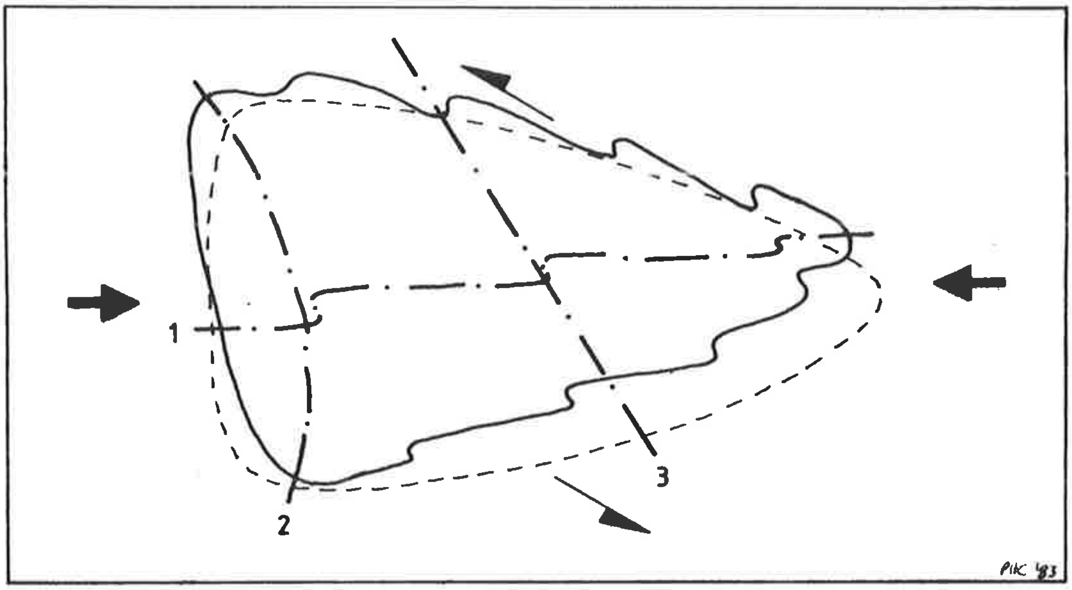

Fig. 7.30 Schematic model demonstrating how two apparent folding events can arise from the one generation of deformation. Given an initial folding event (1), compressional strains will produce cross- folds (2), giving rise to a hybrid 'dome-and-basin'/ luniform interference pattern. Shearing strains of the same deformation can then refold the figure (3) (see Fig. 7.31).

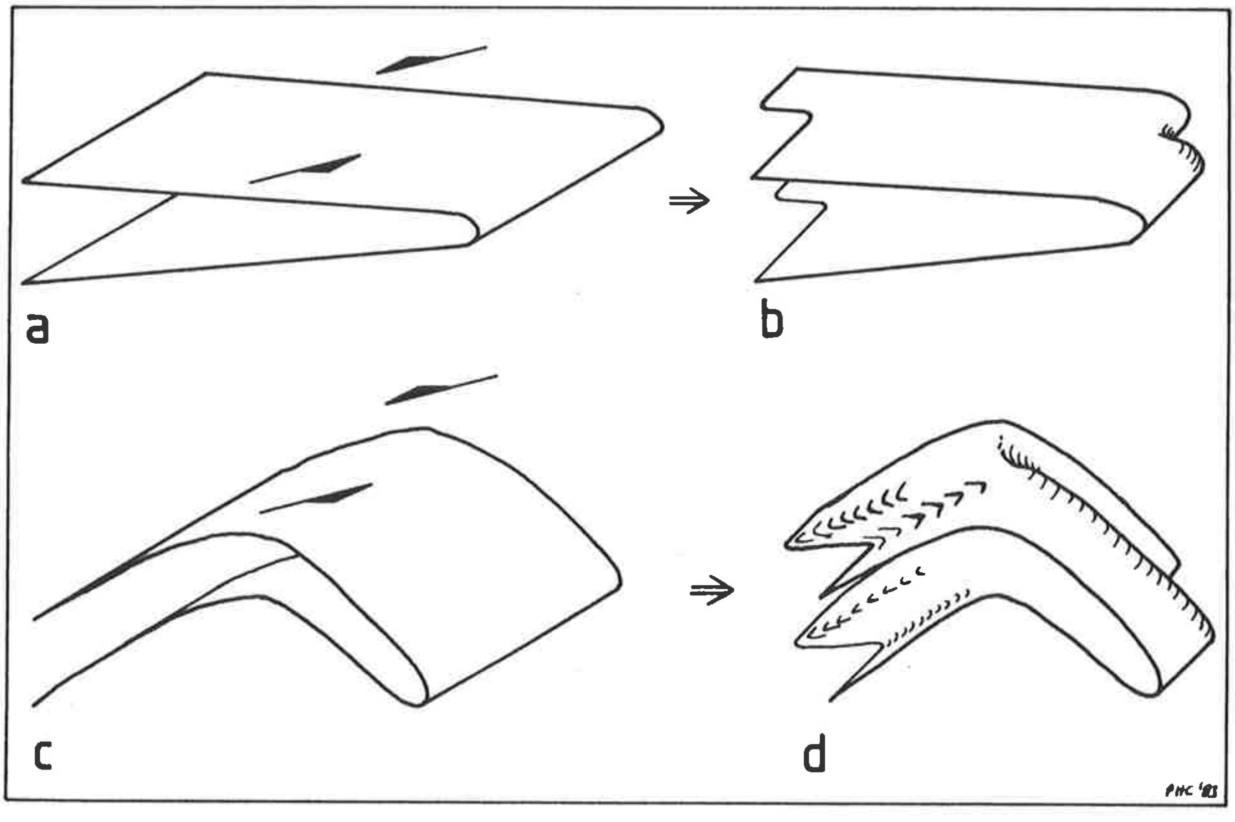

Fig. 7.31 Model showing that shearing stresses on reclined to recumbent folds only appear after considerable folding by the compressional component. Shearing of (a) produces little visible effect (b), but an initial refolding by compression (c) will cause a better expression of the shearing component (d).

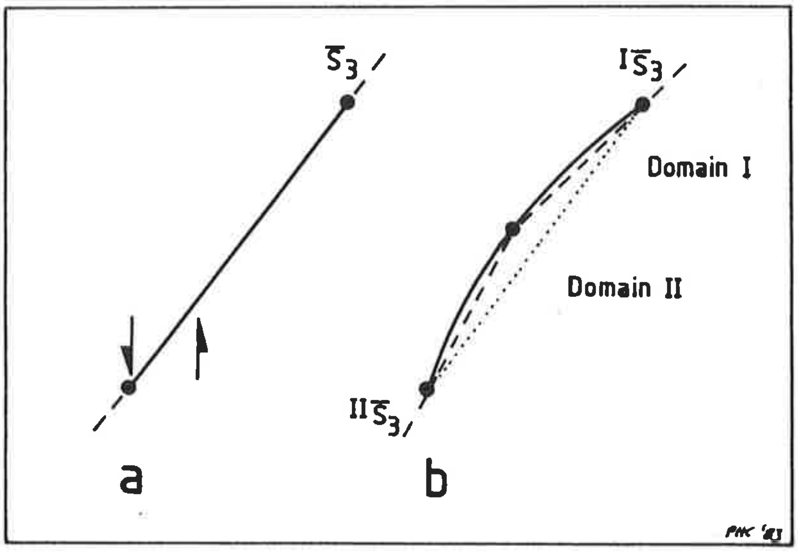

Fig. 7.32 Model to demonstrate how effective sinistral shearing in only part of an area will give rise to a dextral rotation in adjacent areas. The mean F_3 axial plane in (a) is sheared in a small part of the region considered. The result is that the region can be subdivided into two domains (I) and (II), with domain I having a mean S_3 dextrally rotated from the regional mean, and domain II shows a sinistral rotation of the mean S_3.

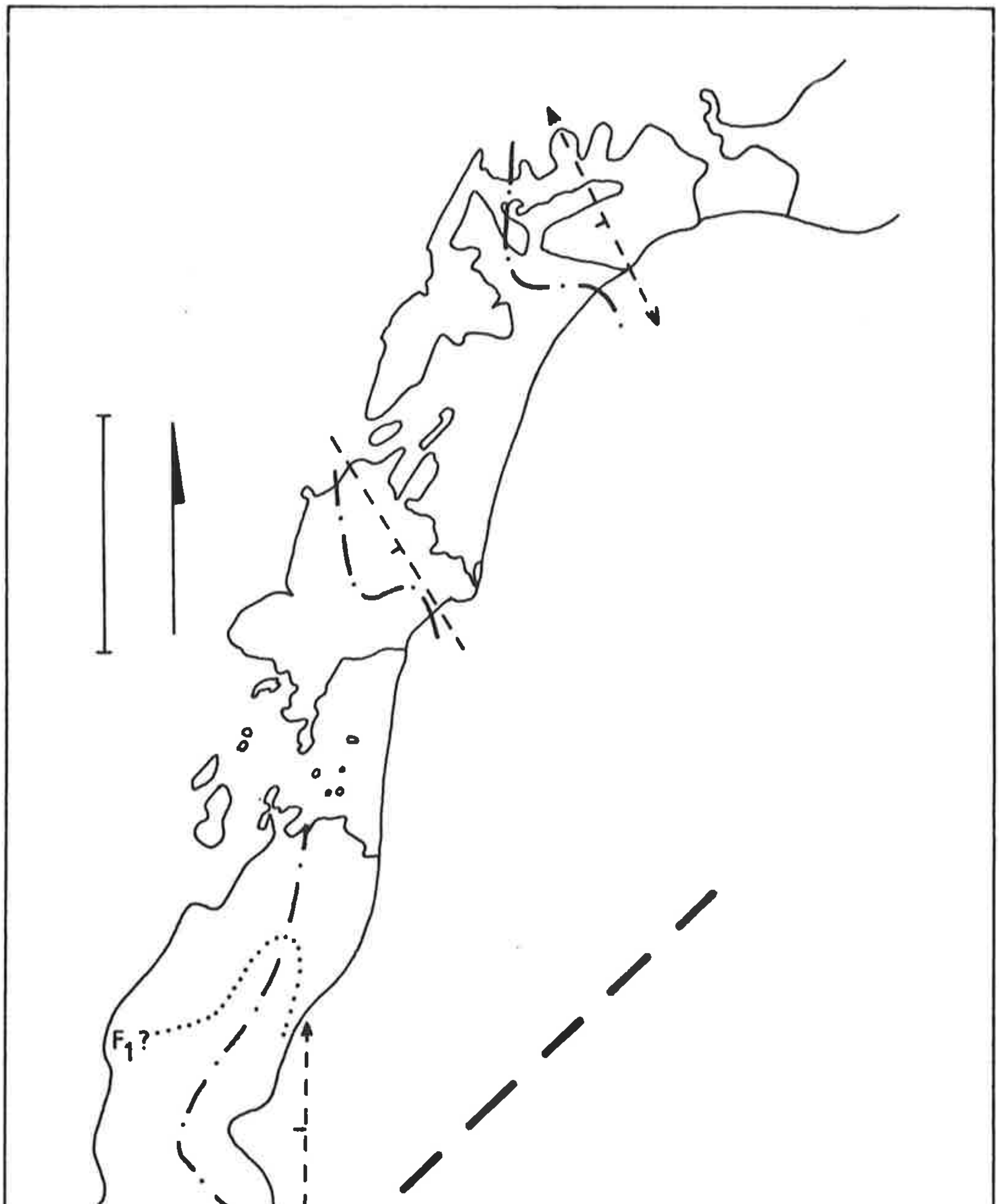

Fig. 7.33 Schematic interpretation of the D_2 structures in submap M789. Refer to Fig. 7.11 for the meaning of symbols.

Fig. 7.34 Structural data maps for Geology Sheet 4.

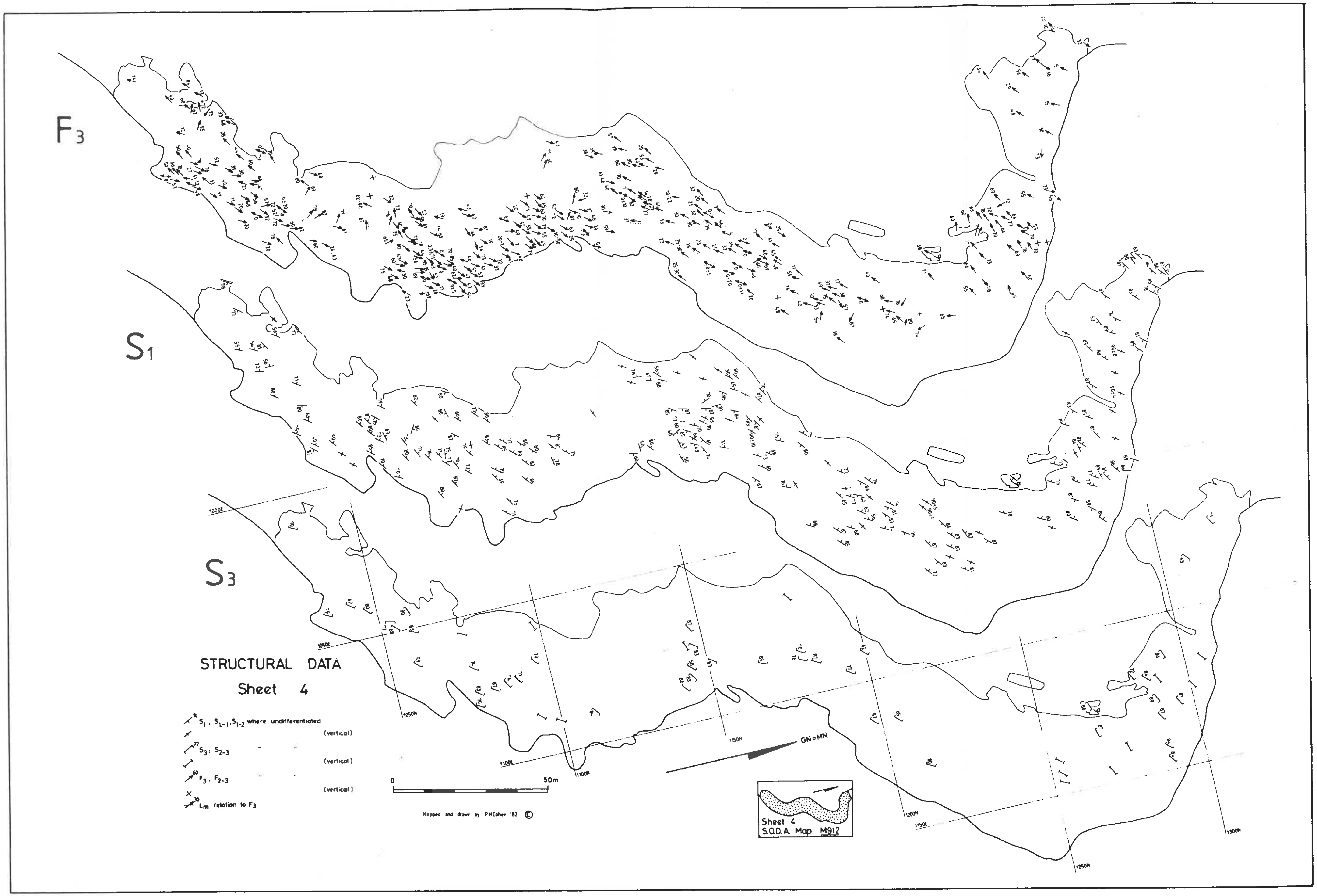
F3
S1
S3
STRUCTURAL DATA
Sheet 4
S1 . SL-1 , S1-2 where undifferentiated
(vertical)
S3 ; S2-3
(vertical)
F3 . F2-3
(vertical)
Lm relation to F3
0
50m
Mapped and drawn by P.H.Cohen '82 ©
GN=MN
Sheet 4
S.O.D.A. Map M912
1000E
1050E
1100E
1150E
1050N
1100N
1150N
1200N
1250N
1300N

Fig. 7.35 Examples of refolded folds from submap M912.

a) (Left) Type 3 fold of Ramsay (1967) in augen gneiss. Scale bar is 6cm. (Location 1120,1290, looking northwest - Sheet 4).

b) (Right) Variable plunges of F_{2-3} folds in augen gneiss. Scale bar is 50cm. (Location 1081,1124, looking southeast - Sheet 4).

c) Similar situation to (b). Scale bar is 20cm. (Location 1083,1176, looking east - Sheet 4).

d) Triangular (Ramsay type 2) interference pattern in granitic gneisses. Lens cap is 55mm in diameter. (Location 1060,1030 - Sheet 4).

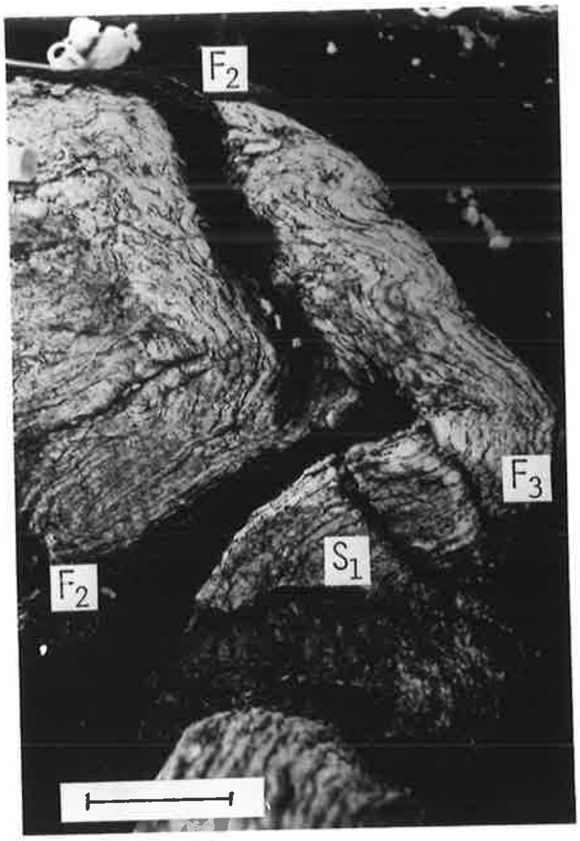
F_2
F_3
S_1
F_2

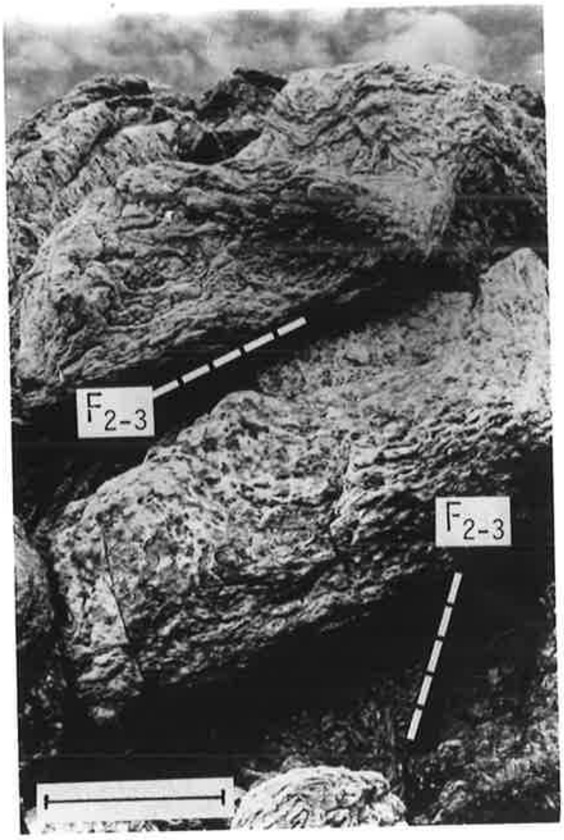
F_{2-3}
F_{2-3}

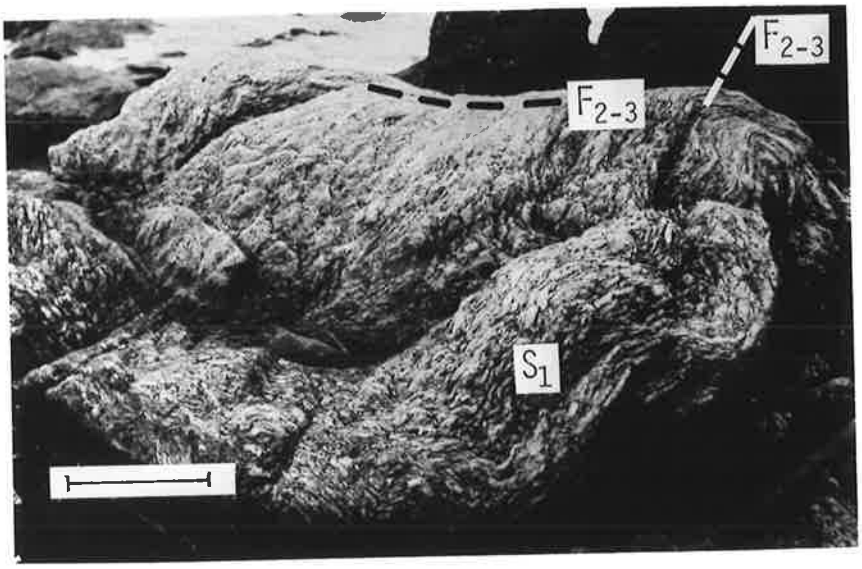
F_{2-3}
F_{2-3}
S_1

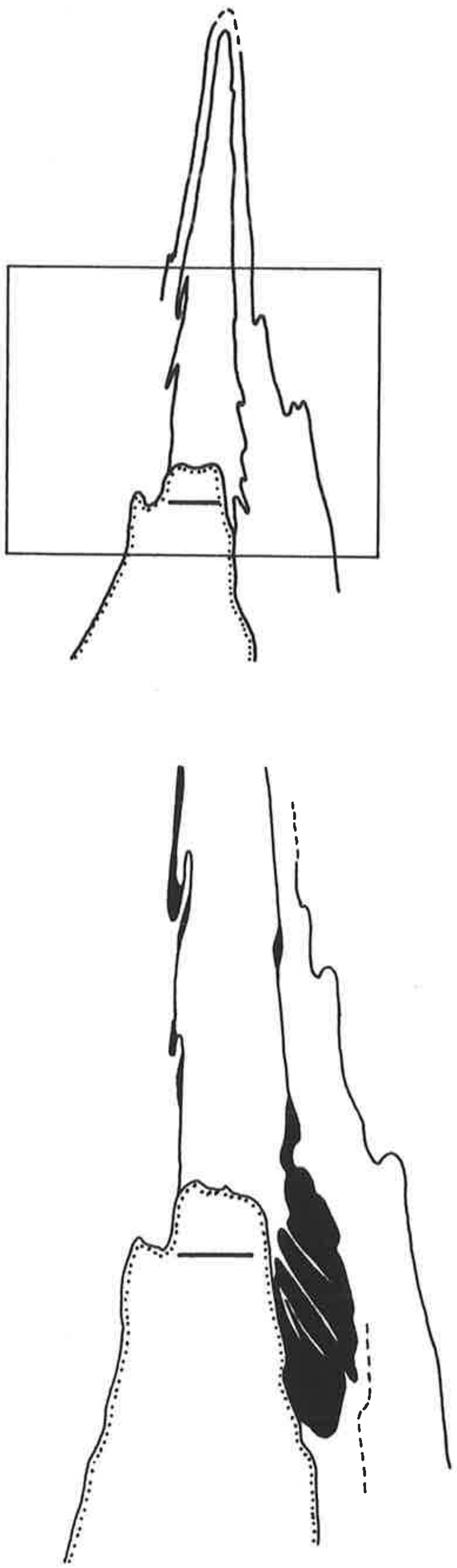

a

b

Fig. 7.36 Sketch from a photograph of an example of a tightly folded quartz ribbon in an amphibolite that has an intense layer-parallel foliation, S_1. The quartz ribbon shows dextral minor folds on the sinistral limb and sinistral minor folds on the dextral limb. A parallel quartz ribbon (which could be the same one) shows the correct sense of vergence on each limb. (Location 1002,1033).

Fig. 7.37 Examples of curved fold hinges and lineations caused by near coaxiality between D_2 and D_3 in submap M912.

c) (Left) Side view of folded quartz veins in biotite gneiss. F_2 folds defined by quartz veins are overprinted by F_3, showing both gently curved F_2 and intensely curved F_3 fold hinges. D_3 produced a mineral lineation defined by the long axes of biotite flakes in the S_3 schistosity, defined by alignment of biotite and quartz ribbons and veins.
(Location 1062,1065 - Sheet 4).

d) (Right) Top view of (c).

a) Curved intersection lineation between S_1 and surface approximately parallel to F_3 axial plane.
(Location 1055,1059 - Sheet 4).

b) Similar situation to (a) except in augen gneiss.
(Location 1087,1180 - Sheet 4).

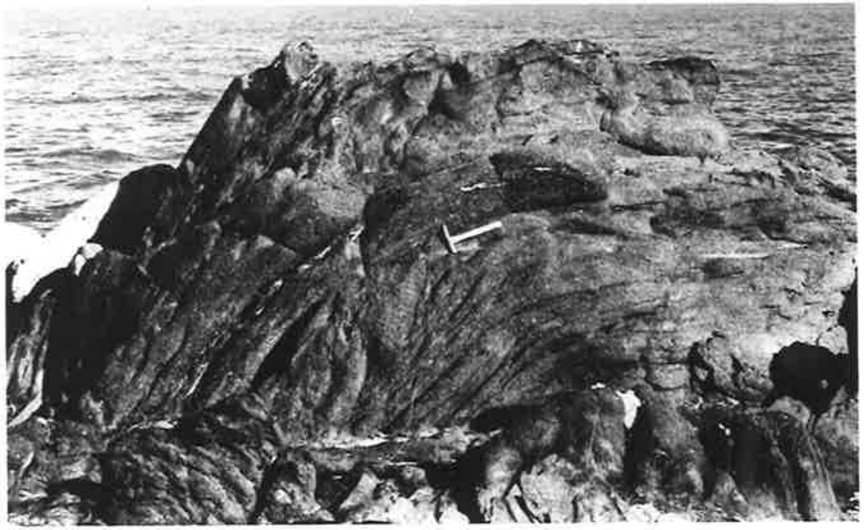

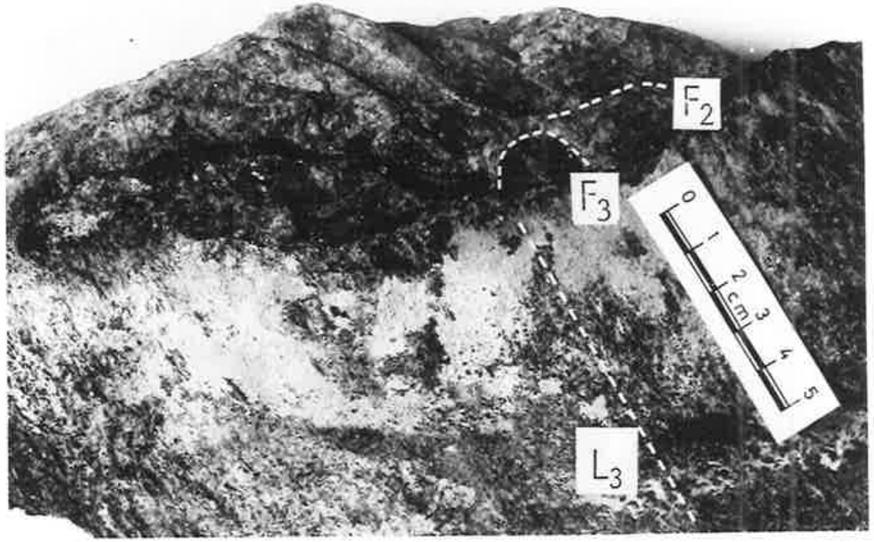
F2
F3
0 1 2 cm 3 4 5
L3

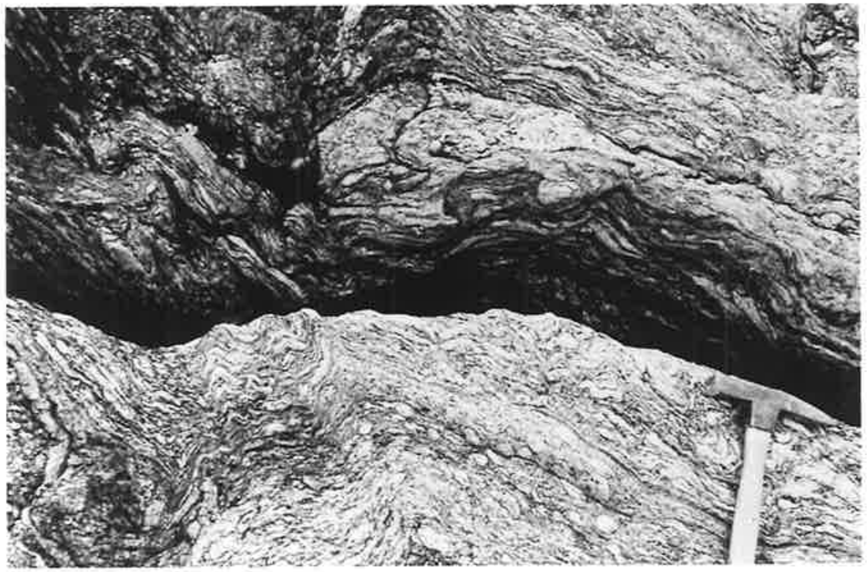

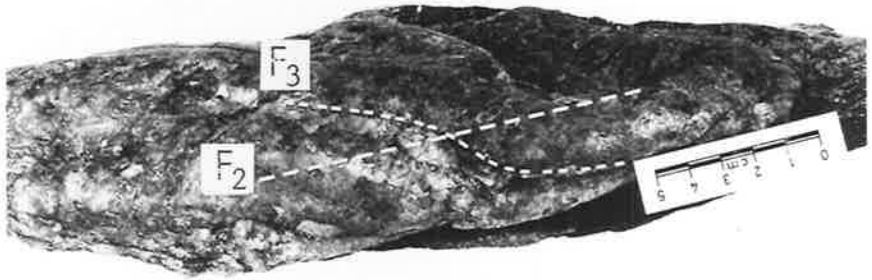
F3
F2
5 4 3 cm 2 1 0

Fig. 7.38 a) A locally horizontal F_3 fold in augen gneiss folding a first generation mineral elongation lineation. Scale bar is 9cm.
(Location 1075,1140 - Sheet 4).

b) Profile of the fold in (a), taken from the left-hand side of (a). F_3 is upright and folds an F_2 fold that has a subhorizontal fold hinge (not shown). The flattened augen define an S_{0-1} foliation. Scale bar is 55mm.

c) Thin-section (in plane light) of augen gneiss from (b) showing folded augen. The augen consist primarily of equigranular feldspar with recrystallised biotite parallel to S_{2-3}, and quartz (less than 5%) between augen. Two populations of biotite grains exist between augen, those defining S_1 and those recrystallised to S_{2-3}. The latter grains are larger than those within the augen. Scale bar is 15mm.


F3
L1

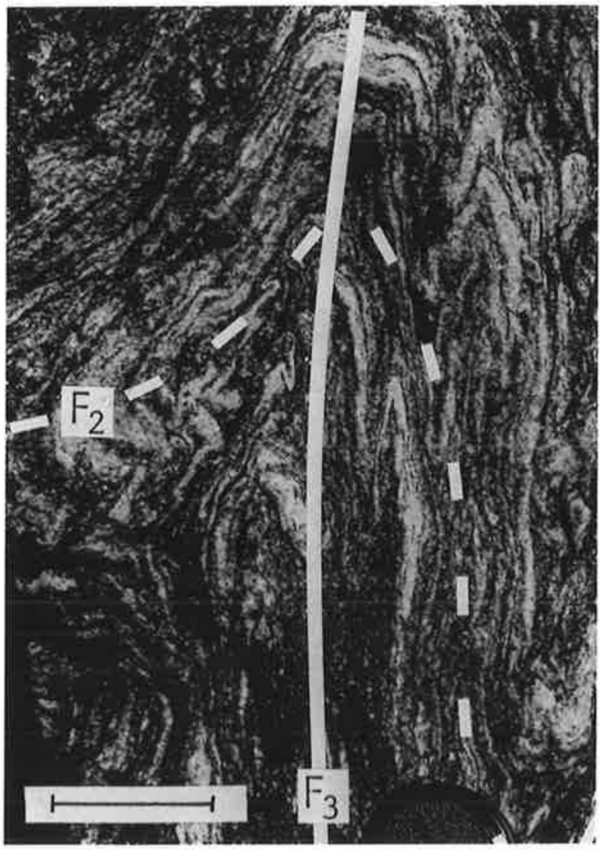
F2
F3

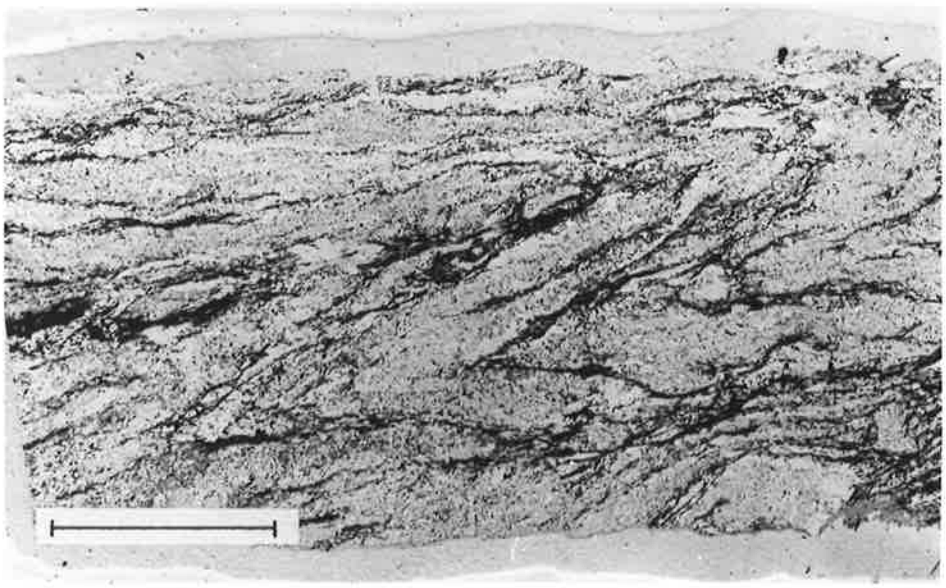

Fig. 7.39 a) View looking northeast of a basin structure in an augen gneiss in the interlayered zone north of the embayment (see Geology Sheet 4). The F_2 fold plunges northeast in the foreground, is horizontal in the inset outlined, and plunges southwest further to the northeast. Inset is enlarged in (b).
(Foreground location 1114.5,1212 - Sheet 4).

b) Enlargement of inset in (a), showing D_2 folding of layer-parallel foliation, S_{0-1} (see (c)). A prominant S_{2-3} cleavage was developed due to the near coaxiality of the two deformations (D_2 and D_3) at this point (the section is on the limb of an F_3 fold).
(Location 1121,1218).

c) Sketch of (b). Scale bar is lm.

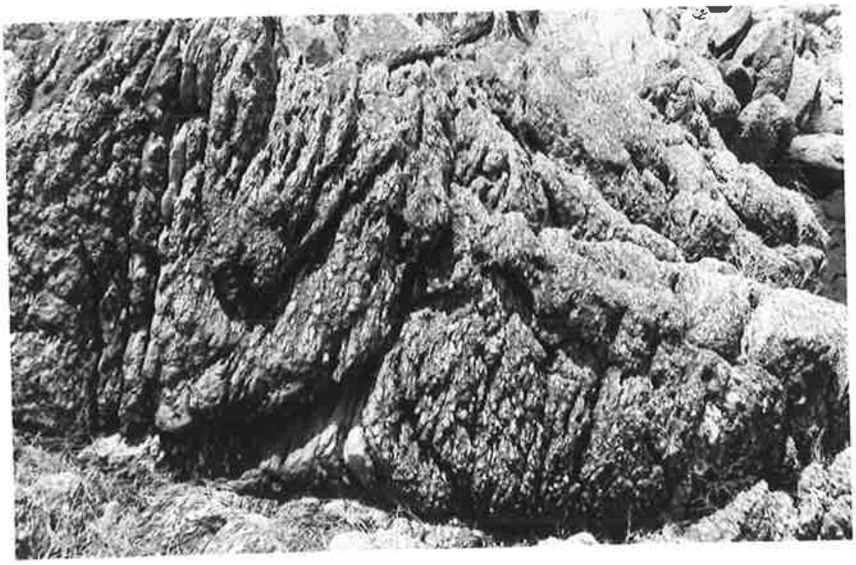

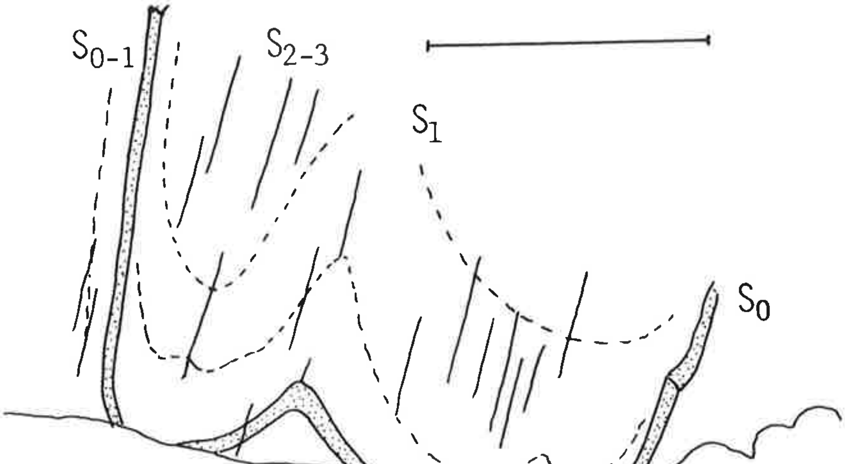

S0-1
S2-3
S1
S0

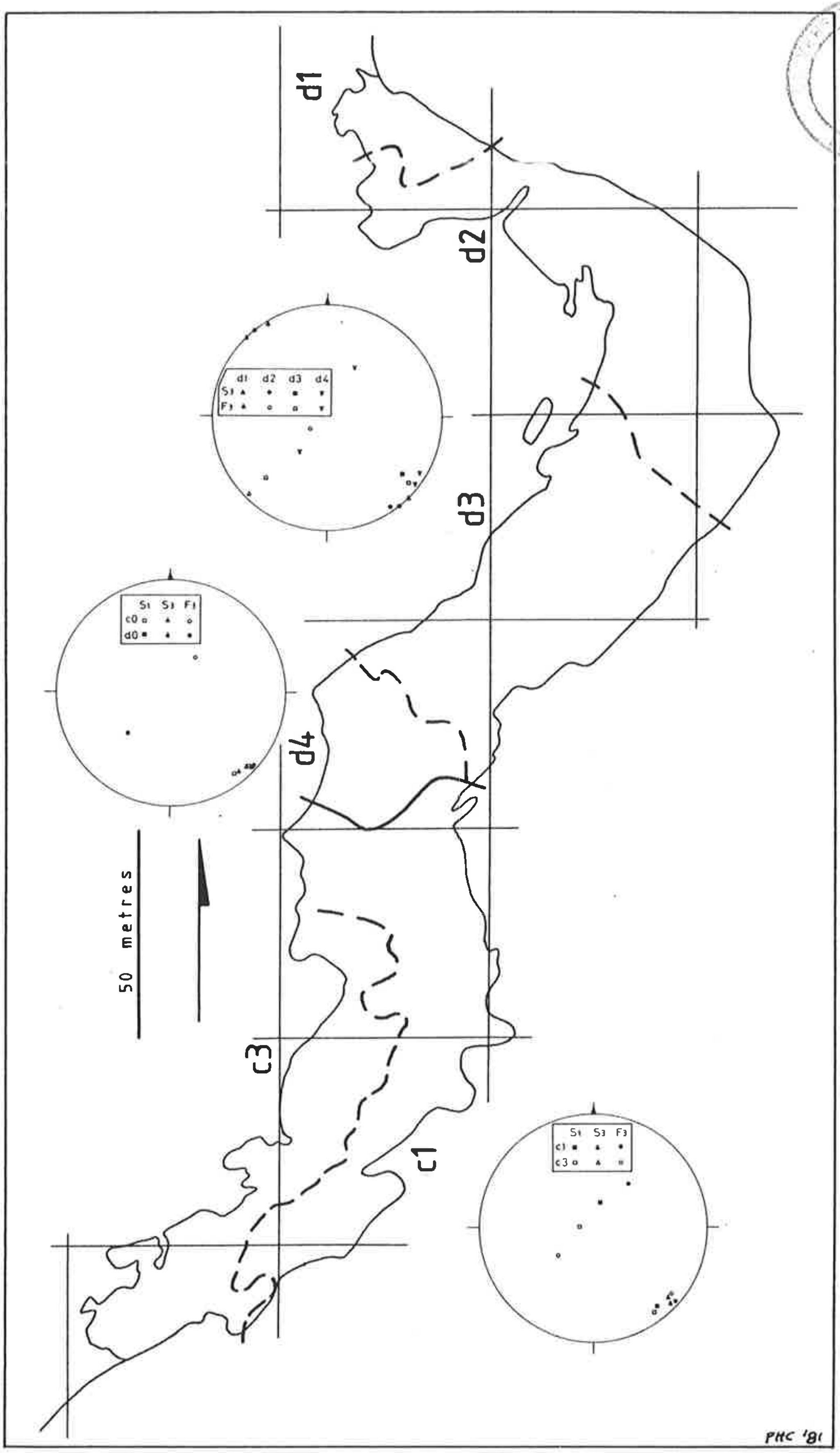

Fig. 7.40 Structural domains of Geology Sheet 4 (Submap M912).
a0 = c0 + d0 , c0 = c1 + c3, d0 = d1 + d2 + d3 + d4.
Synoptic stereonets from Fig. 7.41.

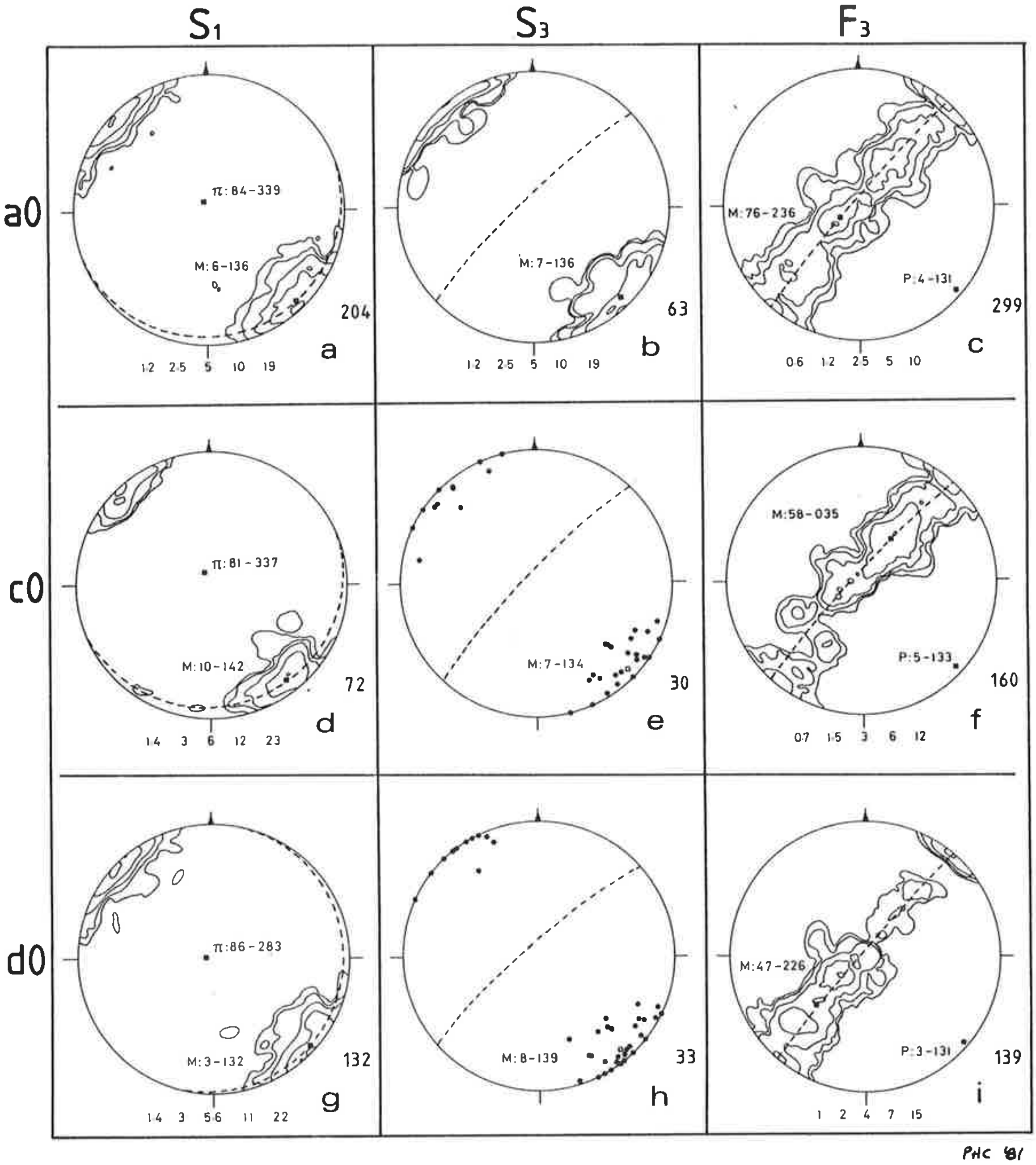

A

Fig. 7.41 Stereoplots of structural domains for Geology Sheet 4. (A) Primary domains; (B) Secondary domains (overleaf).

(Continued)

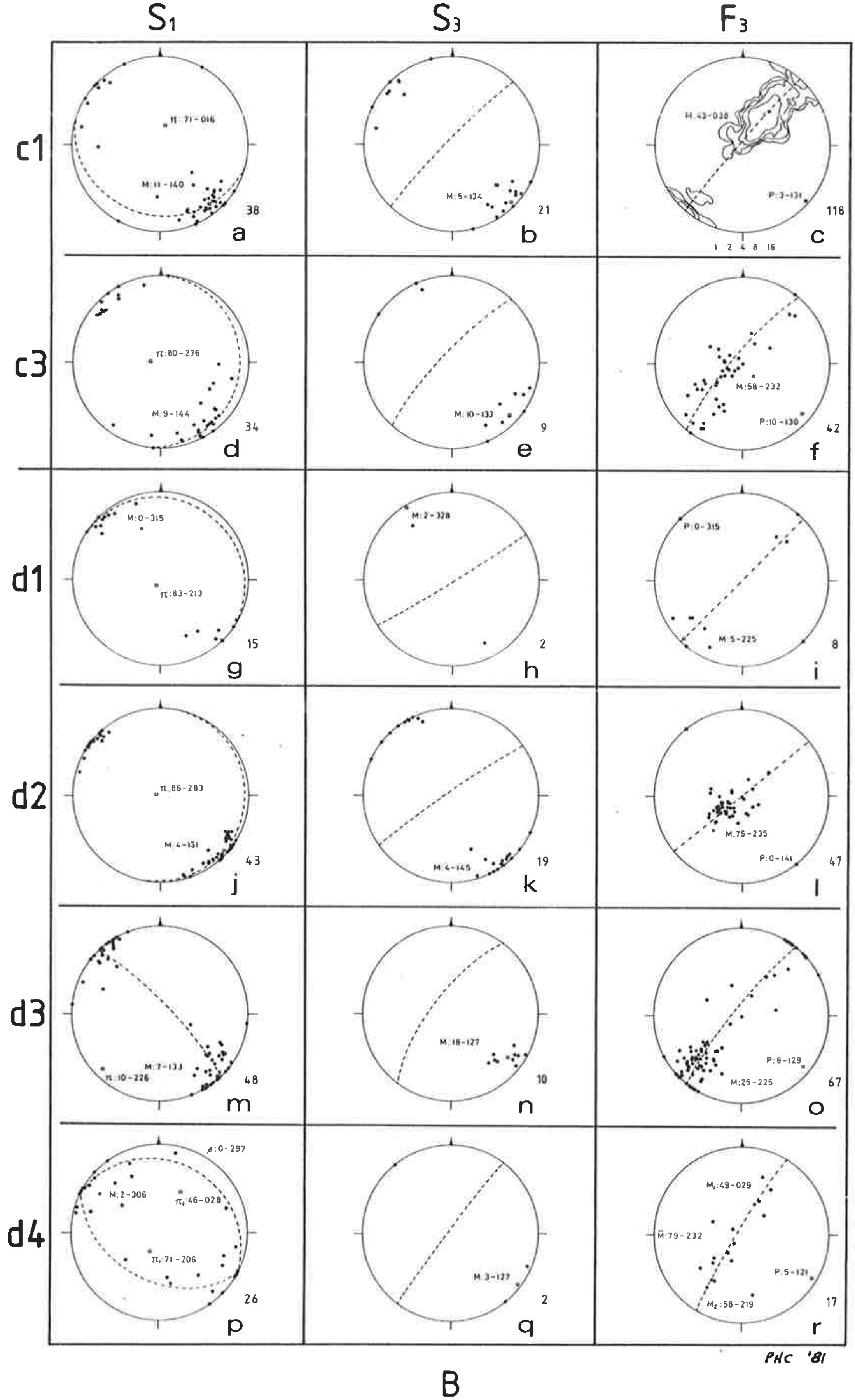

S1
S3
F3
c1
c3
d1
d2
d3
d4
π:71-016
M:11-140
38
a
M:5-134
21
b
M:43-038
P:3-131
118
1 2 4 8 16
c
π:80-276
M:9-144
34
d
M:10-133
9
e
M:58-232
P:10-130
42
f
M:0-315
π:83-213
15
g
M:2-328
2
h
P:0-315
M:5-225
8
i
π:86-283
M:4-131
43
j
M:4-145
19
k
M:75-235
P:0-141
47
l
M:7-133
π:10-226
48
m
M:16-127
10
n
P:8-129
M:25-225
67
o
ρ:0-297
M:2-306
π1 46-028
π2 71-206
26
p
M:3-127
2
q
M1:49-029
M:79-232
P:5-121
M2:58-219
17
r
PHC '81
B

Fig. 7.41 (Cont.)

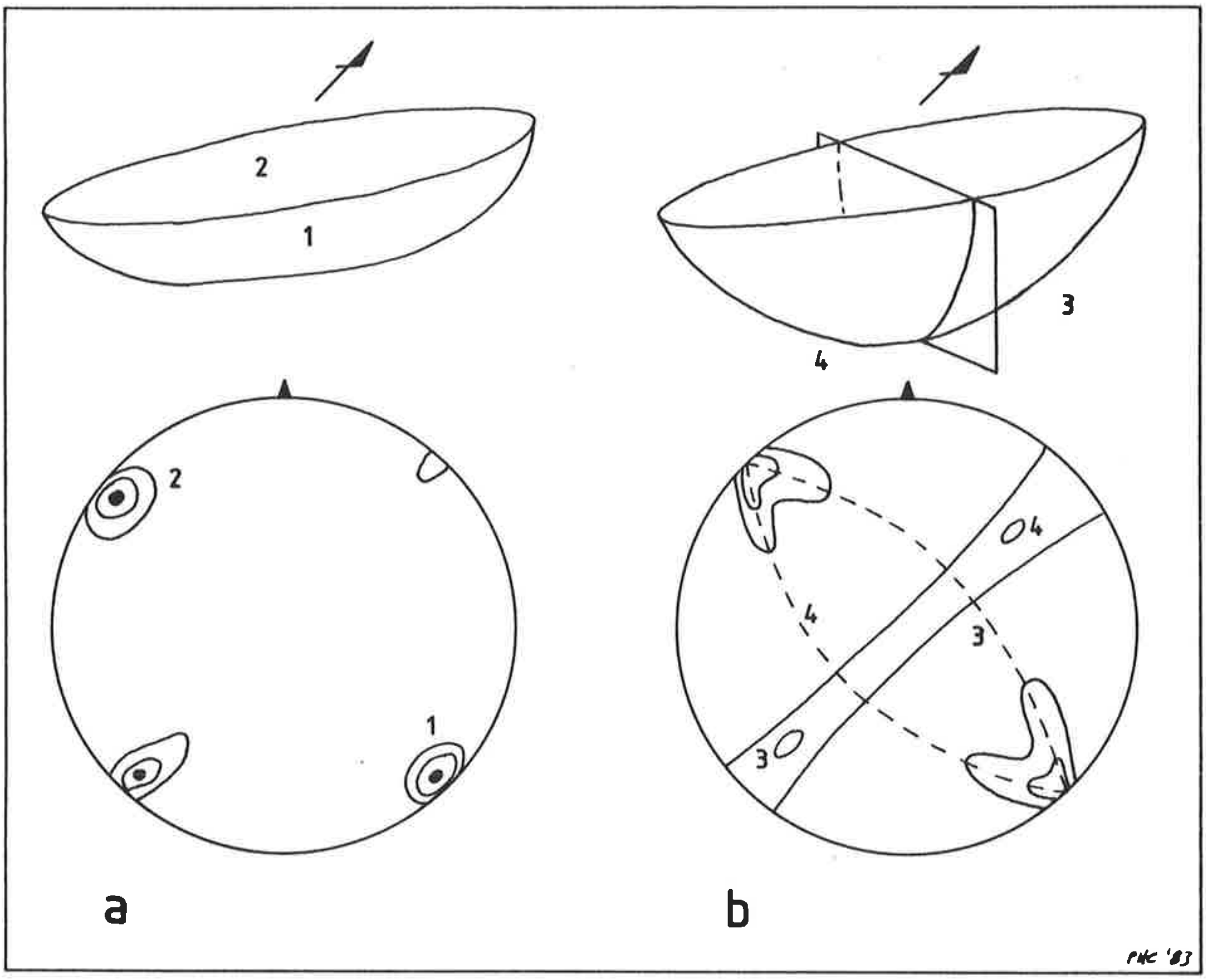

Fig. 7.42 Model demonstrating how a tight 'dome-and-basin' fold can produce stereonet patterns observed in (b) from that in (a). In (a) a tight basin has a shallowly plunging hinge. Flattening of this fold will give rise to pronounced curved fold hinges (Sanderson, 1973) as shown in (b).

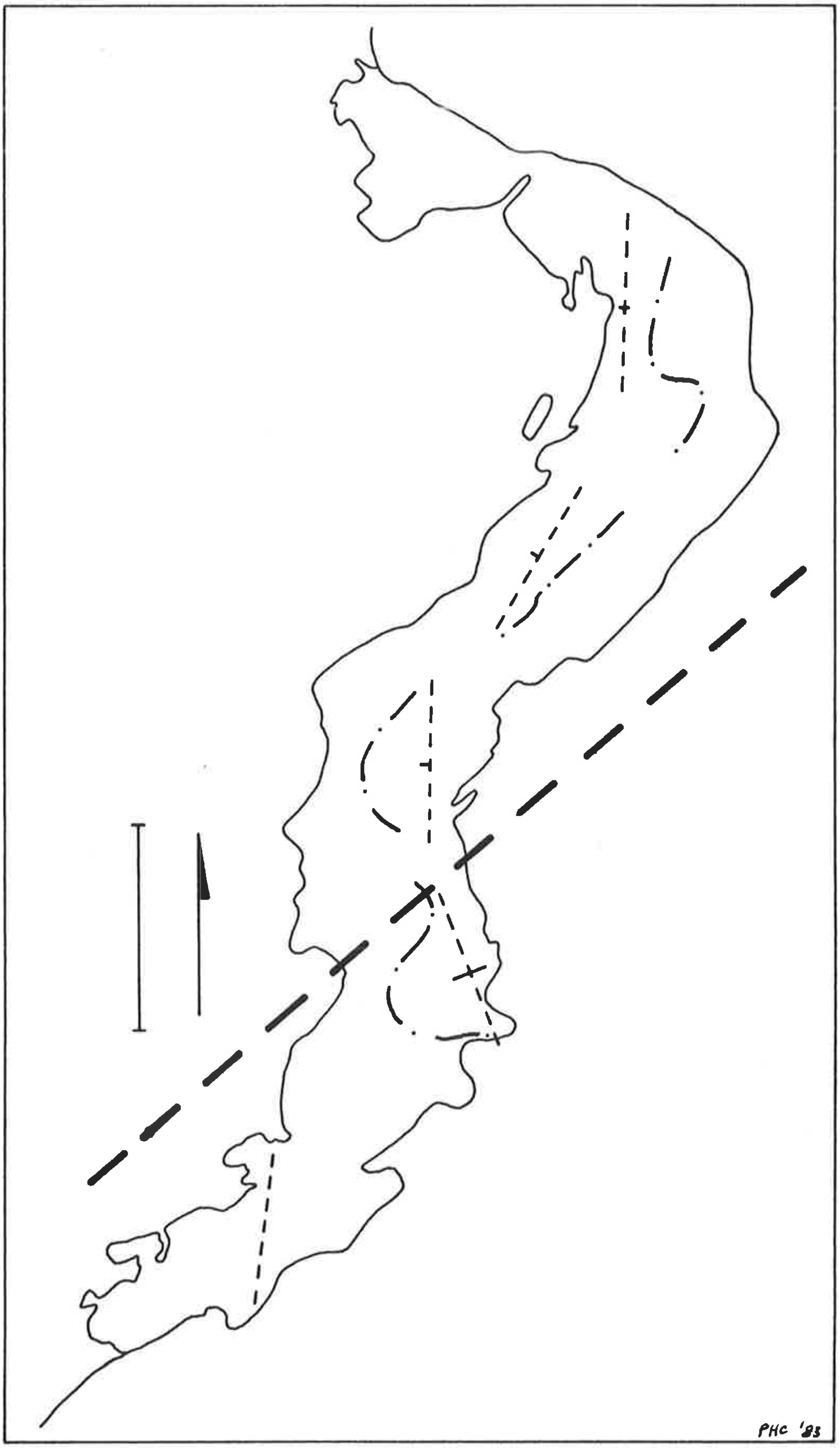

Fig. 7.43 Schematic interpretation of the D_2 structures in submap M912. Refer to Fig. 7.11 for the meaning of symbols.

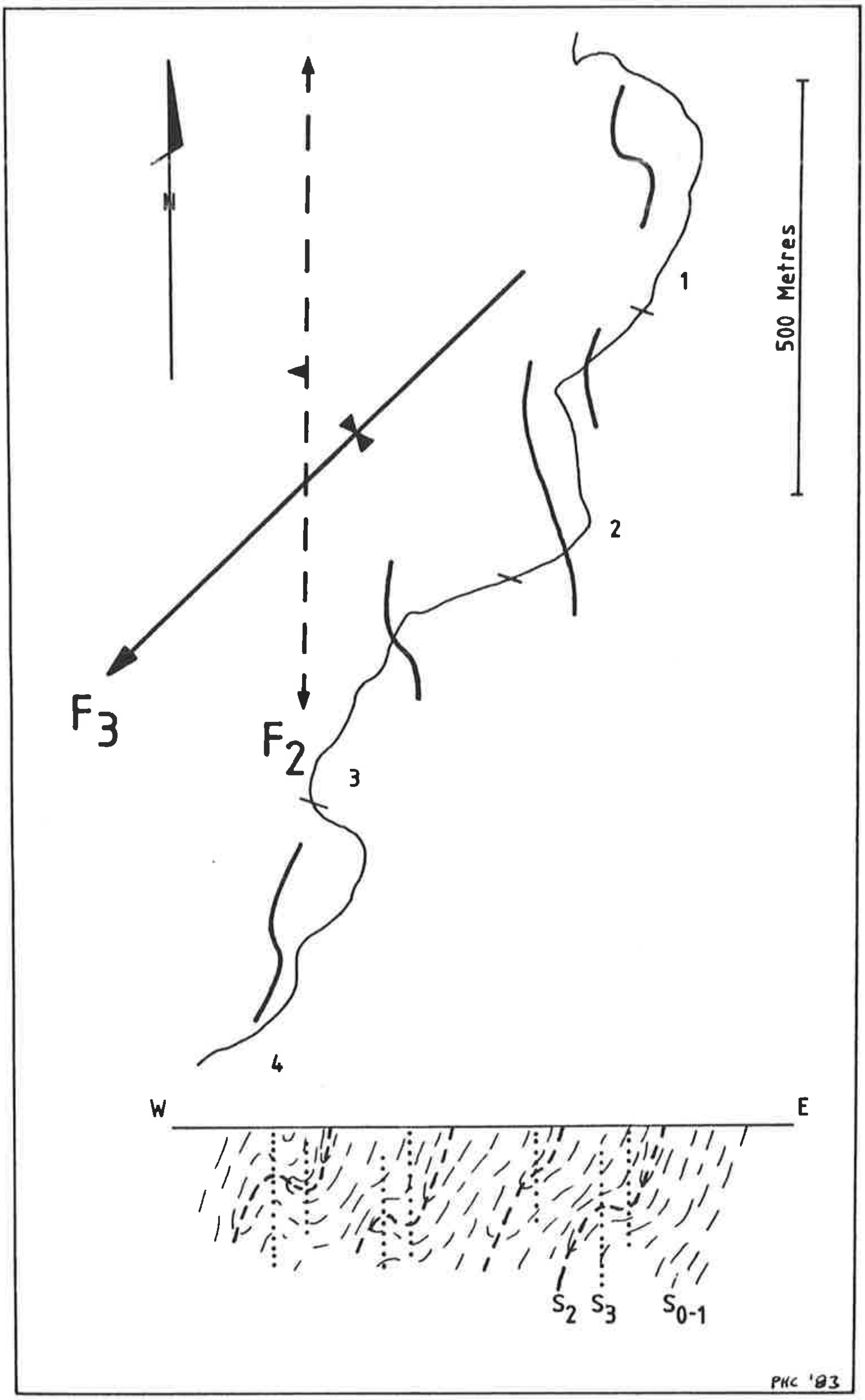

Fig. 7.44 Summary interpretation of the structures in the Lipson Cove area. The numbers refer to the geology sheets (Fig. 6.2). The short lines of the map are the interpreted trends of F_2 folds (see text), and the dashed heavy line is the trend of the macroscopic F_2 folds (which is inclined to the west and has variable plunges but is subhorizontal overall). The solid heavy line is the trend of F_3 folds, and in the mapped area it is a synform plunging southwest. The interpreted trends of the macroscopic F_2 and F_3 folds are correctly orientated but not spatially positioned. The vertical cross-section is a schematic one across the mapped area showing the relationship of the foliations (and axial planes).

Fig. B.1 Plot an assorted number of field measurements.

Set up an equal-area net of 5° step size with a title 17 characters long, a subtitle of 11 characters long, and with the north and centre points marked.

2,2,5,17,11,1,1,1

Pole of plane 300°/40° with symbol "0": 3.48,0,300,40,-9,0,0,0.

Pole of plane 210°/30°NW with symbol "A": 3.65,0,210,30,-8,0,0,0.

The following points with the symbol "X":

Plane 210°/30°NW with a pitch 81.7°E:

-3.88,0,210,30,-4,-1,81.7,0.

Plane 300°/40° with the trend of a sole marking 320°:

300,40,0,320,0,0.

Plane 210°/30°NW with the plunge of crenulation 25°NE:

210,30,-4,25,-1,0.

Finish the function: -1,-1,0,0,0,0.

Plot great circle 300°/40°: 4,1,300,40,0,0,0,0.

Plot great circle 210°/30°NW: 4,5,210,30,-4,0,0,0.

Fig. B.2 Solve a diamond drill hole problem by using the following information to find the orientation of a marker bed (assumed to be planar) which was observed in each of three oblique drill holes.

Hole No.	Bearing	Inclination	Delta angle
1	235°	25°	42°
2	150°	40°	70°
3	50°	24°	30°

Set up the equal-area net.

Enter 2,2,5,30,11,1,1,1.

Mark each drill hole with the hole number.

3.49,0,235,25,0,0,0,0 for hole 1 marked with "1".
3.50,0,150,40,0,0,0,0 " " 2 " " "2".
3.51,0,50,24,0,0,0,0 " " 3 " " "3".

Draw the small circles with radius of the delta angles.

5,1,235,25,42,0,0,0 (hole 1, solid line)
5,4,150,40,70,0,0,0 (hole 2, short dashes)*
5,5,50,24,30,0,0,0 (hole 3, dotted)

Find where all three circles intersect at one point. Overlay the plot on a gridded net of the same type and size and read off the orientation, which is the pole to the marker bed.

* An error occurs in the plot when the centre of the stereonet lies inside the cone.

EXAMPLE OF POINTS

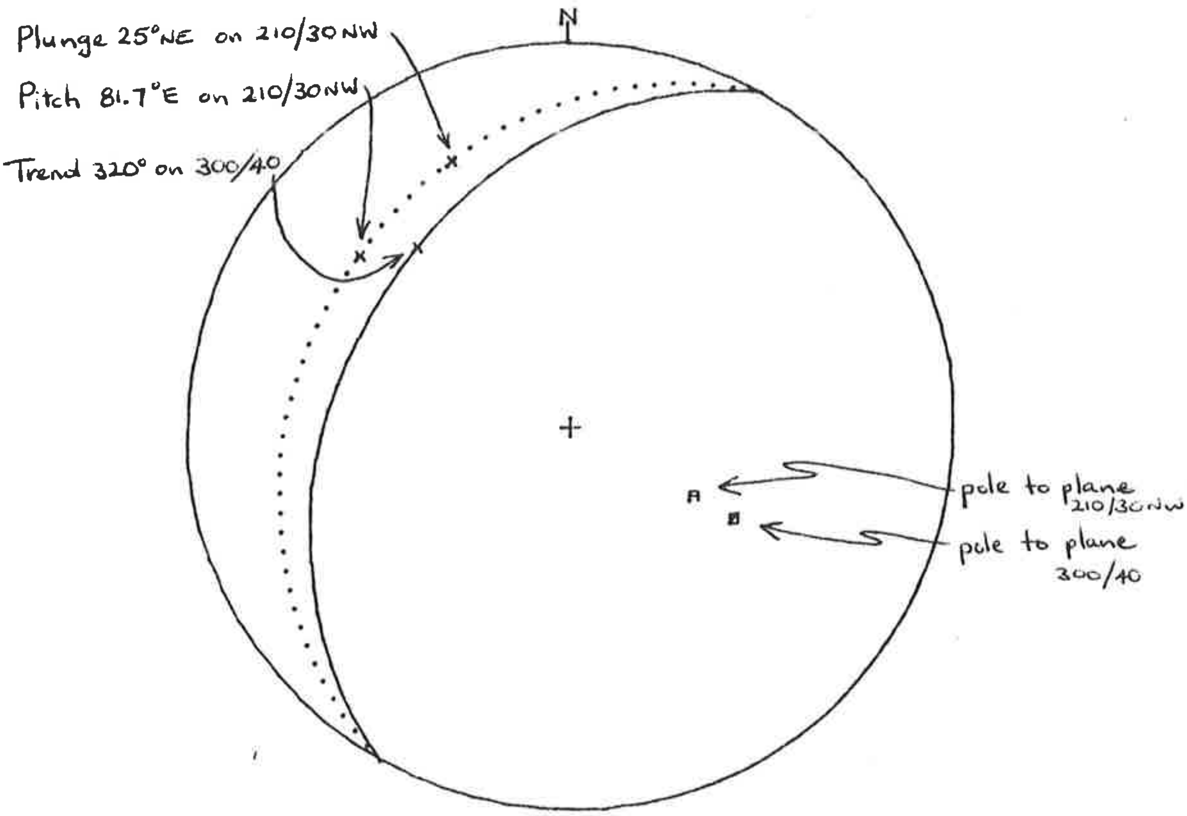

SCHMIDT NET

SOLUTION TO DRILL HOLE PROBLEM

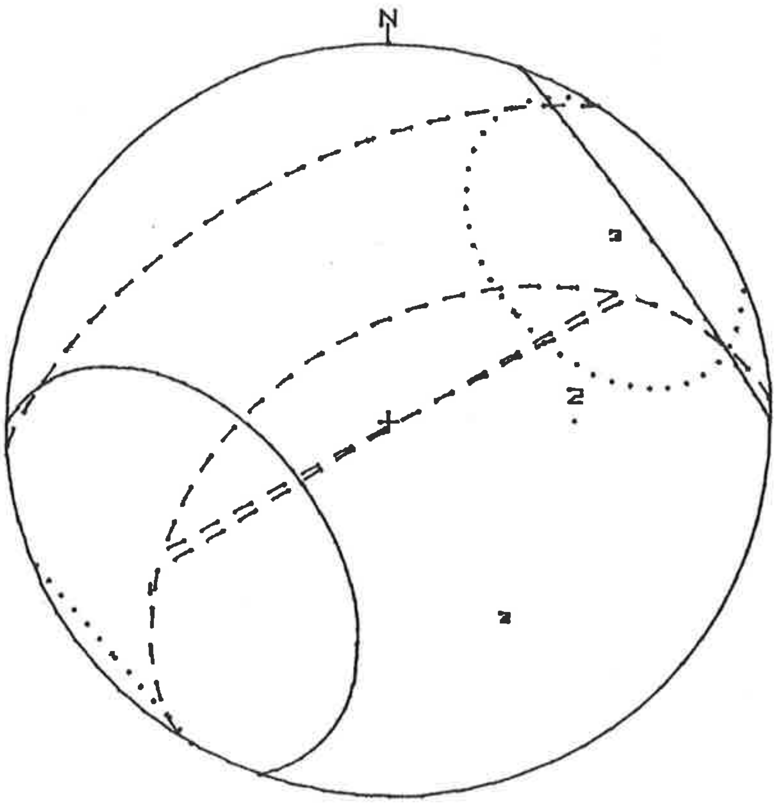

SCHMIDT NET

Fig. B.3 Solve a flow lineation problem. On a titled equal-area net find the true direction of a flow lineation from two measured apparent lineations.

Data: Joint 1 - 018°/50°E, pitch of apparent lineation 32°E
Joint 2 - 064°/70°N, " " " " 66°NE

Set up the net: 2,2,5,22,11,1,1,1

Find trend and plunge of apparent lineations.
Plot the lineation on joint 1 with "X", labelled "1".
3.88,49,18,50,-2,-3,32,0
As for joint 2, but labelled "2".
3.88,50,64,70,-1,-1,66,0

Computed orientations stored in memory:

88	49	176	24
88	50	26	59

Plot the poles of the joints (for a complete picture.).
3.65,0,18,50,-6,0,0,0 for joint 1 with symbol "A".
3.66,0,64,70,-8,0,0,0 for joint 1 with symbol "B".

Draw the joints as solid great circles (for completeness).
4,1,18,50,-2,0,0,0 for joint 1.
4,1,64,70,-4,0,0,0 for joint 2.

Plot the "N" planes for both the joint surfaces as dashed great circles (using data from listing above):
4,4,176,24,0,18,50,-6. "244/50" is displayed.
4,4,026,59,0,64,70,-8. "73/68" is displayed.

Find the intersection of these two "N" planes and plot with "O".
3.79,0,244,50,0,73,68,0
Computed orientations stored in memory (the last value in the listing (160/07) is the desired value):

88	49	176	24
88	50	26	59
65	0	288	40
66	0	154	20
79	0	160	7

If the flow fabric was thought to be planar then find the plane (dotted) containing the two lineations.
4,5,176,24,0,26,59,0. "92/76" is displayed (which is dip direction and dip of the required plane).

Fig. B.4 Contouring of data.

a) Scatter plot (equal-area net) of data to be contoured.

FLOW LINEATION PROBLEM

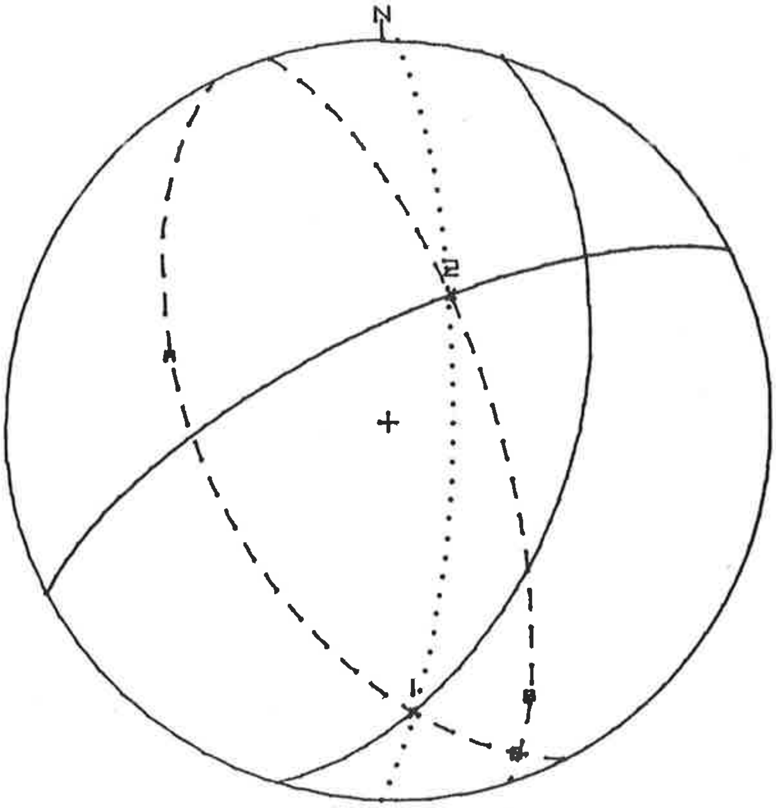

SCHMIDT NET

A DISTRIBUTION OF POINTS

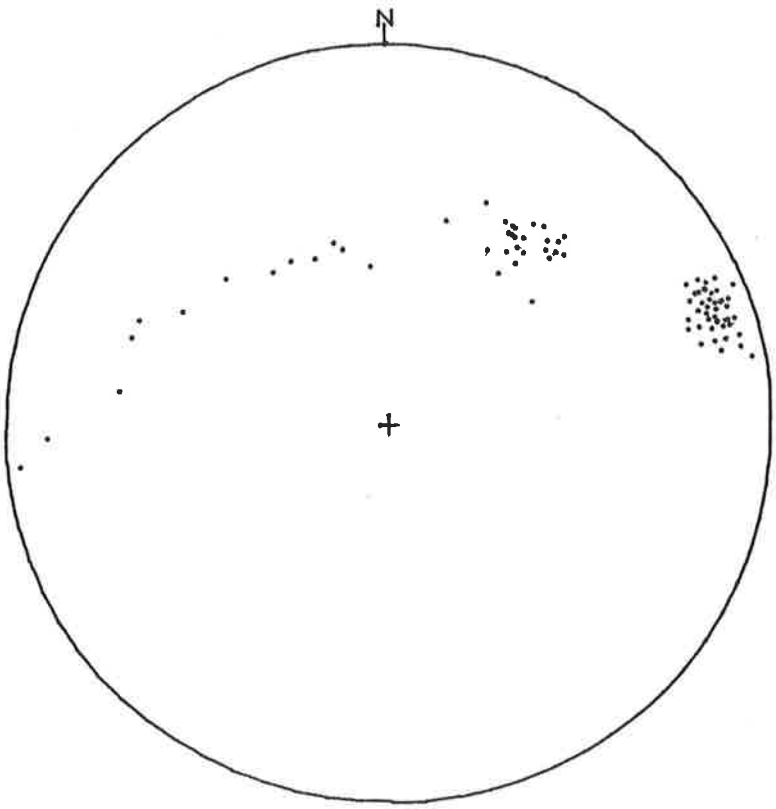

SCHMIDT NET

Fig. B.4 Contouring of data (continued).

Set up net for plotting: 6,0,1,1,1,1,1,2.

b) The count plot

c) The contour plot.

CONTOUR OF POINTS DISTRIBUTION

LEVEL	%	(COUNT)
1.00	2.37	1.97
2.00	4.74	3.93
3.00	9.47	7.86
4.00	18.95	15.72
5.00	37.89	31.45
MAX.	40.96	34.00

```
                              N

                           0  0  0
                  0  0  0  0  0  0  0  0  0
            0  0  0  0  0  0  0  0  0  0  0  0  0
         0  0  0  0  0  0  0  0  0  0  0  0  0  0  0
      0  0  0  0  0  0  0  0  0  1  2  6  2  0  0  0  0
      0  0  0  0  0  2  4  3  1  1  2 17 21  0  0  0  0
   0  0  0  0  2  1  2  3  4  1  0  2  7 11  4  0  1 13 13
   0  0  2  3  1  1  0  0  0  0  0  0  1  1  0  0  2 34 32
   0  0  1  2  0  0  0  0  0  0  0  0  0  0  0  0  1 15 10
0  0  1  1  0  0  0  0  0  0  0  0  0  0  0  0  0  0  0  2  1
0  1  1  1  0  0  0  0  0  0  0  0  0  0  0  0  0  0  0  0  0
3  3  0  0  0  0  0  0  0  0  0  0  0  0  0  0  0  0  0  0  0
   0  0  0  0  0  0  0  0  0  0  0  0  0  0  0  0  0  0  0
   1  0  0  0  0  0  0  0  0  0  0  0  0  0  0  0  0  0  0
   1  0  0  0  0  0  0  0  0  0  0  0  0  0  0  0  0  0  0
      0  0  0  0  0  0  0  0  0  0  0  0  0  0  0  0  0
      0  0  0  0  0  0  0  0  0  0  0  0  0  0  0  0  0
         0  0  0  0  0  0  0  0  0  0  0  0  0  0  3
            0  0  0  0  0  0  0  0  0  0  0  0  0
                  0  0  0  0  0  0  0  0  0
                           0  0  0
```

SCHMIDT NET

CONTOUR OF POINTS DISTRIBUTION

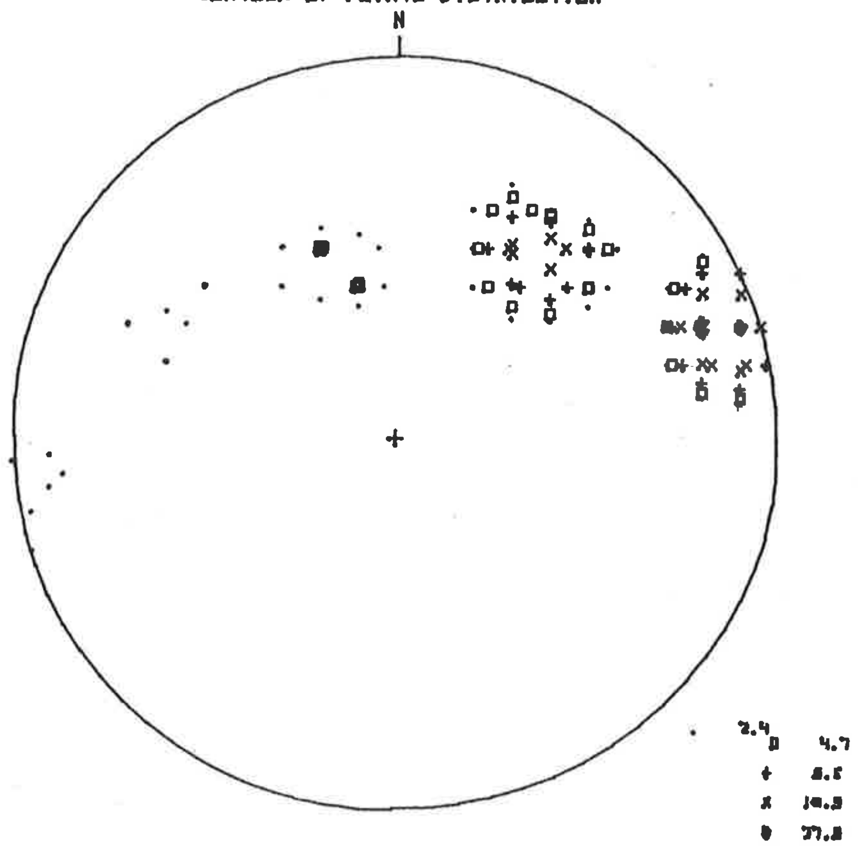

SCHMIDT NET

Fig. B.5 Rotate the data in Fig. B.4a by 107° clockwise around the axis 090°/40° and replot them with the symbol "X".

Set up the net with: 2,2,5,28,11,1,1,1.

Rotate the data: 7,0.88,0,40,90,107,0,0.

Fig. B.6 Replot Fig. B.5, find the mode, and find and plot the best fit great and small circles.

Set up the net with: 2,2,5,21,18,1,1,1.

Replot points (symbol "X"): 3.88,0,-1,0,0,0,0,0.

Find best fit circles and mode: 9,88,1,1,1,0,0,0.
The results below are printed:

```
MODE FIT TO SYMBOLX = 124/ 29
CONE AXIS FIT TO SYMBOLX = 359/ 58 1/2 APEX ANGLE 87
POLE OF PLANE FIT TO SYMBOLX = 360/ 53
```

Plot the great circle with a solid line: 4,1,360,53,-9,0,0,0.

Plot the small circle with a solid line: 5,1,359,58,87,0,0,0.

ROTATION OF POINTS CONTOURED

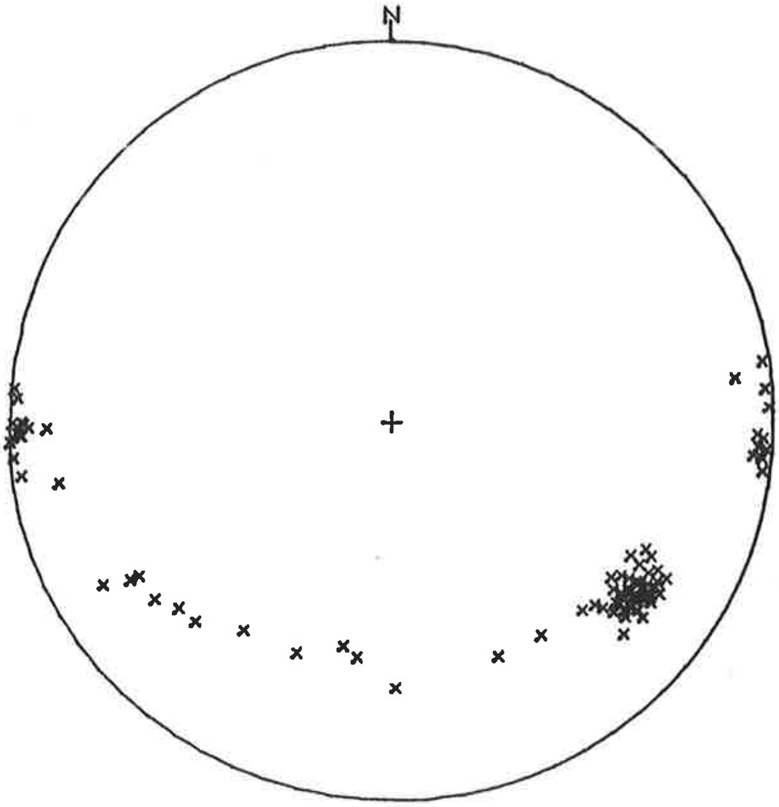

SCHMIDT NET

FIT OF PLANE AND CONE

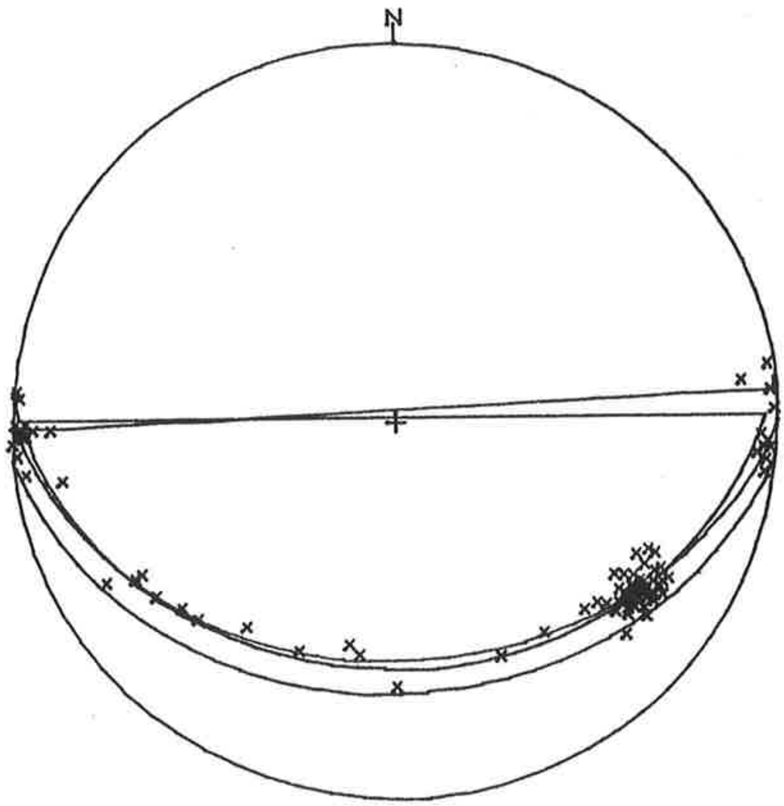

(POINTS REPLOTTED)

Aspect	Class	Value
Age	2400 Ma	7
	2300 MA	6
	1800 Ma	5
	1600 Ma	4
	1500 Ma	3
	1400 Ma	2
	600 Ma	1
	430 Ma	0
Sedimentary	Not sedimentary	0
	Mudstone	1
	Siltstone	2
	Shale	3
	Sandstone	4
	Limestone	5
	Conglomerate	6
	Greywacke	7
Metamorphic	Not metamorphosed	0
	Greenschist	1
	Amphibolite	2
	Granulite	3
Igneous	Not igneous	0
	Granite	1
	Syenite	2
	Basalt	3
Mineralisation	Cu yes/no	0/1
	Pb yes/no	0/1
	Zn yes/no	0/1
	Mn yes/no	0/1

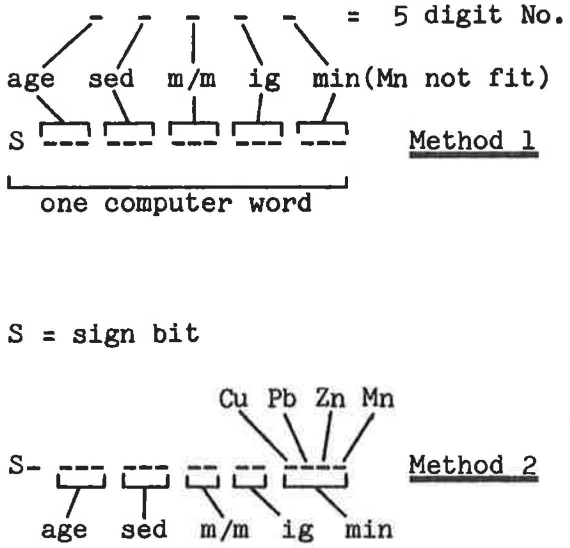

PKC '81

Fig. C.1 Two methods for coding geological data into 15 bit computer words.

Condition = "1800 Ma, sandstone, Cu and Pb mineralised".

```
                 2   6   0   1   2
match    = 0 010 110 000 001 010  = 26012_8
                4   4   0  0  10_10 = class numbers

                 3   7   4   1   2
control  = 0 011 111 100 001 010  = 37412_8
                7   7   0  0  10_10 = mask for aspects
```

Condition = "1800 Ma, metamorphosed siltstone to amphibolite grade, Cu and Pb mineralised but no Zn".

```
                 2   5   2   1   2
match    = 0 010 101 010 001 010  = 25212_8
                4   2   2  2  10_10 = class numbers

                 3   7   7   1   6
control  = 0 011 111 111 001 110  = 37716_8
                7   7   3  0  14_10 = mask for aspects
```

PHC '81

Fig. C.2 Two examples of conditions, using data from Fig. C.1, method (2).

(a)

Sediment	Class (octal)	Bit Pattern (binary)
Turbidite	0	000
Conglomerate	1	001
Greywacke	2	010
Moraine	3	011
.	.	.
.	.	.

(b)

Sediment	Class (octal)	Bit Pattern (binary)
Turbidite	0	000
Greywacke	1	001
.	.	.
Conglomerate	4	100
Moraine	5	101
.	.	.

PHC '81

Fig. C.3 Sequencing of classes for group (property) testing.

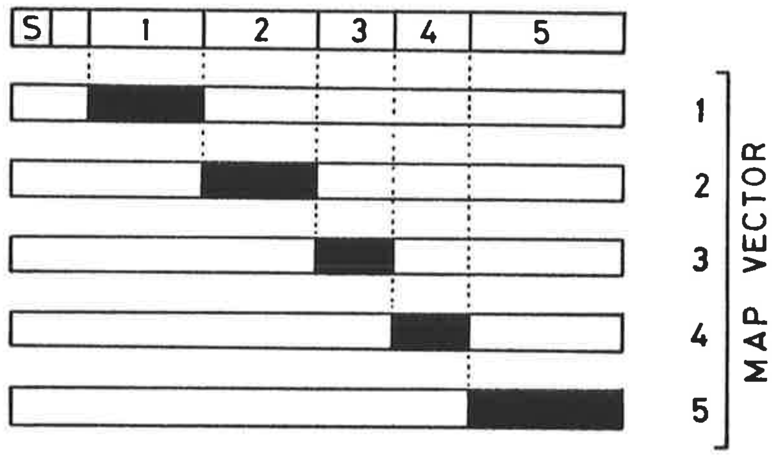

Fig. C.4 Map vector containing location of areas reserved for each coded geological aspect (see text). First (top) word is the D word for Fig. C.1. S is the sign bit. The numbered elements for the map vector (following words) correspond to the numbered aspects. These elements are zeroed, except for the black regions, which are set to ones.

```
STATION S1        S3        F3        SPEG      X         Y

MAP1         1349.7 2297.9 284.   200.     CM
1                 157 80   163 72              50.1      27.0

2          123 90                              50.4      25.1

3          307 82                              50.2      25.3

4                                    270 80    22.6      15.4

5                                              22.2      13.2

6          240 70   146 90                     17.8      20.0

7                   148 90   210 65            16.4      19.2

8                            058 77            14.3      15.3

9                            332 80            14.6      15.7

10                           217 30            15.0      12.0

10A                          278 70            15.0      12.0

11                           051 35            13.5      12.2

12                           211 70            11.8      14.1

13         286 77                              13.0      20.7

14         305 90                              10.8      20.7

15                           216 85             6.9      14.7

21         288 80                              45.9      26.4
```

Fig. D.1 Sample of a source data file, printed by program LOOKMS. (Geological description column excluded.)

```
300.
S1        X         Y
FOLIATION FOR MAPS 9/10 - 12 (AZ = 042)
090.METRES    0.    70. 1120. 1000. 009.   400.     METRES
0
 1 1.0 001001 042.
MAP9/10
1-45, 46-/
MAP10
-/
MAP11
1-84, 85-K0, K1-/
MAP12
-/
```

Fig. D.2 Sample file of map stations to be used in a map required to be extracted. Only S1 data is extracted from: stations 1 to 45, 46 to end of Map9/10; all Map10; 1 to 84, 83 to K0, and K1 to end of Map11; and all Map12. Map title, origin, units, scale, stereonet plots, and grid are specified in lines 3 to 6.

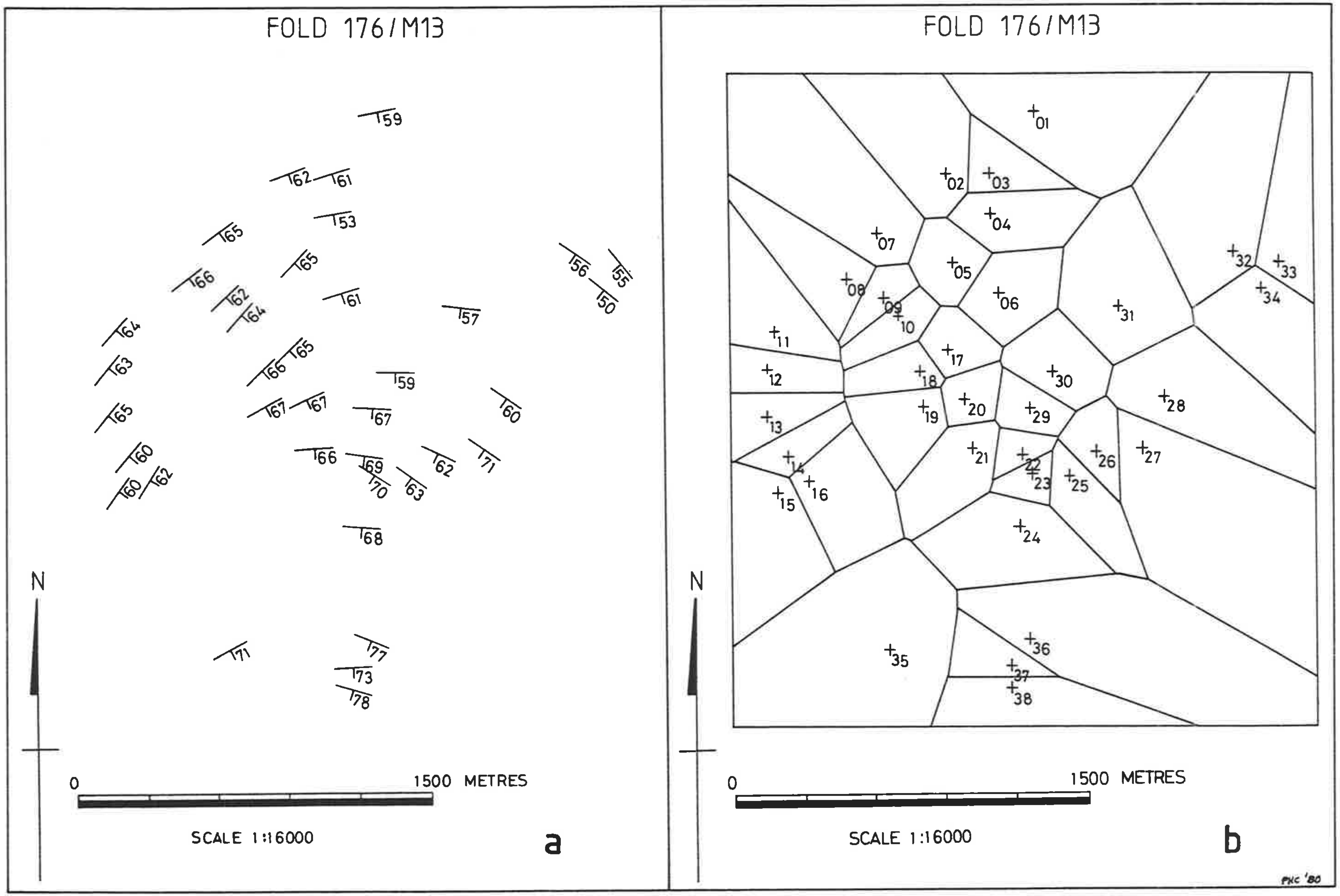

Fig. D.3 Maps produced by program PLTMAP.
a) Strike-dip map. b) Tessellated locality map of (a), using Thiessen polygons (Rhynsburger, 1973).

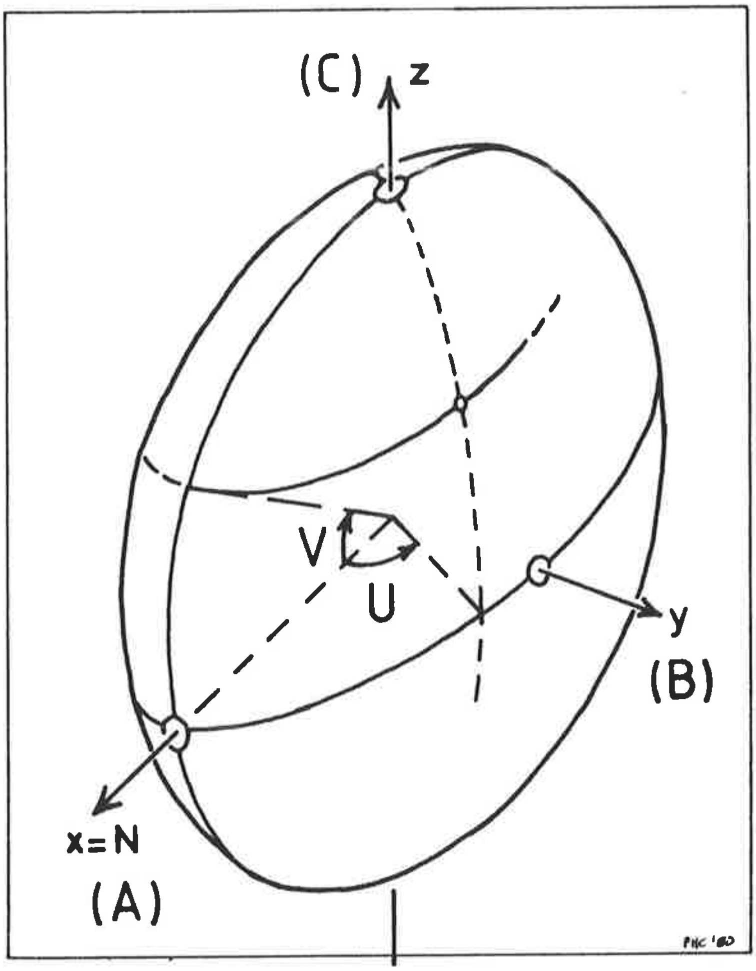

Fig. E.1 Geometrical configuration of a general ellipsoid. (N = north)

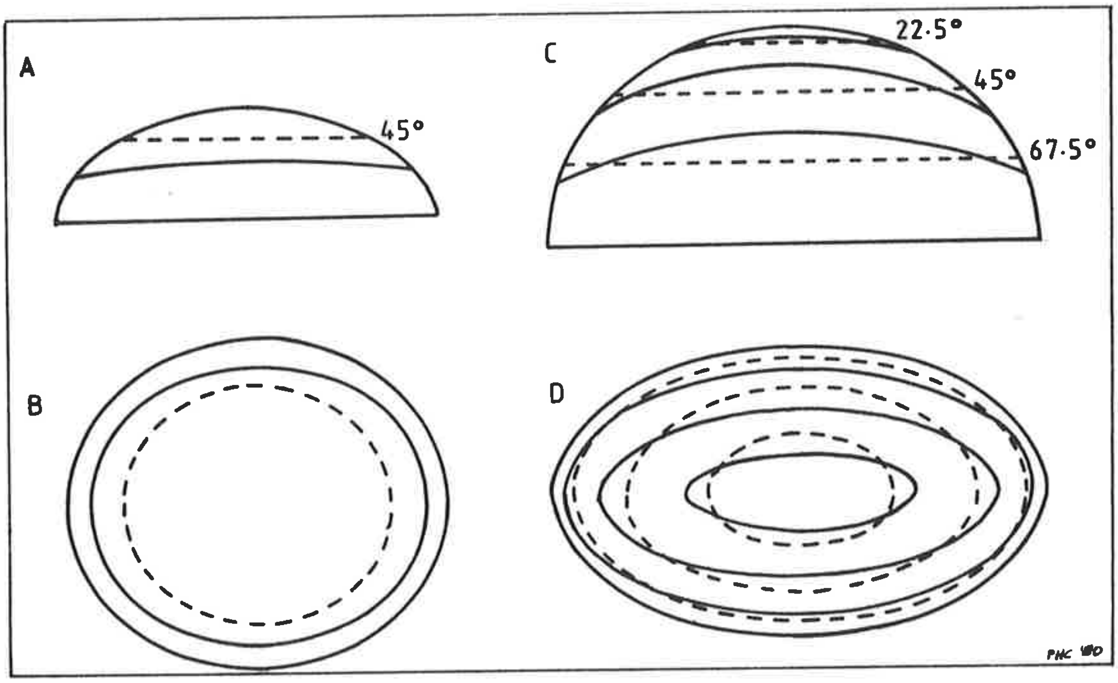

Fig. E.2 Section and plan views of isodip contours for two oblate ellipsoidal domes. Solid lines are isodip contours, dashed lines are corresponding height contours (strike-lines). Angles are for V (equation (E.2)ff).

a) Longitudinal section, and b) plan of dome with z axis vertical.

c) " " , " d) " " " " y " " .

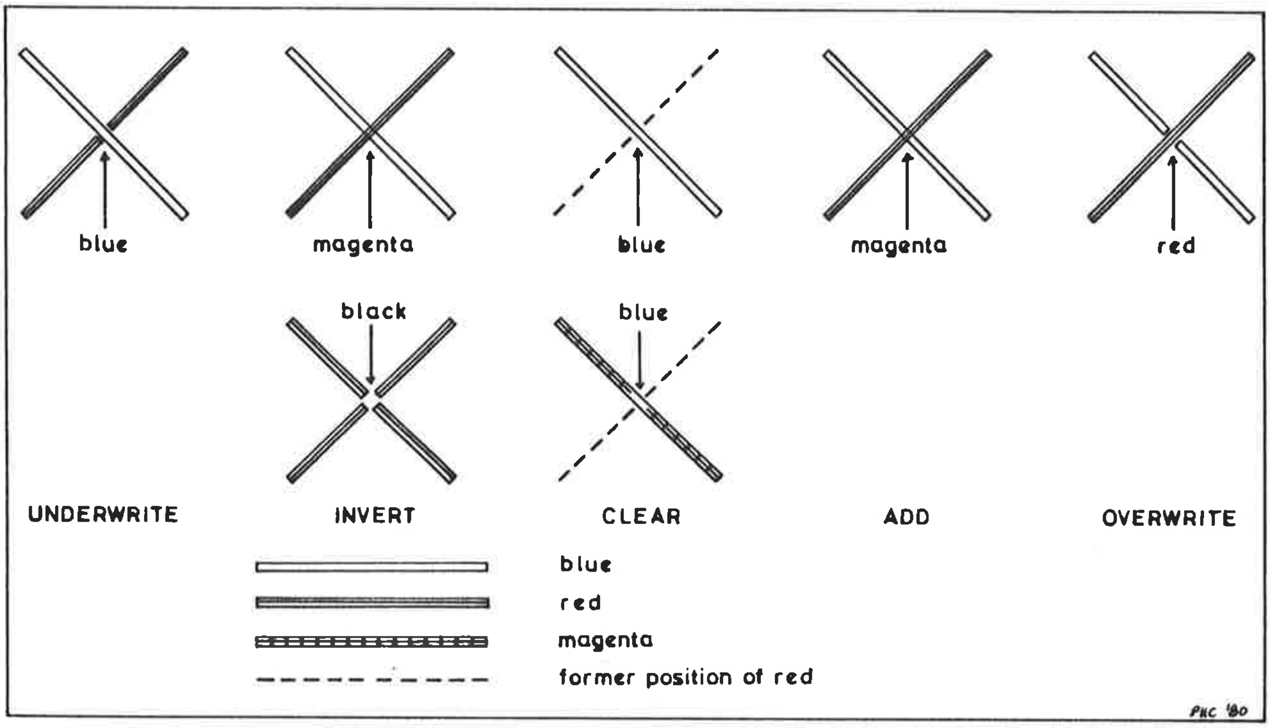

Fig. F.1 A demonstration of the five ways in which screen-pixels can be coloured (using the three colour guns). In each case the top left to bottom right diagonal line was on the display before the plotting of the other diagonal (red) line in the appropriate mode, except for "clear" which had both diagonals plotted before the red line was replotted (cleared).

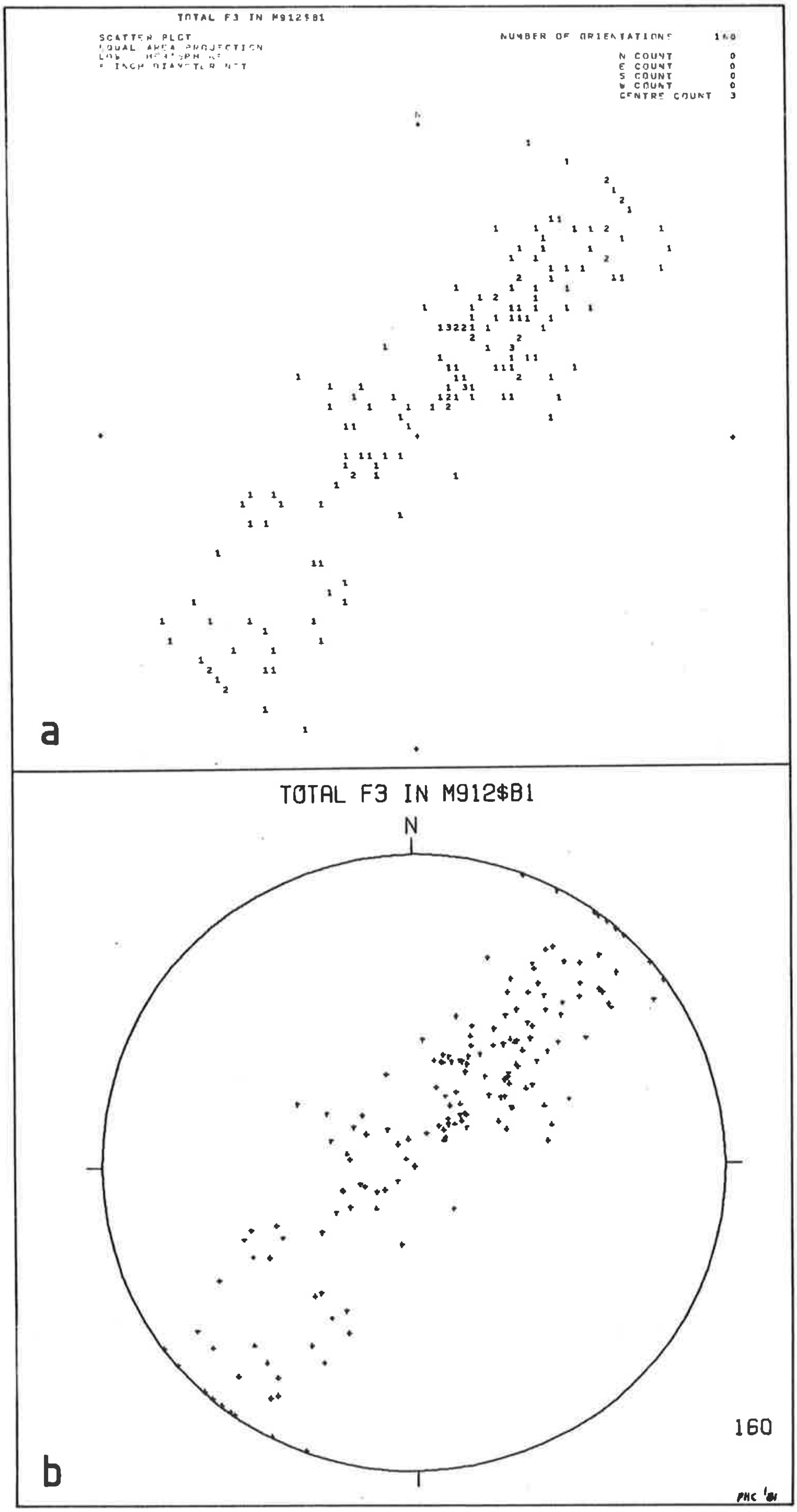

Fig. H.1 Scatter plots by program CNTRFIN. a) Line printer. b) Pen plotter.

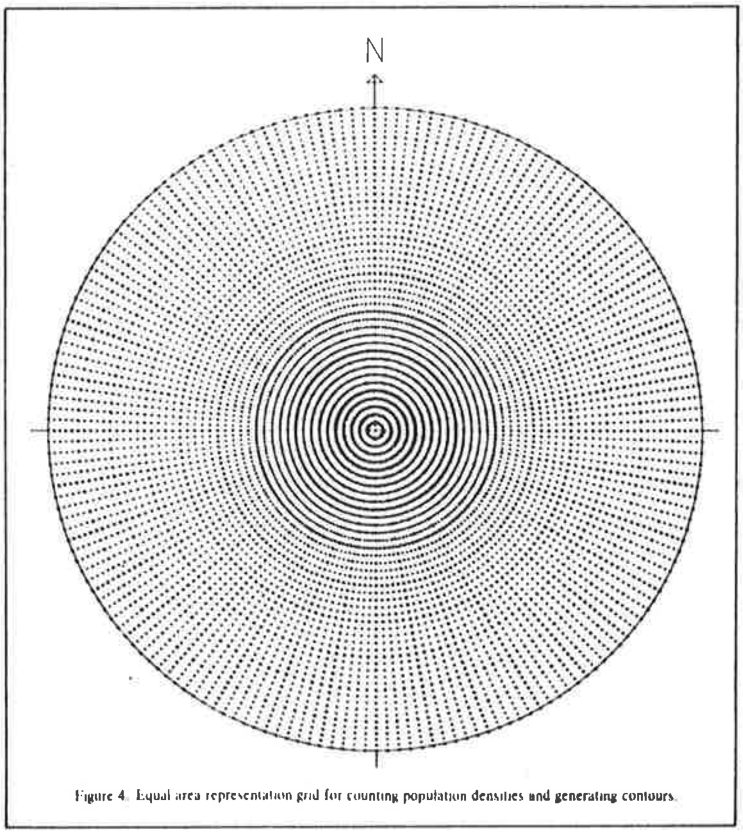

Fig. H.2 Grid used by Kalkani and von Frese (1979, fig. 4), similar to that used by this thesis, except it does not account for increasing distortion towards the vertical.

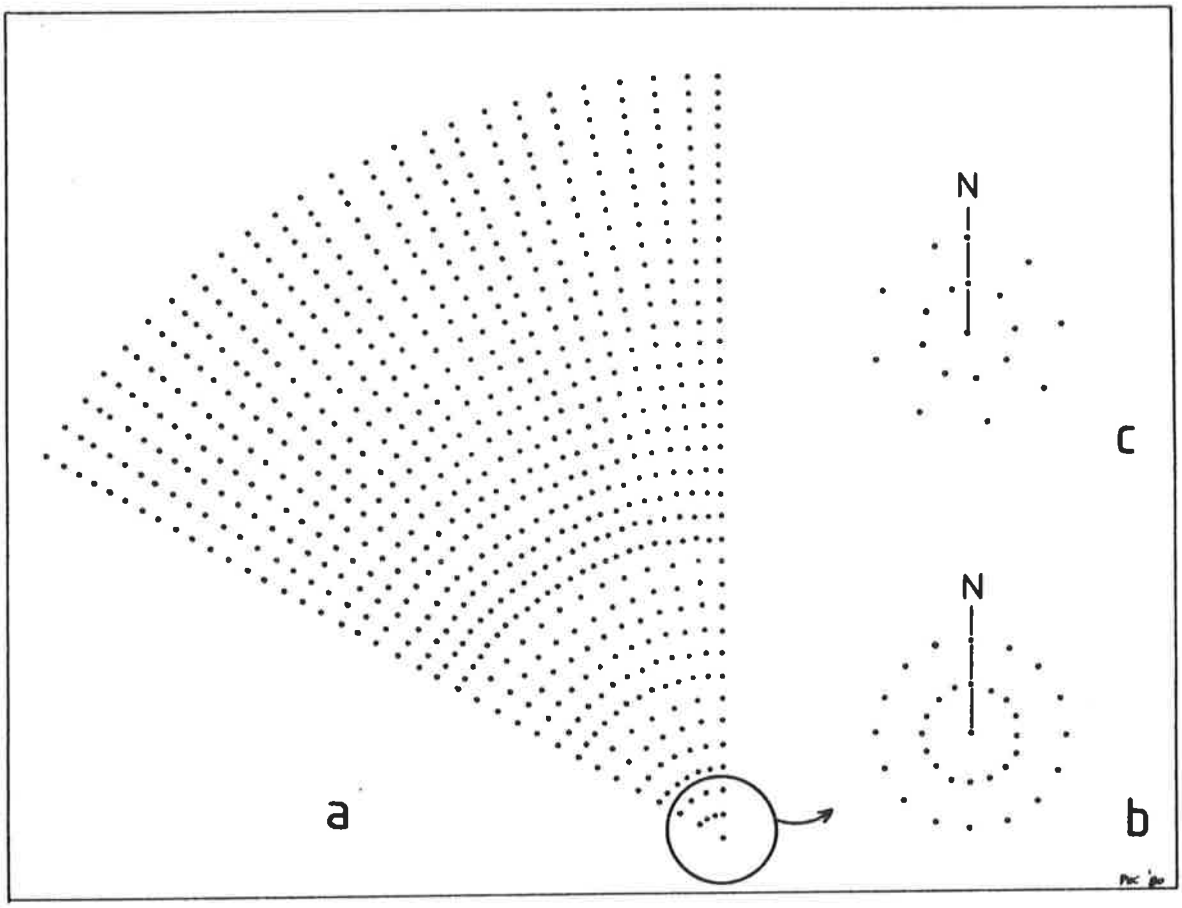

Fig. H.3 a) A 60° sector of the stereonet contouring grid used by CNTRFIN. b) Enlargement of a near vertical portion of the grid, showing its regularity. c) Only grids of certain angles can be used, as otherwise irregular grids arise.

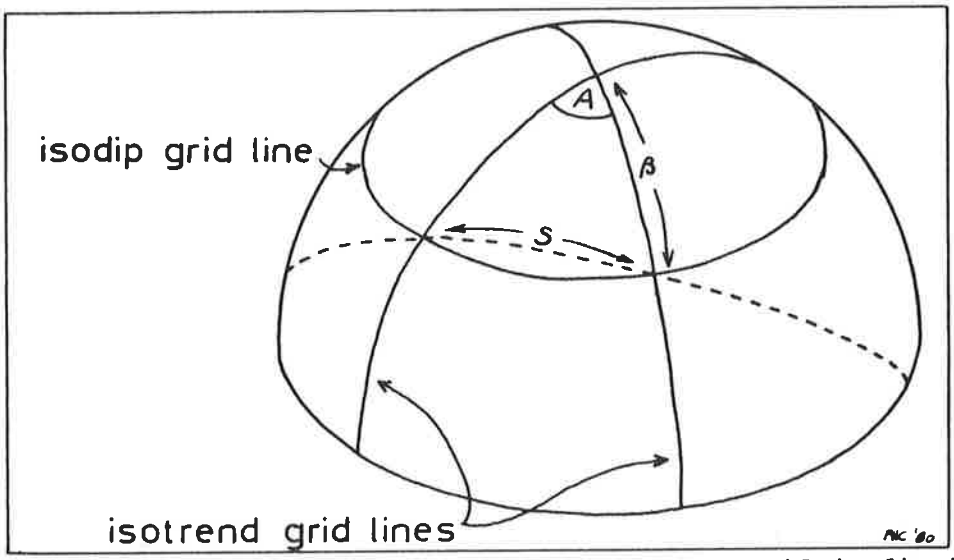

Fig. H.4 Geometry for computing where transition grid isodip lines occur. The sine rule for oblique spherical triangles can be applied to find ß $(=\sin^{-1}([(1-\cos S)/(\cos A-1)]^{-1/2})$. Angles A and S are modulo G (the grid size). Grid isodip lines closest to ß are the transition lines, provided that Fig. H.8 can be satisfied.

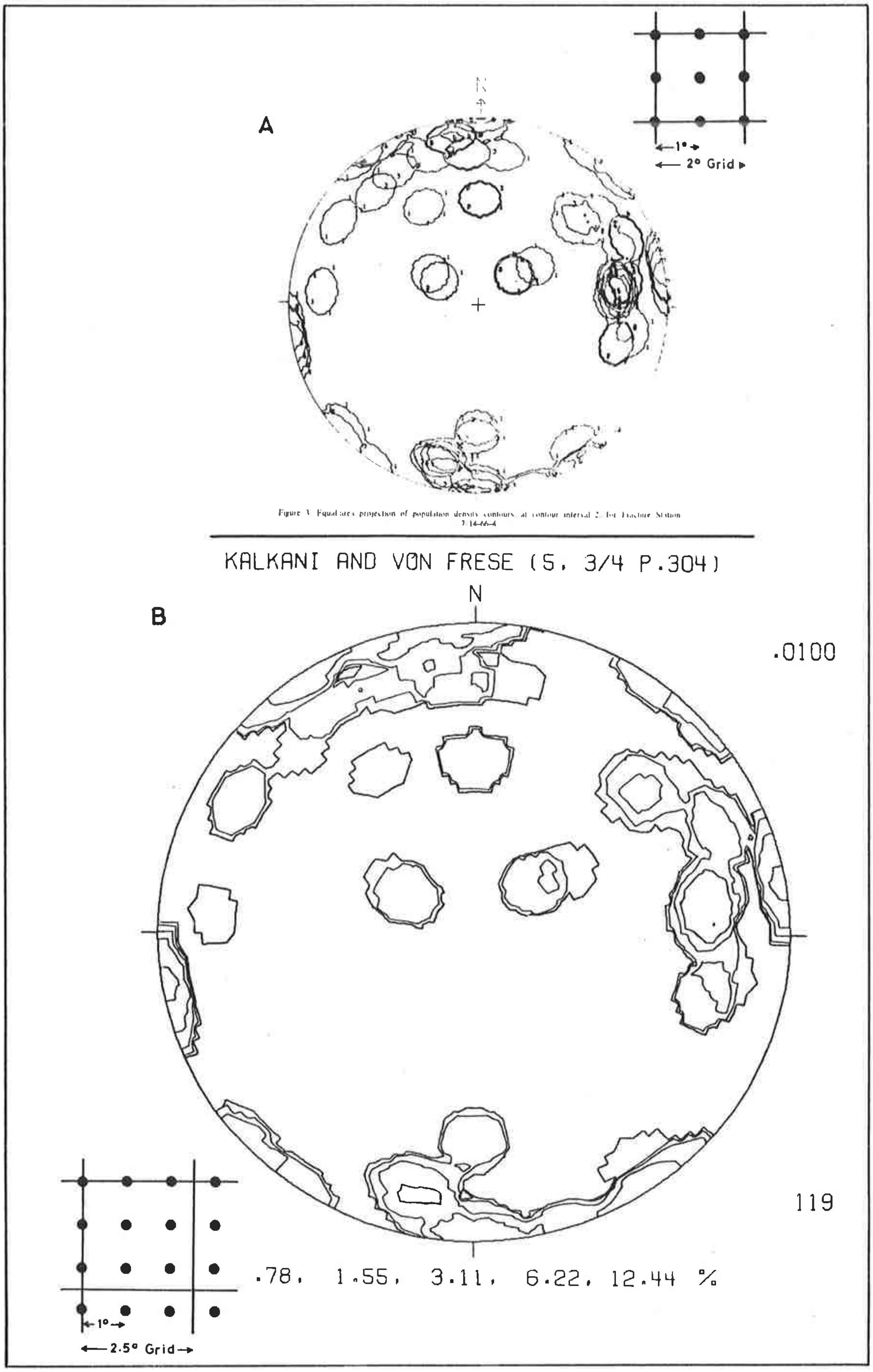

Fig. H.5 Distortion of contours due to grid size.
a) 1° or 2° grids (after Kalkani and von Frese, 1979, fig. 3) show no distortion, provided angles are integers (see inset).
b) A 2.5° grid produces distortion due to asymmetry between some grid nodes and integer degree values (see inset).

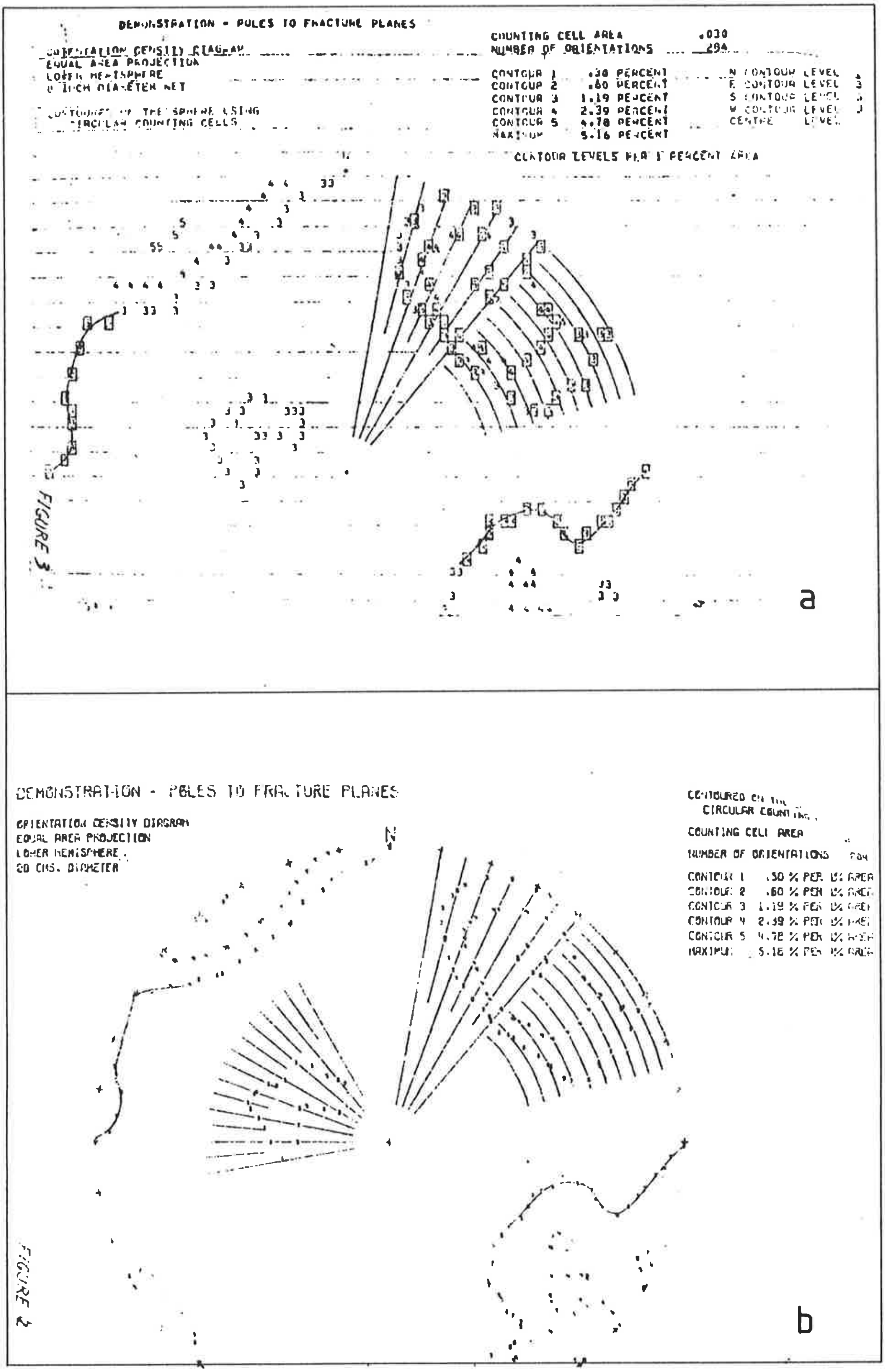

Fig. H.6 Stereonet contours produced by program ORIENT (after Bridges and Etheridge, 1974, figs. 2,3). a) Line printer. b) Pen plotter.

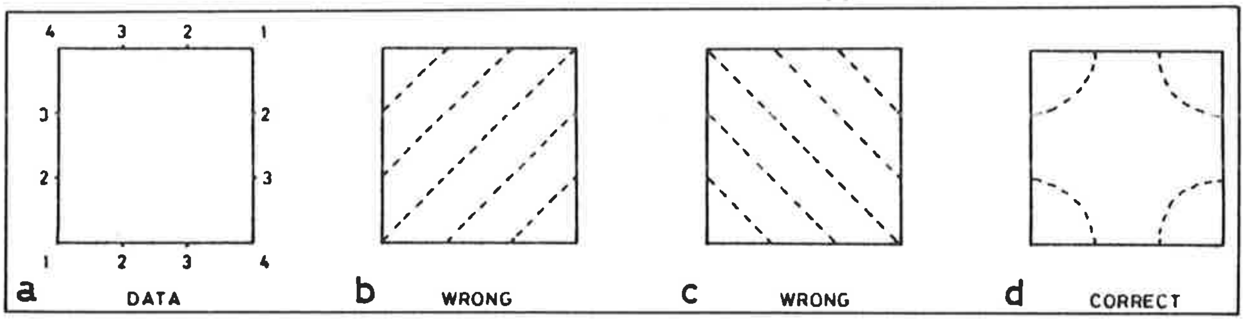

Fig. H.7 Various interpretations of a saddle contained in a grid cell (a). b,c) Incorrect, caused by using only one diagonal to divide the cell into triangles. d) Correct, by dividing the cell using both diagonals, with the centre point as average of the corners.

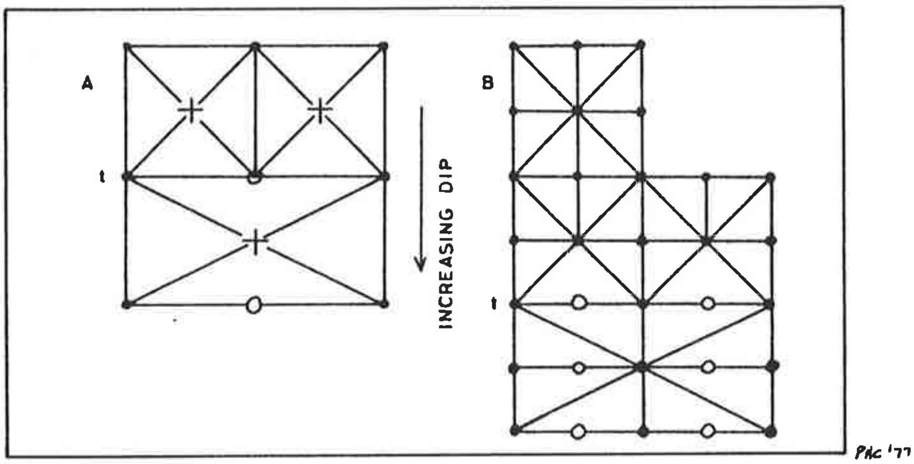

Fig. H.8 Division of grid cells into triangles as used by CNTRFIN.

a) Maximum detail obtained by using Fig. H.7d. (Used for coarse grids, 2.5°.) Discontinuities can occur at transition (t) boundaries, which are eliminated by adopting the strategy (b).

b) For fine grids, alternate diagonals are used. This assumes that no saddle is contained within a single grid cell.

● grid node, o grid node not used, ● the previous combined
+ computed point.

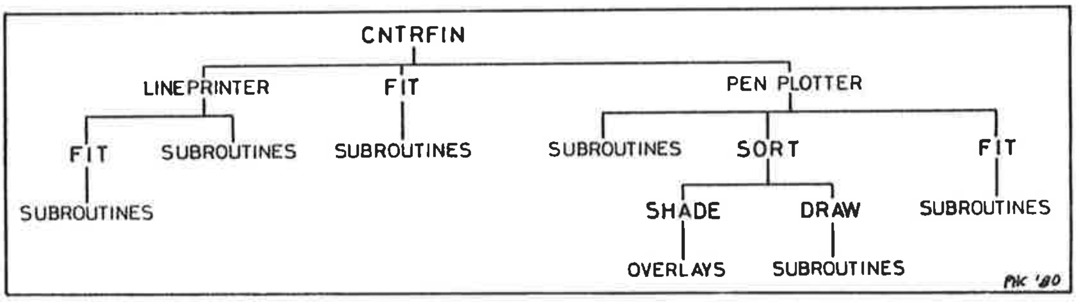

Fig. H.9 Layout of program CNTRFIN into overlays. Heavy type are programs.

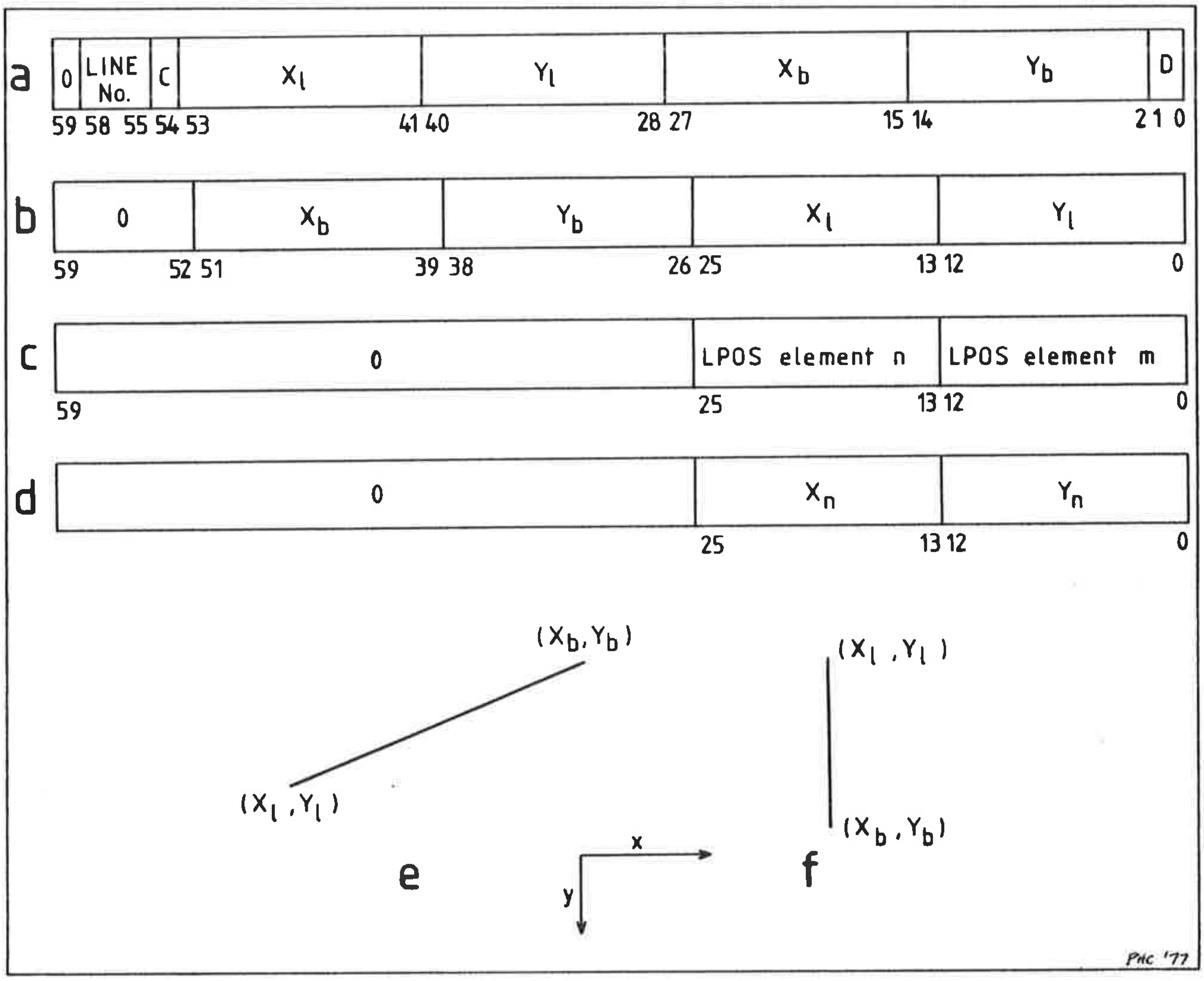

Fig. J.1 Packing of information into 60 bit computer words. Bits are numbered from the right (LSB, least significant bit), to the left (MSB, most significant bit).

a) A binary file record. Fields C and D are reserved for a polygon shading program. LINE No. refers to contour level.

b) An element of vector IV.

c) " " " " LJOIN. Bits 25-13 are used for Fig. J.2a situations, and bits 12-0 for Fig. J.2c.

d) An element of vector JVC. (Refer to Fig. J.3).

e) Line segment showing the most (l) and least (b) significant coordinates of the end points.

f) Same as (e), except $X_l = X_b$.

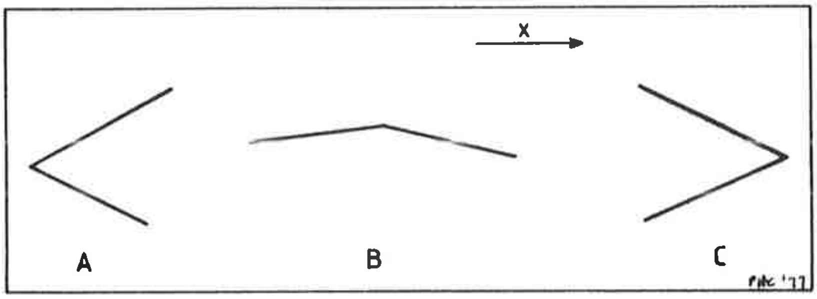

Fig. J.2 Three situations which the sequencing procedure looks for.
a) Sequences (see Fig. J.3) joined at their beginnings.
b) Continuation of a sequence.
c) Sequences joined at their endings.

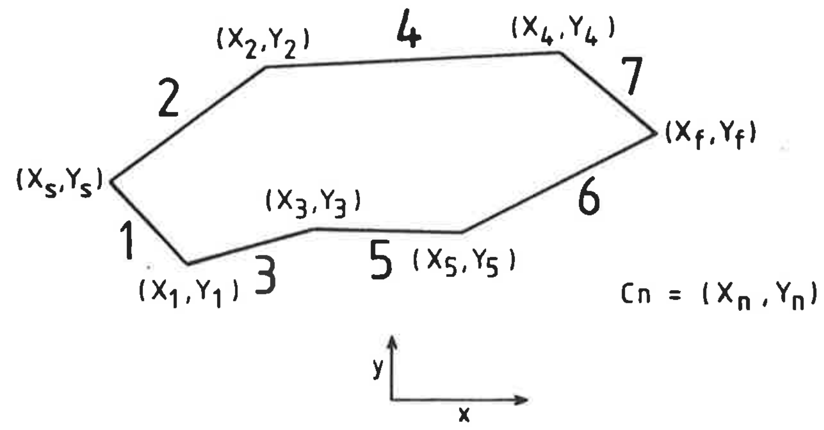

	IV	LAR	LPOS	LJOIN	JVC
1	———	~~0~~2	1	~~0~~~~2~~∞; ~~2~~∞	Cs
2	C1 : Cs	~~0~~~~3~~4	~~2~~~~3~~~~4~~5	~~0~~~~1~~∞; ~~1~~∞	C1
3	C2 : Cs	~~0~~~~2~~6	~~3~~~~4~~~~5~~~~6~~~~7~~8	0	C3
4	C3 : C1	~~0~~~~5~~~~3~~7	0	0	C5
5	C4 : C2	~~0~~~~5~~3	0	0	Cf
6	C5 : C3	~~0~~5	0	0	C4
7	Cf : C5	~~0~~8	0	0	C2
8	Cf : C4	0	0	0	Cs

PHC '77

Fig. J.3 Example of a closed contour to demonstrate segment order, sequencing, and how the arrays are used. Heavy type refer to the order in which the segments appear on the sorted binary file. Two sequences occur: 1,3,5,6 and 2,4,7. The values in LAR are one greater as the first element of IV is not used. LPOS elements refer to the start of each sequence in LAR.

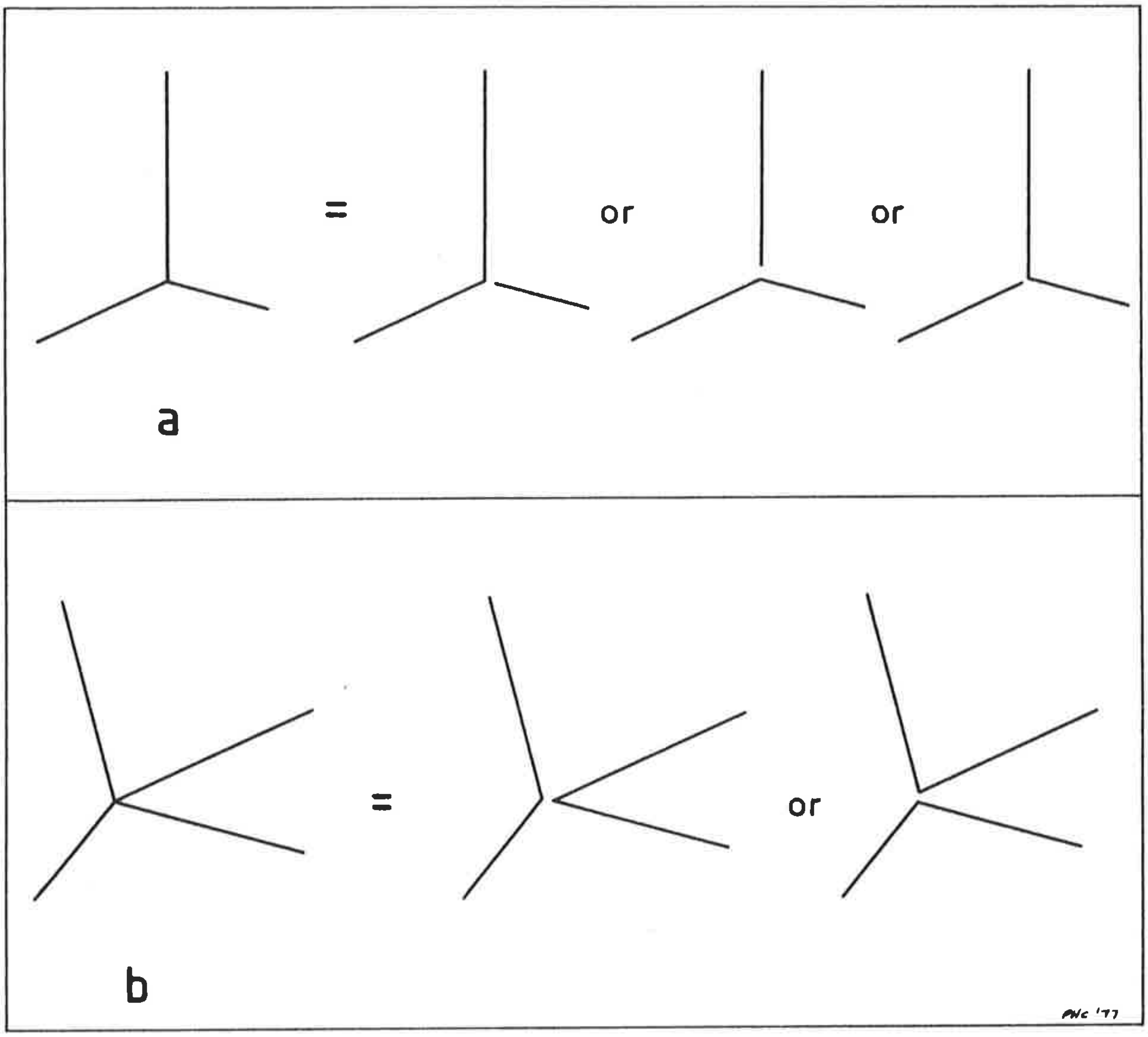

Fig. J.4 Possible interpretations when more than two line segments have a common end-point.

a) Three segments give rise to one continuous contour (Fig. J.2) and an open contour.

b) Four segments give rise to two continous contours.

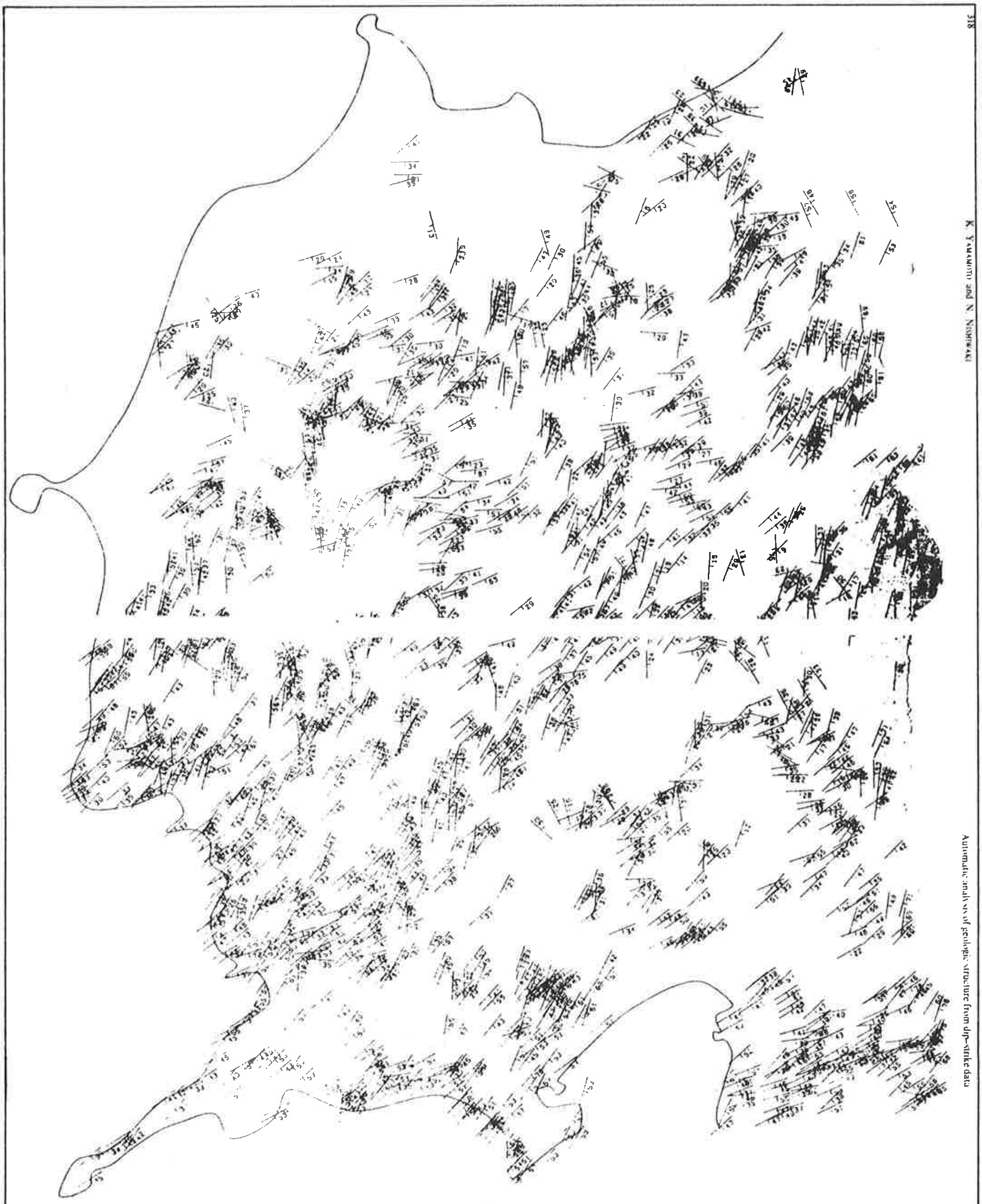

Figure 9. Dip-strike data used in study. Total number of data is 1573, and data of shoreline also are given as reference data.

Fig. K.1 Strike/dip map after Yamamoto and Nishiwaki (1976, fig. 9).

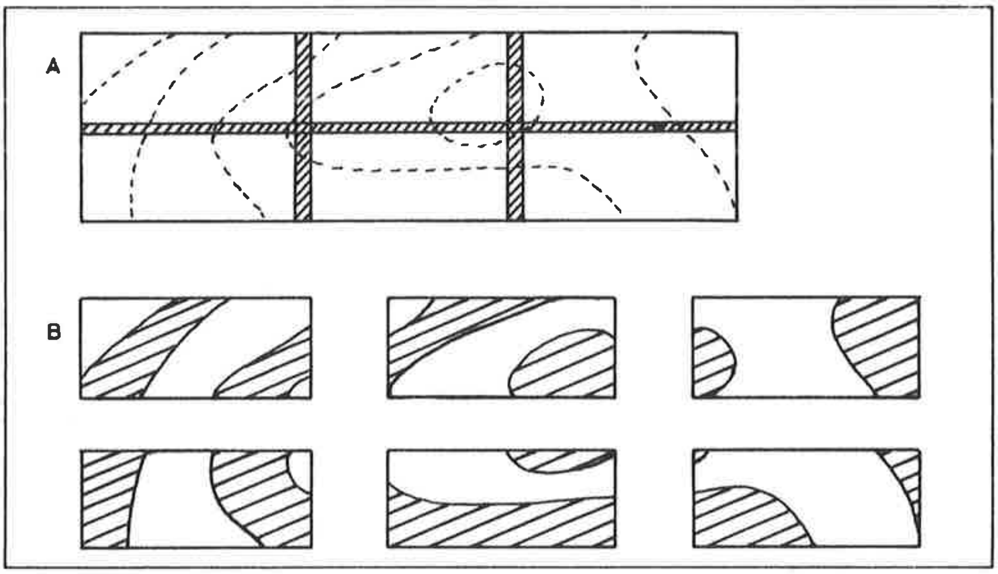

Fig. K.2 Example of output from program MRECON. (a) Reconstituted map showing overlap areas of (b) individually computed submaps. Dashed lines = contours; shading (a) = overlap; shading (b) = contours. (Contours are printed with symbols on a line printer.)

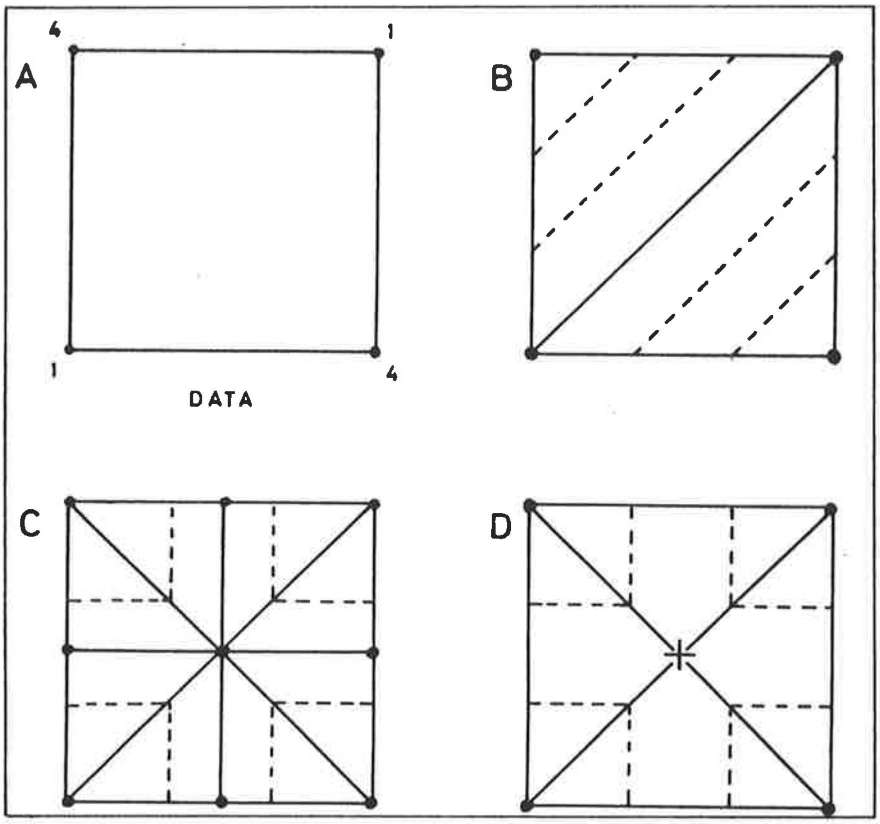

Fig. K.3 Various methods of dividing grid cells into triangles. An ability to detect saddles is preferred.

a) Sample grid cell of a saddle.
b) Method used by program CMPP2.
c) Method of using alternate diagonals (e.g. Starkey, 1977).
d) Method used in program CMPPR, where both diagonals are used and the centre point value is the average of the vertices.

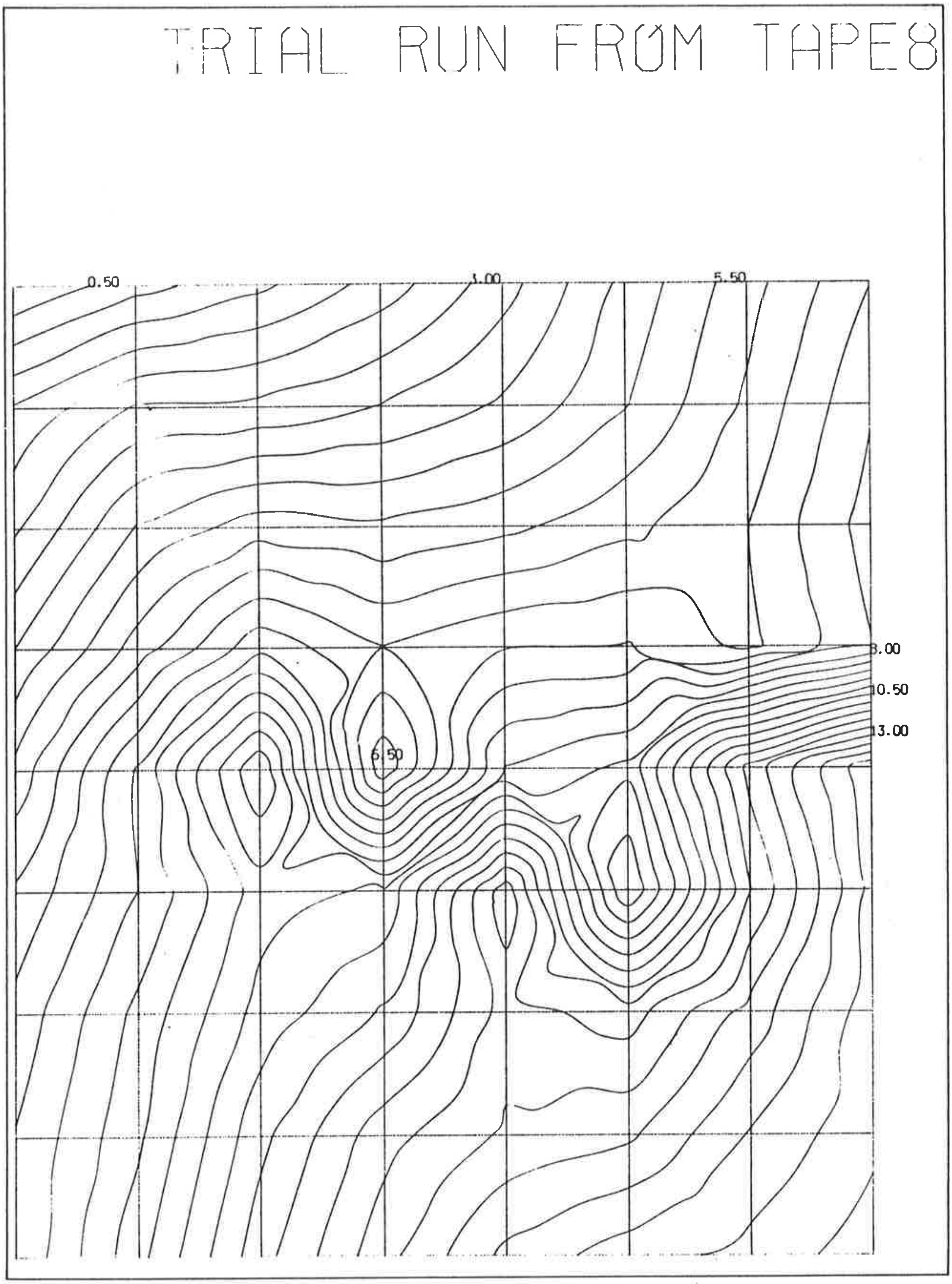

Fig. K.4 Sample output from program CMPPR. (Bias in the NE-SW direction introduced by program CMPP2 is eliminated).

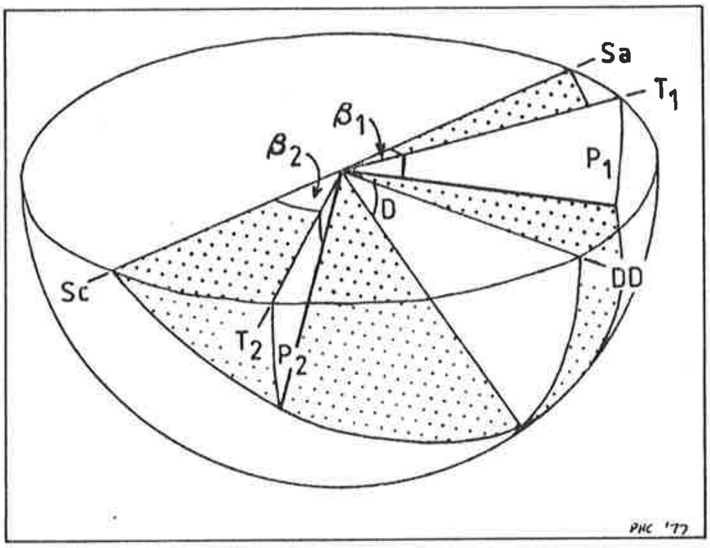

Fig. L.1 Geometry for fitting a plane (DD/D) to two vectors, T_1/P_1 and T_2/P_2. Also used for calculating the intersection of two planes whose poles are the two vectors.

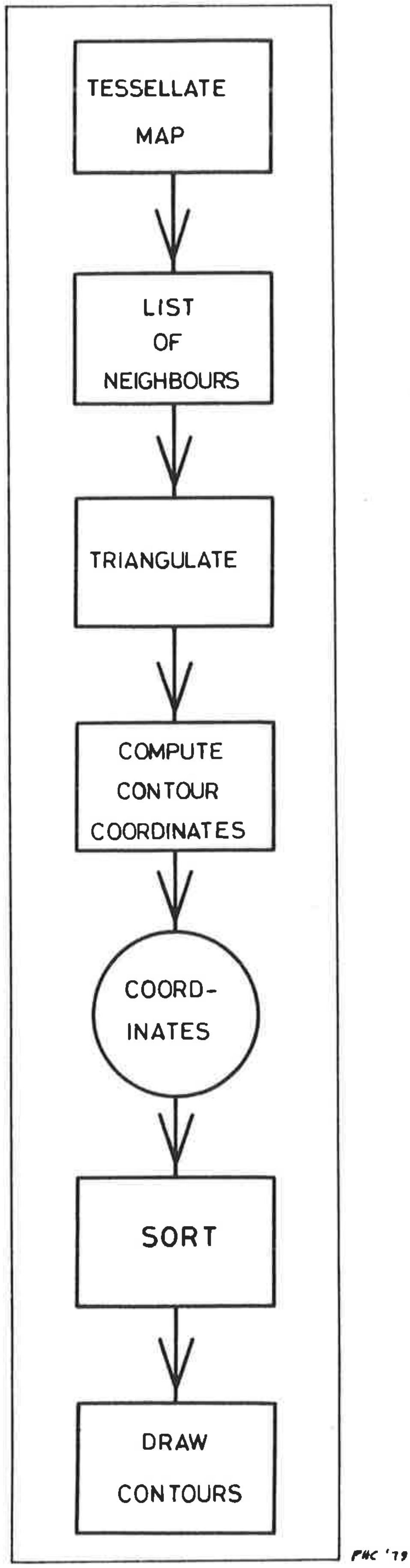

Fig. M.1 Flowchart of program TRICON (see text).

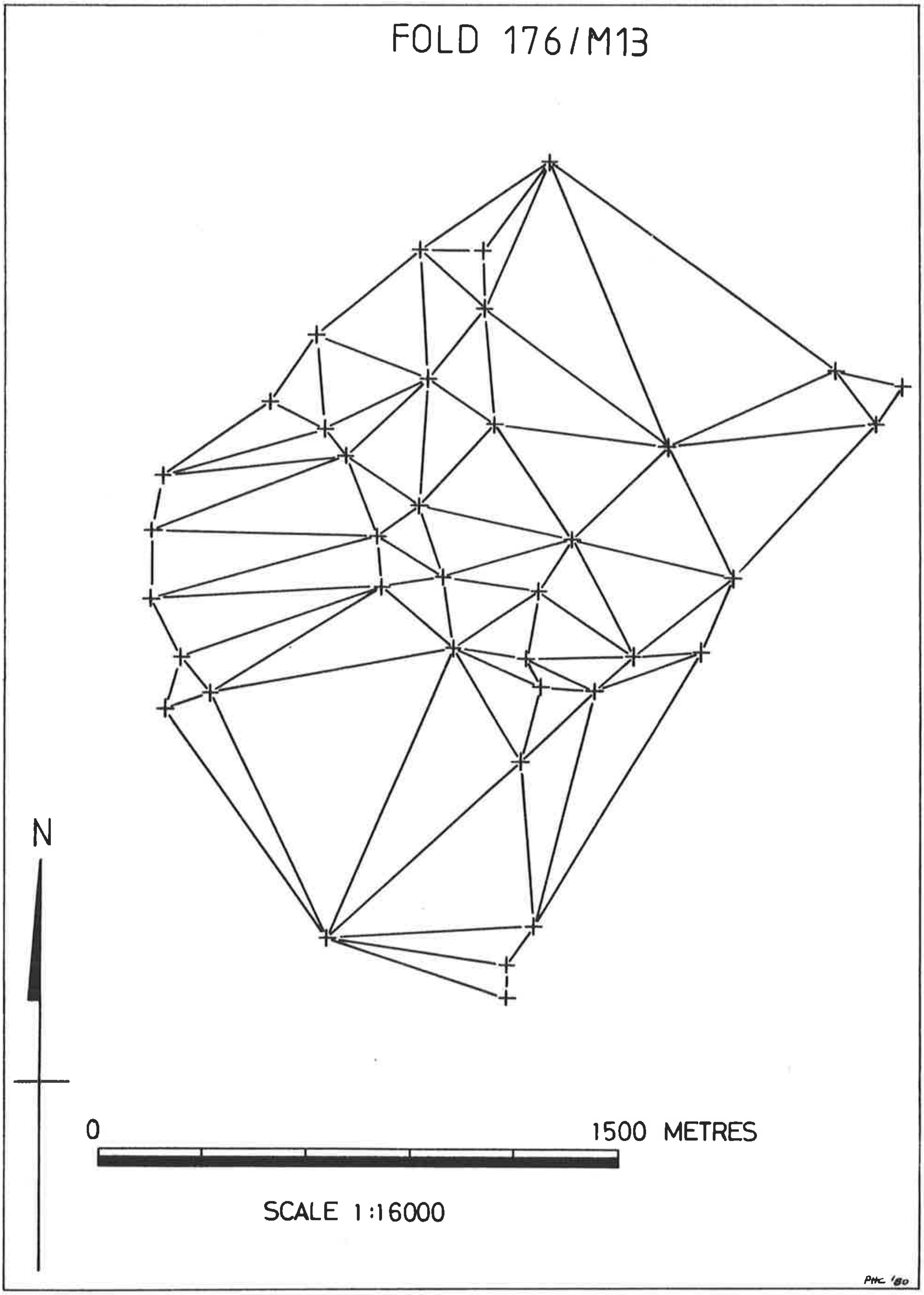

Fig. M.2 Triangulation of a map with data points at the vertices. (The map is the same one figured in Appendix D).

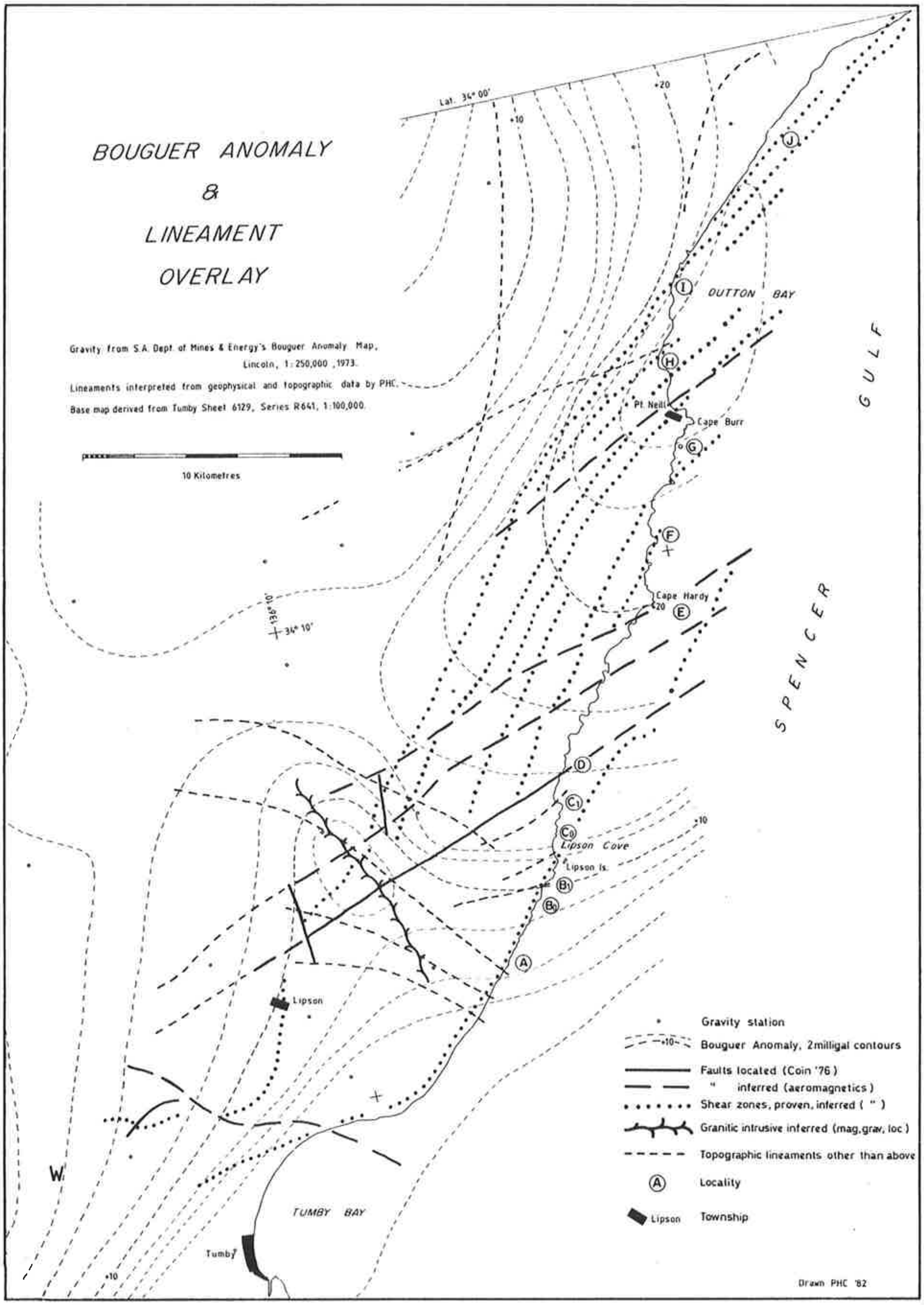

Fig. 0.1 Interpreted lineament map from geophysical and topographic data.

Fig. 0.2 Geological features of interest south of Lipson Cove.

a) Folded boudinaged quartzofeldspathic veins in amphibolites. Scale bar is 12cm. (Locality B_1, Fig. 0.1).

b) A consistent and intense L_3 fabric in augen gneiss plunging towards the northeast. Scale bar is 1m. (Locality B_0, Fig. 0.1)

c) A zoned vein semi-concordant with an intense L-S fabric in the surrounding augen gneiss. The vein (V) shows no tectonic fabric whatsoever. B = beryl, G = garnet, F = feldspar, and M = mica (muscovite). Lens cap is 55mm in diameter. (Locality between A and B_0, Fig. 0.1)

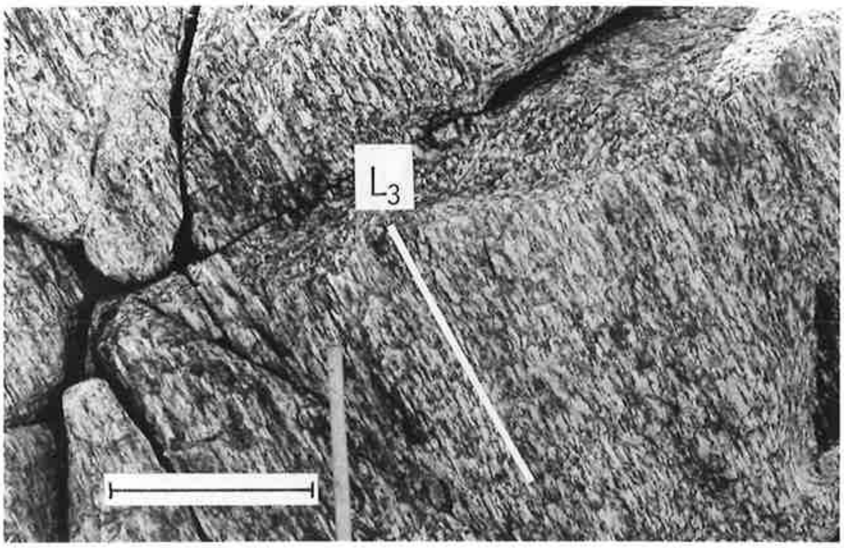
L_3

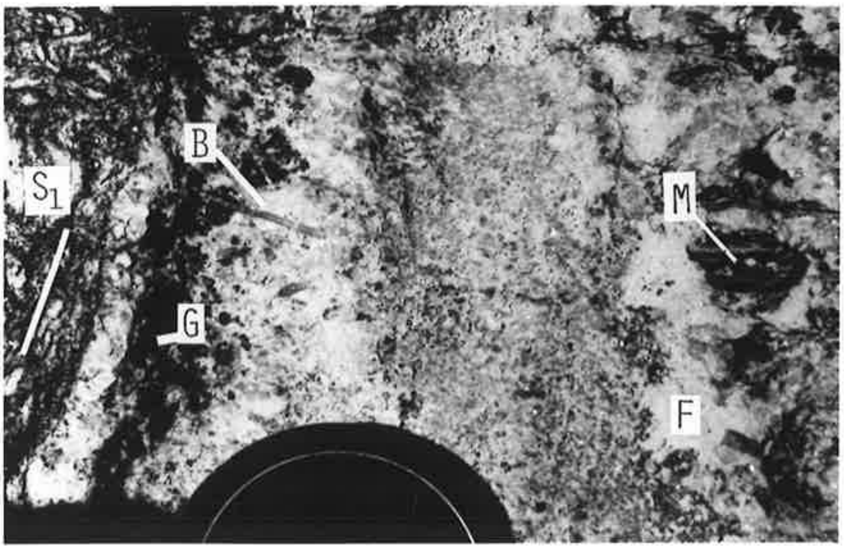
S_1
B
G
M
F

Fig. O.3 L-S fabric in augen gneisses (between localities D and E, Fig. O.1).

a) Variation in augen size across units with a high percentage of dark mineral components. Augen are generally oblate. (Lens cap is 55 mm.)

b) Sketch of LS fabric, drawn from a photograph. Note change in plunge of the lineation (an elongation lineation).

c) Amphibolite boudin in granitic and augen gneisses (between localities D and G, Fig. O.1), showing oblique shearing plane "S", tension fractures "T", and the apophyses "A" demonstrating the intrusive nature of the amphibolite. Scale bar is 40cm.

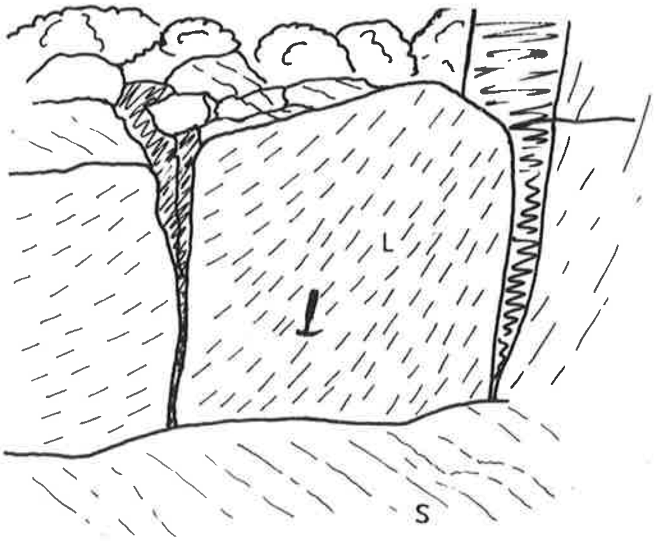
L
S

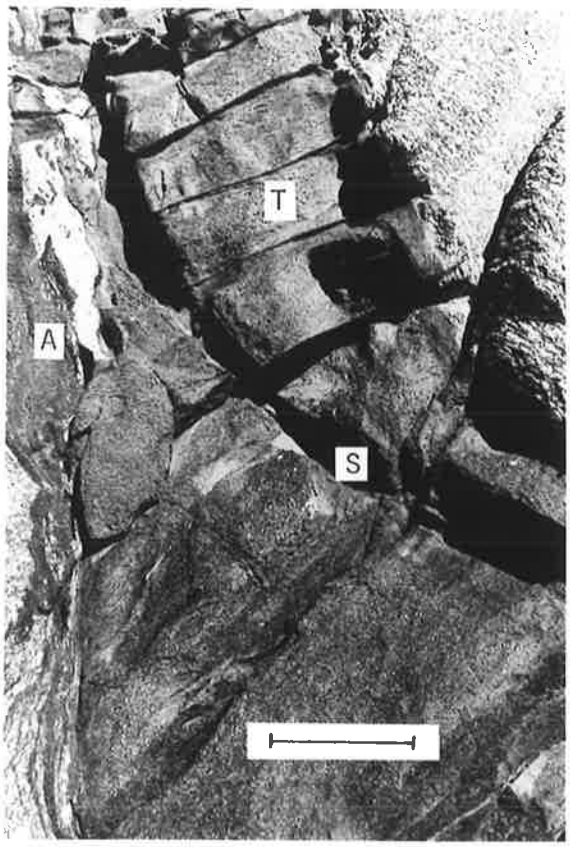
T
A
S

Fig. 0.4 Amphibolite boudins in granitic and augen gneisses (between localities D and G, Fig. 0.1).

c) Vertical section showing "hour-glass" shape in necking of an amphibolite sill.

a) Oblique view showing the three dimensional structure of a large boudin.

b) Vertical section outlined in (a).

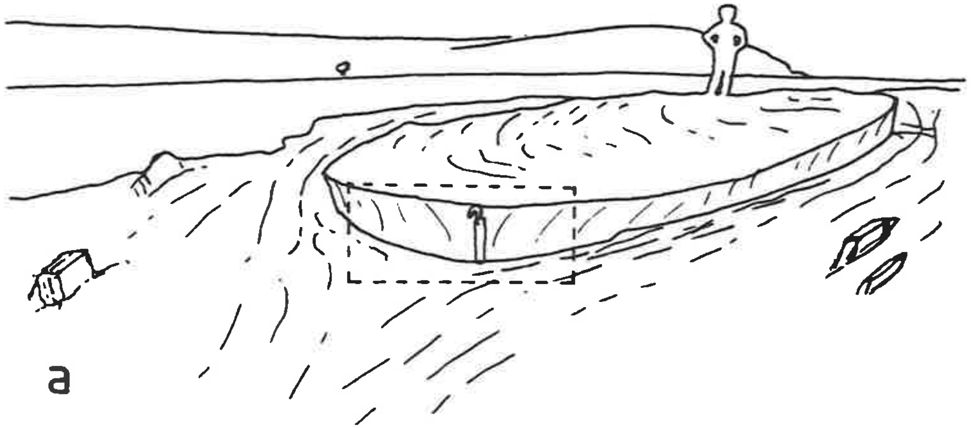

a

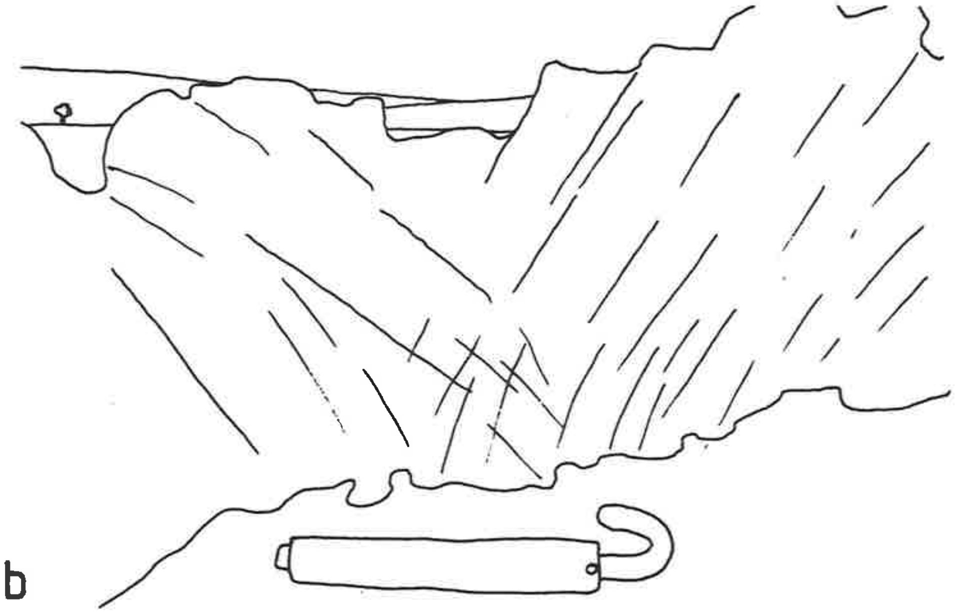

b

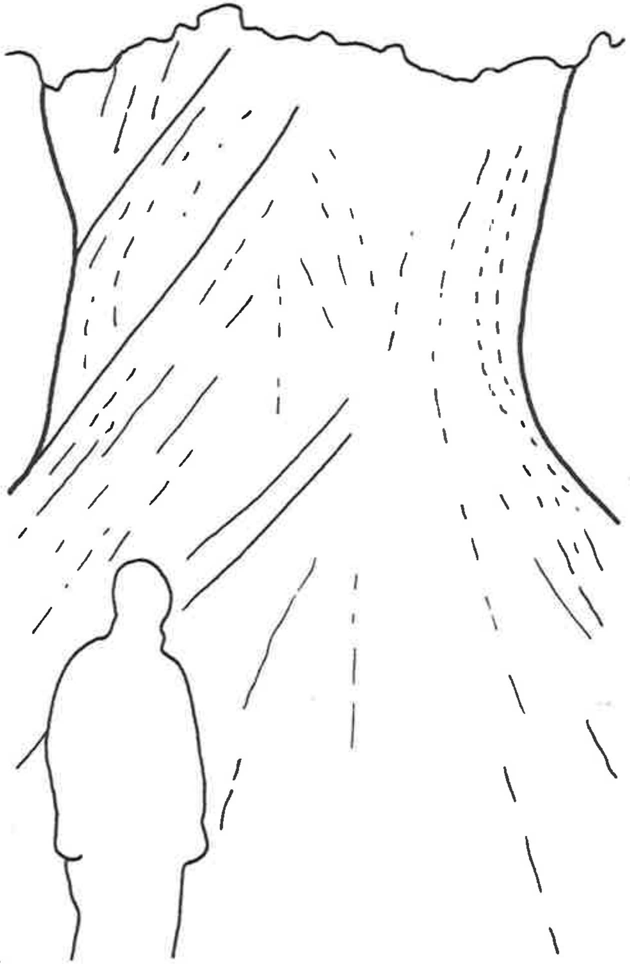

c

Fig. 0.5 Development of a mylonitic foliation from low strain augen (feldspar) gneisses or gneissic megacrystic granites (locality E, Fig. 0.1).

a) Granite showing no strain (approximately 100m in extent) surrounded by (b).

b) Augen gneiss containing low strains.

c) Protomylonite fabric in augen gneiss (locality F, Fig. 0.1).

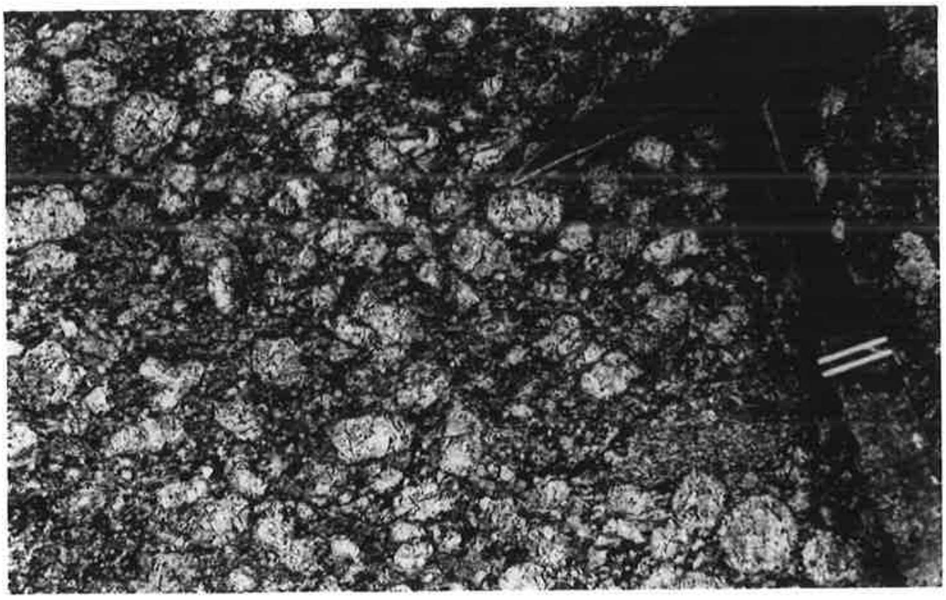

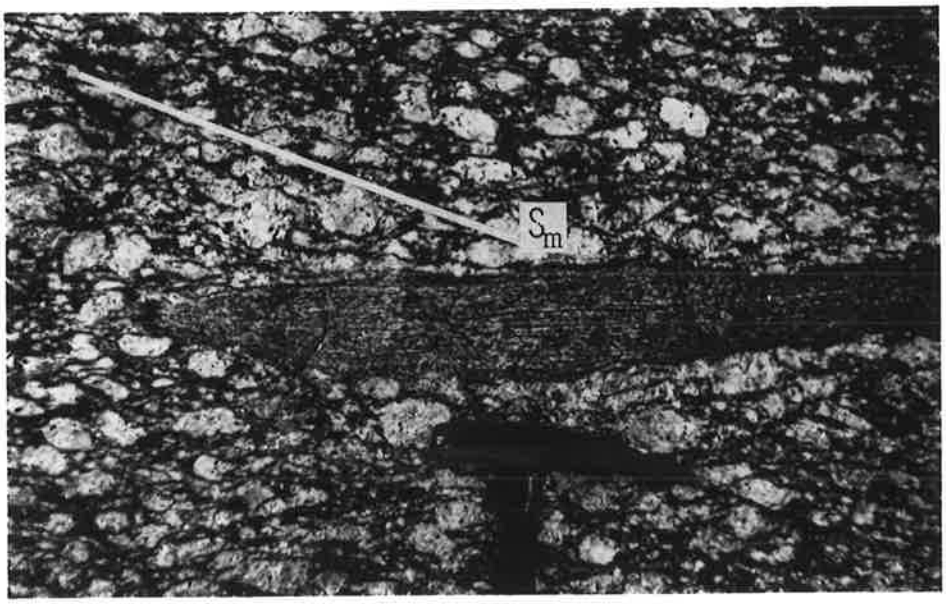
Sm


Sm

Fig. 0.6 F_2(?) folds in granitic gneiss.

a) Fold at locality F (Fig. 0.1). L_i is parallel to the fold hinge. Scale bar is 1 m.

b) (Left) Profile plane of (a). Note lack of a visible folded foliation. Scale bar is 5 cm.

c) (Right) Folds similar to (a) also occur that show that the foliation is folded. Lens cap is 55mm in diameter.

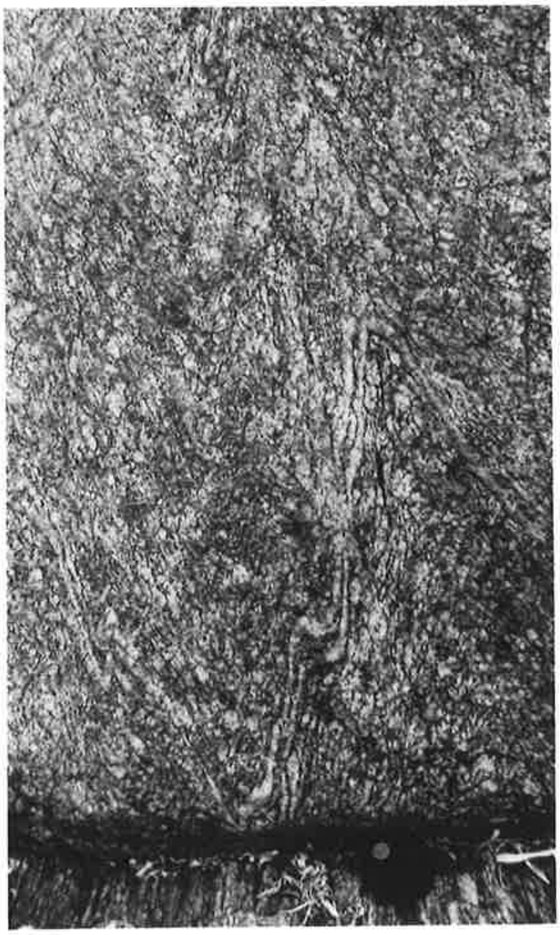

Fig. O.7 Features of the Kalinjala mylonite zone north of Cape Burr.

a) Mylonite fabric in acid granulites. Scale bar is 40 cm.

b) Rotated mylonite fabric in boudins (locality H, Fig. O.1, looking SW). The rocks are gneisses, and the boudins are separated by pegmatites (dominantly feldspar) veins trending NE-SW. (The bucket has a 2 gallon capacity.)

c) (Left) Intrafolial folds in acid granulite adjacent to mylonites. (Lens cap is 55mm.)

d) (Right) Boudins of isoclinally folded mafic granulites in acid granulites.

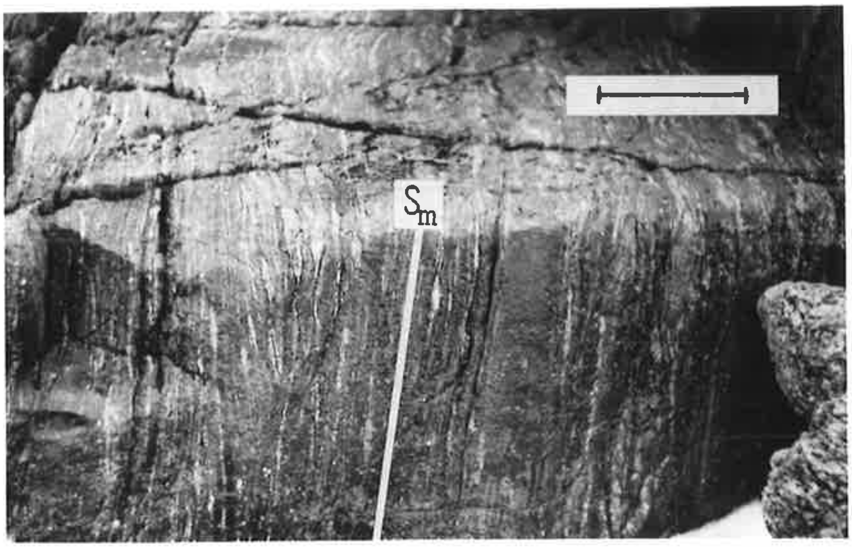
Sm

Fig. 0.8 Geological features at Waterfall (Mine) Creek (Locality W, Fig. 0.1).

a) Augen gneiss near mylonite zone. The mylonite fabric S_m dominates over the earlier foliations (not visible as they are coaxial in this view). Scale bar is 13 cm.

b) An approximately profile view of tight, reclined F_2 folds in quartzofeldspathic gneisses 1 km east of the mylonite zone. Scale bar is 1 m.

c) Small scale tight folds in the vicinity of (b). Scale bar is 12 cm.

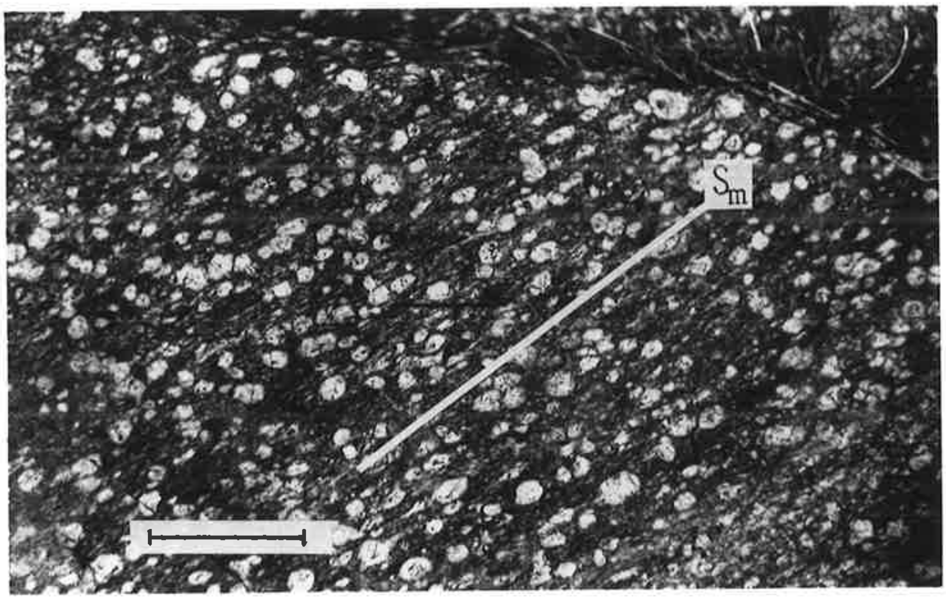
S_m

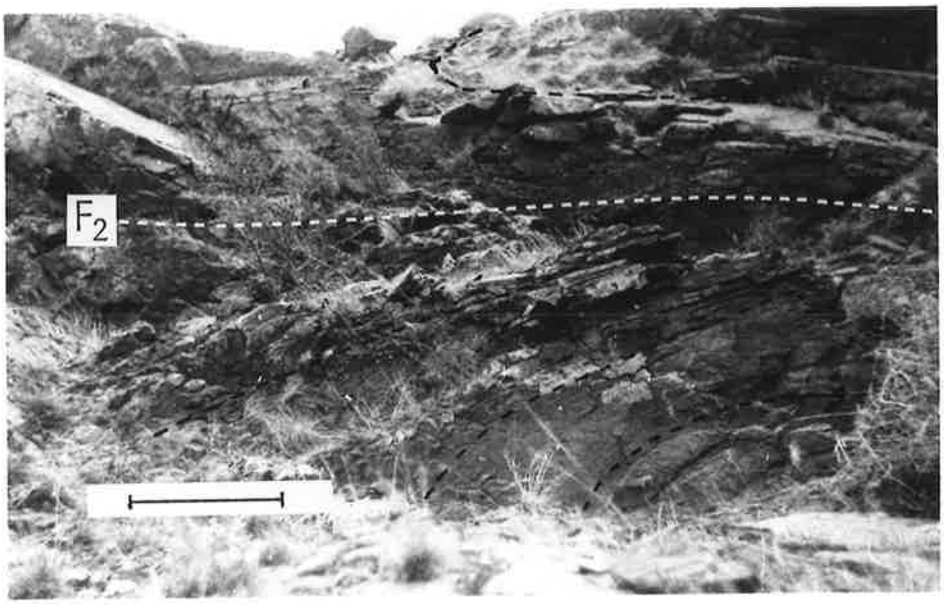
F_2

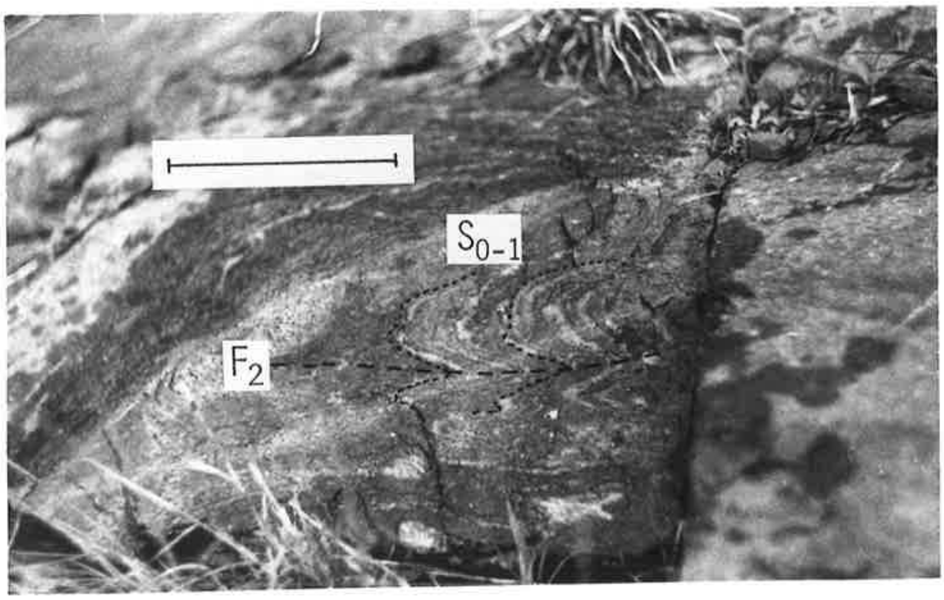
S_0-1
F_2

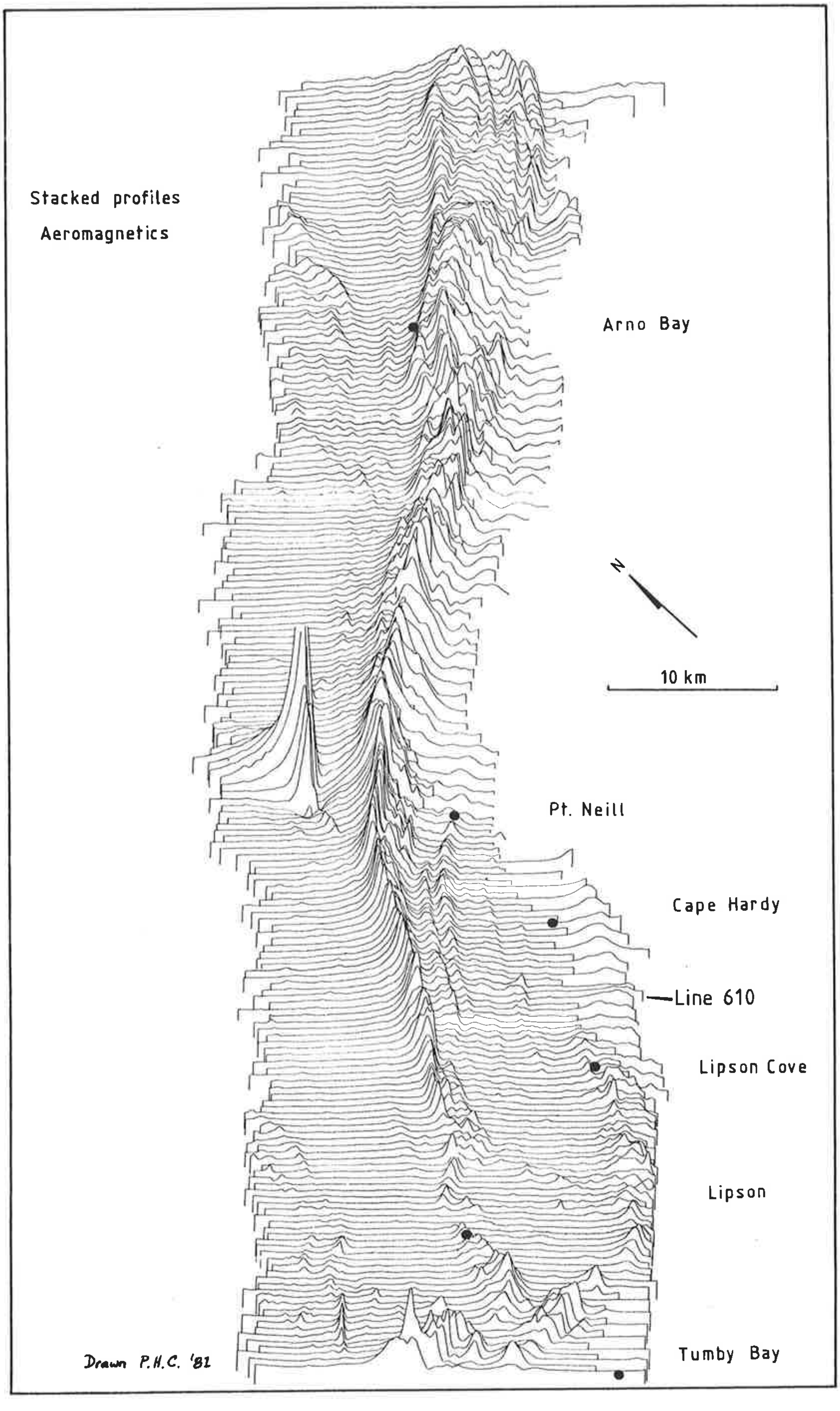

Fig. P.1 Stacked magnetic profiles showing magnetic surface topography. Data from magnetic profile sheets produced by B.H.P. from their low-level aeromagnetics of the Arno Bay area, 1976.

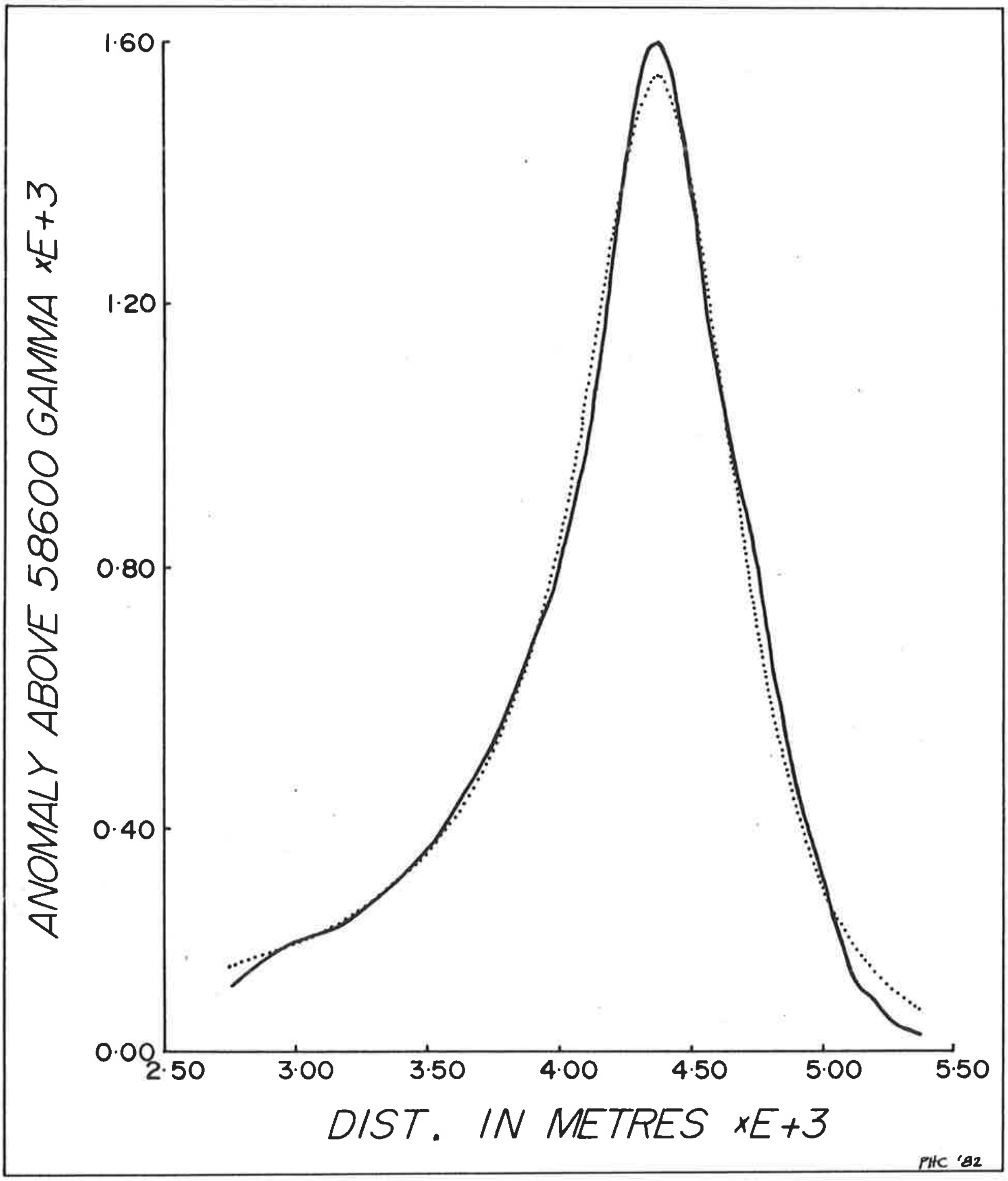

Fig. P.2 Sample aeromagnetic profile (Line 610, Fig. P.1) across the Kalinjala mylonite zone, interpreted using a computer program developed by Ukaigwe (personnal communication).
Given: Dike strike = 130°*, Inclination = -65°, Field intensity = 58600 gammas. 39 sample points were used.
Computed: Magnetic susceptibility = 0.0214, Dip = 70.1°, Depth = 338.6m (below flight height of 80m), Width = 253.8m, Centre = 64.7m southeast of anomaly peak.

---

* The term 'strike' is used here in a geophysical context and is perpendicular to the geological strike, in this case, 040°.

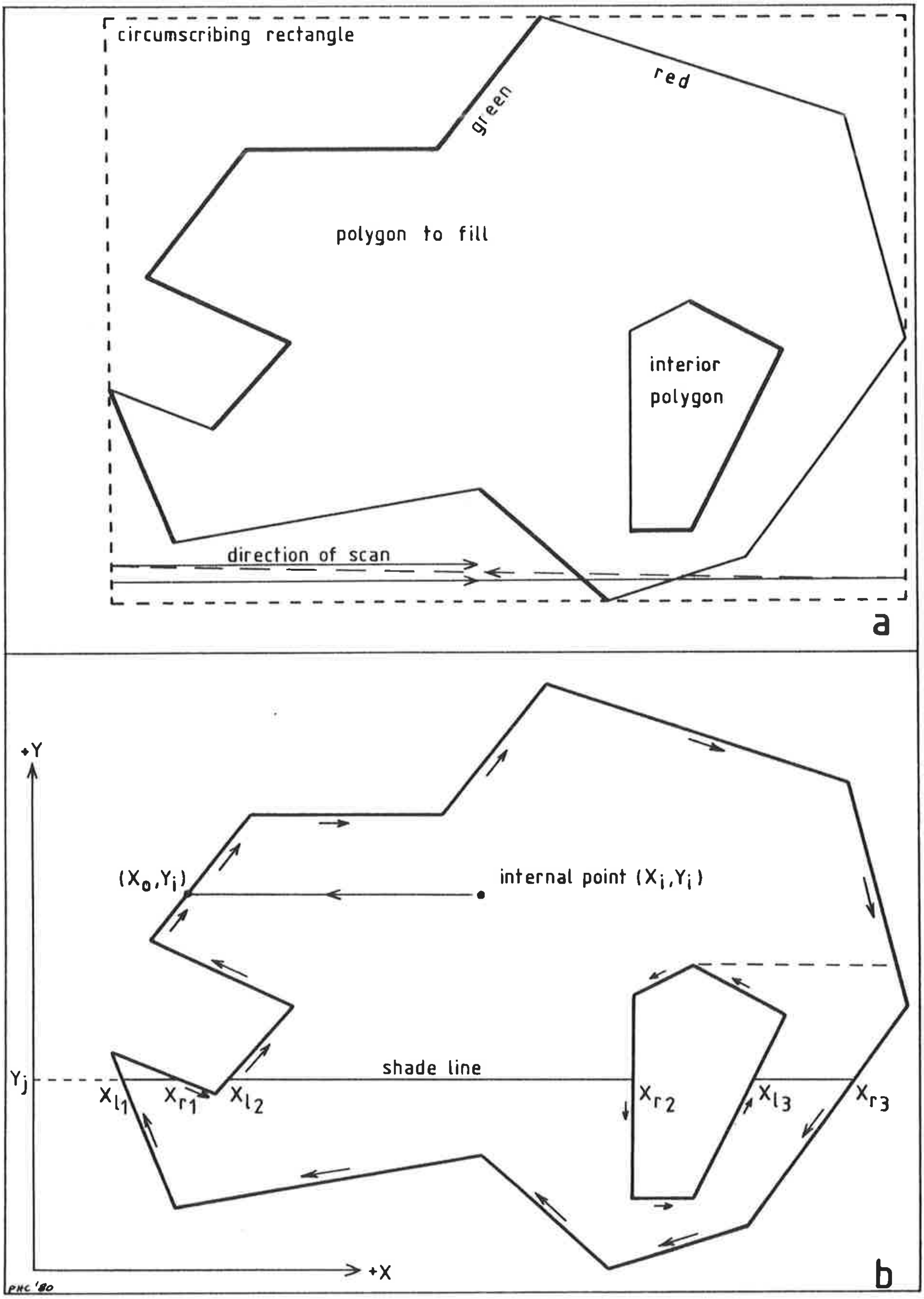

Fig. Q.1 Two situations for polygon fill routines.

a) Set up for filling without a known internal point.

b) Set up for filling with a known internal point.

```
C         SHADE POLYGON IN BLUE

          CALL FCLR(MINX,MINY,MAXX,MAXY,0)    ;BLANK CIRCUMSCRIBING RECTANGLE
          CALL FDBND(BNDX,BNDY,NPT,3,5,1,-1) ;DRAW POLYGON IN GREEN/RED
          CONTINUE
A         LDA      0,MODE1
A         DOC      0,76
A         LDA      0,@.IDY ;SET UP LOOP BY ROWS
A         INC      0,0
A         INC      0,0
A         STA      0,LNY
A         LDA      1,@.MINY
A         NEG      1,1
A         COM      1,1
AL.270:   LDA      0,@.IDX ;SET UP LOOP BY COLUMNS
A         INC      0,0
A         INC      0,0
A         STA      0,LNX
A         LDA      2,@.MINX
A         NEG      2,2
A         COM      2,2
A         SUB      0,0
AL.280:   LDA      3,GREEN ;PULSE FOR GREEN
A         ADD      3,1
A         DOA      1,76
A         DOBP     2,76
A         LDA      3,GREEN ;PREPARE FOR RED
A         ADD      3,1
A         JMP      .+1
A         JMP      .+1
A         JMP      .+1
A         DIB      3,76      ;GET GREEN BIT
A         DOA      1,76      ;PULSE FOR RED
A         DOBP     2,76
A         COM#     3,3,SNR ;GREEN ?
A         MOV      3,0,SKP ;YES, SET AC0#0
A         SUB      3,3       ;NO
A         STA      3,GBIT    ;SAVE GREEN
A         MOVL     1,1       ;PREPARE FOR BLUE
A         MOVZR    1,1
A         DIB      3,76      ;GET RED BIT
A         COMZ     3,3,SNR ;RED ?
A         SUB      0,0       ;YES
A         LDA      3,GBIT    ;AC3=GREEN, CARRY=RED
A         MOVL#    3,3,SNR ;ON BORDER ?
A         JMP      L.290     ;NO
A         MOV#     3,3,SBN ;YES, AT VERTEX ?
A         JMP      L.300     ;NO
A         LDA      0,BBIT    ;YES
A         JMP      L.300+2
AL.290:   MOV#     0,0,SNR ;INSIDE ?
A         JMP      L.300     ;NO
A         DOA      1,76      ;YES, SHADE BLUE
A         DOB      2,76
A         SUBZL    3,3,SKP
AL.300:   SUBCL    3,3
A         STA      3,BBIT
A         INC      2,2       ;NEXT COLUMN
A         DSZ      LNX
A         JMP      L.280
A         INC      1,1       ;NEXT ROW
A         DSZ      LNY
A         JMP      L.270
A         JMP      L.330     ;EXIT
A
AMODE1:   217
AGREEN:   040000
A  LNX:   0
A  LNY:   0
A BBIT:   0
A GBIT:   0
A.MINX:   .GADD    V4,12.
A.MINY:   .GADD    V4,16.
A .IDX:   .GADD    V4,19.
A .IDY:   .GADD    V4,20.
```

PHC '80

Fig. Q.2 Routine to shade a polygon without an internal starting point.

(A)

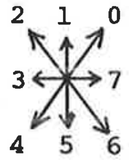

(B)

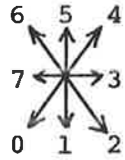

(C)

0	1	2	3	4	5	6	7
6 → 3	0 → 4	0 → 5	2 → 6	2 → 7	4 → 0	4 → 1	6 → 2

(D)

0	1	2	3	4	5	6	7
0,1,2,3,4,5	always	always	never	0	1,0	2,1,0	3,2,1,0

PHC '80

Fig. Q.3 Method of tracking boundaries and determining where the boundary is in position to shade lines.

a) Labelled directions of searching for the next boundary point.

b) As for (a) but rotated 180°.

c) To track a polygon boundary in a clockwise direction the search for the next boundary point is anticlockwise around the current boundary point, as it is conducted inside the polygon (analogous to gearing). The top line is a list of directions (a) with which the current boundary point was found, and the second line gives the appropriate direction sequence to search. Tracking polygon boundaries anticlockwise can be done using the (b) directions.

c) Conditions which must prevail if a boundary point is to be to the left of a shade line (use (a) directions). The top line is the same as for (b), and the second line is the direction in which the next boundary point must lie. To determine if a boundary point is to the right of a shade line, use (b) directions.

A) XY$key.DT

Line		
1	FORMAT(S51)	Title of map.
2	FORMAT(8I5,1X,F10.2)	Map origin (X,Y), no. of data columns (including descriptions), map border (X_{min}, Y_{min}, X_{max}, Y_{max}), fine/coarse digitising, map scale.
3	FORMAT(15(S7))	Names of data columns (including descriptions).
4	FORMAT(I1,2I5,15(1X,I3,1X,I2,1X))	Colour, X, Y, description, data.
5	"	
.	.	
.	.	

B) RF$key.DT and PY$key.DT

1	FORMAT(I1,I2,I1,2I5,1X,A10)	Colour, point-type, "start-of-line" flag, X, Y, name-of-item.
2	"	
.	.	
.	.	

C) XYkeyXY.BN

Word Location	
0 - 35+4*NCOL (=n)	Binary dump of lines 1 to 3 of XY$key.DT .
n+1 - n+3+NCOL	Data point coordinate and colour (X/colour*, Y), Description word, Data ($plunge_j/trend_j$+, $1 \leq j \leq NCOL$).
.	.
.	.

* | X | ICOL | 0 |

\+ | TR | PL |

D) PYkeyPY.BN

0 - 1	X/"start-of-line" flag#, Y
.	.
.	.

\# | X | FLC |

PHC '80

Fig. R.1 Source files. Each referenced box (*,+,#,%) represents a single 16 bit computer word. Lengths of the fields within each word are not specified here.

A) XYkey1v.BN

0 - 50	Title
51 - 54	ISIZ, OSIZ, OSCX, OSCY
55	No. of boundary points (NPT)
next NPT*2 words	Subarea boundary coordinates
(n = 56+NPT*2)	(x_1,y_1; x_2,y_2; ...)
n - n+2	Data record no. in XY$key.DT, coordinate/colour (X/colour#, Y)
n+3 - n+5	" " " " " , " , "
.	.
.	.

| X | ICOL | 0 |

B) RFkey1v.BN

0 - 1	"start-of-line" flag/colour/X+, point-type/Y%
2 - 3	" " , "
.	.
.	.

+ | FLC | ICOL | X | % | IPT | Y |

C) PYkeyPY.BN and PYkey1v.DT

0 - 1	X/"start-of-line" flag*, Y
.	.
.	.

* | X | FLC |

PHC '80

Fig. R.2 Subarea files. (See caption to Fig. R.1.)

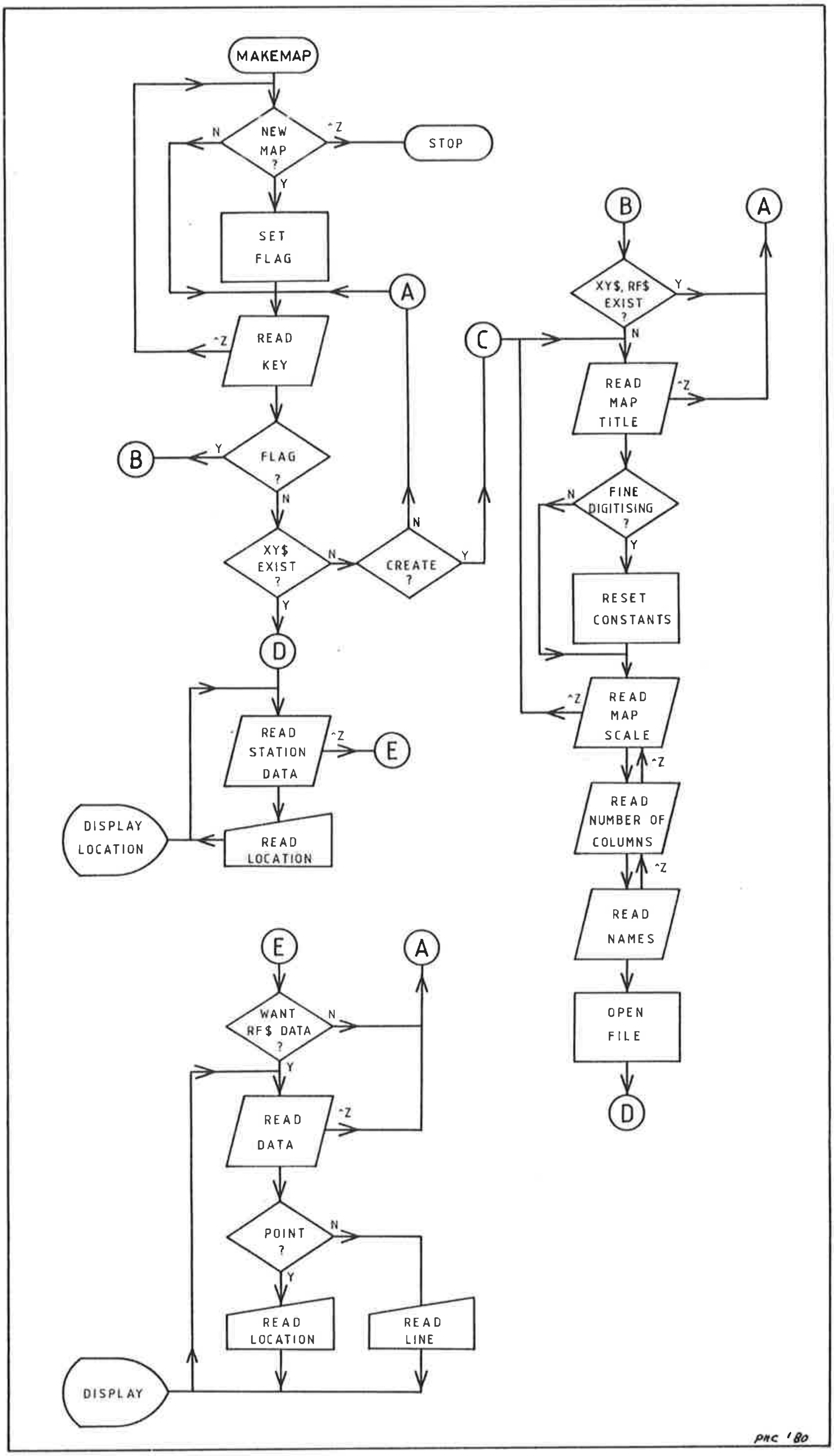

Fig. R.3 Flow chart for program MAKEMAP.

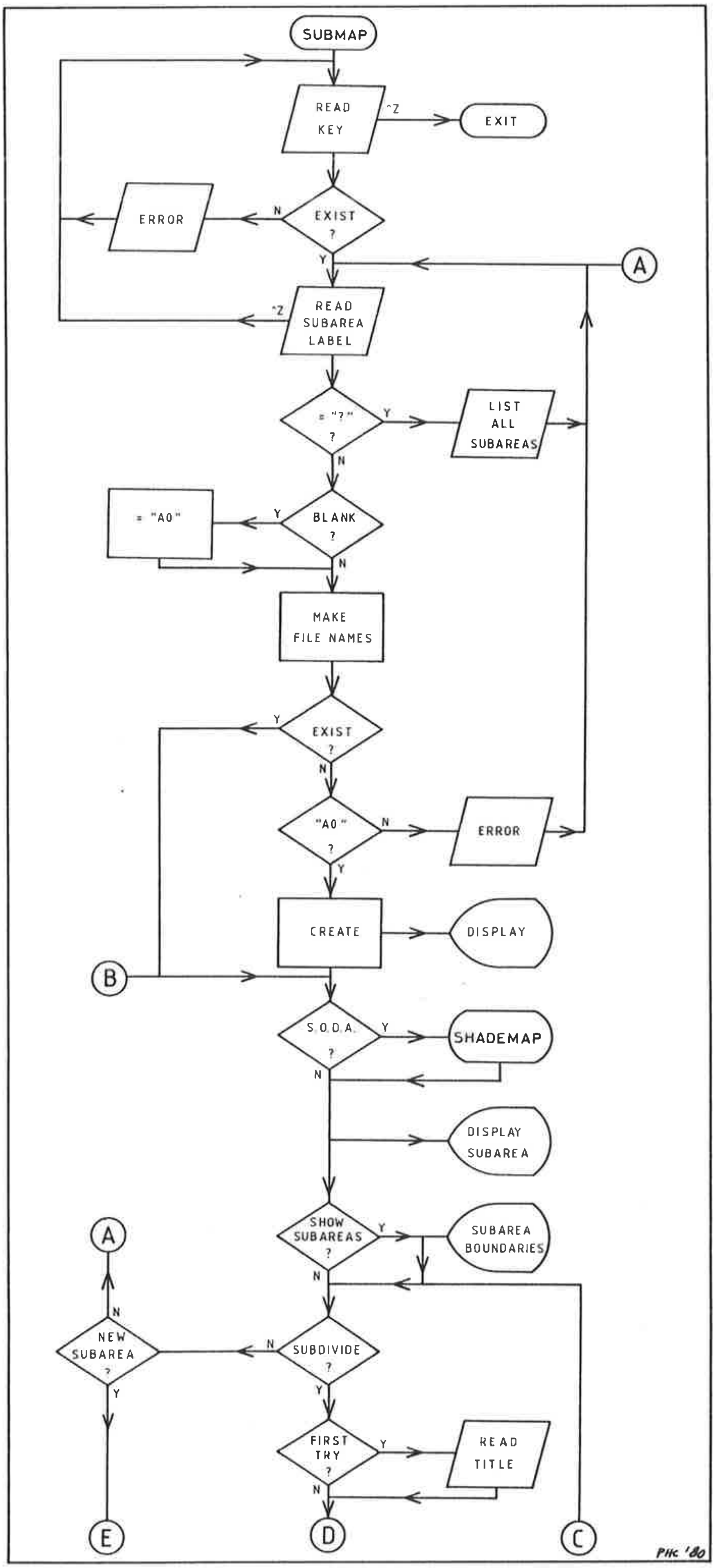

Fig. R.4 Flow chart for program SUBMAP.

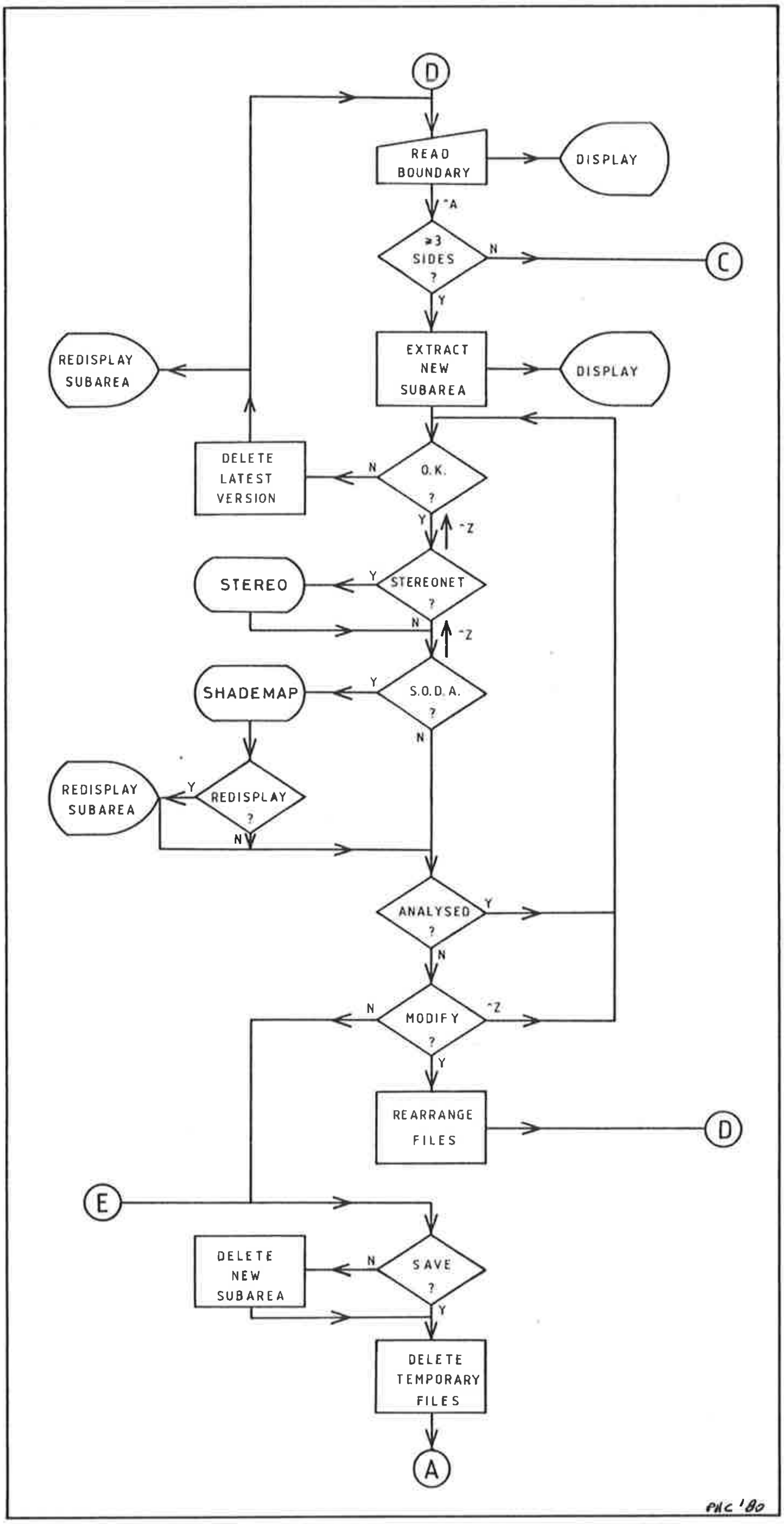
D
READ
BOUNDARY
DISPLAY
~A
≥3
SIDES
?
N
C
Y
EXTRACT
NEW
SUBAREA
DISPLAY
REDISPLAY
SUBAREA
DELETE
LATEST
VERSION
N
O.K.
?
Y
~Z
STEREO
Y
STEREONET
?
N
~Z
SHADEMAP
Y
S.O.D.A.
?
N
REDISPLAY
SUBAREA
Y
REDISPLAY
?
N
ANALYSED
?
Y
N
N
MODIFY
?
~Z
Y
REARRANGE
FILES
D
E
DELETE
NEW
SUBAREA
N
SAVE
?
Y
DELETE
TEMPORARY
FILES
A
PHC '80

Fig. R.4 (cont.)

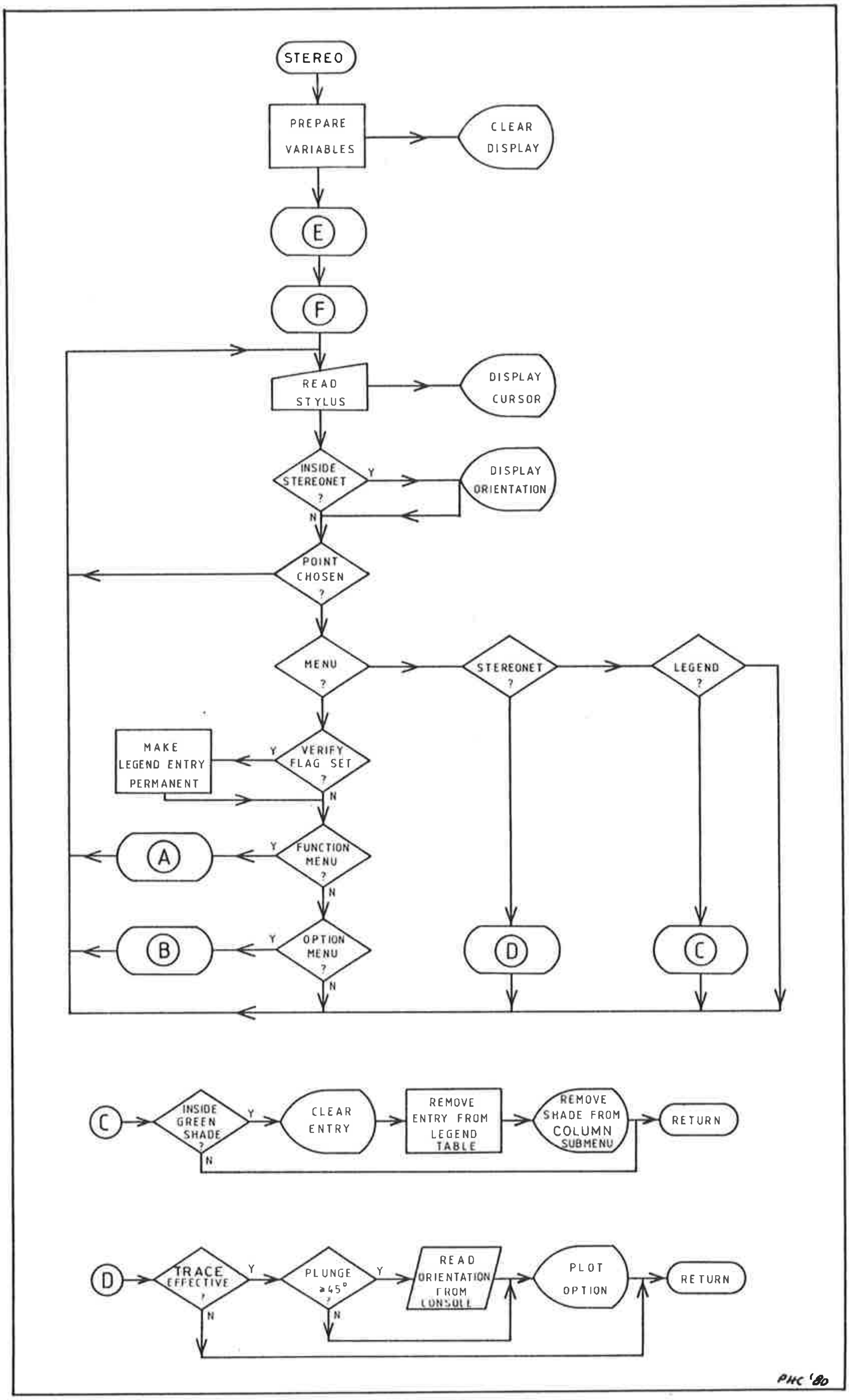

Fig. R.5 Flow chart for program STEREO.

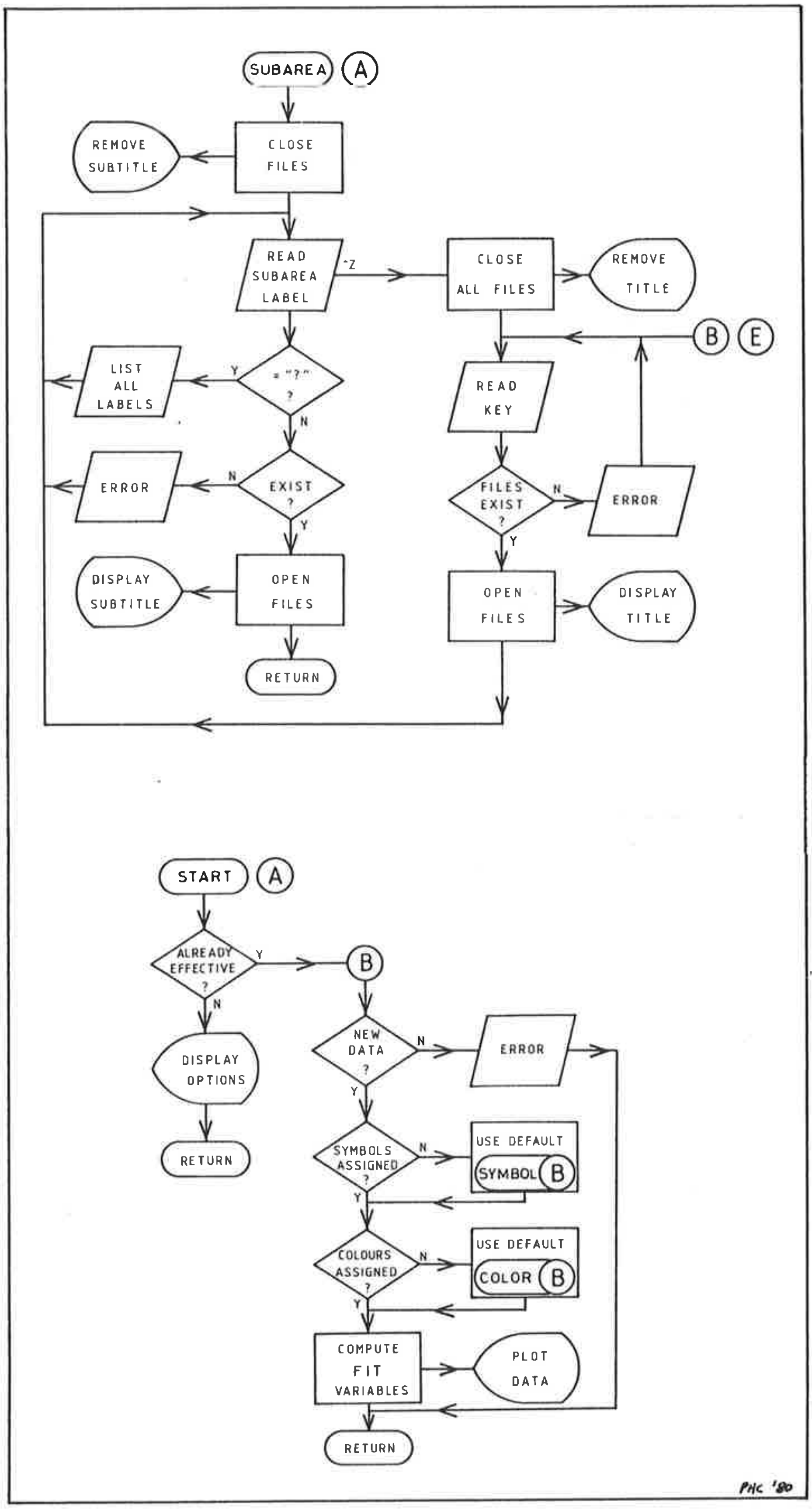
SUBAREA
A
CLOSE FILES
REMOVE SUBTITLE
READ SUBAREA LABEL
^Z
CLOSE ALL FILES
REMOVE TITLE
B
E
= "?" ?
Y
N
LIST ALL LABELS
READ KEY
EXIST ?
ERROR
FILES EXIST ?
ERROR
OPEN FILES
DISPLAY SUBTITLE
OPEN FILES
DISPLAY TITLE
RETURN
START
ALREADY EFFECTIVE ?
DISPLAY OPTIONS
RETURN
NEW DATA ?
ERROR
SYMBOLS ASSIGNED ?
USE DEFAULT
SYMBOL
COLOURS ASSIGNED ?
USE DEFAULT
COLOR
COMPUTE FIT VARIABLES
PLOT DATA
RETURN
PHC '80

Fig. R.5 (cont.)

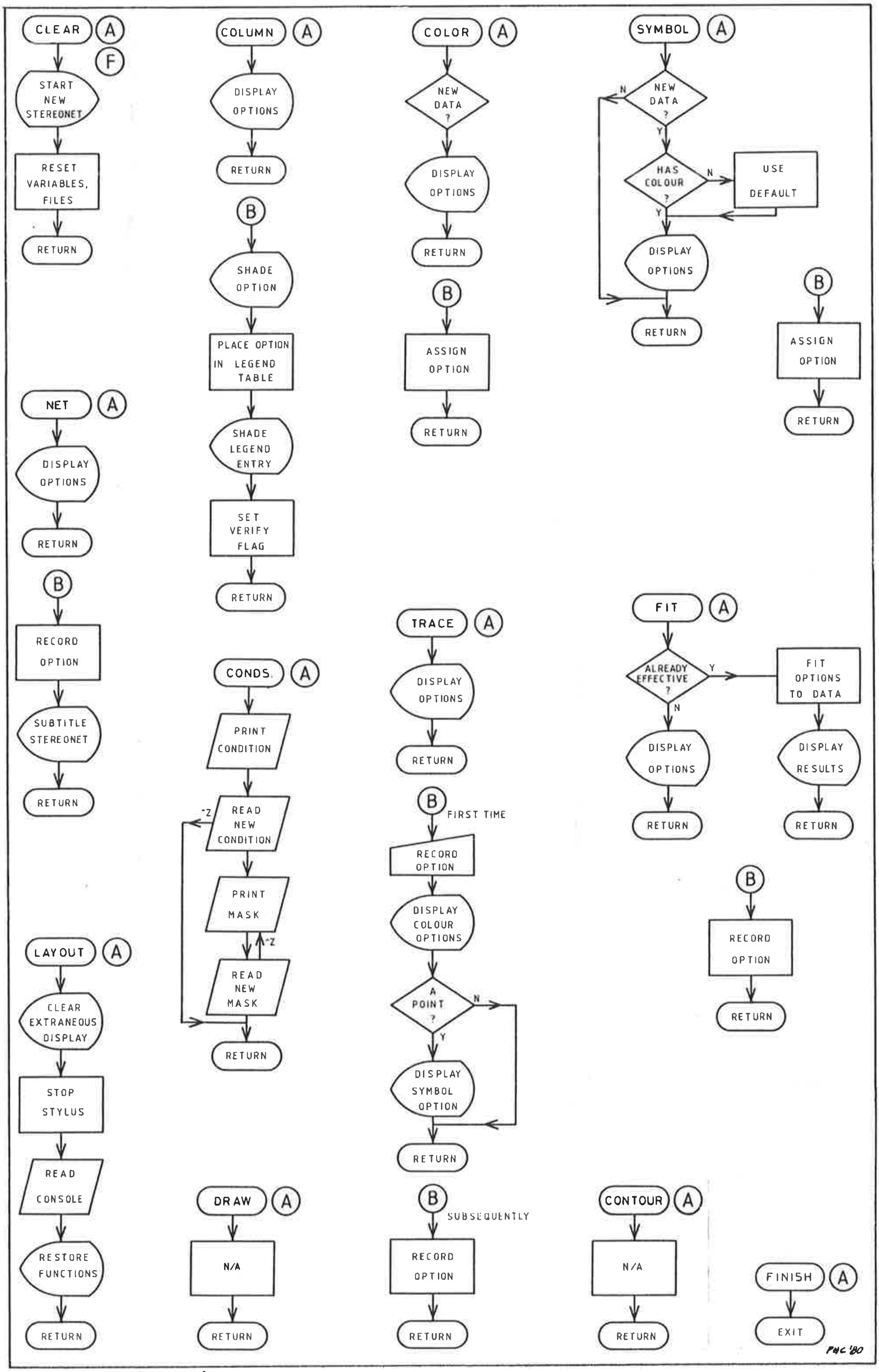
CLEAR
A
F
START NEW STEREONET
RESET VARIABLES, FILES
RETURN
COLUMN
DISPLAY OPTIONS
RETURN
B
SHADE OPTION
PLACE OPTION IN LEGEND TABLE
SHADE LEGEND ENTRY
SET VERIFY FLAG
RETURN
COLOR
NEW DATA ?
DISPLAY OPTIONS
RETURN
ASSIGN OPTION
RETURN
SYMBOL
NEW DATA ?
N
Y
HAS COLOUR ?
USE DEFAULT
DISPLAY OPTIONS
RETURN
ASSIGN OPTION
RETURN
NET
DISPLAY OPTIONS
RETURN
RECORD OPTION
SUBTITLE STEREONET
RETURN
CONDS
PRINT CONDITION
READ NEW CONDITION
^Z
PRINT MASK
READ NEW MASK
RETURN
TRACE
DISPLAY OPTIONS
RETURN
FIRST TIME
RECORD OPTION
DISPLAY COLOUR OPTIONS
A POINT ?
DISPLAY SYMBOL OPTION
RETURN
FIT
ALREADY EFFECTIVE ?
FIT OPTIONS TO DATA
DISPLAY OPTIONS
DISPLAY RESULTS
RETURN
RECORD OPTION
RETURN
LAYOUT
CLEAR EXTRANEOUS DISPLAY
STOP STYLUS
READ CONSOLE
RESTORE FUNCTIONS
RETURN
DRAW
N/A
RETURN
SUBSEQUENTLY
RECORD OPTION
RETURN
CONTOUR
N/A
RETURN
FINISH
EXIT
PHC '80

Fig. R.5 (cont.)

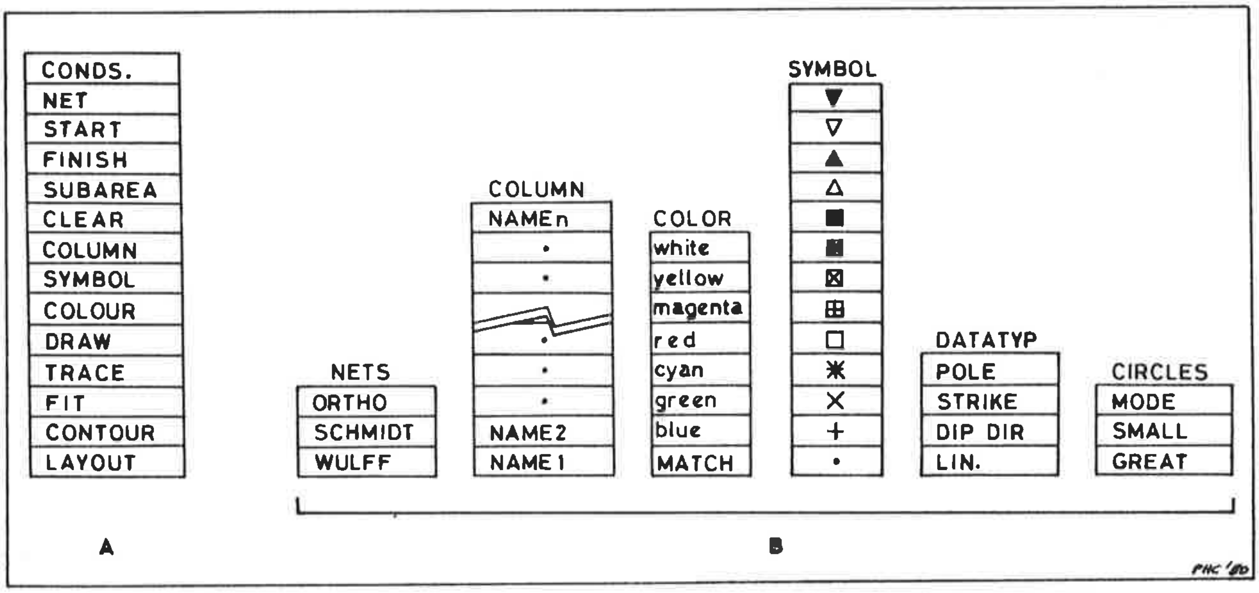

Fig. R.6 Interactive menus for controlling on-screen stereonet plotting.

a) Primary, or functions, menu.

b) Secondary, or options, menus.

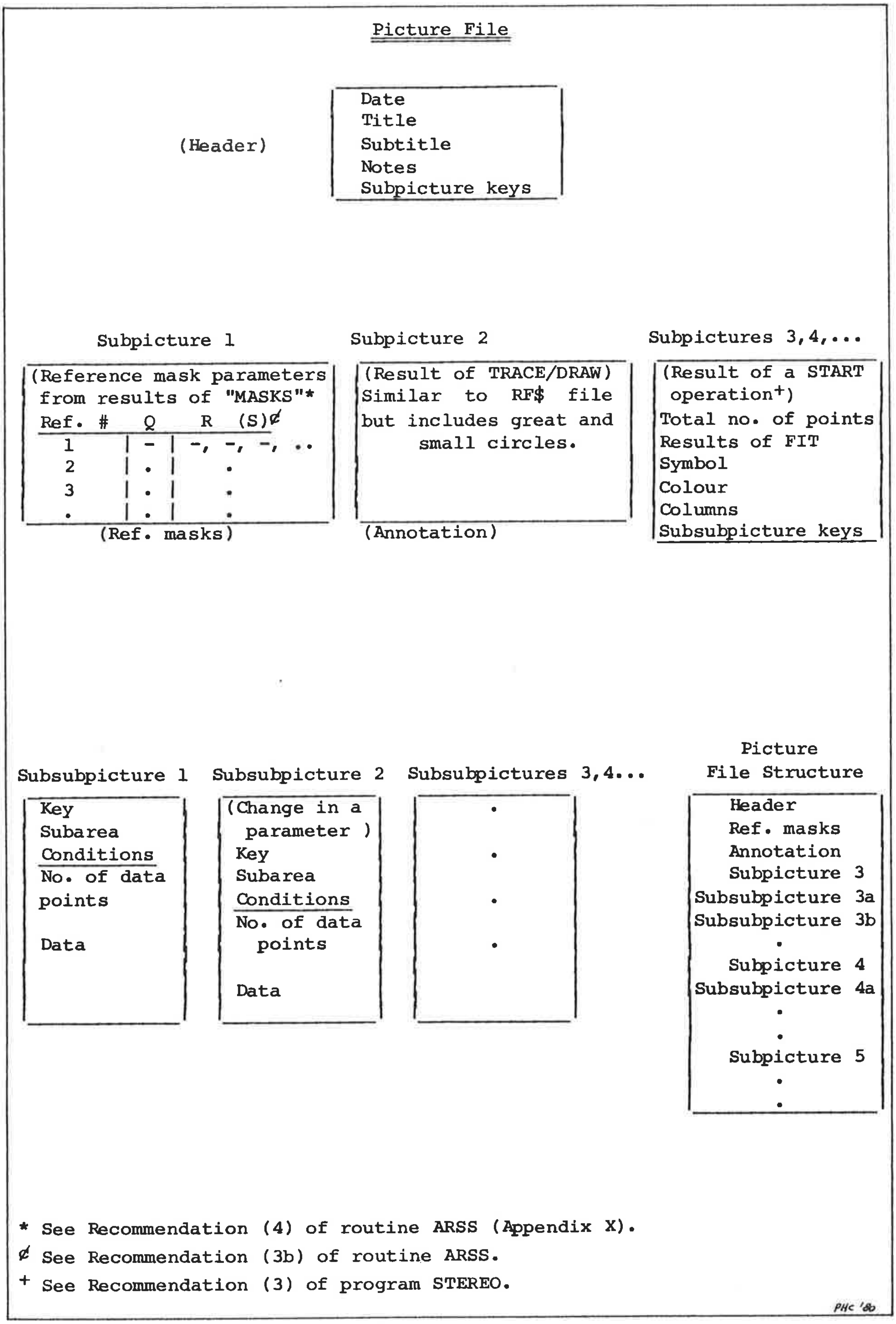

Fig. R.7 A possible design for a picture file for program STEREO.

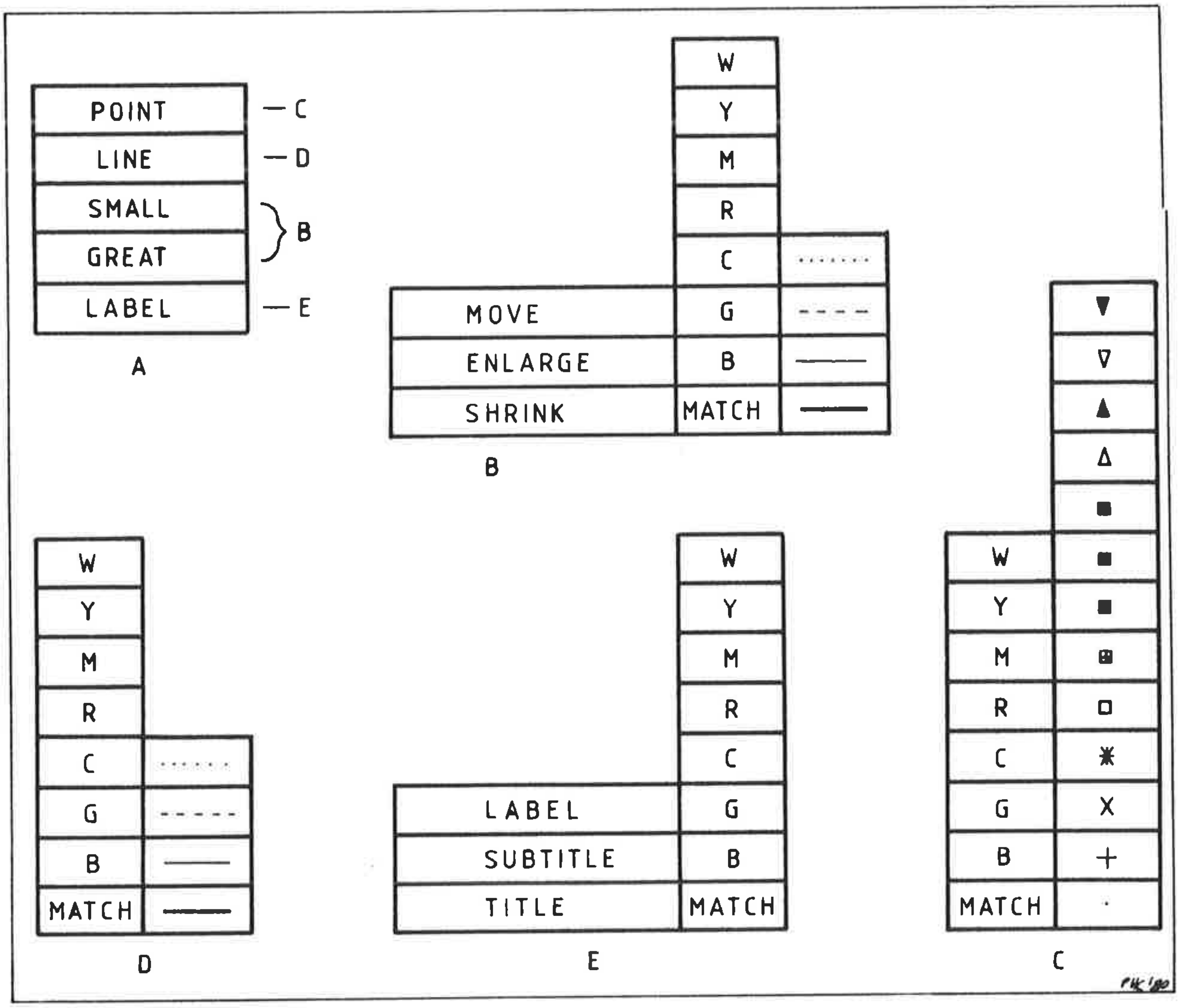

Fig. R.8 Proposed options submenu for a merged TRACE/DRAW function (a), which calls other submenus (b-e).

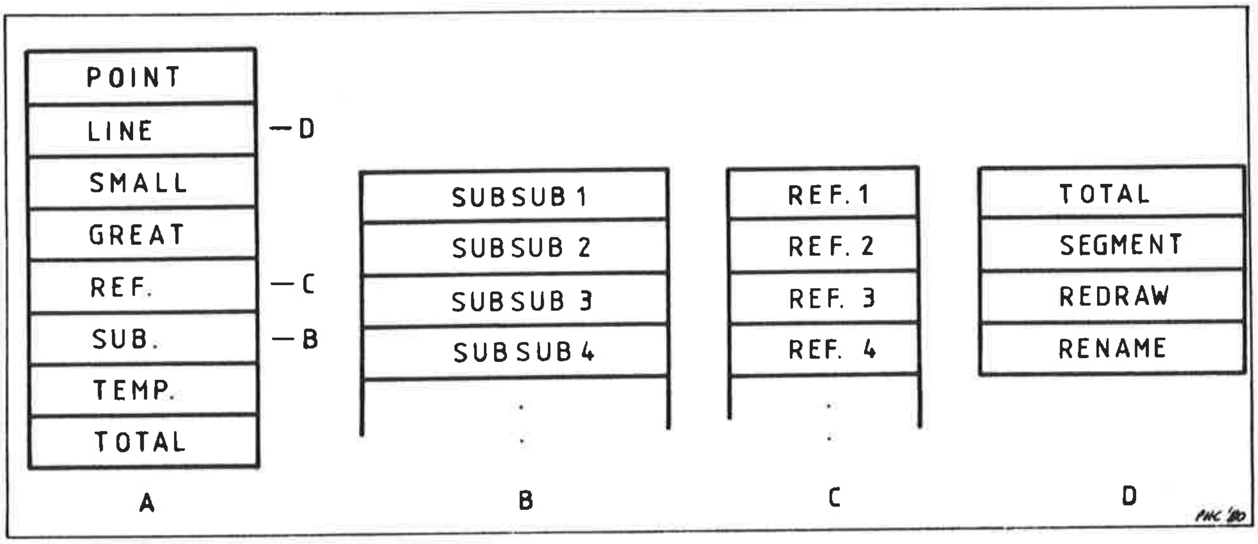

Fig. R.9 Proposed options submenu for CLEAR to modify the display, and subsequently picture files.

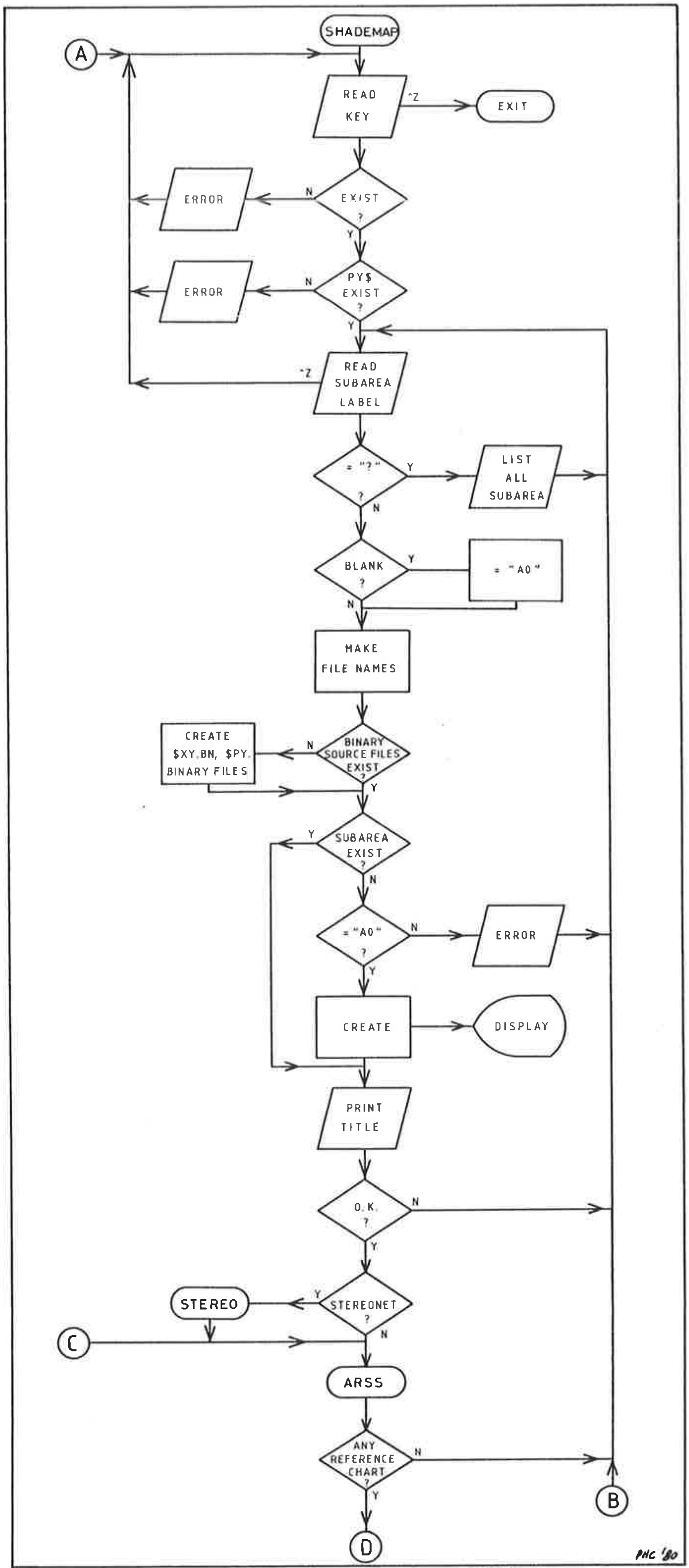

Fig. R.10 Flow chart for program SHADEMAP, a S.O.D.A. program.

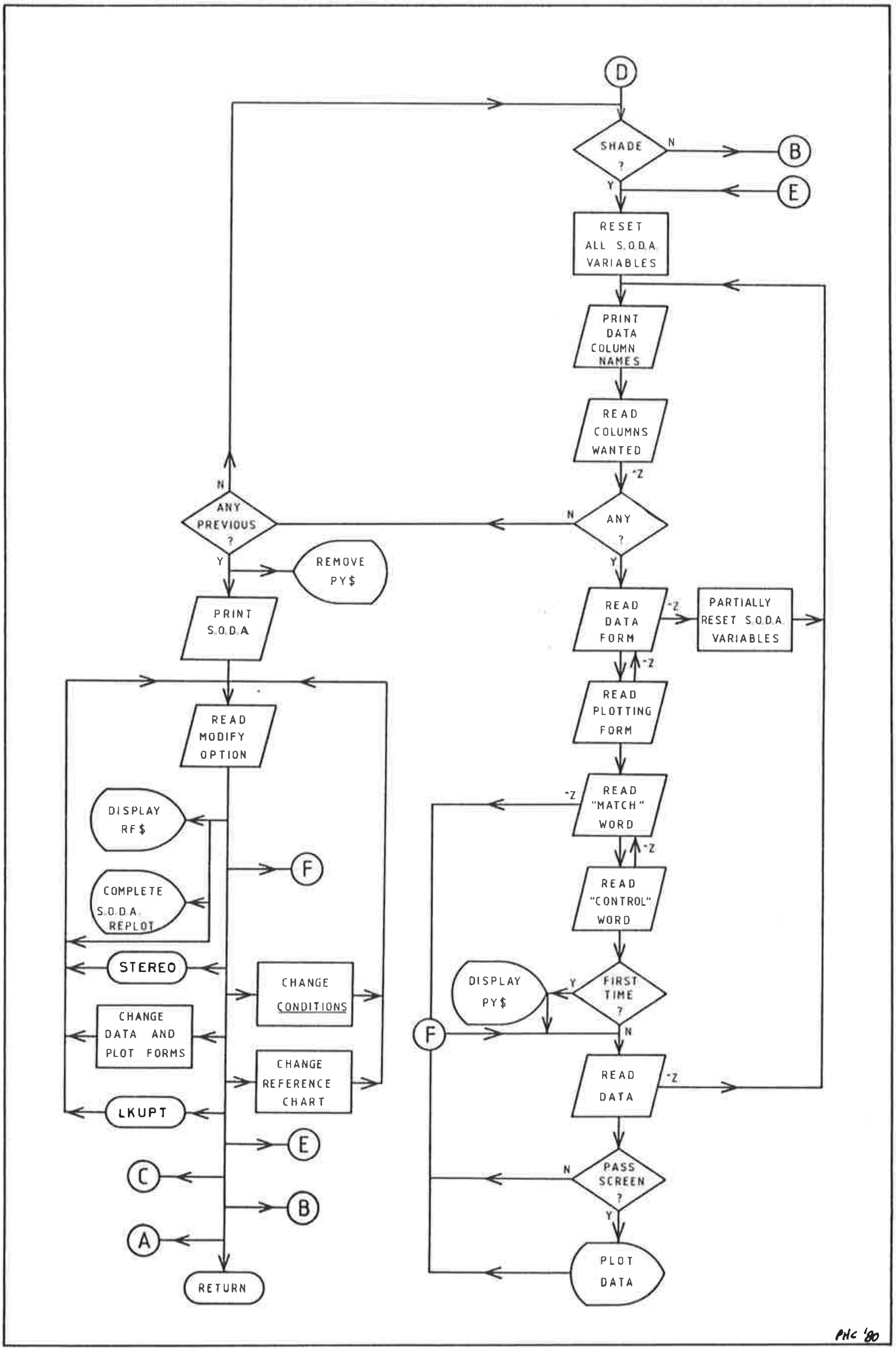
D
SHADE ?
N
Y
B
E
RESET ALL S.O.D.A. VARIABLES
PRINT DATA COLUMN NAMES
READ COLUMNS WANTED
ANY ?
ANY PREVIOUS ?
REMOVE PY$
PRINT S.O.D.A.
READ MODIFY OPTION
DISPLAY RF$
COMPLETE S.O.D.A. REPLOT
F
STEREO
CHANGE CONDITIONS
CHANGE DATA AND PLOT FORMS
CHANGE REFERENCE CHART
LKUPT
E
C
B
A
RETURN
READ DATA FORM
PARTIALLY RESET S.O.D.A. VARIABLES
READ PLOTTING FORM
READ "MATCH" WORD
READ "CONTROL" WORD
DISPLAY PY$
FIRST TIME ?
F
READ DATA
PASS SCREEN ?
PLOT DATA
PHC '80

Fig. R.10 (cont.)

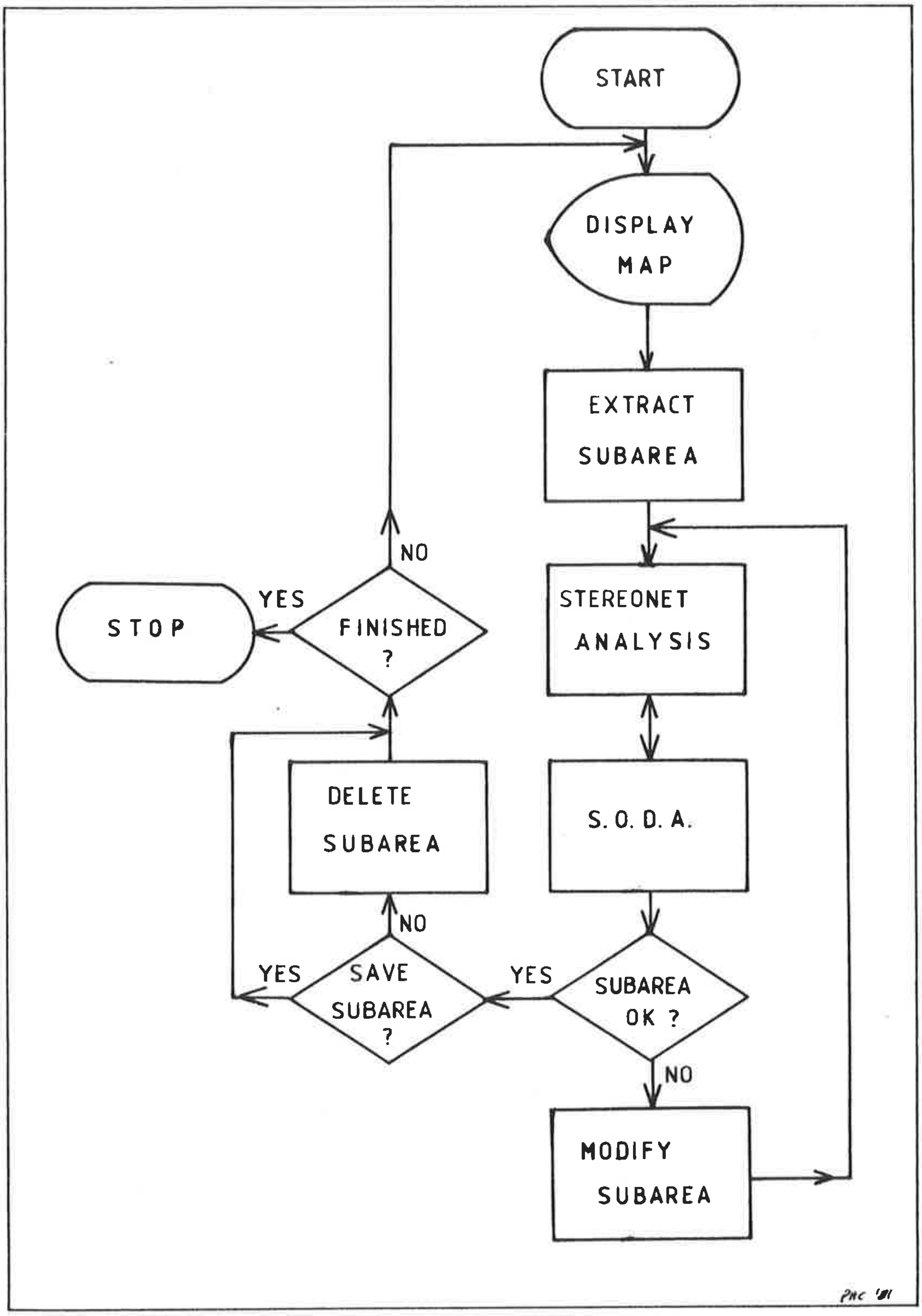

Fig. S.1 Flow chart for application of the S.O.D.A. technique.

Fig. U.1. Masks and charts to aid in sectioning stereonets. Any combination of portions of each mask may be selected to mask out unwanted portions of the stereonet. One of the three charts (predefined stereonet sectioning) may be chosen for modifying and rotating. Colouring and contrast may be set by the user.

A) Mask Q (quadrant mask) may be fixed relative to north, or rotated by STR.

B,C) Mask R (reference mask) defines a reference girdle that can be rotated into any position by defining STR, DIP, and PCH. The last allows a reference point to be defined. TOL determines the angular distance that a point may lie from the girdle and still be considered to belong to that girdle.

(D) Standard chart (isotrend RES fixed at 30° and isodip RES fixed at 18° due to machine limitations; Cohen, in prep.[b]).

E) Isotrend chart for contouring trends. The chart may be unidirectional (every trend value, 000°-359° is unique) or bidirectional (opposite trends undifferentiated).

F) Isodip chart for contouring dips, may be uni- or bi-directional. The charts may be rotated about the vertical and can be rotated to be centred on i) the vertical (default), ii) the pole to the reference girdle, or iii) the reference point. If the chart is not centred on the vertical then the contours become functions of both trend and plunge.

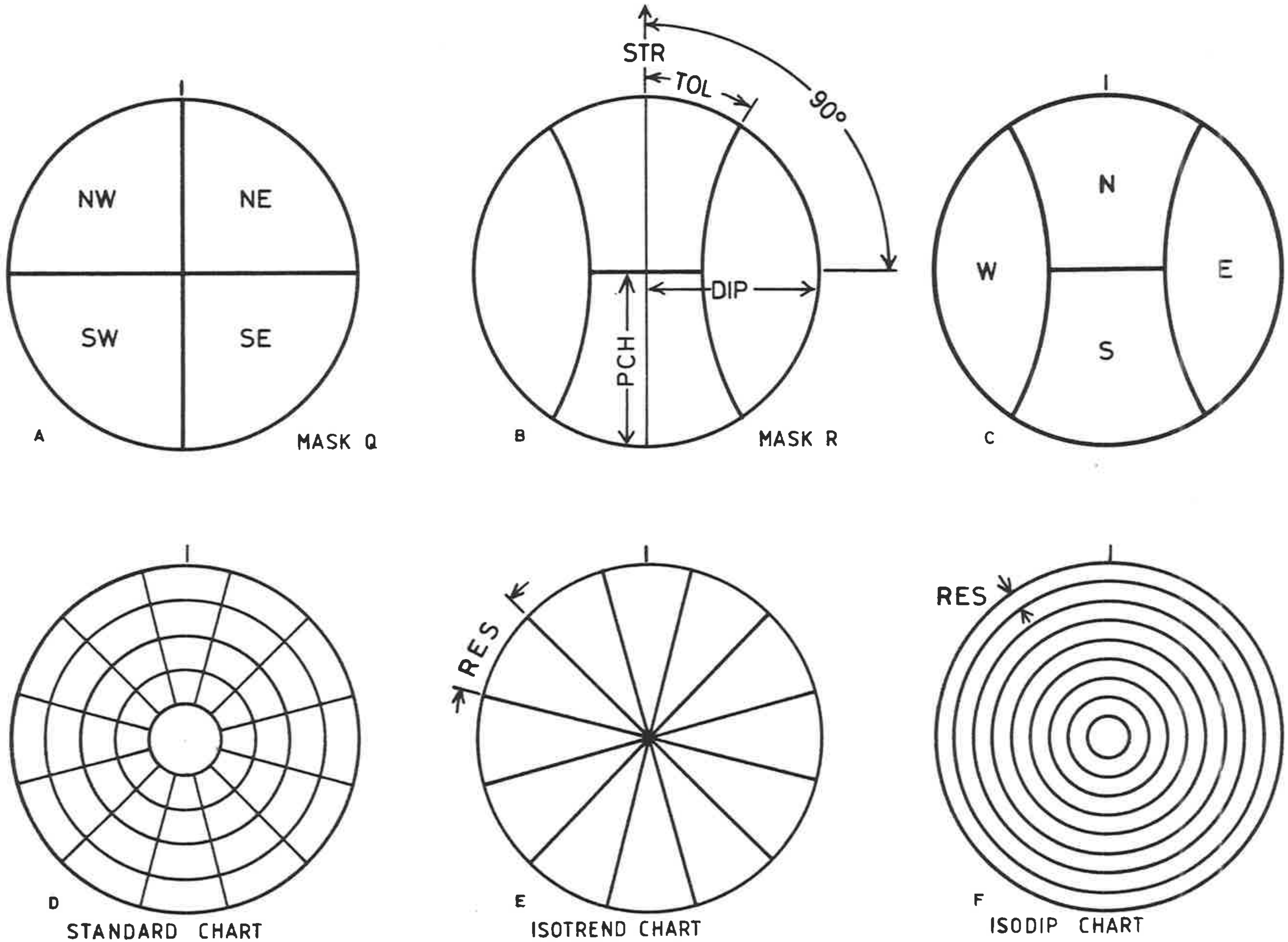
NW
NE
SW
SE
A
MASK Q
STR
TOL
90°
DIP
PCH
B
MASK R
N
W
E
S
C
D
STANDARD CHART
RES
E
ISOTREND CHART
RES
F
ISODIP CHART

Fig. U.2. An example of quartz fabric A.V.A. using figure 11B of, and data supplied by, Wilson, (1973).
(A) A.V.A. plot, and (B) Sectioned equal-area net using a bi-directional isotrend chart (RES=30) centred on the pole to the reference girdle (STR=144, DIP=90, PCH=90, TOL=20). E and W are masked out to produce the central portion (using a medium contrast look-up colour table), and are then each assigned a "fixed" colour to override the predefined sectioning in those portions.
(C) Stereonet plot. The quartz fabric has a conical distribution which is approximate enough to a great circle for a valid usage of the reference girdle shown.

Fig. U.3. Two examples of faults. In both, two upright, horizontal anticlines separated by a syncline have been faulted.
(A) A strike-slip fault of a quarter wavelength.
(B) A vertical fault where tighter folds have been juxtaposed against open folds such that their respective anticline/syncline hinges are aligned.
(C) The unrotated standard chart used for the analysis.

Fig. U.4. A subvertical fold can be classified (two-dimensional) according to Ramsay's (1967) fold classification by using a standard bidirectional isotrend chart so that the trend contours become the dip isogons. (A) A type 2 (similar) fold. (B) The chart used (RES=15).

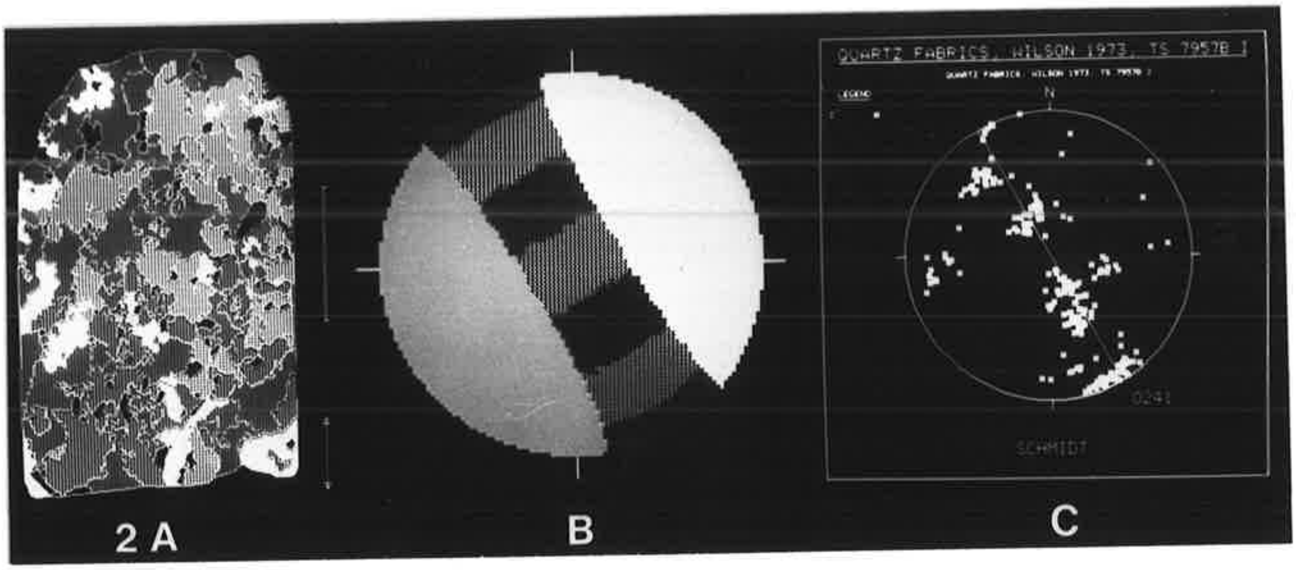
QUARTZ FABRICS, WILSON 1973, TS 7957B I
LEGEND
N
0241
SCHMIDT
2 A
B
C

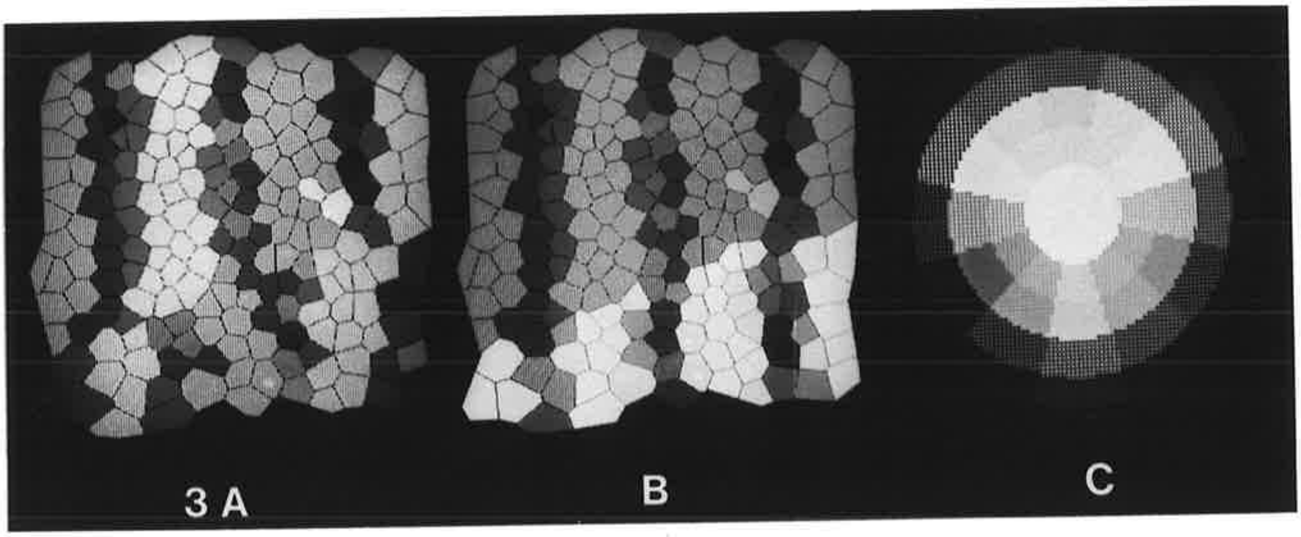
3 A
B
C

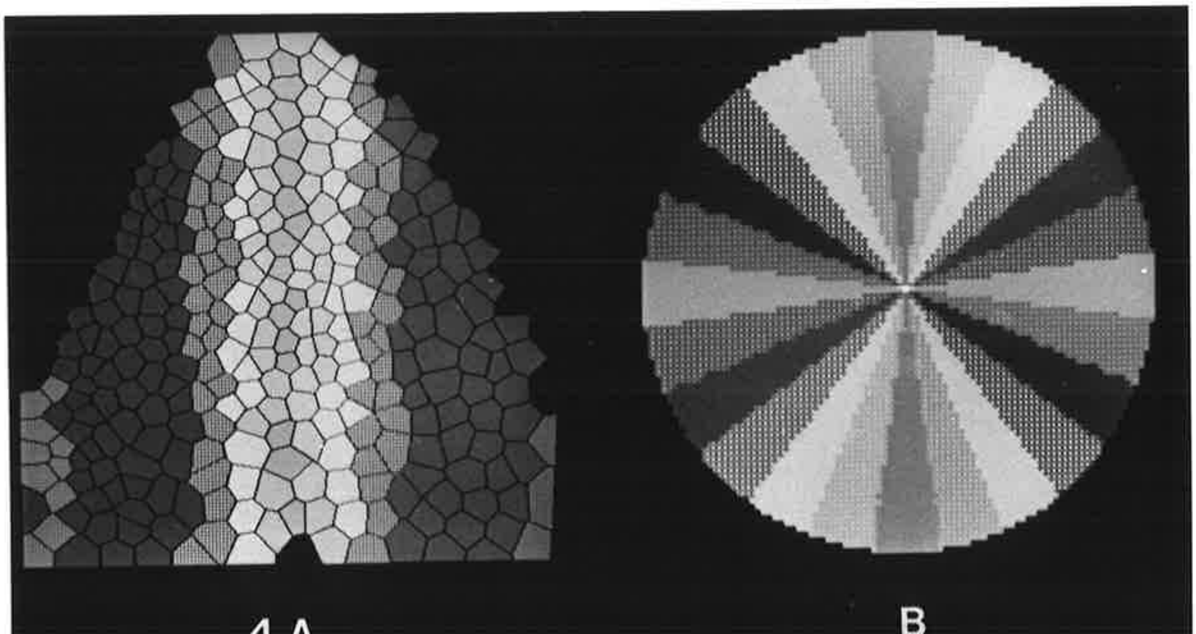
4 A
B

Fig. V.1. Thin section of an amphibolite schist with an S_1 fabric, folded by F_2 and overprinted by D_3 crenulations. The crenulations best occur in only one limb, where the hornblende grain orientations allow them to form.

Fig. V.2. Stereonet plots of combined [100] and [001] axes for (A) combined limbs of F_2, which are separately displayed in (B) the north limb, and (C) the south limb.

Fig. V.3. Stereonet plots and the respective S.O.D.A. charts used for the axial distribution analysis of the quartz fabrics of Wilson's (1973) (A) figure 9A, and (B) figure 11B.
(Note that the data have not been rotated into their field orientations.)

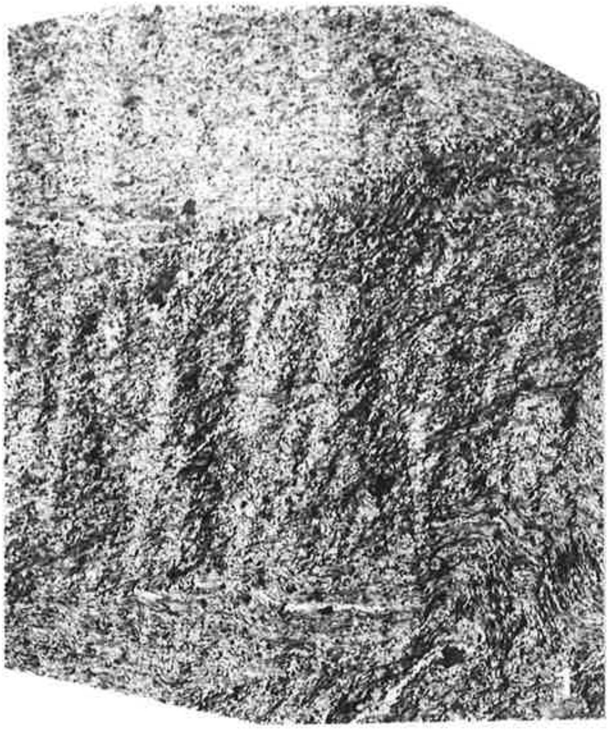

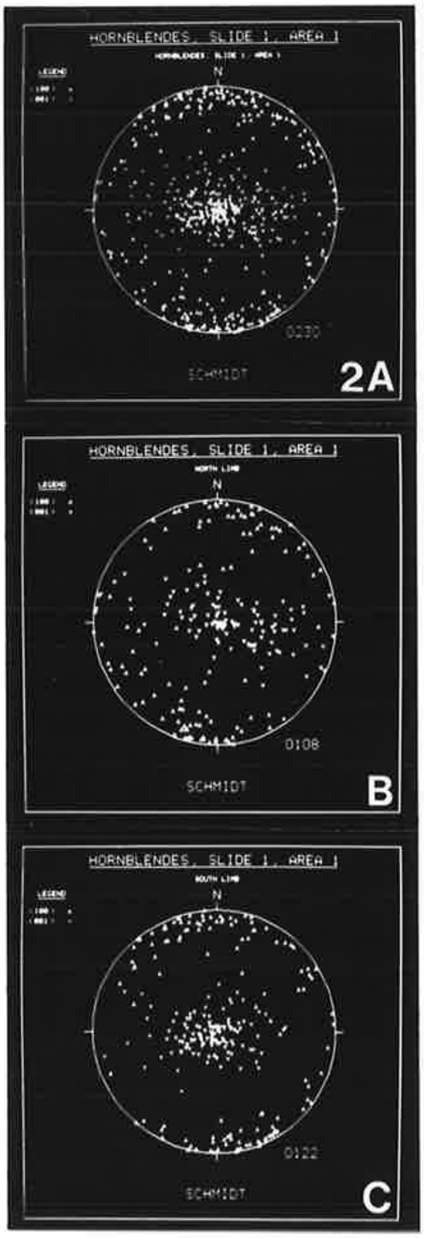

HORNBLENDES, SLIDE 1, AREA 1
N
0230
SCHMIDT
2A
HORNBLENDES, SLIDE 1, AREA 1
N
0108
SCHMIDT
B
HORNBLENDES, SLIDE 1, AREA 1
N
0122
SCHMIDT
C

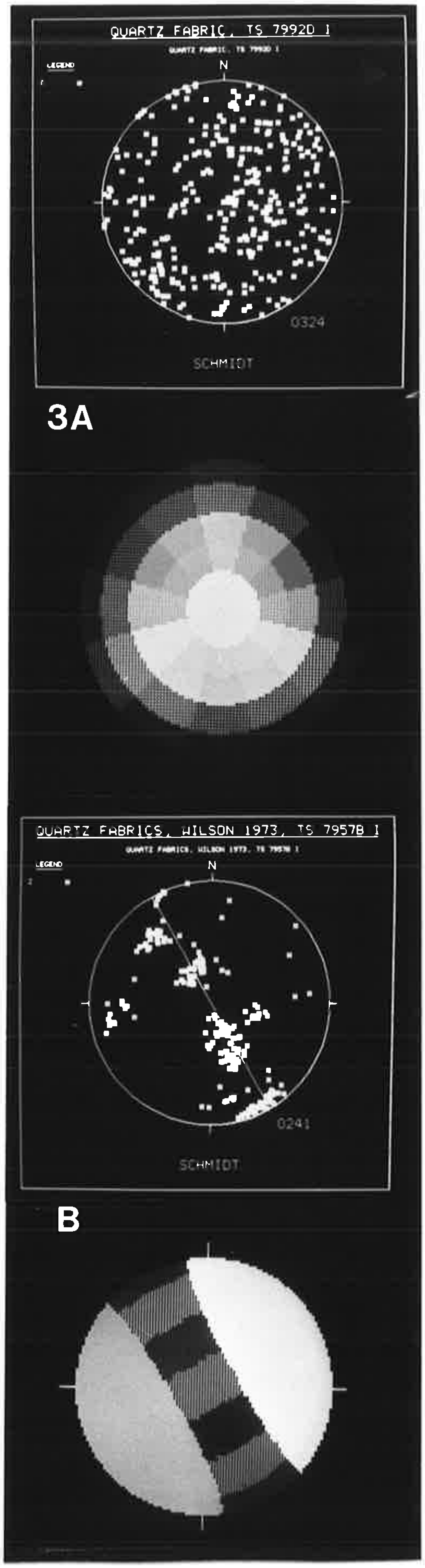

QUARTZ FABRIC, TS 7992D 1
N
0324
SCHMIDT
3A
QUARTZ FABRICS, WILSON 1973, TS 7957B 1
N
0241
SCHMIDT
B

Fig. V.4. A.V.A. plots produced by S.O.D.A. (A) Plot for fig. V.2A. (B,C) Plot of D_3 crenulation using a bidirectional isotrend chart (RES=45). (D) Plot for fig. V.3A. (E) Plot for fig. V.3B.

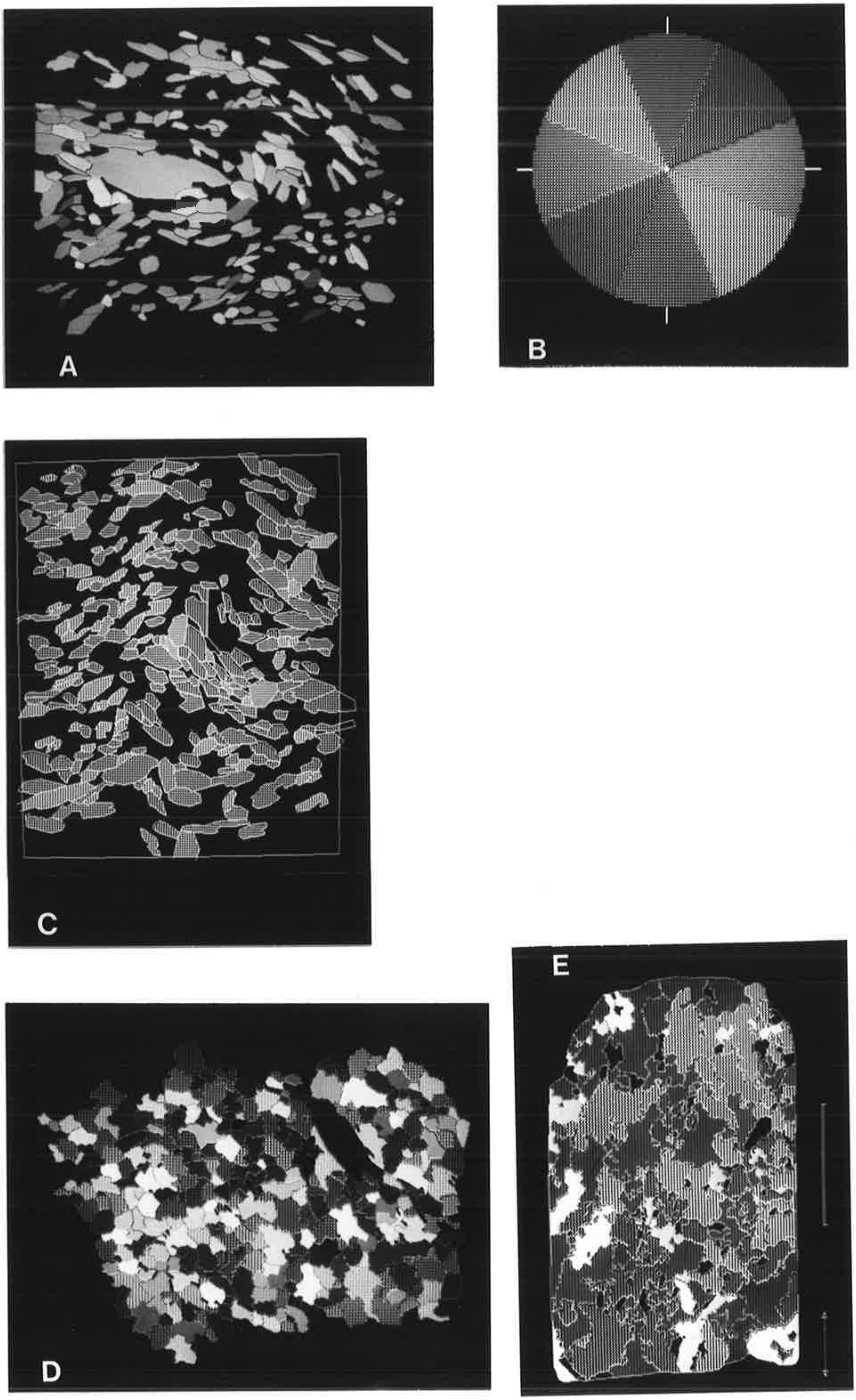
A
B
C
D
E

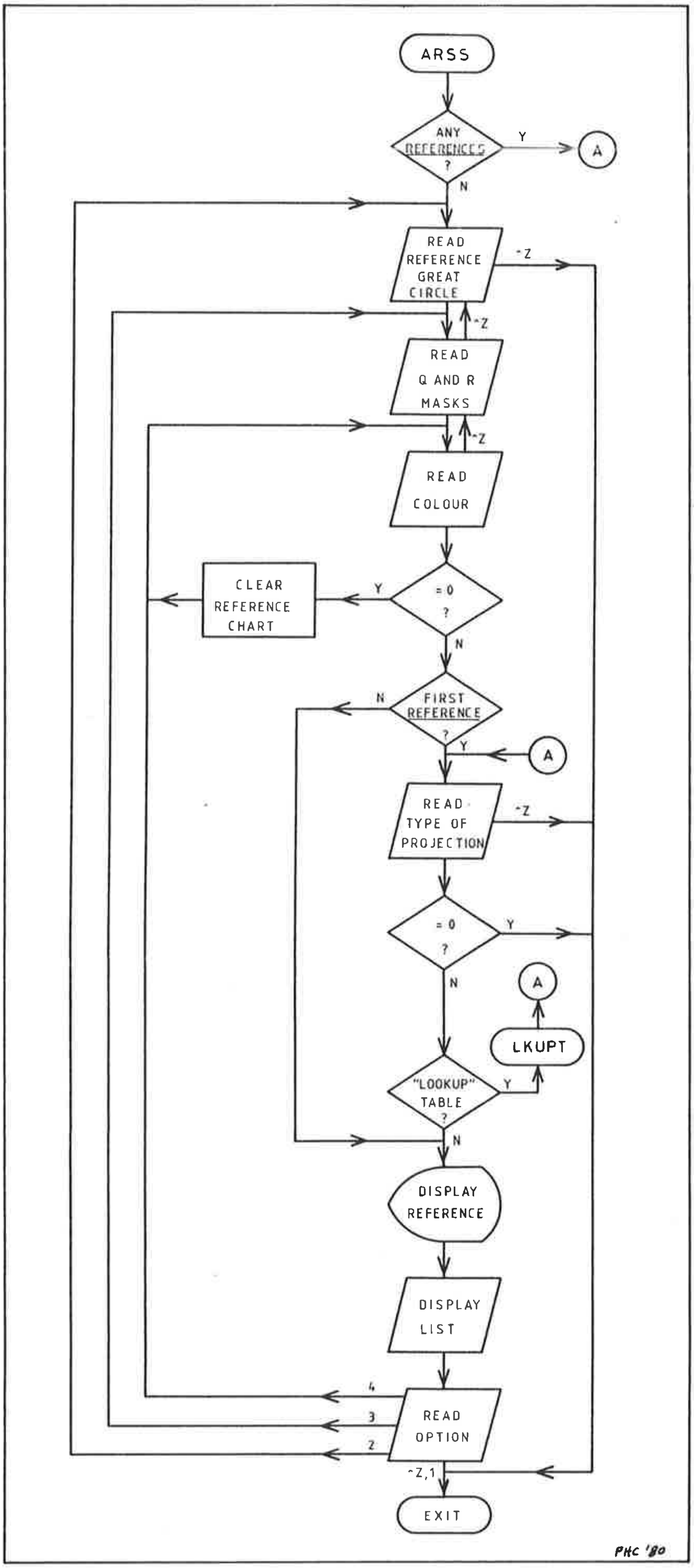

Fig. X.1 Flowchart of subroutine ARSS; a reference chart generator.

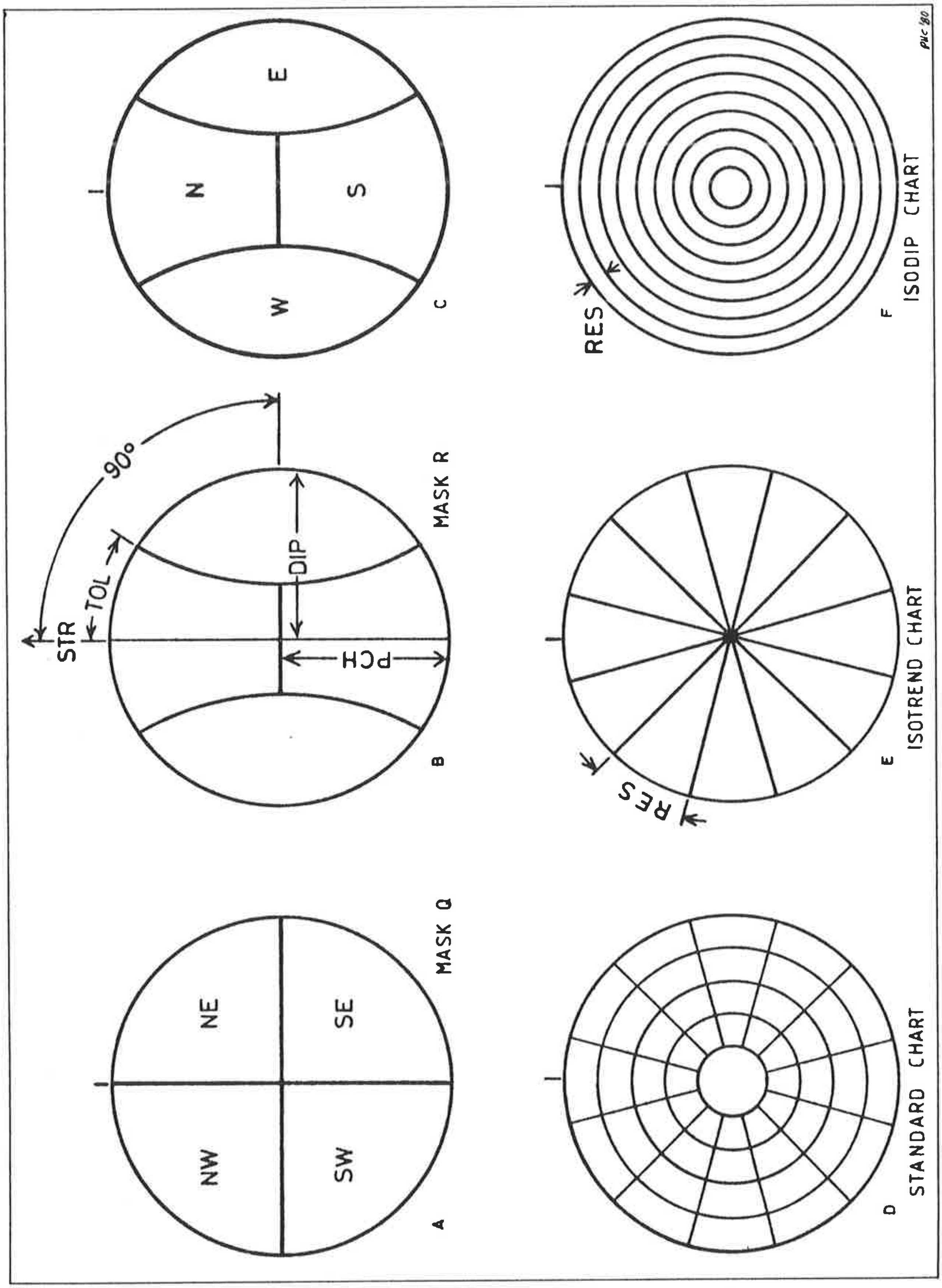

Fig. X.2 Masks and basic subdivisions of stereonets for use in producing S.O.D.A. plots.

a) Quadrant mask "Q" for selecting quadrants.

b) Reference mask "R" for defining portions of stereonets related to the geometry of cylindrical folds, and c) their names.

d) The standard chart made from (e) and (f), with RES values of 30° and 18° respectively.

e,f) Isotrend and isodip charts respectively.

Red	+ Green	+ Blue	= 3 bit pixel	
0	0	0	0	Black
0	0	1	1	Blue
0	1	0	2	Green
0	1	1	3	Cyan
1	0	0	4	Red
1	0	1	5	Magenta
1	1	0	6	Yellow
1	1	1	7	White

PHC '80

Fig. X.3 Colour monitor colour schemes and coding array. With a three bit word, eight hues can be produced. The three primary colour columns show whether each hue requires it (1) or not (0).

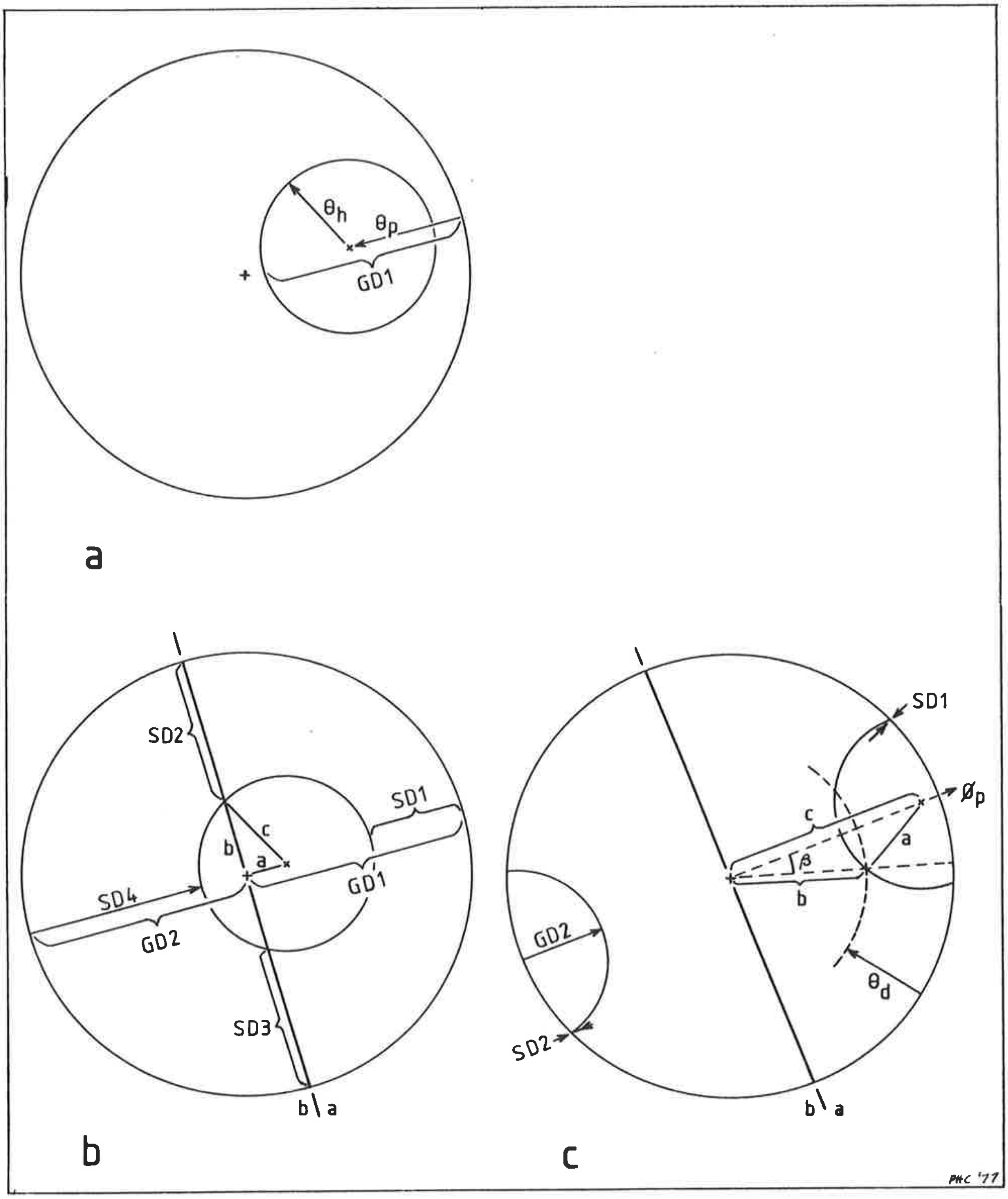

Fig. Z.1 Definitions of variables required to compute grid nodes that lie within a counting circle centred on a data point. Three possibilities occur, (a), (b), and (c). To avoid a combination of (b) and (c), the maximum counting circle size must be < 25%. (b) and (c) are divided into two separate problems, with portion "a" containing the data point.

Fig. CP.1 Design of standard colour chart.

a) Blue gun

b) Red gun

c) Green gun

d) Standard colour chart (all guns)

e) Close up of northern portion of colour chart. Patterns due to colour-pixel masks are observable. Individual screen-pixels and the physical monitor screen-mask can be seen.

f - j) Colour masks for various colour-pixel intensities. Each square is a screen-pixel. Those screen-pixels with dots are used.

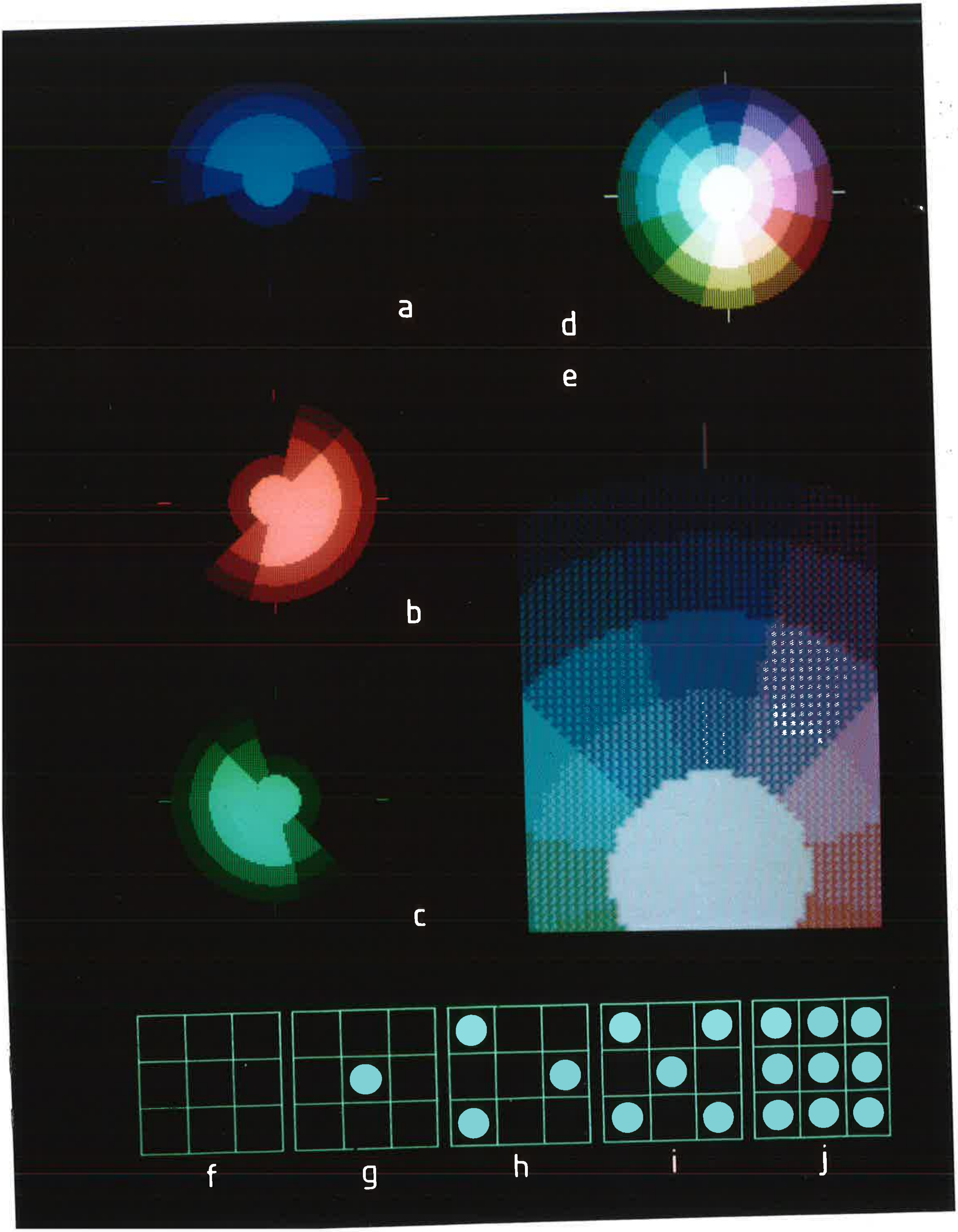
a
d
e
b
c
f
g
h
i
j

Fig. CP.2 Examples of reference charts.

a)	Standard colour chart, Equal-area net "1 (0) ; 0 90 90 0 00 7" .								
b)	" " " , Equal-angle net.								
c)	" " " , Orthographic projection.								
d)	U-isotrend chart.	2 30	;	000	90	90	0		
e)	B-isotrend " .	3 60 [1]	;						
f)	B-isodip " .	4 5	;						
g)	B-isotrend " .	3 60 [2]	;						
h)	" " .	3 60 [3]	;						
i)	Q mask " .	1 (0)	;	000	90	90	0	10	-2
								20	-1
								30	-4
								40	-6
j)	R mask " .	1 (0)	;	000	90	90	0	01	-4
								02	-2
								03	-1
								04	-6
		1 (0)	;	000	90	90	0	00	40
k)	Rotated standard chart.	1 (0)	;	315	-45	90	30	00	7
l)	Double rotated standard chart.	1 (-90)	;	315	-45	90	30	00	7
m)	Modal chart.		;	037	60	90	55	05	-1
			;	088	85	90	60	05	-2
			;	325	145	90	32	05	-4
n)	Modal b-isotrend chart.	3 10	;	315	-90	90	30	06	7
								02	-2
								01	-4
o)	U-isotrend (second colour chart)	-2 3	;	000	90	90	30	06	7
			;	090	90	90	30	06	7
			;	000	00	90	00	00	-7

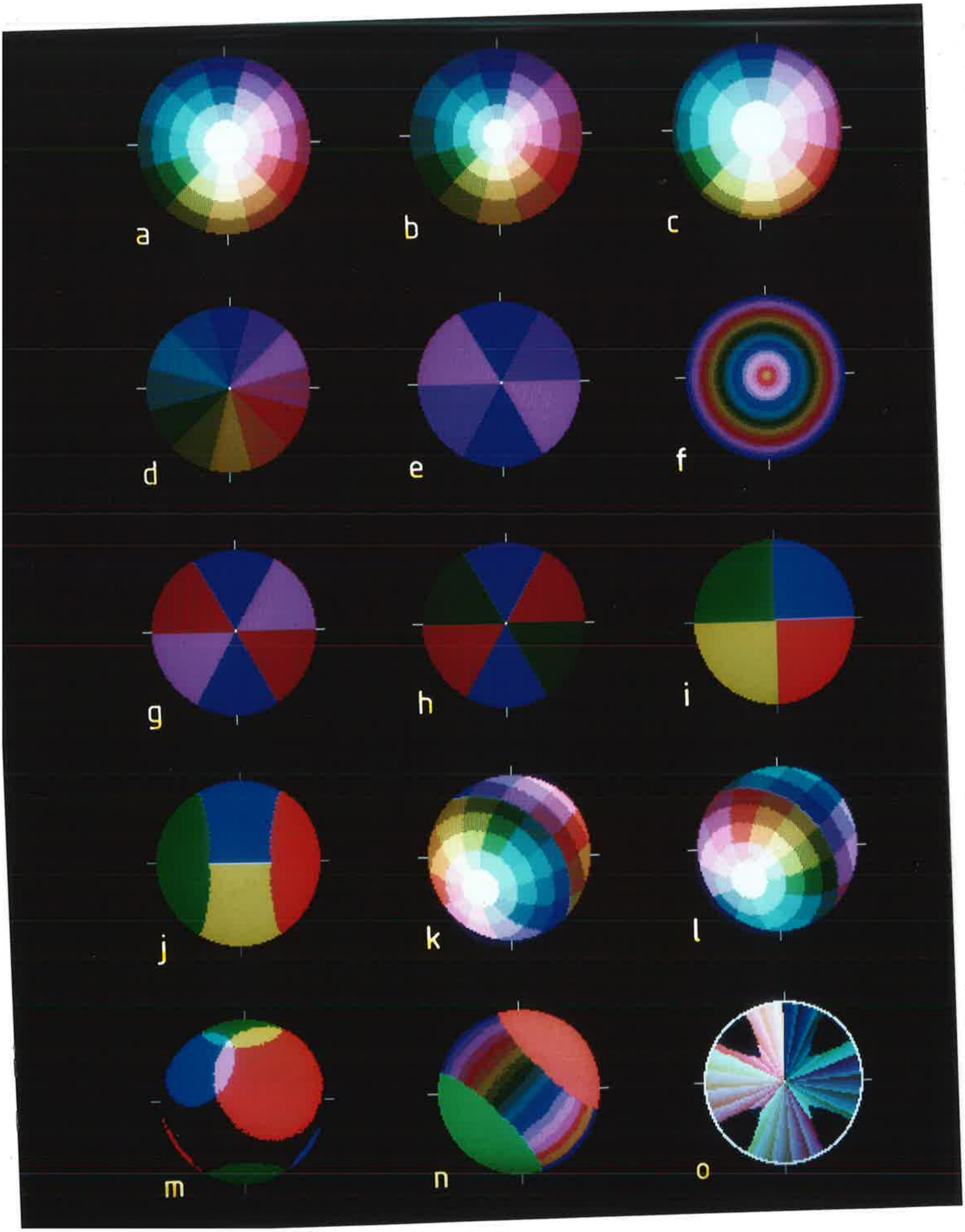
a
b
c
d
e
f
g
h
i
j
k
l
m
n
o

Fig. CP.3 Upright horizontal "similar" style folds with north-south hinge lines (refer to Fig. 4.1a,b,c), demonstrating patterns in isodip contours due to hinge tightness (see text for details). S.O.D.A. plots are produced by plotting dip vectors on the standard colour chart (g).
Pole figures for each fold (red points), and corresponding dip vector figures (green points) are given in (b),(d),(f).

a) Rounded fold.

c) Intermediate.

e) Angular (chevron) fold.

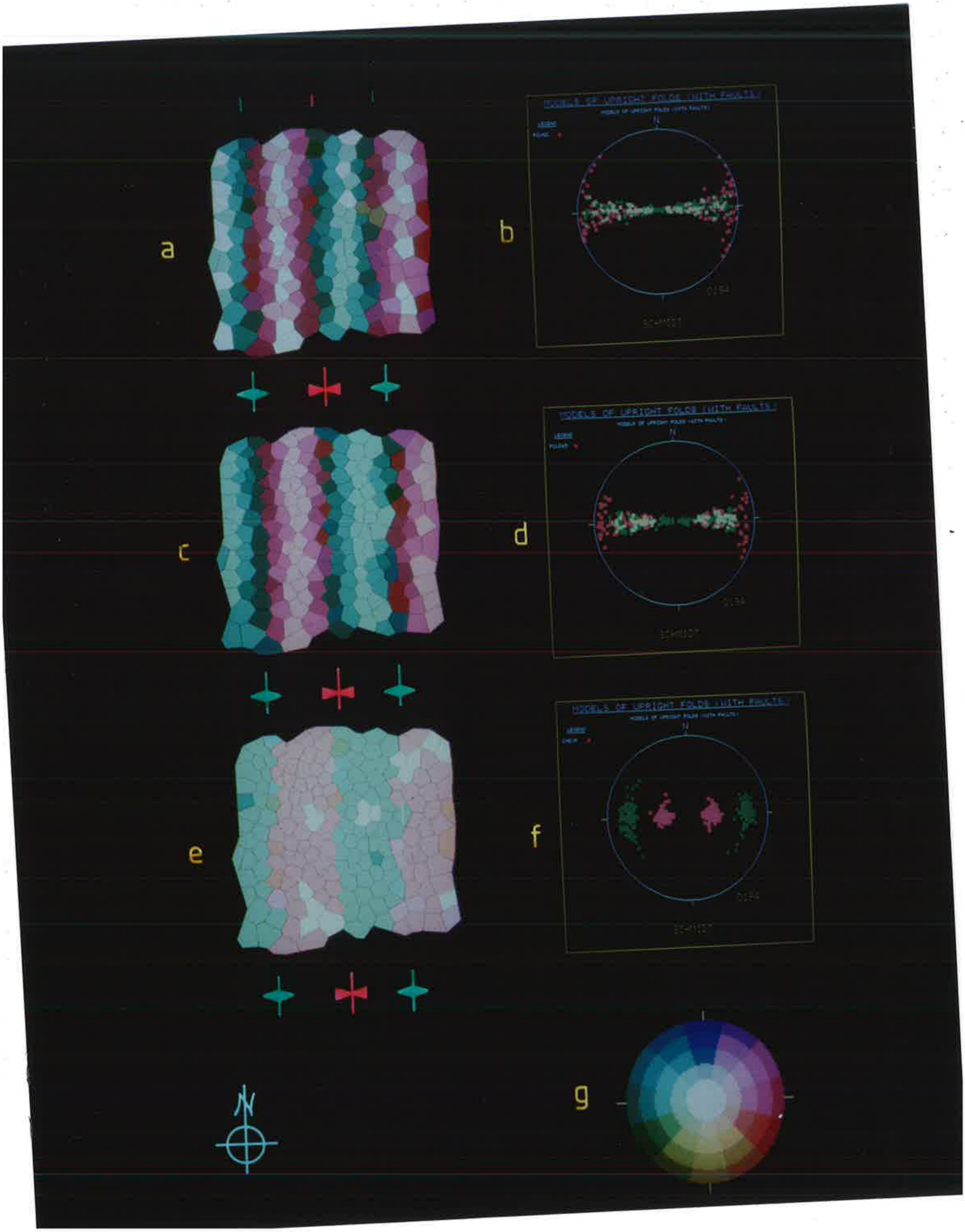
a
b
MODELS OF UPRIGHT FOLDS (WITH FAULTS)
N
SCHMIDT
c
d
MODELS OF UPRIGHT FOLDS (WITH FAULTS)
N
SCHMIDT
e
f
MODELS OF UPRIGHT FOLDS (WITH FAULTS)
N
SCHMIDT
g
N

Fig. CP.4 S.O.D.A. maps of upright "similar" style fold rotated into various plunges, trending due north (refer to Figs. 4.1d,e,f,g) made by plotting dip vectors on the standard colour chart (h) (unless otherwise stated).

a) Initial horizontal position.

b) Plunging 10° north.

c) Plunging 65° north.

d) Vertical (produced by plotting poles on standard chart (g)).

e) Replot of vertical fold using poles on colour chart (f).

f) B-isotrend colour chart with 15° resolution.

g) Composite dip vector figures of (a),(b),(c),(d) data.

h) Standard colour chart.

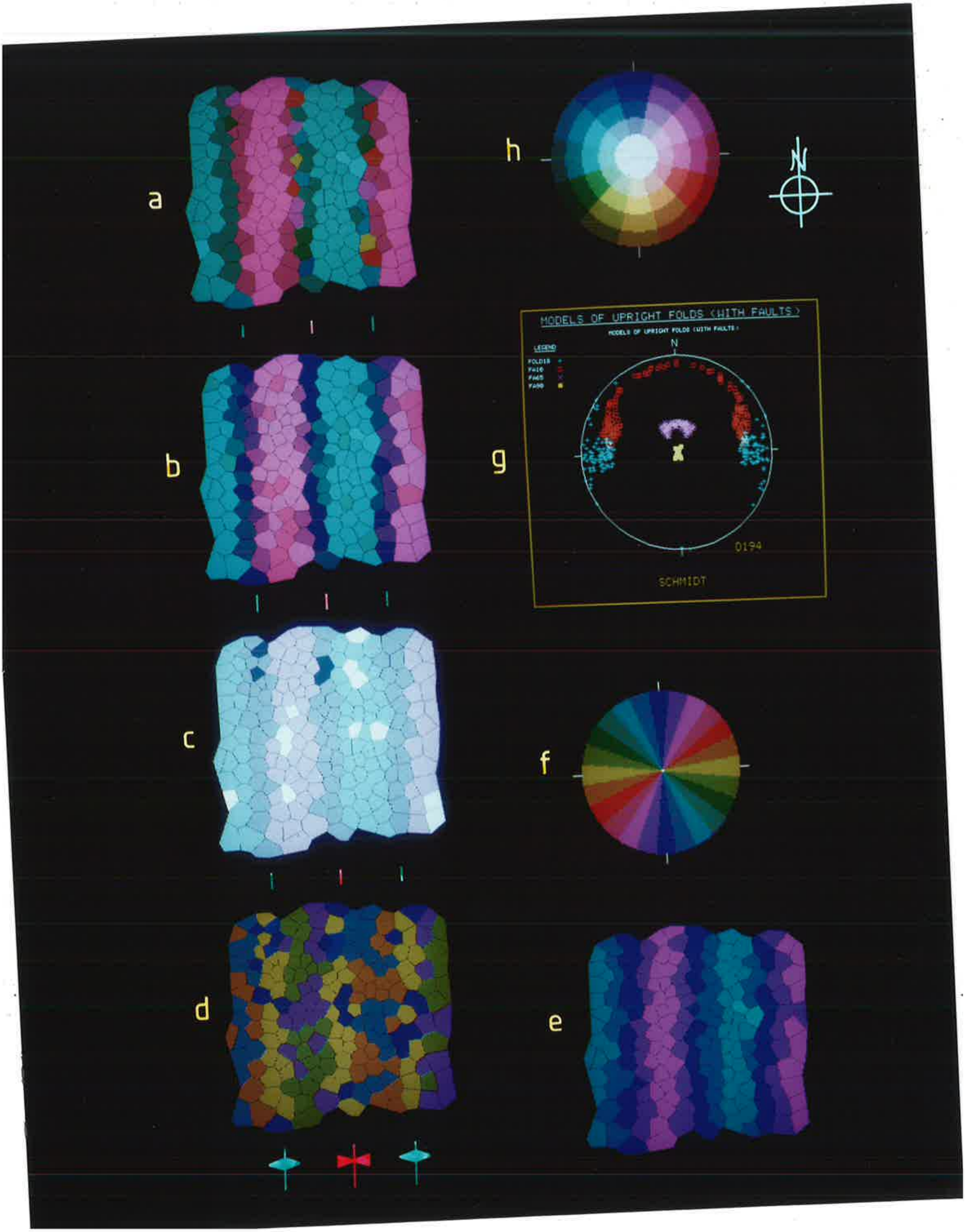

a
b
c
d
e
f
g
h
N
MODELS OF UPRIGHT FOLDS (WITH FAULTS)
MODELS OF UPRIGHT FOLDS (WITH FAULTS)
LEGEND
FOLDIR
FA10
FA65
FA90
N
0194
SCHMIDT

Fig. CP.5 S.O.D.A. plots of models in Fig. 4.1d,e,f,g; demonstrating the changes in isotrend contours, (a),(b),(c), respectively (model Fig. 4.1g) not included; and isodip contours, (d),(e),(f),(g), respectively. Isotrend contours produced by plotting poles on u-isotrend chart (h), and isodip contours by plotting poles on b-isodip chart (i).

h) 15° resolution u-isotrend chart.

i) 3° resolution b-isodip chart.

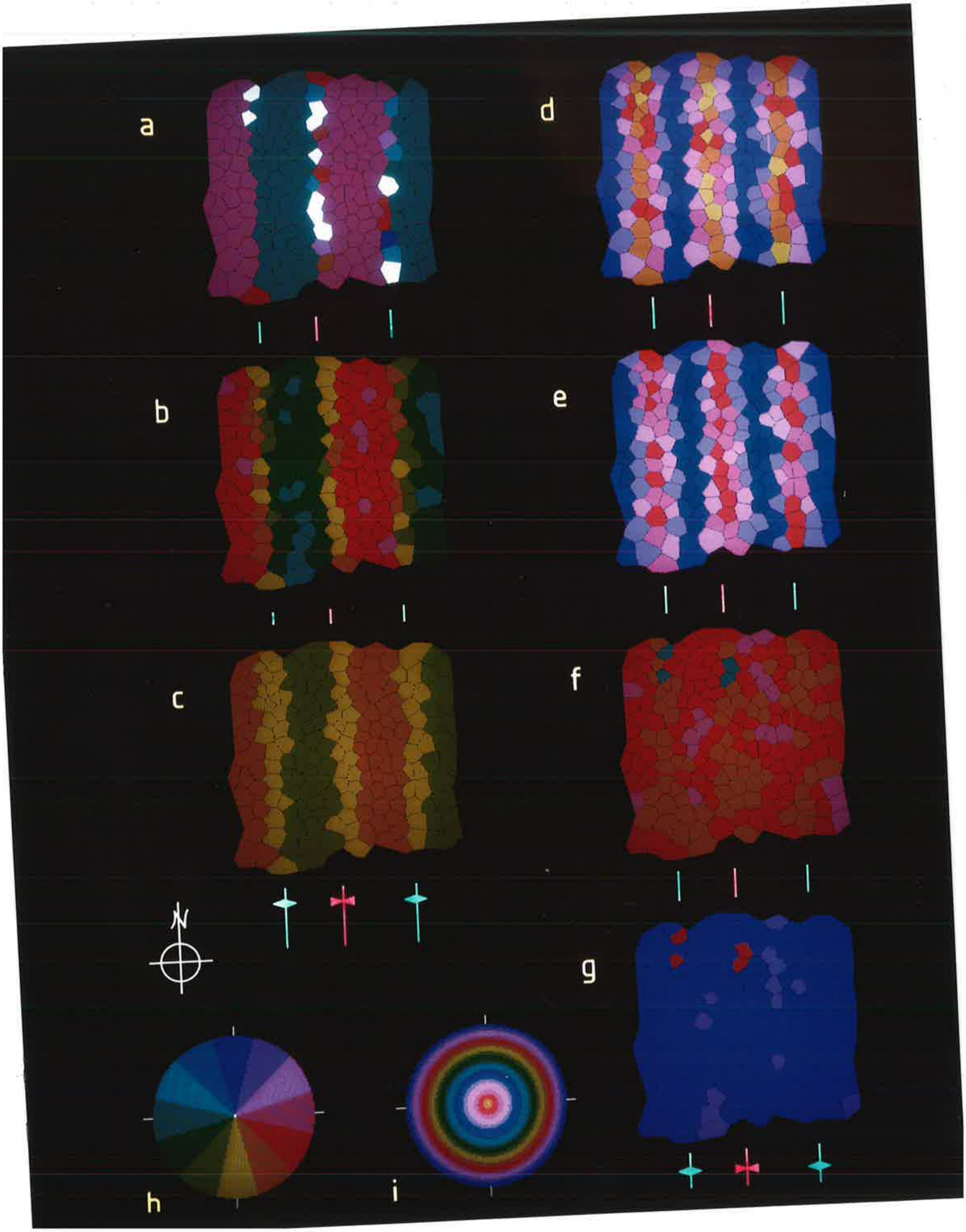
a
b
c
d
e
f
g
h
i
N

Fig. CP.6 S.O.D.A. map classification of vertically plunging folds, profiles after Ramsay (1967, figure 7.24). Maps are produced by plotting poles on a b-isotrend colour chart (f).

a) Class 1A

b) 1B

c) 1C

d) 2

e) 3

f) B-isotrend colour chart of 15° resoloution.

g) A representative pole figure using data for (b).

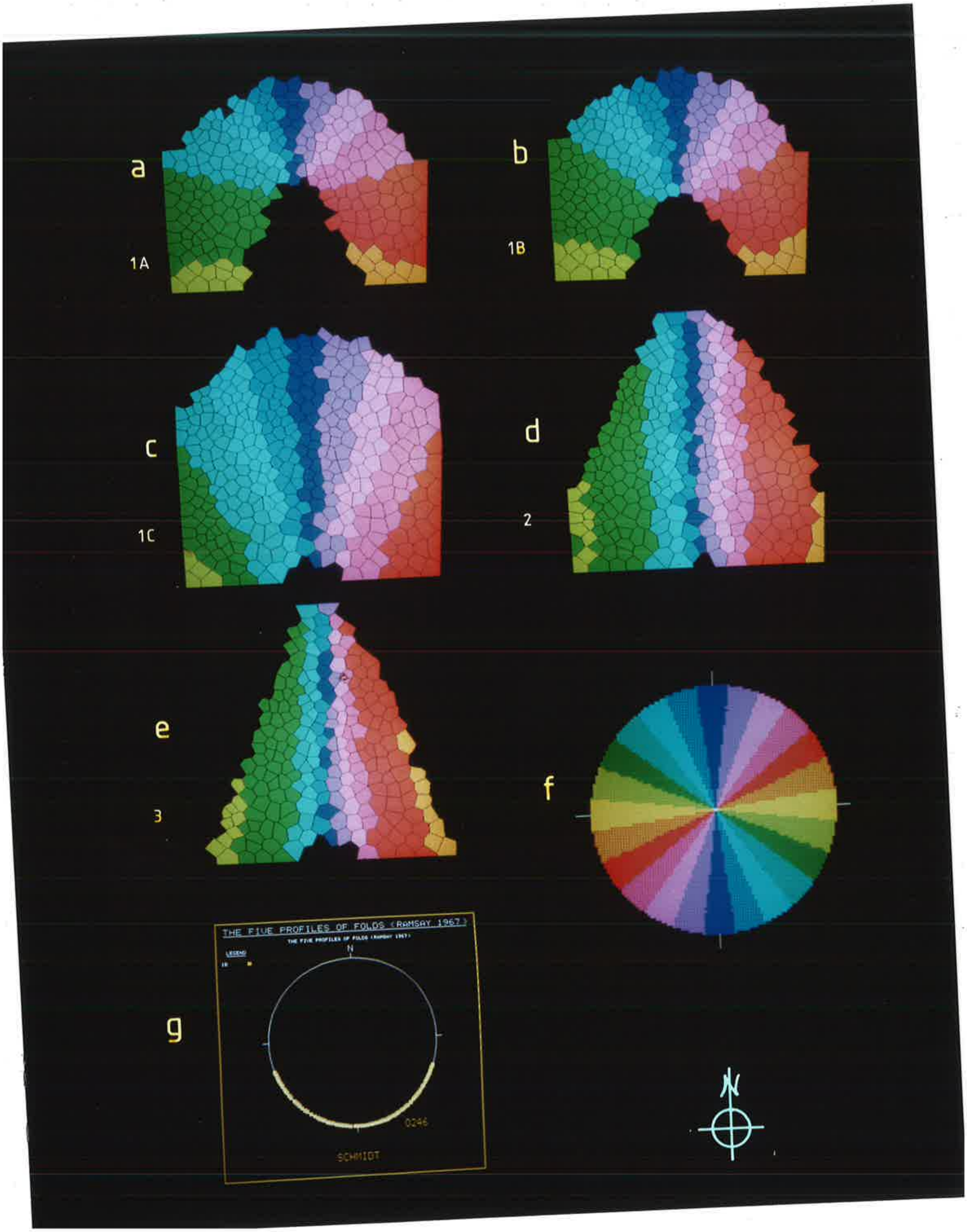
a
1A
b
1B
c
1C
d
2
e
3
f
g
THE FIVE PROFILES OF FOLDS (RAMSAY 1967)
N
0246
SCHMIDT
N

Fig. CP.7 S.O.D.A. maps demonstrating dislocations. Maps produced by plotting dip vectors on a standard colour chart.

a) Strike-slip fault model (Fig. 4.2a).

b) Dip vector figure for (a) plotted in green, corresponding pole figure plotted in red. (Any overlap produces yellow.)

c) Vertical fault model (Fig. 4.2b).

d) As for (b), except data is for (c).

e) Similar to (c) except northern portion after Fig. 4.1a and southern portion after Fig. 4.1b.

f) Dip vector figure for northen portion of (e) plotted in green, dip vector figure for southern portion in red.

g) Similar to (c) except northern portion after Fig. 4.1b and southern portion after Fig. 4.1c.

h) As for (f), except data is for (g).

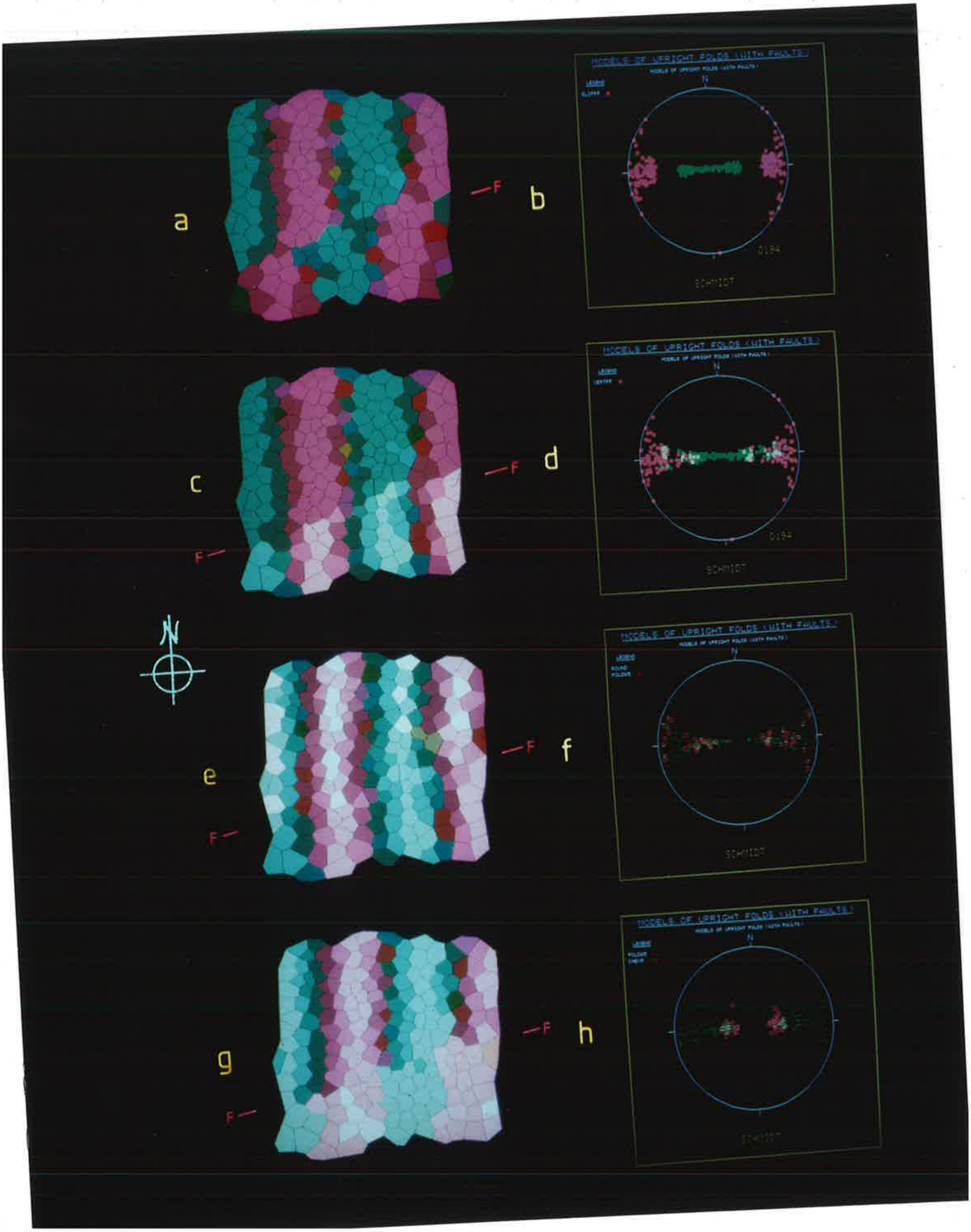

a
b
c
d
e
f
g
h
F
N
MODELS OF UPRIGHT FOLDS (WITH FAULTS)
SCHMIDT

Fig. CP.8 Analysis of two different structures that have identical orientation data sets (see text).

a) S.O.D.A. map of u-isotrends for a dome (Fig. 4.3); made by plotting dip vectors on colour chart (c).

b) S.O.D.A. map of b-isodips for dome of (a); made by plotting dip vectors on colour chart (d).

c) U-isotrend chart of 30° resolution.

d) B-isodip chart of 5° resolution.

e) Pole figure of data for dome above (identical to that for the dislocated plane below).

f) S.O.D.A. map of a dislocated plane (Fig. 4.4); made by plotting dip vectors on the chart (h). Two possible subareas can discerned (the boundary marked by F-F).

g) S.O.D.A. map of (f) after determining two subareas by domain analysis (marked by F-F); made by plotting dip vectors on chart (i).

h) Standard colour chart.

i) Colour chart used to separate the two domains of (g), derived from dip vector figure (j).

j) Composite dip vector figure for the two subareas in (g). Western portion (west of F-F) plotted in red, eastern portion in green.

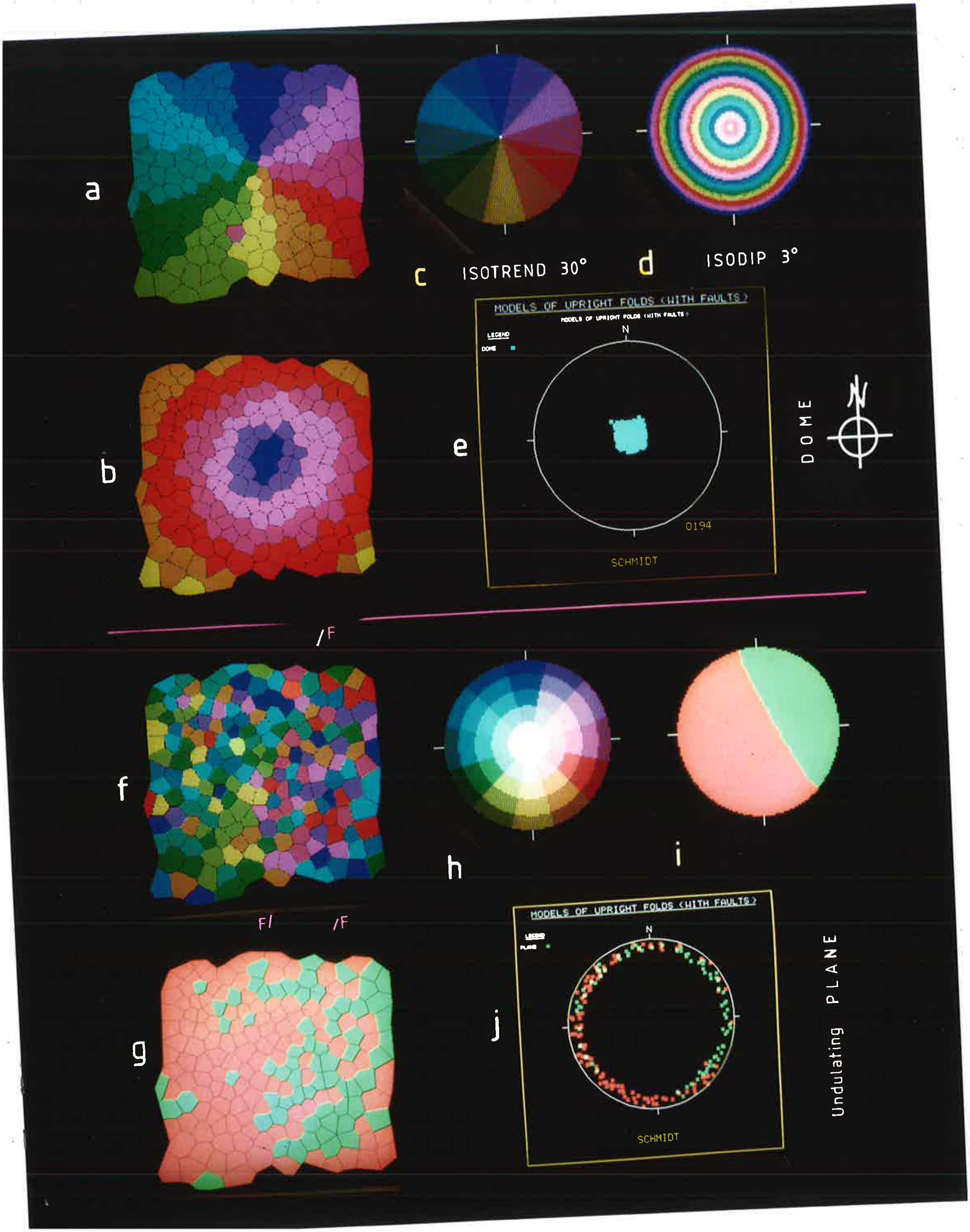

a
c
ISOTREND 30°
d
ISODIP 3°
MODELS OF UPRIGHT FOLDS (WITH FAULTS)
LEGEND
DOME
N
b
e
0194
SCHMIDT
DOME
N
/F
f
h
i
F/
/F
g
MODELS OF UPRIGHT FOLDS (WITH FAULTS)
N
j
SCHMIDT
Undulating PLANE

Fig. CP.9 S.O.D.A. plots for a fold in Llangedwyn-Dyffryn-Clwyd (§5.2.1).

a) Plot of S_0, using poles on (b).

b) Colour chart: 4 10 (0) [3]; 326 -115 45 0.

c) Plot of S_0, using poles on (d).

d) Colour chart: 2 30 (0) [1]; 326 115 -135 0.

e) Plot of S_1, using poles on (f).

f) Colour chart: 2 30 (0) [1]; 326 -115 45 0.

g) Plot of L_1, using (h).

h) Colour chart: 4 5 (0) [1]; 326 115 -45 0.

i) Composite stereoplot of data.
S_0 green 84 points,
S_1 red 13 points,
L_1 cyan 15 points,
Great circles: 236°/62°, 351°/50°.

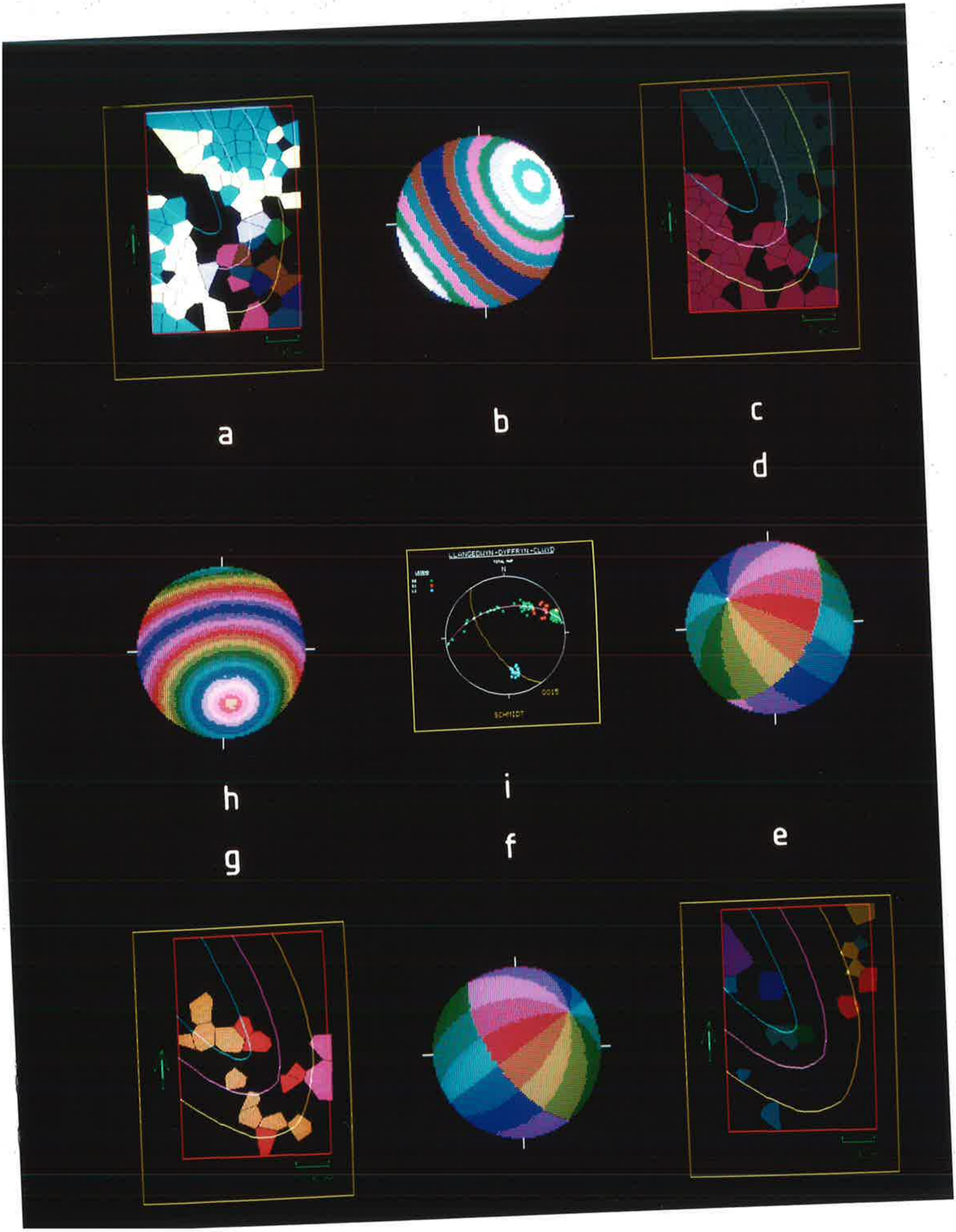

a
b
c
d
LLANGEDWYN-DYFFRYN-CLWYD
N
SCHMIDT
h
i
e
g
f

Fig. CP.10 S.O.D.A. plots of poles to bedding for the whole map of Fig. 5.4.

a) According to (b).

b) Colour chart: 2 -30; 323 96 -75 0.

c) According to (d).

d) Colour chart: 4 -10; 323 -96 75 0.

e) According to (f).

f) Standard colour chart.

g) Mineralized areas in blue.

h) Pole figure. Great circle: 233°/84°.

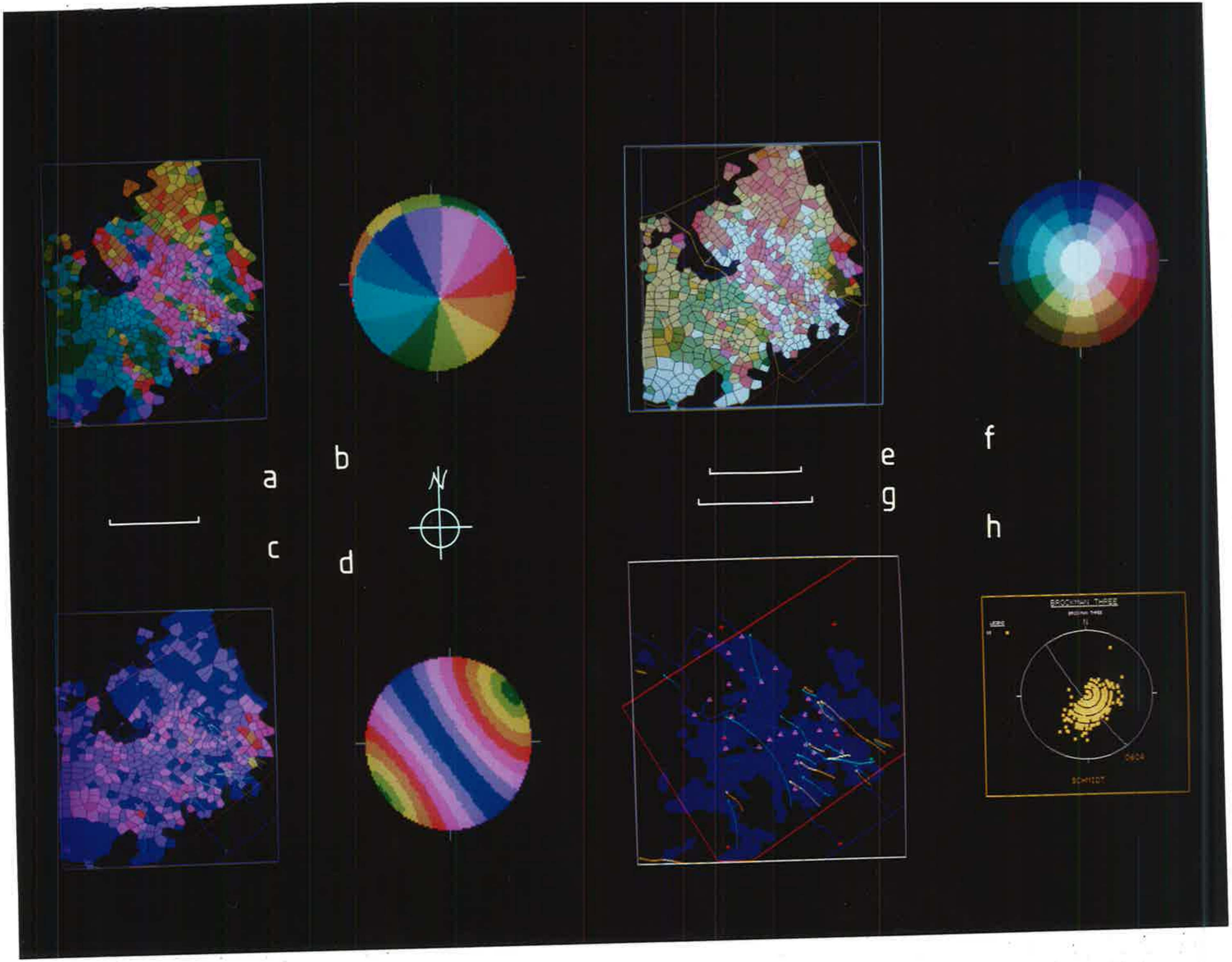
a
b
c
d
e
f
g
h
N
BROCKMAN THREE
N
0604
SCHMIDT

Fig. CP.11 S.O.D.A. plots of primary domains derived from Fig. CP.10 .

a) Domain b0 according to (c).

b) Domain c0 according to (e).

c) Colour chart: 2 30 (0); 323 96 75 0.

d) Composite pole figure.
b0 green 224 points,
c0 red 206 points,
Great circle: 233°/84°.

e) Colour chart: 2 180 (0); 303 90 -75 0.

f) Composite pole figure of domain d0, consisting of d1 (dark green area in southeast of (g)), d2 (the red area adjacent to d1, in the west), and d3 (the remaining area to the north).

d1	white	11 points,	(comparable to domain h1)
d2	magenta	16 points,	(" " " h2)
d3	blue	147 points	(" " " h3).

Great circle: 233°/84°.

g) Domain d0 according to (h).

h) Colour chart: 3 15 (90); 323 95 -0 0.

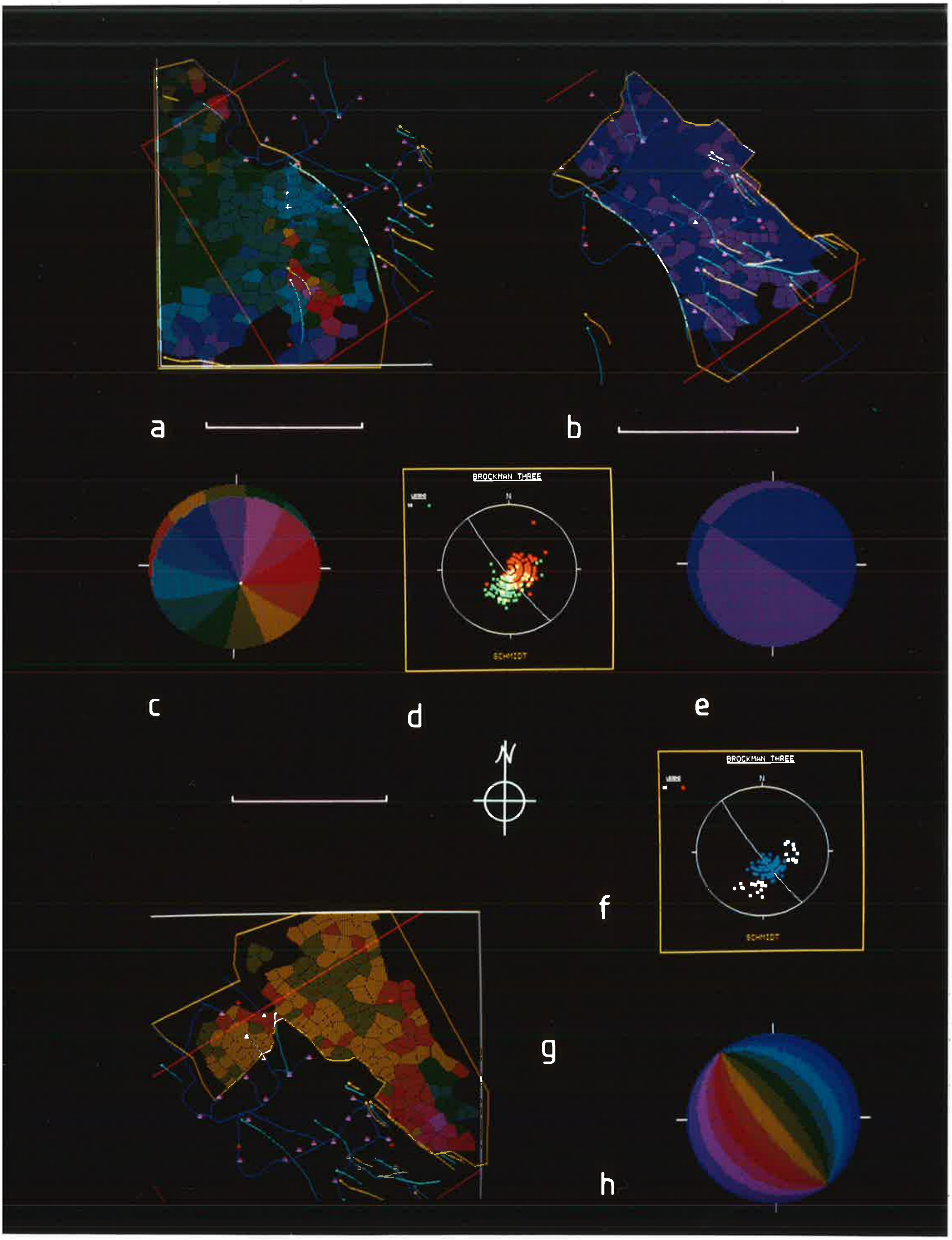
a
b
BROCKMAN THREE
N
SCHMIDT
c
d
e
f
g
h

Fig. CP.12 S.O.D.A. plots of random quartz fabrics. Specimens after Wilson (1973). (a) and (c) after his figures 9A,C.

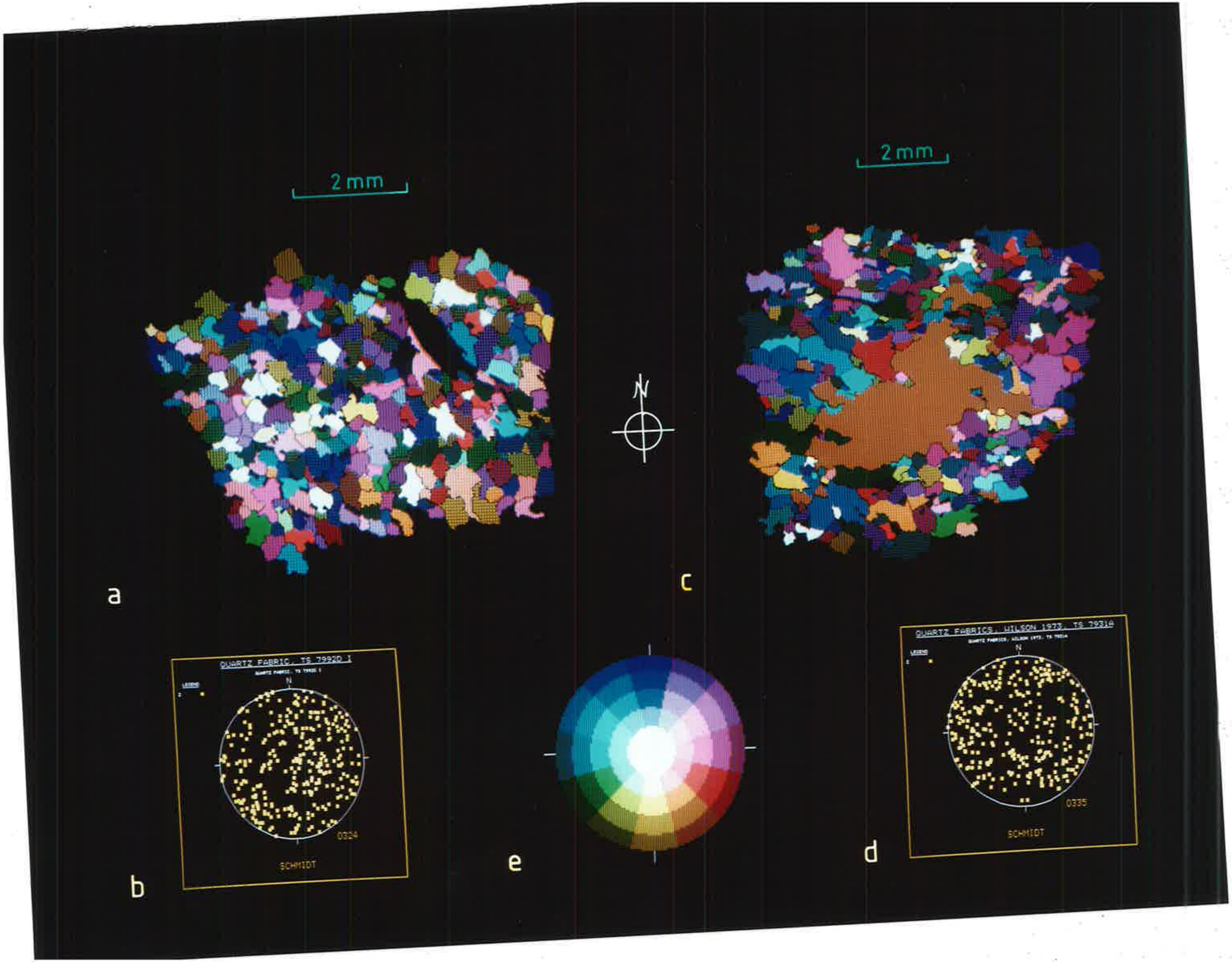
2 mm
2 mm
N
a
c
QUARTZ FABRIC, TS 7992D I
N
0324
SCHMIDT
b
e
QUARTZ FABRICS, WILSON 1973, TS 7931A
N
0335
SCHMIDT
d

Fig. CP.13 S.O.D.A. plots of non-random quartz fabrics. Specimens after Wilson (1973). A foliation in each of the specimens lies parallel to the scale bars.

a) After figure 11A, using colour chart (c).

b) Stereoplot for (a). Great circles: 284°/84°, 023°/80°.

c) Standard colour chart.

d) After figure 11B, using colour chart (c).

e) Stereonet plot for (d). Great circle: 060°/90°.

f) Colour chart: 3 30 (0) [3]; 330 -90 90 30 06 7
01 -4
02 -2

g) After figure 11B, using colour chart (f).

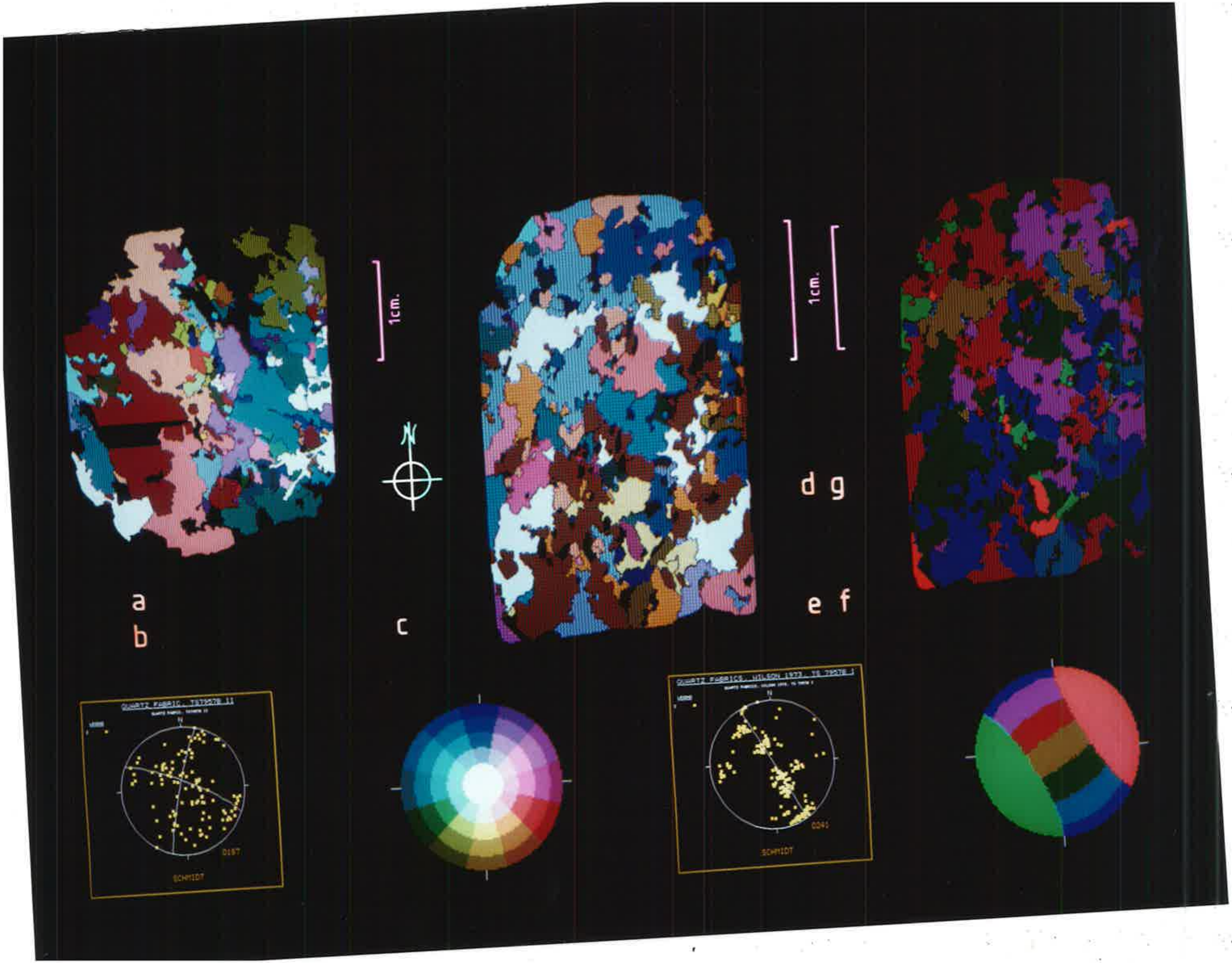

1cm.
N
1cm.
d g
a
b
c
e f
QUARTZ FABRIC, TS79578 11
N
SCHMIDT
QUARTZ FABRICS, WILSON 1973, TS 79578 1
N
SCHMIDT

Fig. CP.14 S.O.D.A. plots of hornblende grains in thin section HB1 (unorientated) (see Fig. 5.15).

a) S.O.D.A. plot using (100) axes with colour chart (b).

b) Colour chart: 3 30 (25) [3]; 000 90 90 0.

c) S.O.D.A. plot using (001) axes with colour chart (d).

d) Colour chart: 3 30 (15) [3]; 280 -90 90 0.

e,f,g) Stereoplots of (100),(010) and (001) axes in domain a0 respectively (see Fig. 5.15).
Great circles: 100/90, 190/90.

h,i,j) As above for domain b0.
Great circles: 110/90, 200/90.

k,l,m) As above for domain c0.
Great circles: 158/90, 068/90, 203/90.

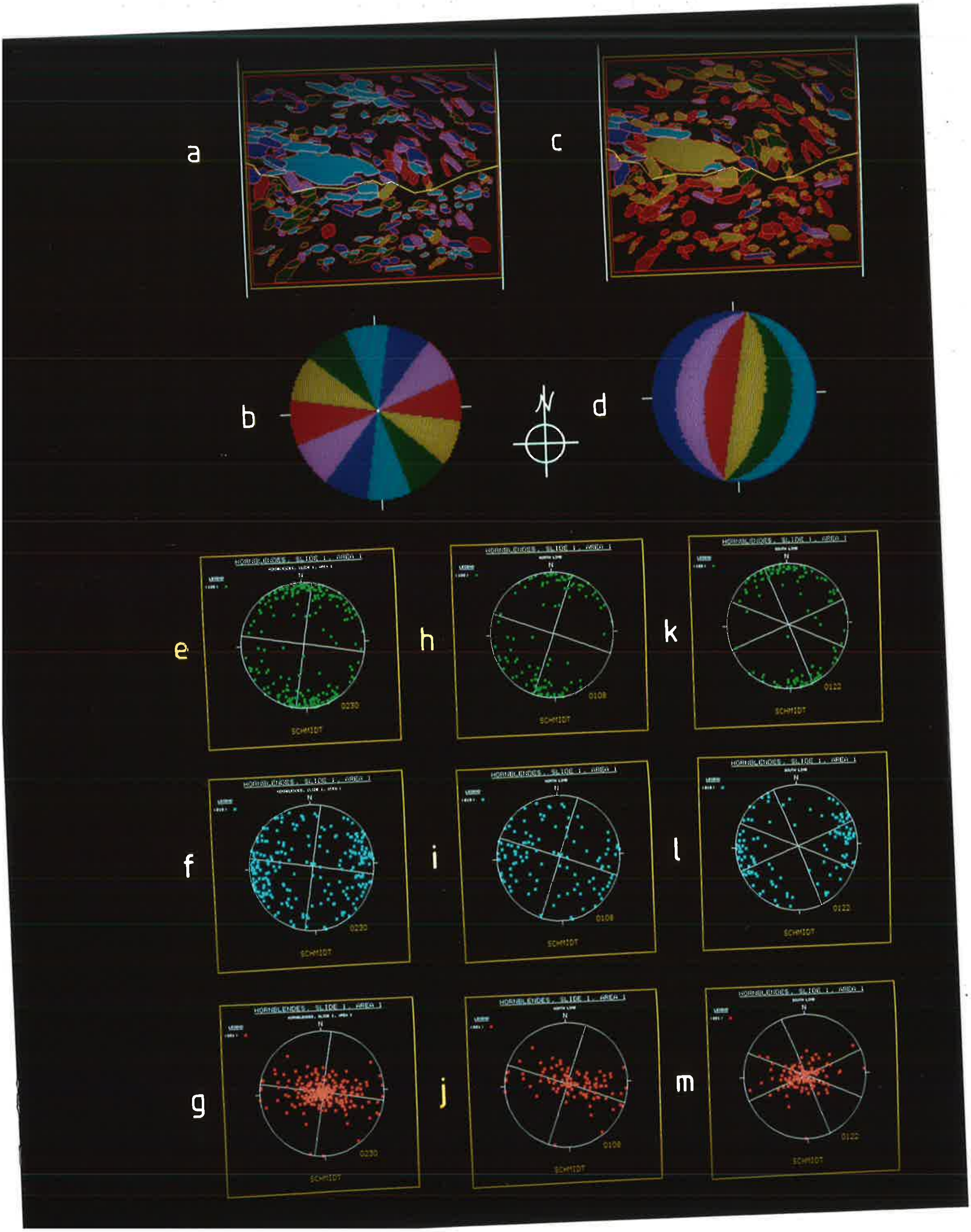
a
c
b
N
d
e
h
k
f
i
l
g
j
m
HORNBLENDES, SLIDE 1, AREA 1
N
0230
0108
0122
SCHMIDT

Fig. CP.15 S.O.D.A. plots of hornblende grains in thin section HB1 (unorientated) (see Fig. 5.17).

a,b,c) S.O.D.A. plots using (100), (010) and (001) axes respectively, with colour chart (d).

d) Colour chart: 3 30 (15) [3]; 000 90 90 0.

e,f,g) Stereoplots of (100), (010) and (001) axes respectively.
Great circles: 184/85, 094/95.

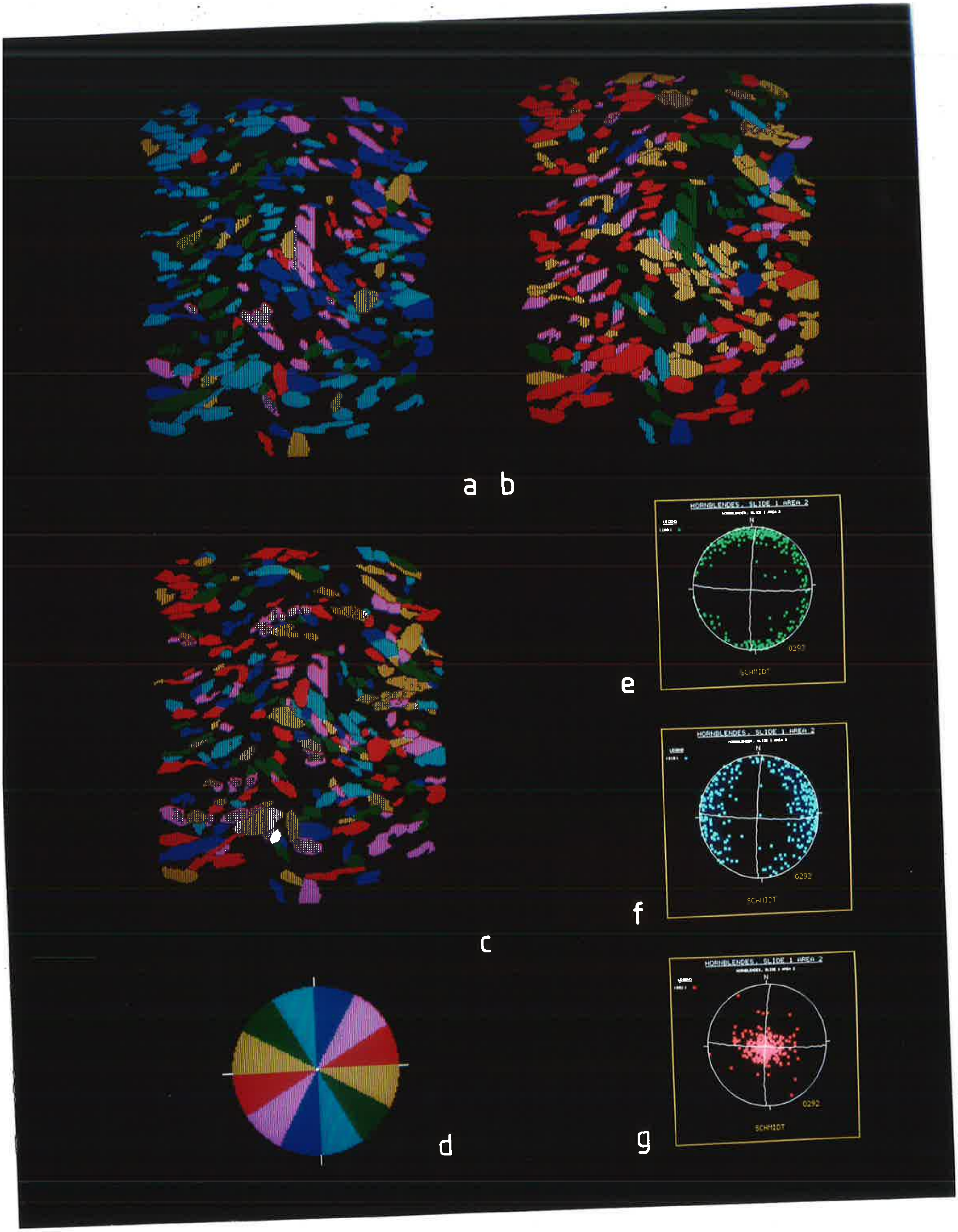
a
b
c
d
HORNBLENDES, SLIDE 1 AREA 2
N
0292
SCHMIDT
e
HORNBLENDES, SLIDE 1 AREA 2
N
0292
SCHMIDT
f
HORNBLENDES, SLIDE 1 AREA 2
N
0292
SCHMIDT
g

Fig. CP.16 S.O.D.A. plots of submap M13 (Fig. 7.6). Scale bar 100 metres. (All colour charts for this and following plates have north orientated parallel to the stereonet north, not the north of the S.O.D.A. maps.)

a) Poles to S_1 using colour chart (d).

b) Composite stereoplot of data. S_1 green, 92 points; S_3 red, 43 " ; F_{2-3} cyan, 98 " ;
Great circles: 317/90, 036/19.

c) Poles to S_3 using colour chart (d).

d) Colour chart: 2 -30 (50); 50 90 90 0.

e) F_{2-3} using colour chart (f).

f) Colour chart: 4 -9 (50); 50 90 -71 0.

g) Poles to S_1 demonstrating nonsensical domains, using colour chart (h).

h) Colour chart: 2 15 (0); 50 -90 71 0.

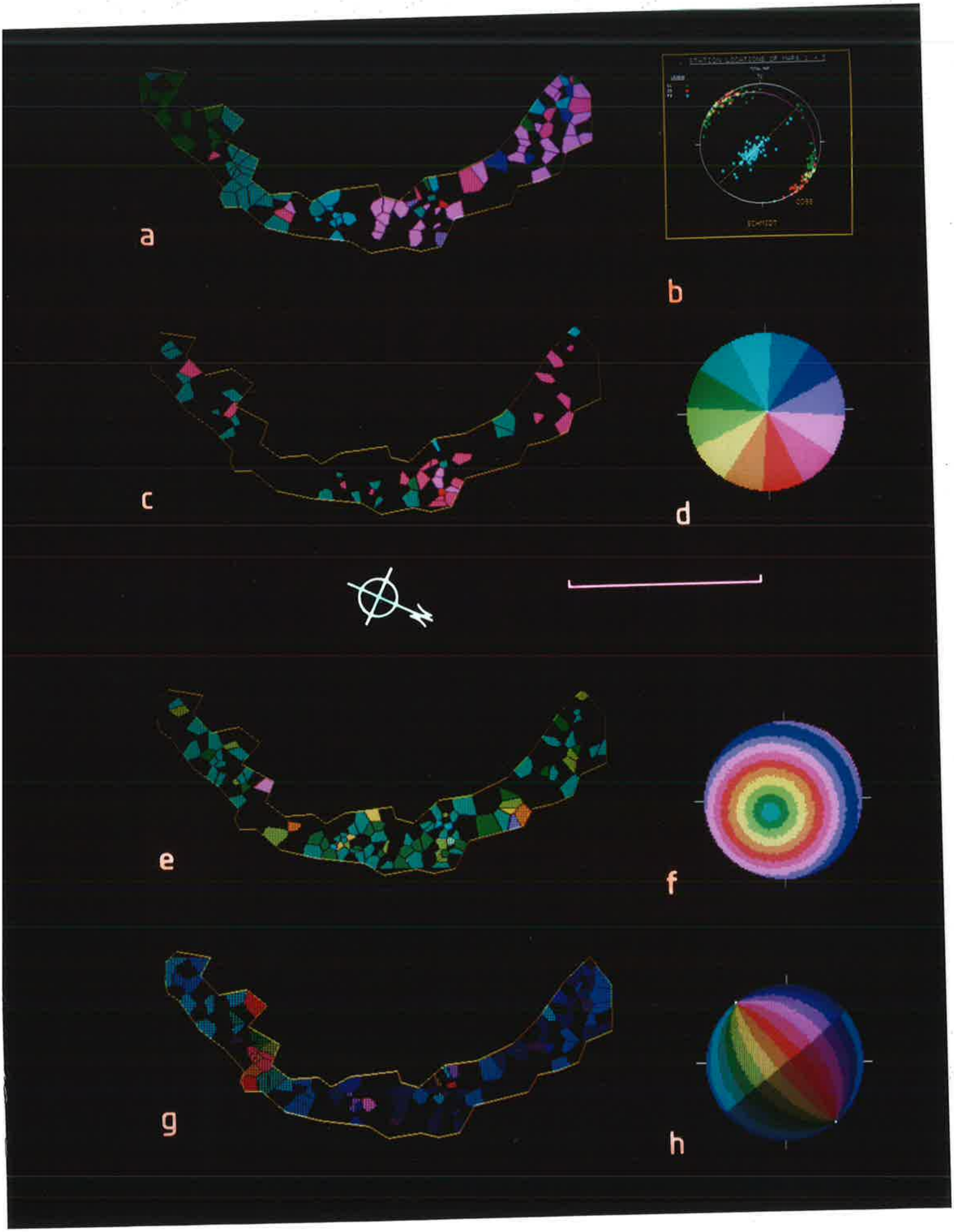
a
b
c
d
e
f
g
h

Fig. CP.17 S.O.D.A. plots of submap M45 (Fig. 7.17). Scale bar 100 metres.

a) Poles to S_1 using colour chart (d).

b) Composite stereoplot of data. S_1 green, 46 points;
S_3 red, 9 " ;
F_{2-3} cyan, 74 " ;
Great circles: 126/90, 140/84, 048/04.

c) Poles to S_3 using colour chart (d).

d) Colour chart: 2 -30 (36); 36 90 90 0.

e) F_{2-3} using colour chart (f).

f) Colour chart: 3 -15 (0); 36 -90 90 0.

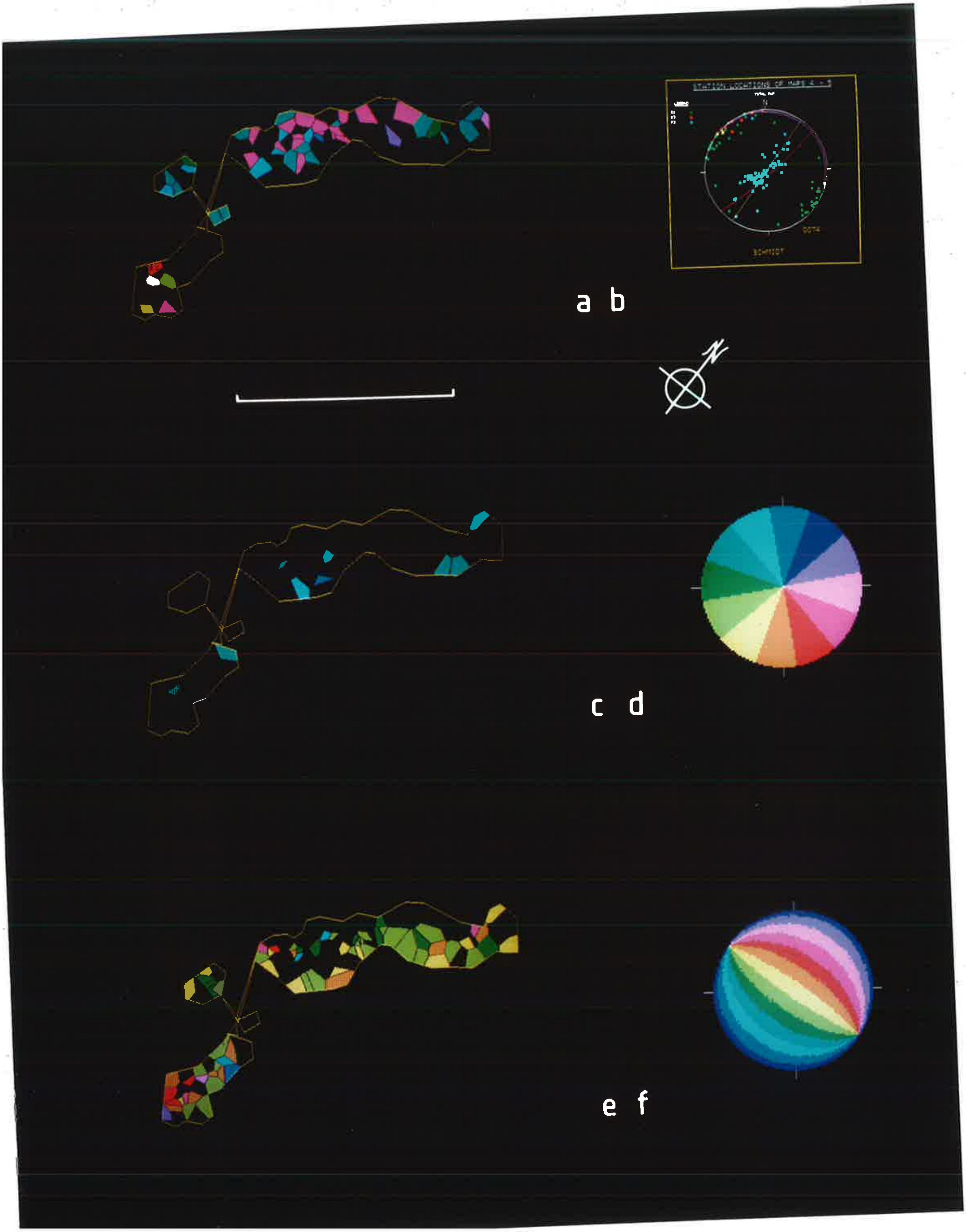
SCHMIDT
a b
c d
e f

Fig. CP.18 S.O.D.A. plots of submaps M6AB (a-d) and M789 (e-j) (Fig. 7.28). Scale bar 100 metres.

a) Poles to S_1 using colour chart (d) of Fig. CP.17 .

b) Poles to S_3 " " " " " " .

c) F_{2-3} " " " (f) " " .

d) Composite stereoplot of data. S_1 green, 60 points;
S_3 red, 4 " ;
F_{2-3} cyan, 33 " ;
Great circles: 306/85, 101/08.

---

e) Composite stereoplot of data. S_1 green, 98 points;
S_3 red, 37 " ;
F_{2-3} cyan, 126 " ;
Great circles: 130/90, 126/90, 040/20.

f) Poles to S_1 using colour chart (i).

g) Poles to S_3 " " " " .

h) F_{2-3} " " " (j).

i) Colour chart: 2 -30 (40); 40 90 90 0.

j) Colour chart: 3 -15 (0); 40 -90 90 0.

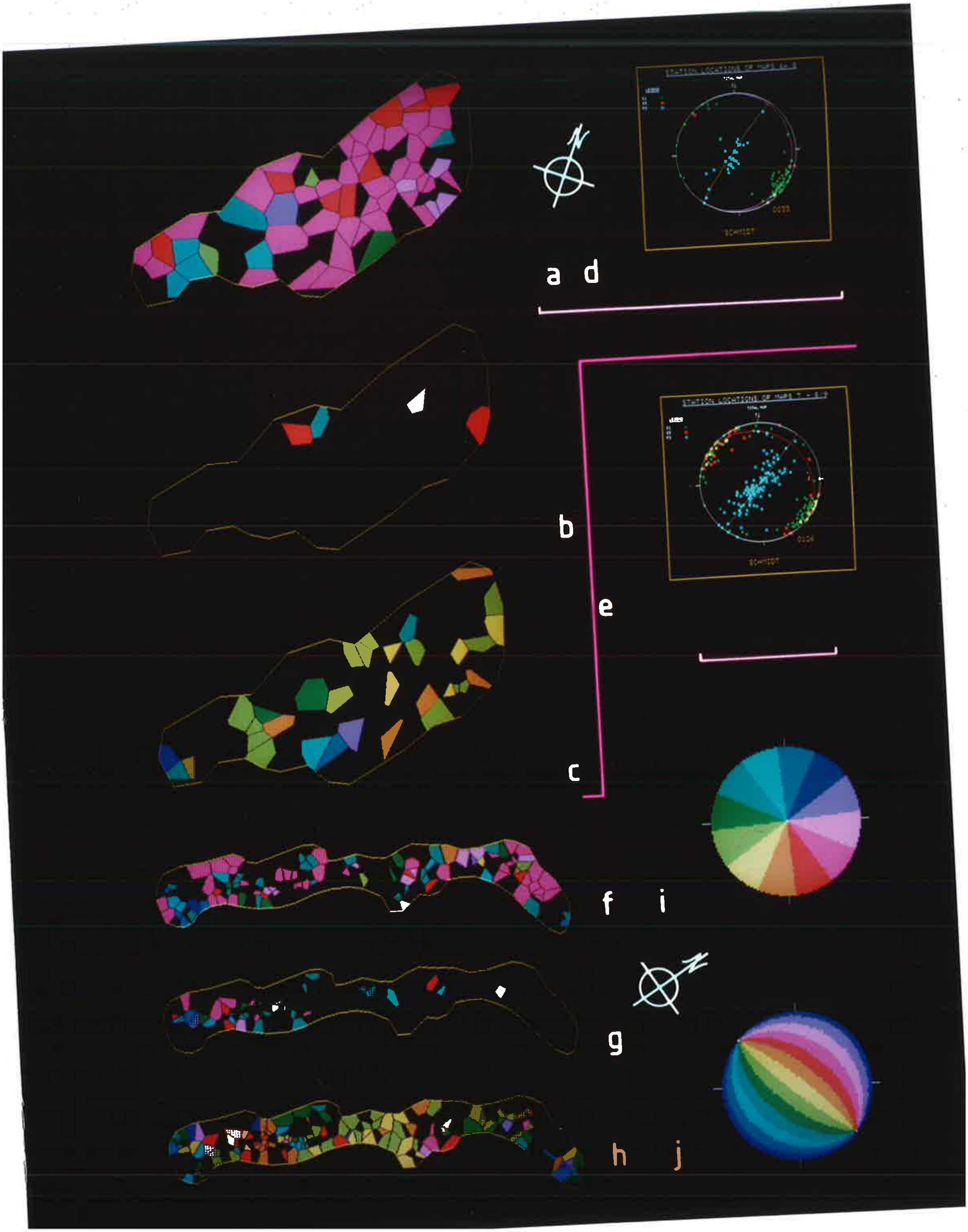
a
d
b
e
c
f
i
g
h
j

Fig. CP.19 S.O.D.A. plots of submap M912 (Fig. 7.40). Scale bar 100 metres.

a) F_{2-3} using colour chart (b).

b) Colour chart: 4 -11 (0); 45 90 90 0.

c) F_{2-3} using colour chart (d).

d) Colour chart: 3 -15 (0); 45 -90 90 0.

e) Composite stereoplot of data. S_1 green, 204 points;
S_3 red, 63 " ;
F_{2-3} cyan, 299 " ;
Great circles: 315/85.

f) Poles to S_1 using colour chart (g).

g) Colour chart: 2 -30 (45); 45 90 90 0.

h) Poles to S_3 using colour chart (g).

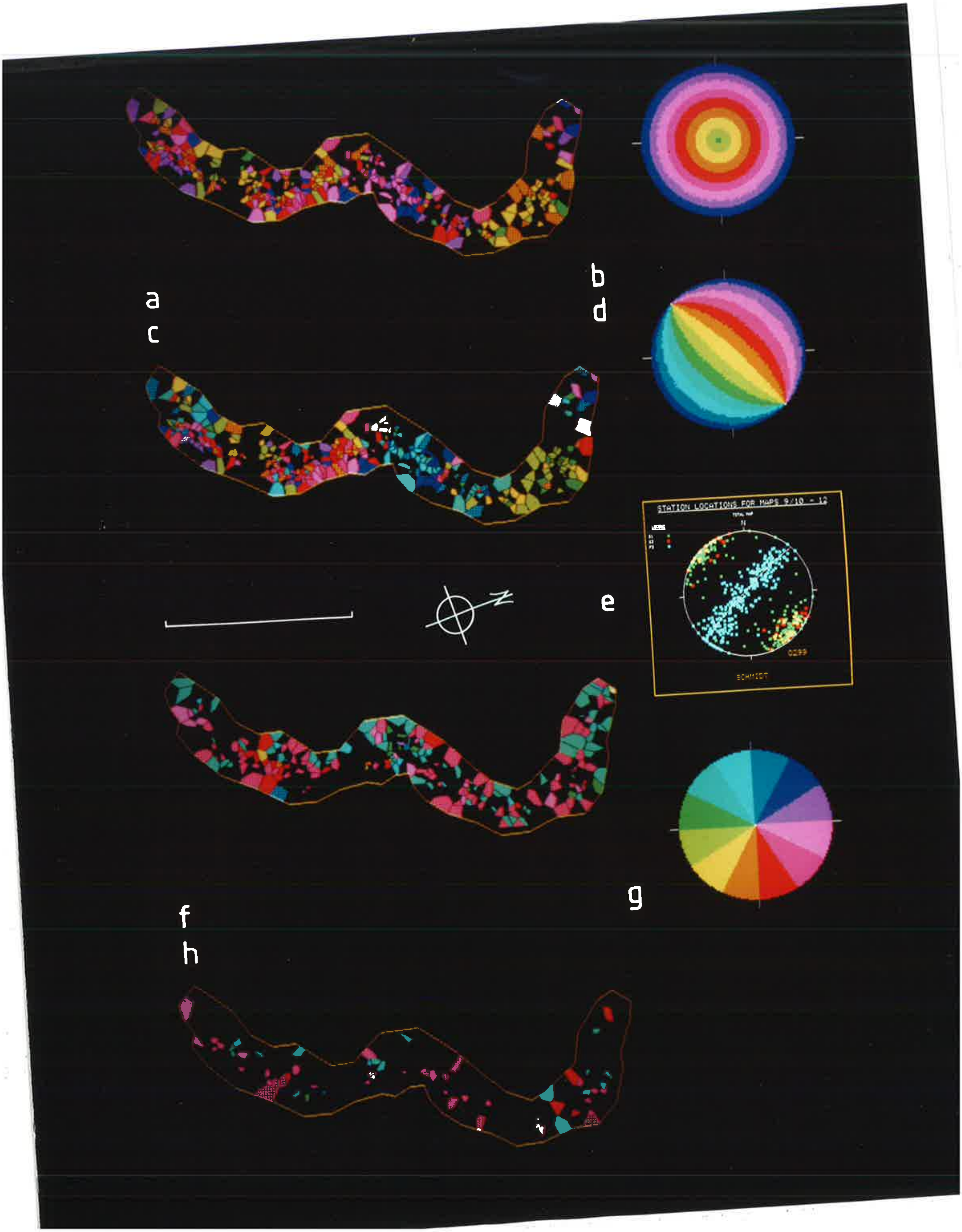
a
b
c
d
e
STATION LOCATIONS FOR MAPS 9/10 - 12
TOTAL MAP
N
0299
SCHMIDT
f
g
h